Towards Understanding the Mechanism of Clioquinol Neurotoxicity

by

Jamuna Chhetri

BPharm (Hons), Kathmandu University, Nepal
MPharmSc, University of Tasmania, Australia

Submitted in fulfilment of the requirements for the Doctor of Philosophy
Division of Pharmacy, School of Medicine,
Faculty of Health

University of Tasmania, Hobart

October 2016

Declaration of Originality

This thesis contains no material which has been accepted for a degree or diploma by the University or any other institution, except by way of background information and duly acknowledged in the thesis, and to the best of my knowledge and belief no material previously published or written by another person except where due acknowledgement is made in the text of the thesis, nor does the thesis contain any material that infringes copyright.

Jamuna Chhetri

4 October 2016

Authority of Access

This thesis is not to be made available for loan or copying for two years following the date this statement was signed. following that time, the thesis may be made available for loan and limited copying and communication in accordance with the Copyright Act 1968.

Jamuna Chhetri

4 October 2016

Statement of Ethical Conduct

The research associated with this thesis abides by the international and Australian codes on human and animal experimentation, the guidelines by the Australian Government's Office of the Gene Technology Regulator and the rulings of the Safety, Ethics and Institutional Biosafety Committees of the University. All animal experiments were approved by the Animal Ethics Committee (AEC), University of Tasmania, Australia (Animal Ethics approval numbers: A12817 and A0015097).

Statement Regarding Published Work Contained in Thesis

The publishers of the papers comprising Chapters 1 and 2 hold the copyright for that content, and access to the material should be sought from the respective journals. The remaining non published content of the thesis may be made available for loan and limited copying and communication in accordance with the Copyright Act 1968.

List of Publications and Statement of Co-authorship

The following people and institutions contributed to the publication of the work undertaken as part of this thesis:

Candidate: Jamuna Chhetri[1] (JC)

Author 1: Nuri Gueven[1] (NG)

Author 2: Glenn Jacobson[1] (GJ)

Author 3: Anna E. King[2] (AEK)

[1]Pharmacy, School of Medicine, Faculty of Health, University of Tasmania, Hobart, Tasmania, Australia

[2]Wicking Dementia Research and Education Centre, Faculty of Health, University of Tasmania, Hobart, Tasmania, Australia

Author details and their roles:

Peer-reviewed journal publications

Paper 1, Chhetri J, Jacobson G, Gueven N. Zebrafish-on the move towards ophthalmological research. Eye 2014;7(10):19. (IF: 2.213)

Located in chapter 1

Candidate was the primary author and with NG and GJ contributed to the idea, its formalisation and refinement. NG and GJ assisted in editing the manuscript.

Paper 2, Chhetri J, Gueven N. Targeting mitochondrial function to protect against vision loss. Expert Opin Ther Targets 2016:1-16. (IF: 4.79)

Located in chapter 1

Candidate was the primary author and with NG contributed to the idea and its formalisation and refinement. NG also assisted in evaluating and editing the manuscript.

Paper 3, Alzheimer's Disease and NQO1: Is there a Link? (Accepted for Publication: Current Alzheimer Research) (IF: 3.58)

Located in chapter 1 and chapter 2

Candidate was the primary author and with NG and AEK contributed to the idea, its formalisation and refinement. NG and AEK also assisted in evaluating and editing the manuscript.

Conference abstracts (Oral) (Presenting author is underlined)

1. Chhetri J, Gasperini R, Jacobson G, Foa L, Gueven N. Mechanism of Clioquinol Toxicity-relevance to neurodegenerative diseases. APSA-ASCEPT (29 Nov-2 Dec 2015), Hobart, Australia.

Conference abstracts (Poster) (Presenting author is underlined)

1. Chhetri J, Jacobson G, Gueven N. Development of a zebrafish model to detect mitochondrial dysfunction-induced vision loss. University of Tasmania Graduate Research conference (Aug 2013, Hobart, Australia).
2. Chhetri J, Jacobson G, Gueven N. Detoxification of clioquinol by NQO1. University of Tasmania Higher Degree Research (HDR) conference (Jul 2014, Hobart, Australia).

3. Chhetri J, Dilek J, Jacobson G, Gasperini R, Foa L, Gueven N. Clioquinol induces mitochondrial dysfunction by inhibiting NQO1. AussieMit conference (Dec 1-3 2014, Perth, Western Australia).
4. Chhetri J, Gasperini R, Jacobson G, Foa L, Gueven N. Mechanism of Clioquinol Toxicity-relevance to neurodegenerative diseases. APSA-ASCEPT (29 Nov-Dec 2015, Hobart, Australia).
5. Chhetri J, Farooq M, Dilek J, Jacobson G, Gasperini R, Foa L, Gueven N. NQO1-dependent toxicity of clioquinol. United Mitochondrial Disease Foundation, Mitochondrial Medicine (15-18th of June 2016, Seattle, WA, USA, presented by N Gueven).

We the undersigned agree with the above stated "proportion of work undertaken" for each of the above published (or submitted) peer-reviewed manuscripts contributing to this thesis:

Signed:

A/Prof Nuri Gueven	Prof Ben Canny
Supervisor	Head of School
School of Medicine	School of Medicine
University of Tasmania	University of Tasmania

Date: 22/9/2016

Acknowledgements

This PhD thesis would have never been possible if I was not given an opportunity in the first place. Therefore, first and foremost I would like to thank the University of Tasmania, in particular, Professor Gregory Peterson, Deputy Dean (Research), in believing my potential and providing me with an opportunity to pursue PhD study at the University of Tasmania.

I am very much grateful to my primary supervisor, A/Professor Nuri Gueven who introduced me to research in a real sense and nurtured my enthusiasm for research. I appreciate his time, immense support and expert suggestions for my PhD study. He has always been a tremendous mentor who has always encouraged my research and allowed me to grow as an independent researcher. I am so much impressed with his immense knowledge of the subject matter, problem-solving skills, and networking skills. All in all, it has been a great honour to be his PhD student.

I would also like to express my sincere gratitude to my co-supervisors A/Professor Lisa Foa, Dr Robert Gasperini and Dr Glenn Jacobson for their support and insightful comments on my research project. In addition, I am thankful to Lisa for letting me use the zebrafish facility at Medical Science Precinct (MSP) for the *in-vivo* experiments.

My special thanks go to Dr Peter Traill, Anthony Whitty, Melissa Aubrey of Pharmacy and Dr David Steele, Sarah Kane of Medical Science Precinct (MSP) for the efficient management of logistics to facilitate the smooth running of my day-to-day research work. I could not stay without thanking Mr Steven Weston, Ms Narelle Phillips, Dr Ellen Bennett from MSP for so willingly sharing their histology expertise with me whenever I required them. I would also like

to thank A/Professor Noel Davies, Central Science Laboratory, University of Tasmania, for his help with mass spectrometric analysis, Petr Smejkal and Aliaa Shallan for their help with 3D printing, Adrian Thompson for providing me with zebrafish eggs for the experiments, Jem Dilek for the initial drug screening and Mohammed Farooq for assisting me with some of the *in-vitro* studies.

I would also like to express my sincere thanks to Emeritus Professor Stuart Mclean for providing me insightful feedback on my write-up, Dr Rosanne Guijt, Dr Rahul Patel and Dr Syed Tabish R. Zaidi for their support and suggestions on my research project and future career.

I am thankful to my colleagues in Pharmacy for their companionship, emotional support and of course for the wonderful time we spent together. Last but not the least, I am very much indebted to my family, who has always been a source of inspiration to me and has always stood by me in all my pursuits. They are the reason why I am here today and I happily dedicate this thesis to them.

List of Abbreviations

Acronym	Definition
8-HQ	8-hydroxyquinoline
Acetyl-CoA	acetyl-coenzyme A
AD	Alzheimer's disease
ADOA	autosomal dominant optic atrophy
ADP	adenosine diphosphate
AEC	animal ethics committee
AEG	advance glycation end products
ALDH4	aldehyde dehydrogenase 4
AMD	age-related macular degeneration
ANOVA	analysis of variance
ANT	adenine nucleotide transporter
APA	acetaminophen
APP	amyloid precursor protein
APS	ammonium persulphate
ARE	antioxidant response element
ATP	adenosine triphosphate
AVMA	American Veterinary Medical Association
Aβ	amyloid beta
BSA	bovine albumin serum
CAG	cytosine adenine guanine
Cat	catalase
CM-H_2DCFDA	chloromethyl 2',7'-dichlorodihydrofluorescein diacetate

CoQ	coenzyme ubiquinone
Cu	Copper
Cu/ZnSOD	copper/zinc superoxide dismutase
Cul 3	cullin 3
Cys	cysteine
Cytc	cytochrome c
DAB	3, 3’-diaminobenzidine
DCPIP	dicholorophenolindophenol
DCs	double cones
Dic	dicoumarol
DLG	dorsal lateral geniculate nucleus
DMD	digital micromirror device
DMEM	dulbecco’s modified eagle’s medium
DMSO	dimethylsulfoxide
DNA	deoxyribonucleic acid
DR	diabetic retinopathy
DTT	dithiothreitol
E2	ubiquitin-conjugation enzyme
ECL	enhanced chemiluminescence
EDTA	ethylenediaminetetraacetic acid
EGTA	ethylene glycol-bis(β-aminoethyl ether)-N,N,N',N'-tetraacetic acid
EMA	European Medicines Agency
ER	escape response
ETC	electron transport chain
$FADH_2$	flavin adenine dinucleotide reduced

Fe	iron
Fe-S	iron-sulphur centres
FMN	flavin mononucleotide
GAPDH	glyceraldehyde-3-phosphate dehydrogenase
GLS-2	glutaminase 2
GPT	glutamate pyruvate transaminase
GPx1	glutathione peroxidase 1
GSH	glutathione
GSR	glutathione reductase
GSSG	glutathione disulphide
GST	glutathione-s-transferase
H & E	haematoxylin and eosin
H_2O_2	hydrogen peroxide
HBSS	hank's balance salt solution
HD	Huntington's disease
HEK293	human embryonic kidney cells
HepG2	human hepatocarcinoma cells
HO-1	heme oxygenase1
HTG	high tension glaucoma
IHC	immunohistochemistry
INL	inner nuclear layer
IPL	inner plexiform layer
keap1	kelch-like ECH-associated protein 1
LDH	lactate dehydrogenase
LGB	lateral geniculate body

LHON	Leber’s hereditary optic neuropathy
LSCs	long single cones
MD	mitochondrial disease
MELAS	mitochondrial encephalopathy, lactic acidosis and stroke-like episodes
MERRF	myoclonus epilepsy with ragged-red fibres
MnSOD	manganese superoxide dismutase
MRM	multiple reaction monitoring
MS	multiple sclerosis
MS-222	tricaine methanesulfonate
mt PTP	mitochondrial permeability transition pore
mt- rRNAs	mitochondrial ribosomal RNA
mt-tRNAs	mitochondria transfer RNAs
MTC	maximum tolerated concentration
mtDNA	mitochondrial DNA
Na_3VO_4	sodium orthovanadate
NAC	n-acetyl cysteine
NaCl	sodium chloride
NADH	nicotinamide adenine dinucleotide
NADPH	nicotinamide adenine dinucleotide phosphate
NaOH	sodium hydroxide
NBT	nitro-blue tetrazolium
nDNA	nuclear DNA
NF-kB	nuclear factor kappa-light-chain-enhancer of activated B
NGF	nuclear growth factor
NQO1	NAD(P)H quinone oxidoreductase 1

Nrf2	nuclear factor erythroid 2-related factor 2
NTG	normal tension glaucoma
OKR	optokinetic response
OMR	optomotor response
ONH	optic nerve head
ONL	outer nuclear layer
OPA	optic atrophy protein
OPL	outer plexiform layer
ox	oxidant
OXPHOS	oxidative phosphorylation
PBS	phosphate-buffered saline
PD	Parkinson’s disease
PET	petstore
PFA	paraformaldehyde
pi	inorganic phosphate
PKC	polyol protein kinase
PL	plexiform layer
PMSF	phenylmethanesulfonyl fluoride
POAG	primary open-angle glaucoma
PPMS	primary progressive MS
PR	photoreceptor layer
Prx3	peroxiredoxin 3
PTB	phototactic behaviour
RAGE	receptor for AGE
RGC	retinal ganglion cells

RNA	ribonucleic acid
RNFL	retinal nerve fibre layer
ROS	reactive oxygen species
Rot	rotenone
RPE	pigment epithelium layer
RPMS	relapsing remitting MS
RRMS	relapsing-remitting MS
RT	room temperature
SD	standard deviation
SD-OCT	spectral domain optical coherence tomography
SDS-PAGE	sodium dodecyl sulfate-polyacrylamide gel
SEM	standard error of mean
SMON	subacute mylo-optic neuropathy
SOD	superoxide dismutase
SPMS	secondary progressive MS
SR	startle response
SSCs	short single cones
TBS-T	tris-buffered saline-tween
TCA	tricarboxylic citric acid
TEMED	tetramethylenediamine
TIGAR	TP53-induced glycolysis and apoptosis regulator
TM	trabecular meshwork
TON	toxic optic neuropathy
Trx	thioredoxins
$Trx(SH)_2$	Trx reduced

Trx(SS)	Trx oxidised
VDAC	voltage-dependent anion channels
VEGF	vascular endothelial growth factor
VKORC1	vitamin k oxidoreductase C1
VMR	visual motor response
WST	1(2-(4-iodophenyl)-3-(4-nitrophenyl)-5-(2,4-disulphonyl)-2H-tetrazolium)
Zn	Zinc
γGCL	γ-glutamyl-cysteine-ligase

List of Contents

List of Tables

List of Figures

Abstract

The quinoline derivative clioquinol (CQ) was widely used as a topical disinfectant for skin conditions and as an oral antibiotic against diarrhoea. However, in 1970 the oral formulation was taken off the market in many countries after it was linked to about 10 000 cases of subacute myelo-optic neuropathy (SMON) in Japan. SMON was characterised by optic neuritis and axonopathy of the spinal cord. Although a clear mechanistic connection is still disputed, a clear reduction in SMON cases was witnessed following drug withdrawal from the market. Furthermore, the common pathological features of SMON-associated neurotoxicity have been successfully recapitulated in CQ-treated animals, which support a direct connection. Several hypotheses have tried to explain CQ-dependent toxicity such as CQ-induced DNA damage and oxidative stress. However, none of these studies has attempted to explain the restriction of CQ-induced neurotoxicity to the Japanese population. Despite this toxicity, CQ and its structural analogues are currently under investigation as a disease modifying treatment for the neurodegenerative disorders such as Alzheimer's and Huntington's Disease, with some encouraging preclinical and clinical results. In light of the re-emergence of CQ and its structural analogues, it is crucial to understand the underlying mechanism of CQ-induced toxicity beyond the scope of SMON to prevent any potential CQ-associated risks to future patients.

From a previous research project that screened marketed drugs and drug-like compounds against their potential to cause mitochondrial dysfunction *in vitro*, CQ and 8-HQ were identified as hits (unpublished). The mitochondrial liability of these compounds (0.5-10) µM was subsequently confirmed in RGC5 cells by measuring galactose-hypersensitive ATP levels, lipid peroxidation and cellular viability. However, the confirmation of CQ-induced mitochondrial toxicity in another cell line, HepG2, failed. Prior unrelated observations (N.

Gueven, unpublished) showed that these cell lines differ in the response to oxidants, which is associated with different cellular levels of the antioxidant enzyme NADPH Quinone Oxidoreductase 1 (NQO1). NQO1-dependent CQ associated-mitochondrial-dysfunction was confirmed in isogenic cell lines that differ only in the expression levels of NQO1. NQO1 expression was inversely correlated to CQ-induced mitochondrial-dysfunction. While cells with low NQO1 were highly sensitive to CQ-induced mitochondrial-dysfunction, recombinant NQO1 expression in these cells provided protection against CQ-toxicity. CQ-induced reduction of cellular ATP levels, increased lipid peroxidation and elevated cell death could be attenuated by concomitant treatment with different antioxidants, implicating oxidative stress as the core mechanism of CQ-induced toxicity. Furthermore, biochemical studies also revealed that CQ and 8-HQ directly inhibited NQO1 enzyme activity at a concentration range of 10-100 µM.

In order to translate the *in-vitro* findings of NQO1-dependent CQ toxicity into an *in-vivo* situation, zebrafish were selected as a suitable animal model. Zebrafish are characterised by variable NQO1 expression in the retina during different stages of their life. While larval zebrafish are reported to lack retinal NQO1 expression, the protein is highly expressed in the adult zebrafish retina. The observed general CQ-induced toxicity in zebrafish was strain-dependent. Petshop (PET) strain zebrafish larvae were less sensitive compared to a commonly used laboratory strain (AB). The maximum tolerated concentration of CQ that did not lead to systemic toxicity was 10 µM in PET and 3 µM in AB. To demonstrate retinal CQ effects in this model, visual CQ toxicity in PET zebrafish larvae was determined by measuring eye velocity as a function of different stimulus velocities. Comparable to the human situation, CQ inhibited visual function in a dose-dependent manner between 3-10 µM, which is surprisingly consistent with the concentration range that caused mitochondrial-dysfunction *in-vitro*. In

contrast to larval responses, even the highest CQ concentration (10 µM) did not affect visual function in the adult zebrafish. This is in line with the *in-vitro* results where high NQO1-expressing HepG2 cells were resistant to CQ-induced mitochondrial-dysfunction. NQO1-dependent protection against CQ-induced visual impairment was confirmed by the presence of NQO1 enzyme activity in the adult zebrafish retina. Consistent with this, pharmacological inactivation of NQO1 resulted in CQ-induced oxidative stress in the retina and acute systemic toxicity in the adult fish.

Overall, these results highlight the importance of NQO1 expression in mitigating CQ toxicity both *in-vitro* and *in-vivo* and that CQ induces mitochondrial-dysfunction through the generation of oxidative stress. Strikingly, nearly 50 years after the drug was retracted from the market, this connection between NQO1 and CQ-toxicity might explain the geographic restriction of SMON cases. It is important to note that a much higher prevalence of the inactivating C609T NQO1 polymorphism has been reported for the Japanese population compared to the European population. Based on the results of this study, this population group should, therefore, be highly susceptible to the toxicity of CQ. The results of the present study could for the first time explain the geographic restriction of CQ-induced neurotoxicity to Japan. Currently, this hypothesis is tested by assessing the presence of the C609T NQO1 polymorphism in Japanese SMON survivors. Furthermore, if CQ or its derivatives are to be employed for the treatment of neurodegenerative diseases, it appears imperative that NQO1 status of the patients should be ascertained before the start of the treatment. Therefore, in addition to potentially solving a long-standing medical mystery, this project offers a significant benefit towards personalised medicine to minimise drug treatment-associated risk to a specific group of patients.

CHAPTER 1

Chapter 1: General Introduction

1.1 Mitochondria

Mitochondria, also known as the powerhouses of cells, generate the majority of the energy needed for cellular life. Mitochondria are dynamic intracellular organelles that exist as a reticulum and constantly undergo biogenesis and degradation to maintain the overall health of the mitochondrial pool within each cell. The number of mitochondria per cell varies from hundreds to thousand depending on the metabolic demand of the specific cell. Since the brain and the visual system have very high energy demands, they are highly populated with mitochondria [1]. The structure of mitochondria consists of an outer and inner membrane (**Figure 1**) [2]. The permeability of the outer mitochondrial membrane is regulated by a family of channel-forming proteins, known as porins or voltage-dependent anion channels (VDAC), which are permeable to uncharged low molecular weight molecules up to 10 kDa [3]. The inner membrane is relatively impermeable compared to the outer membrane. The space between the outer and the inner membrane of mitochondria is called the inter-membrane space [2]. Bounded by the inner membrane is the matrix, which contains the enzymes that make up the Tricarboxylic Citric Acid (TCA) cycle, enzymes for beta-oxidation of fatty acids, mitochondrial DNA (mtDNA), RNA, and mitochondrial ribosomes [2]. The mitochondrial genome consists of thousands of copies of maternally inherited mtDNA as well as approximately 1500 genes that are coded in the nuclear DNA (nDNA) [4]. Mitochondrial DNA encodes 37 genes, 13 of which code for proteins essential for the process of mitochondrial oxidative phosphorylation (OXPHOS), 22 genes that code for mitochondrial transfer RNAs (mt-tRNAs) and 2 that encode mitochondrial ribosomal RNAs (mt-rRNAs), which are essential for the synthesis of OXPHOS proteins [4]. All proteins that are responsible for other aspects of mitochondrial function, such as mitochondrial biogenesis, are encoded by nuclear genes [4].

Apart from energy production, mitochondria are also responsible for other essential cellular functions such as fatty acid synthesis, maintenance of calcium homeostasis, biosynthesis of haem and iron sulphur proteins, production and regulation of reactive oxygen species (ROS), as well as regulation of cell death through the activation of the mitochondrial permeability transition pore (mt PTP) [4,5].

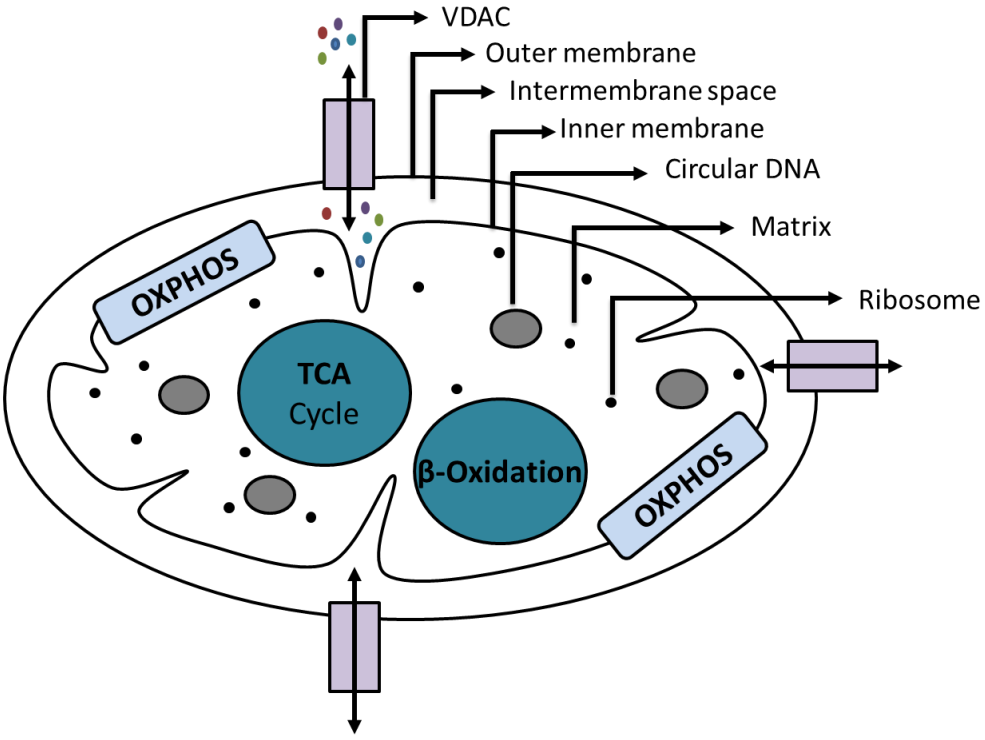

Figure 1: Schematic representation of mitochondrial structure.

Mitochondria are organelles consisting of an outer and an inner membrane. The space between the outer and the inner membrane is called the intermembrane space. The permeability of the outer membrane is regulated by voltage gated anion channels (VDAC). Embedded on the matrix side of the inner membrane are components of the oxidative phosphorylation (OXPHOS) complexes. The matrix mainly contains the enzymes of the Tricarboxylic-Citric Acid cycle (TCA), enzymes for β-oxidation as well as mtDNA and mitochondrial ribosomes.

1.1.1 Mitochondria and Energy Metabolism

Mitochondria produce energy by oxidizing glucose, amino acids and fatty acids present in food, to generate chemical energy mainly in the form of adenosine triphosphate (ATP). This energy is stored in the covalent phosphate bond of ATP and is released upon hydrolysis of this bond to generate ADP as a reaction product (a lower energy molecule). Cellular energy production occurs via different metabolic pathways. Glycolysis occurs in the cytoplasm, oxidative phosphorylation (OXPHOS) occurs exclusively in the mitochondrial inner membrane in the presence of oxygen while the tricarboxylic-cyclic acid (TCA) cycle takes place in the mitochondrial matrix [6].

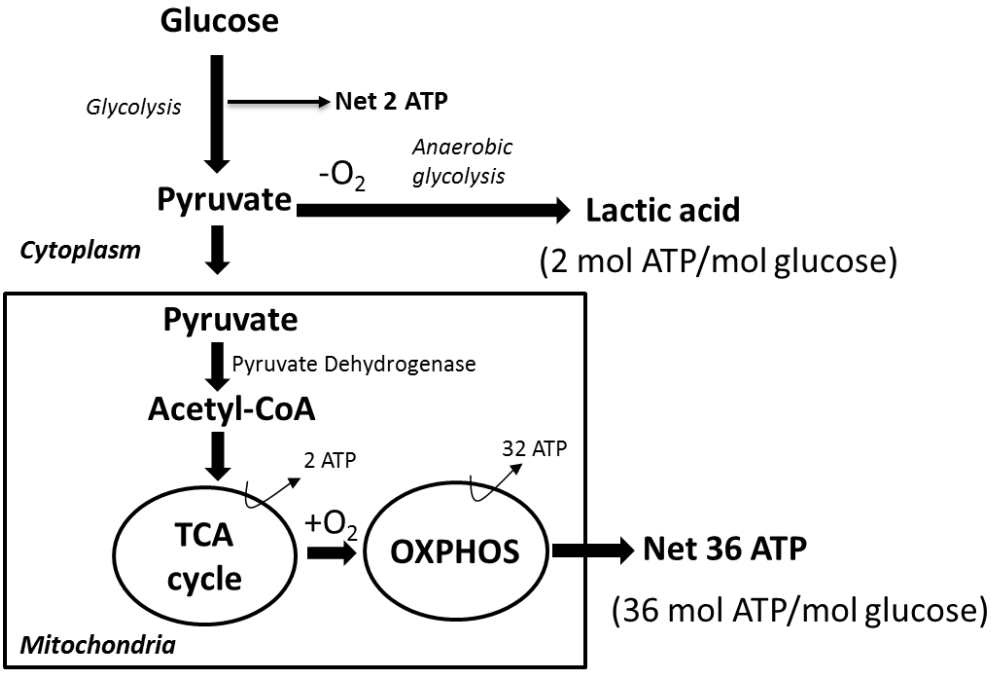

Figure 2: Cellular energy metabolism.

Glucose is metabolised to pyruvate via glycolysis in the cytoplasm. Pyruvate is then completely oxidised in the mitochondrial TCA cycle to provide energy equivalents for oxidative phosphorylation. In total, this process generates 36 molecules of ATP per molecule of glucose. When oxygen is limiting, cells divert the glycolysis-generated pyruvate towards the production of lactic acid (anaerobic glycolysis), a highly inefficient process that generates only a net of 2 molecules of ATP per molecule of glucose.

Glycolysis is a multistep metabolic pathway that consists of ten enzymes, which metabolize glucose to pyruvate. This process starts by the addition of two phosphate groups to the glucose molecule at the expense of two ATP molecules and in turn generates two molecules of pyruvate and four molecules of ATP. Hence glycolysis in total provides a net of two ATP molecules and two molecules of the reduced form of the electron donor nicotinamide adenine dinucleotide (NADH). The pyruvate molecules either enter the mitochondrial TCA cycle or are converted to lactate in the presence of the enzyme lactate dehydrogenase. Both pathways generate NAD^+ that is continuously required to maintain the process of glycolysis (**Figure 2**). During anaerobic glycolysis, mitochondria are non-functional with regards to oxidative phosphorylation due to the lack of oxygen as terminal electron acceptor. Under these conditions, pyruvate is converted to lactate with a net production of two ATP and 2 NAD^+ molecules (**Figure 2**) [7]. In contrast, under conditions of adequate oxygen supply, pyruvate is entirely metabolized in the mitochondria.

In the mitochondrial matrix, pyruvate is decarboxylated by the pyruvate dehydrogenase complex yielding one molecule of CO_2, NADH and acetyl-coenzymeA (acetyl-CoA). Acetyl-CoA then enters the TCA cycle to generate one molecule of ATP, one molecule of the reduced form of the electron carrier flavin adenine dinucleotide ($FADH_2$) and three molecules of NADH per acetyl-CoA. The NADH and $FADH_2$ molecules act as electron carriers by transferring electrons derived from glycolysis and TCA cycle into OXPHOS to provide maximal ATP production.

OXPHOS involves series of reduction/oxidation (redox) reactions that ultimately leads to the production of ATP through phosphorylation of ADP. OXPHOS is comprised of the electron transport chain (ETC; complexes I to IV) and the ATP synthase (complex V). The ETC consists

of four different large multi-protein complexes embedded in the inner mitochondrial membrane: Complex I (NADH: Ubiquinone oxidoreductase), complex II (succinate ubiquinone oxidoreductase), complex III (cytochrome bc1 complex) and complex IV (cytochrome c oxidase). During each ETC cycle, these complexes accept electrons from 10 NADH and 2 $FADH_2$ generated during glycolysis, mitochondrial conversion of pyruvate to acetyl-coA and TCA cycle. Complex I accepts electrons from NADH while complex II accepts electrons from $FADH_2$. These high-energy electrons then pass through series of redox centres including FMN, iron-sulphur centres (Fe-S) within the complexes and finally are used to reduce the mobile electron carrier ubiquinone by a 2 electron conversion to ubiquinol. Complex III then accepts electrons from reduced ubiquinone (ubiquinol) and reduces another electron carrier, cytochrome c, which transports the electrons to complex IV. Complex IV ultimately transfers the electrons to the final electron acceptor oxygen to produce water (**Figure 3**). The energy released during this electron transport is used to pump protons across the inner mitochondrial membrane from the matrix into the inter-membrane space by complexes I, III and IV. This creates an increased pH in the inter-membrane space and a highly negative membrane potential, $\Delta\Psi m$ ($>-240mV$) across the inner mitochondrial membrane. This electrochemical proton gradient is used by the ATP synthase (complex V) to drive mitochondrial ATP production by phosphorylation of ADP to ATP when protons are allowed to re-enter the matrix [8]. For each molecule of glucose, a total of 32 molecules of ATP are produced by this mechanism, 2 additional ATP are derived from glycolysis and 2 ATP originate directly from the TCA cycle. This is a total yield of 36 ATP produced via aerobic respiration. Therefore, functional mitochondria increase the efficiency of the energy production by 34 ATP or 17-fold in comparison to glycolysis alone.

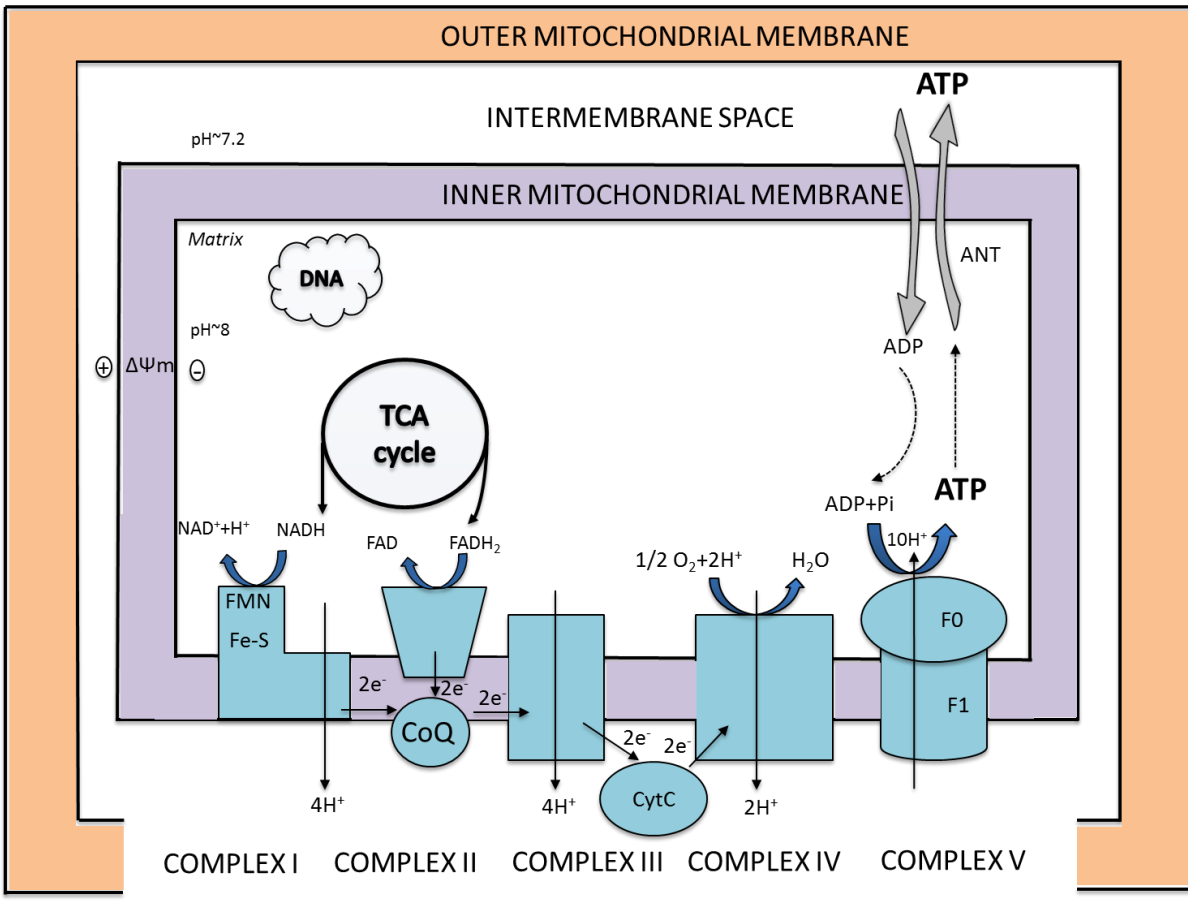

Figure 3: Mitochondrial OXPHOS.

Mitochondrial OXPHOS consists of the electron transport chain (ETC; complexes I-IV) and the F0-F1 ATPase (complex V). OXPHOS is located on the matrix-side of the inner mitochondrial membrane. The electron carriers $NADH_2$, $FADH_2$ derived from the TCA donate electrons to complexes I and II respectively thus activating the ETC which leads to a proton gradient across the inner mitochondrial membrane and the generation of ATP via complex V. The generated ATP is then translocated to cytosol with the help of ANT. ANT: Adenine Nucleotide Transporter; ATP: Adenosine triphosphate; ADP: Adenosine diphosphate; pi: inorganic phosphate; NADH: Nicotinamide Adenine Dinucleotide; FADH: Flavin Adenine Dinucleotide; FMN: Flavin Mono Nucleotide; CoQ: Coenzyme ubiquinone; Cytc: Cytochrome C.

It is now thought that the complexes I, III and IV within the inner mitochondrial membrane occur as a supercomplex known as the respirasome, which is in stark contrast to the classically depicted model of complexes floating individually in the inner membrane [9]. A 3D reconstruction of this supercomplex suggests that the ubiquinone and cytochrome c binding

sites in this supercomplex are facing each other. This structural organization of the supercomplex is thought to promote the higher efficiency of electron transfer and also increase the stability of the complexes. It has been reported that the supercomplex, containing complexes I, III and IV, is more stable and displays higher activity compared to a supercomplex without complex IV [10]. Although the overall structure of the respirasome has yet to be elucidated in detail, the identification of novel components of this complex, such as the novel mitochondrial complex I (CI) assembly factor, C17orf89 [11], has already provided new insights into the role of mitochondria under physiological as well as pathological conditions. [11]. The suppression of C17orf89 markedly reduced CI activity and lack of which has been associated in an unresolved cases of isolated CI deficiency [11].

1.1.2 Mitochondria and Reactive Oxygen Species

1.1.2.1 Reactive Oxygen Species (ROS)

Besides their role in producing cellular energy, mitochondria are also one of the main sources of reactive oxygen species (ROS). ROS encompasses oxygen free radicals such as superoxide anion ($O_2^{\cdot-}$), hydroxyl anion ($OH^{\cdot}$) and non-radical oxidants such as hydrogen peroxide (H_2O_2) and singlet oxygen ($^1O_2$) [12]. ROS are known to have both beneficial and detrimental effects on cellular function depending on their concentration [13]. At low concentration, ROS can regulate cellular functions through redox-dependent signalling and redox-dependent transcription factors [14]. However, at high concentrations ROS can damage cellular processes as a consequence of their detrimental effects on biomolecules such as protein, lipids and DNA. Therefore, a balance between ROS production and removal is essential for normal cellular functions. Any imbalance in production and removal of ROS results in oxidative stress and is likely to result in pathological conditions. Mitochondria are a known source of ROS production

and at the same time, these organelles themselves are highly susceptible to the effect of oxidative stress imposed by ROS [15].

1.1.2.2 Mitochondria as a Major Source of Intracellular ROS

The majority of ROS are generated locally within the mitochondrial ETC [13,15]. Partial reduction of molecular oxygen either by electrons that leak predominantly from complexes I and III of the ETC during cellular respiration or by enzymatic reduction (xanthine/xanthine oxidase, uncoupled nitric oxide synthase, cytochrome p450 isoform and NADPH-dependent oxidase) lead to the formation of superoxide anions ($O_2^{\cdot -}$) [15,16]. Recent studies have demonstrated that besides complexes I and III complex II also contributes to ROS production [17]. It is estimated that approximately 2-4 % of the oxygen consumed during OXPHOS is converted to ROS (10^7 ROS molecules/mitochondrion/day) [18]. ROS the main source of oxidative stress and are invariably linked to many pathological conditions such as neurodegeneration and aging [19].

Since mitochondria are major sources of ROS (80-90 % of cellular ROS) cells have developed powerful antioxidative strategies, which protect against ROS-induced macromolecular damage [20]. These detoxification systems predominantly involve antioxidant defence systems containing non-enzymatic molecules such as GSH (glutathione) and thioredoxins (Trx), alpha-tocopherol, as well as enzymatic systems such as superoxide dismutases (SODs), catalase (cat), coenzyme Q (CoQ), and cytochrome c (cyt C) [15,21]. The GSH system consists of the glutathione reductase (GSR) and glutathione peroxidase 1 (GPx1) while the Trx system includes Trx reductase 2 (TrxR2), Trx2 and peroxiredoxin 3 (Prx3). These antioxidative systems respond to the cellular stressors by interacting with the pool of cellular redox couples

including NADPH/$NADP^+$, NADH/NAD^+, GSH [reduced glutathione]/GSSG [oxidised glutathione], $Trx(SH)_2$ [reduced Trx]/ Trx(SS) [oxidised Trx] [22] (**Figure 4**). For any antioxidative strategy to be successful it is important to precisely understand the source and nature of generated ROS. Superoxide generated by complex I for example is released into the mitochondrial matrix whereas superoxide generated from Complex III is released to inter-membrane space [23]. Consequently, superoxides that are released into the matrix are detoxified by MnSOD to H_2O_2 while those that are released into the inner-membrane space are dismutated to H_2O_2 by Cu/Zn SOD [23]. Subsequently, H_2O_2 is reduced to water by catalase, peroxiredoxins (Prx) and glutathione peroxidase 1 (GPx1) [23]. Peroxiredoxins reduce H_2O_2 by employing mitochondrial Trx whereas GPx1 employs mitochondrial GSH [23].

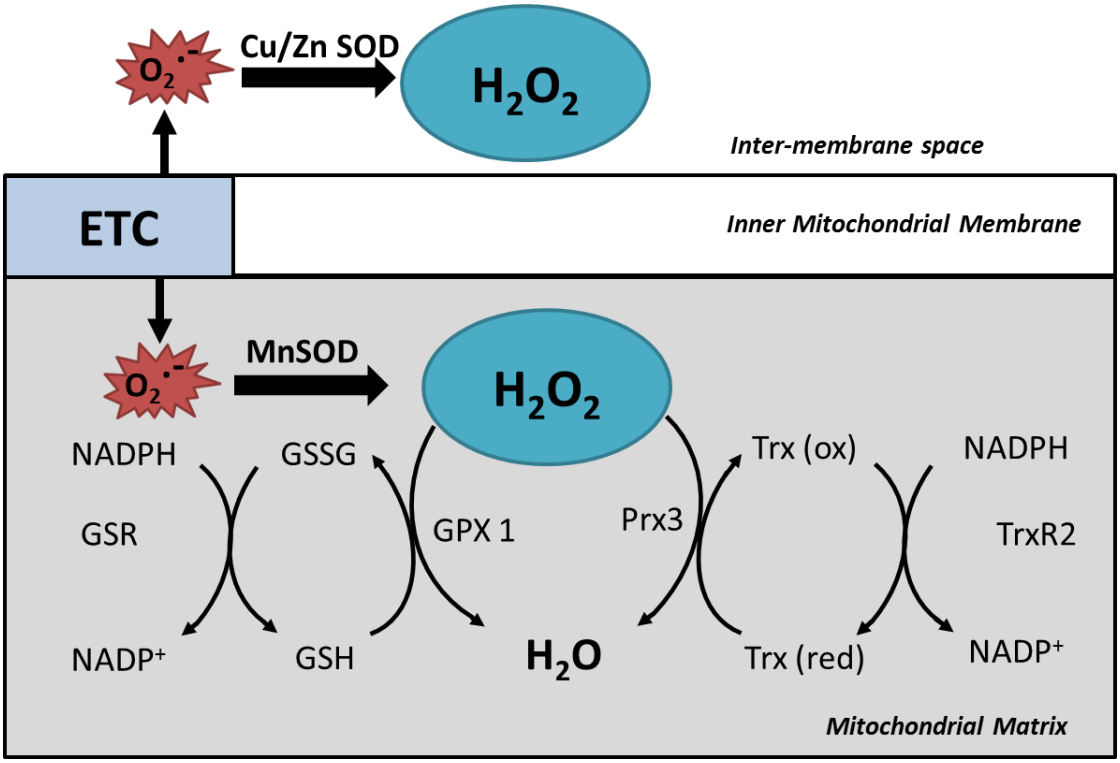

Figure 4: Mitochondrial ROS and antioxidative defence systems.
Superoxide generated by the mitochondrial ETC gets dismutated to hydrogen peroxide via Cu/Zn SOD or MnSOD. Hydrogen peroxide is further detoxified to water by either GPx, which utilizes reducing equivalents of NADPH via GSH. During this process, GSH gets oxidised to GSSG, which is then converted back to GSH by NADPH-dependent GSR. In the thioredoxin pathway, hydrogen peroxide is detoxified to water via utilizing Prx3 which is then reduced by Trx, the oxidation of which is then reduced by TrxR2. ETC: Electron transport chain; MnSOD: Manganese superoxide dismutase; Cu/ZnSOD: Copper/Zinc superoxide dismutase; GSH: Glutathione; GSSG: Glutathione disulphide; GPx: Glutathione peroxidase; Prx3: peroxiredoxin 3; Trx: Thioredoxin; TrxR2: Thioredoxin reductase 2.

Given the fact that mitochondria are essential for many cellular functions, it is not surprising that mitochondrial dysfunction leads to diverse pathologies in a multitude of human diseases. These include neurodegenerative diseases [24], cardiac dysfunction [25], kidney failure [26], liver dysfunction [27], cancer [28] and diabetes [29]. There is also significant evidence that mitochondrial dysfunction is implicated in the pathogenesis of many disorders associated with impaired vision [15]. Not only do nearly all mitochondrial diseases show some form of visual

impairment [30], mitochondrial dysfunction has also been reported for the majority of ophthalmological disorders [31].

1.1.3 Mitochondria and the Eye

1.1.3.1 Molecular Pathology of Mitochondrial Dysfunction

Mitochondrial dysfunction can occur as a result of many physiological events including inherited mitochondrial mutations, age related cumulative mitochondrial DNA (mtDNA) damage, oxidative damage, calcium dysregulation and perturbation in mitochondrial dynamics. Mitochondrial dysfunction in turn can result in defective ATP synthesis, defects in mitochondrial biogenesis, elevated levels of oxidative stress and cell death. [32-34]. However, it has to be noted that these pathological events hardly ever occur in isolation and frequently affect each other [34-36].

1.1.3.2 Susceptibility of Visual Function by Mitochondrial Dysfunction

The visual information from the eye is transmitted to the brain via the axons of retinal ganglion cells (RGC). The visual inputs from these axons are first received in the lateral geniculate nucleus and then in the superior colliculus, from where it is relayed to the higher visual processing centres in the brain. As mention earlier these cells are extremely vulnerable to mitochondrial dysfunction. It has been hypothesized that RGC, which are some of the most metabolically active neuronal cells in the body, possess a unique structural feature, which predisposes them to toxicity caused by mitochondrial dysfunction [37]. Intriguingly, RGC axons are only partially myelinated (**Figure 5**). While RGC axons in the optic nerve are myelinated, the retinal, pre-laminar parts of these axons lack myelination [37]. These non-

myelinated areas within the retina require much higher levels of energy to sustain efficient signal transmission, and as a consequence, contain significantly higher numbers of mitochondria [38]. On the other hand, mitochondrial numbers decrease significantly in the myelinated, post-laminar optic nerve, where mitochondria are predominantly located around the nodes of Ranvier [38]. This unique absence of myelination of the intraocular part of the axons, together with the significantly increased energy demand in this area could be responsible for the selective vulnerability of RGC to impaired energy supply.

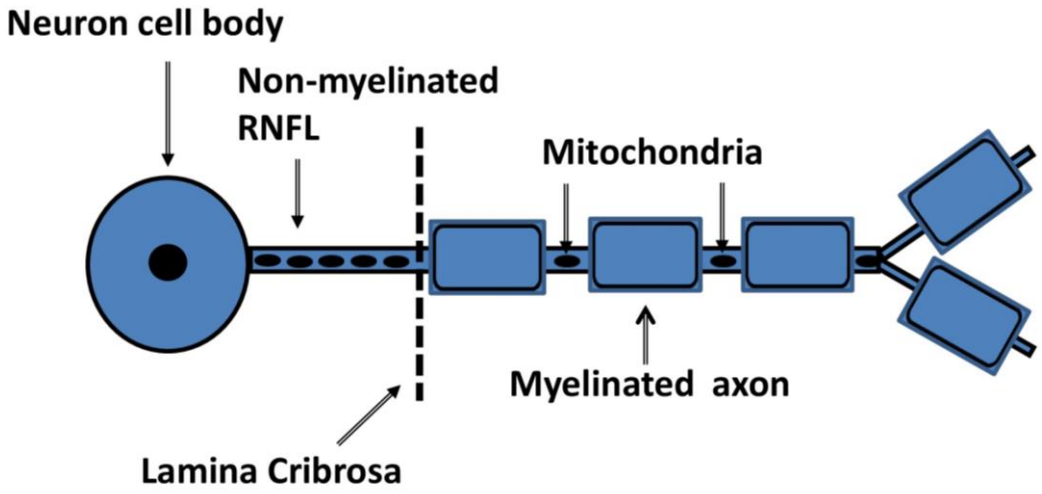

Figure 5: Graphical representation of the structure of retinal ganglion cells (RGC).
RGC are partially myelinated. Axons in the retinal nerve fibre layer (RNFL), anterior to the lamina cribrosa is unmyelinated and shows high concentrations of mitochondria, while axons posterior to the lamina cribrosa are myelinated and contain much lower numbers of mitochondria that are located around the nodes of Ranvier.

1.1.3.3 Hereditary Mitochondrial Diseases (MDs)

MDs are a heterogeneous group of disorders caused by mutations in either nuclear or mitochondrial genes that code for mitochondrial proteins. These disorders typically involve a variety of tissues from the brain to muscles [39] and the diagnosis of mitochondrial diseases is

difficult since a direct correlation between the specific mutation and the clinical phenotype is not always present [40]. Specific mutations can be responsible for symptoms specific to a particular disorder but can also produce symptoms associated with other conditions. However, most consistently associated with nearly all MDs are ophthalmological manifestations such as optic atrophy, retinal degeneration, visual field loss, ptosis, and ophthalmoplegia. Leber's hereditary optic neuropathy (LHON) and Autosomal dominant optic atrophy (ADOA) are the most common hereditary optic neuropathies and serve as a model to understand the role of mitochondrial dysfunction in the molecular pathogenesis of other optic neuropathies.

1.1.3.3.1 Leber's Hereditary Optic Neuropathy (LHON)

One of the best-described examples of visual defects directly caused by mitochondrial dysfunction is LHON, which is one of the most common mitochondrial disorders with an incidence of 1:30 000 to 1:50 000 [41]. It is maternally inherited and manifests with acute or subacute loss of vision usually in one eye, followed by loss of visual acuity in the second eye within 6-8 weeks, although simultaneous involvement of both eyes has been described in few cases [42]. Visual acuity in patients can worsen over a period of one month dropping to less than 20/200 (legal blindness). During the early course of the disease, colour vision is frequently affected [41,43]. LHON is mostly seen in young adults between 15-35 years of age with a predilection to males (80-90% pedigree), but a few cases of LHON have been reported in children and geriatrics [41]. Although at least 18 different mtDNA point mutations in complex I genes are known to be associated with LHON, over >95% of all cases occur as a result of one of the three pathogenic "primary LHON mutations" in mitochondrial DNA (11778G>A, 3460G>A or 14484T>C) [41]. Despite LHON being one of the best-studied MDs, there are

still many unanswered questions relating to its incomplete penetrance, gender bias and most importantly why the visual system is predominantly affected [44].

Almost all LHON cases are homoplasmic, meaning all mtDNA copies harbor mutations and only a few (10-15 %) cases are heteroplasmic containing both wild type and mutated mtDNA, which leads to phenotypic variability among the pedigrees [41]. In addition, genetic mitochondrial haplotypes also play key roles in determining the degree of severity in patients [45]. Higher risk of visual failure was associated with the 11778G>A or 1448T>C mutations in patients carrying haplogroup J whereas the identical mutation (11778G>A) in haplogroup K significantly reduced the risk of visual loss [45]. Vision loss is observed in around 50 % of male carriers and only 10 % of female carriers. The gender predilection seen among symptomatic 11778G>A LHON carriers may possibly be associated with a neuroprotective role of oestrogen in female carriers of LHON [46].

Although in most LHON cases vision loss is permanent, spontaneous visual recovery was reported in some patients, even several years after visual deterioration [47]. The probability for recovery of vision is different for the three LHON mutations, with the highest recovery rates (50 % or more) associated with the 14484T>C mutation. On the other hand, the 11778 G>A and 3460G>A mutations are associated with only low to intermediate recovery rates (4-20 %) [41,47,48]. The presence of visual recovery in LHON patients, even several years after the onset of the disease, strongly suggest that loss of visual acuity is not immediately associated with cell loss but rather represents cellular dysfunction that prevents the signal being transmitted from the retina to the brain [49]. Only in the later stages of the disease will cell loss make visual recovery impossible. Therefore, the time period between the cellular dysfunction

and the cell death can be regarded as a window of opportunity where in principle it could be possible to restore vision loss [49].

It is interesting to note that the pathology of LHON is predominantly restricted to the visual system, although all somatic cells harbour the same mitochondrial DNA mutation. Histochemical studies in LHON have shown selective loss of RGCs and thinning of the retinal nerve fibre layer (RNFL) in the chronic stage of the disease [42,50].

1.1.3.3.2 Autosomal Dominant Optic Atrophy (ADOA)

A second mitochondrial optic neuropathy with similar clinical symptoms compared to LHON but with a slower disease progression is ADOA. Similar to LHON, this disease is characterized by insidious bilateral loss of central vision with a marked decrease in colour perception and relative preservation of pupillary reflex and optic pallor [51]. Vision loss in ADOA commonly starts during childhood at the age of 6-10 and adolescence and equally affects both males and females [3]. As the disease progresses, visual acuities in the patients deteriorate from 20/80 to 20/120 [30]. However, unlike LHON, spontaneous visual recovery was not reported in ADOA [51]. Although ADOA and LHON differ in terms of disease onset and progression, both diseases are characterised by decreased RNFL thickness, RGC dysfunction with preferential loss of small neurons in a papillomacular bundle, axonal degeneration, swelling and demyelination in the optic nerve [52-54].

Although ADOA can result from mutations in four nuclear genes *OPA1, OPA3, OPA4 and OPA5,* the majority of ADAO cases (60 % - 70 %) are associated with mutations in *OPA1* [55,56]. *OPA1* is highly expressed in brain and retina [57], resides in the inner mitochondrial

membrane and is implicated in different functions including mitochondrial fusion, cristae structure, mitochondrial membrane maintenance and OXPHOS [55-57]. Therefore the pathological hallmarks of *OPA1* mutations are mitochondrial network fragmentation and disorganised cristae [3]. *OPA1* also sequesters cytochrome c, a pro-apoptotic factor in the mitochondria, and thus inhibits its release into the cytoplasm and consequently apoptotic cell death [58]. Dysfunctional *OPA1* in ADOA patients was also shown to negatively affect mitochondrial ATP synthesis and respiration in skeletal muscles similar to LHON [59,60]. Despite the systemic presence of *OPA1* mutations, optic atrophy is the most dominant clinical symptoms documented in ADOA. Interestingly reduced *OPA1* expression was also reported in LHON [61]. This suggests that ADOA and LHON might share their pathology by converging on to the same biochemical pathway.

1.1.3.3.3 Mitochondrial Encephalomyopathy with Lactic Acidosis and Stroke-like Episodes (MELAS)

In contrast to LHON and ADOA, some mitochondrial optic neuropathies may occur as more complex disorders with multiple pathologies as a result of mtDNA mutations. MELAS is a maternally inherited mitochondrial disease and is characterised by variable phenotypes including stroke like episodes, seizures, dementia and lactic acidosis [41]. Additional symptoms of MELAS include migraine, depression and cardiac conduction defects [41]. Consistent with a causal relationship of mitochondrial and visual function, MELAS is also associated with a loss of visual acuity [41,48]. The ophthalmological features of MELAS patients are bilateral ptosis, chronic external ophthalmoplegia, choroidal atrophy degeneration of outer segment of photoreceptors, hyperpigmentation in the macular region as a result of retinal pigment epithelium (RPE) hyperplasia, as well as RPE atrophy in the macular area, as

well as iris stroma atrophy and optic atrophy [62,63]. For MELAS, the age of onset is generally before 15 years of age [64]. Although MELAS has been linked to a number of heteroplasmic point mutations in mt-DNA coding for complex I subunits including 3380 G>A in *MT-ND1* and m.13513 G>A in *MT-ND5* [65,66], nearly 80% of MELAS cases result from an A3243G mutation in the *MTTL1* gene encoding the mitochondrial tRNA (Leu(UUR)) [64]. Since mitochondrial complex I is dysfunctional in both LHON and MELAS, it is not surprising that cases of LHON/MELAS overlap syndrome have been reported associated with the heteroplasmic m.3376G>A mutation in *MTND1* [67]. Although the pathogenesis of MELAS is still not fully understood, it was proposed that the mtRNA mutation causes decreased expression of mitochondrial respiratory chain complexes, leading to bioenergetic failure [41].

1.1.3.3.4 Myoclonic Epilepsy and Ragged Red Fibres (MERRF)

MERRF is another multiple system mitochondrial disorder with common ocular involvement. Almost all MERRF patients are affected by a mutation in mtDNA (m.8344T>C in the *MT-TK* gene) encoding tRNA Lys [48]. The age of onset is generally between 5-15 years. Comparable to the situation in MELAS, MERRF patients present with variable clinical phenotypes including myoclonus seizures, cerebellar ataxia, myopathy, dementia bilateral deafness and peripheral neuropathy. The most prominent ocular pathologies include progressive bilateral vision loss, retinal dystrophy, pigmentary retinopathy and macular pattern dystrophy [39,68]. Dysfunction of mitochondrial complex I or IV or occasionally both have been reported in MERRF [69]. The similarity of MERRF to other mitochondrial disorders is highlighted by the recent description of patients with two mutations in mitochondrial tRNA genes (m. 8356 T>C and m.3243A>G) that are responsible for the MERRF/MELAS overlap syndrome [70]. Overall the similarity of these disorders was described by a retrospective study where patients with

known mitochondrial diseases MERRF, MELAS and LHON showed a common ocular phenotype of retinal dystrophy [68].

Based on the evidence described above it appears that no matter how mitochondrial dysfunction arises, either by mtDNA or nDNA mutations, the most consistent clinical symptom is that of vision impairment.

1.1.3.4 Neurodegenerative Diseases, Mitochondria and Vision

Neurodegenerative diseases are a heterogeneous group of disorders characterised by loss of selected neuronal systems, with aging as a major risk factor. Since neurons are heavily dependent on a constant energy supply, it is increasingly recognized that mitochondrial dysfunction acquired during aging as a result of accumulated mtDNA mutations likely contributes to subsequent neurodegenerative pathologies such as Parkinson's disease, Alzheimer's disease [71].

1.1.3.4.1 Parkinson's disease (PD)

A multisystem disorder associated with mitochondrial dysfunction with a wide variety of motor and non-motor symptoms is PD. This disease is the second most common neurodegenerative disease that affected 4.3 million people in 2005 and is projected to increase to 9 million by 2030 [72]. This dramatic increase in the incidence of PD could likely be a cause of age-related mitochondrial dysfunction in an aging population [73]. PD is associated with resting tremor, bradykinesia and rigidity. About 90-95 % cases of PD are sporadic while for only 5-10 % a genetic origin has been identified. PD is caused by loss of dopaminergic neurons responsible

for motor, cognitive and limbic function in the substantia niagra and is characterized by the presence of Lewy bodies (cytoplasmic inclusions containing α-synuclein protein) [71]. Oxidative stress as a result of mitochondrial dysfunction has been implicated in the pathogenesis of PD [74]. Initially, mitochondrial complex I defects were demonstrated in the substantia niagra of PD patients [75]. Later, reduced activities of complexes IV, V have also been reported in platelets and lymphocytes of patients suggesting that mitochondrial dysfunction is not only restricted to the substantial niagra [71] but comparable to classic MD's detectable in all tissues. Consistent with these observations, complex I inhibitors such as rotenone and 1-methyl-4-phenyl-1,2,3,6-tetrahydropyridine (MPTP) have been used to generate pre-clinical models of PD [75]. Chronic exposure of rats to rotenone produces a phenotype strikingly similar to PD, such as loss of dopaminergic neurons, the appearance of Lewy bodies, microglial activation, and the presence of biomarkers of oxidative damage [76]. Furthermore, mutations in genes such as *α-synuclein, parkin, PINK1,* and *DJ-1* have been implicated in the hereditary forms of PD. Defects in these genes lead to oxidative stress, mitochondrial dysfunction and ultimately cell death [77]. In line with the mitochondrial dysfunction in PD, it is therefore not surprising that this disease also affects the visual system [54,78]. Decrease in visual acuity, contrast sensitivity, impaired colour vision, nystagmus are some of the features seen in PD patients [78]. Furthermore, a significant reduction in RNFL thickness has also been documented in PD patients compared to their aged-matched control [79].

1.1.3.4.2 Alzheimer's disease (AD)

The most common neurodegenerative disease and the most common cause of dementia affecting more than 26.6 million patients globally is AD [80]. AD is characterized by a slow

progressive loss of cognitive function, and a gradual decline in memory and intellectual function [81]. The hallmark of AD is the extracellular deposition of the amyloid beta (Aβ) protein and the appearance of intracellular neurofibrillary tangles composed of hyperphosphorylated tau proteins [81]. Many studies have highlighted mitochondrial defects in the disease progression of AD [81]. Evidence of mitochondrial Aβ deposition within the visual cortex of AD patients and in the brain of AD animal models supports the notion of mitochondrial involvement in AD [81]. It has been suggested that Aβ enters the mitochondria via a translocase in the outer membrane and subsequently accumulates in mitochondrial cristae [82]. Thus, accumulated Aβ then causes an imbalance of mitochondrial fusion and fission, which results in mitochondrial fragmentation [83]. Mitochondrial dysfunction is proposed to occur as an early event during development and progression of sporadic AD and includes abnormalities in mtDNA, OXPHOS enzymes, mitochondrial gene expression, mitochondrial dynamics and mitochondrial trafficking [71,81].

Consistent with a connection between mitochondrial and visual function, changes to the visual system such as reduced visual acuity, contrast sensitivity and colour vision defects have also been reported in the early stages of AD patients [84] as well as in animal models of AD [85]. Furthermore, AD patients show pathological changes to the retina and optic nerve and in fact these changes can be regarded as the surrogate markers of the pathological changes in the central nervous system of AD patients [86]. These changes include decreased RGC numbers, reduced macular pigment, optic disc cupping, retinal microvascular abnormalities and a significant reduction in macular RNFL thickness [84,87].

1.1.3.4.3 Multiple Sclerosis (MS)

MS is an inflammatory neurodegenerative disease of a central nervous system characterized by demyelination and progressive axonal degeneration [88]. Although MS is typically depicted as a single disease entity, it has to be noted that it encompasses several distinct clinical phenotypes such as relapsing-remitting MS (RRMS), secondary progressive MS (SPMS), relapsing progressive MS (RPMS) and primary progressive MS (PPMS). Intriguingly, these different forms of the disease are reportedly associated with different levels of mitochondrial impairment, with PPMS reported to have the highest mitochondrial dysfunction. Although it is still unclear what events contribute to the pathogenesis of the disease, accumulating evidence suggest that calcium dysregulation, mitochondrial electron transport chain (ETC) defects, excess free radical production and mitochondrial permeability transition pore opening are responsible for predisposing to MS [88]. MS is often associated with acute onset of vision loss followed by a reduction in contrast sensitivity, loss of colour vision usually in one eye and is associated with pain during eye movements [3]. The loss in visual acuity is not permanent and generally recovers within 2-4 weeks [3]. In 15-20 % of patients, optic neuritis is the first clinical manifestation of MS and 50 % of MS patients develop optic neuritis as the disease progresses [3]. Recently, significant thinning of macular RNFL, reduction of retinal thickness and RGC loss have been reported in MS patients and reduced RNFL thickness, RGC loss, and brain atrophy correlate well with the staging of MS [3,89]. These results suggest that similar to the situation in AD, retinal neurodegeneration can be considered as a surrogate marker of brain atrophy in MS. Interestingly, some MS patients also carry LHON mutations [90]. The resulting LHON-MS overlap syndrome (also known as Harding disease) differs from LHON by its predominance to females; longer time to affect the fellow eye (nearly two years); mostly with more than two visual events [91]. Although Harding disease differs from MS by a higher visual

involvement, lack of painful eye movement; and rare visual recovery [91], both diseases share dysfunctional mitochondrial ETC and defective ATP synthesis [41,88]. However, in contrast to LHON, mitochondrial defects in MS are usually thought to be secondary to the process of acute inflammation [92].

Mitochondrial dysfunction has been universally implicated in the neurodegenerative diseases described above and importantly their visual phenotypes closely resemble those associated with hereditary mitochondrial diseases.

1.1.3.5 Major Ocular Diseases and Mitochondria

Based on the visual impairment in diseases that are characterized by mitochondrial dysfunction and the hypothesis that mitochondrial dysfunction is responsible for vision loss, it is not surprising that most ocular diseases also show mitochondrial dysfunction.

1.1.3.5.1 Diabetic Retinopathy (DR)

DR is one of the major causes of blindness worldwide [93] and is characterised by the abnormal growth of blood vessels in order to supply oxygenated blood to a hypoxic retina. DR patients experience sudden painless loss of visual acuity in one or both eyes that eventually leads to complete blindness [94]. Contrast sensitivity and colour vision can be significantly impaired in diabetic patients before the disease progresses to DR, which is why these ocular features are predictive of DR [95]. Neuronal degeneration along with vascular abnormalities has been reported in the pathogenesis of diabetic retinopathy [96]. In fact, neuronal changes in the retina precede the vascular changes in DR [97]. This statement is supported by a recent cross-

sectional study that compared retinal layers among patients without diabetes, patients with type 2 diabetes without diabetic retinopathy and patients with diabetes but with mild diabetic retinopathy [97]. In this study, the mean ganglion cell layer and retinal nerve fibre layer were thinner in diabetes without retinopathy when compared to healthy individuals [97]. There was a significant reduction in average retinal thickness in mild diabetic retinopathy compared to control and diabetes with no diabetic retinopathy. Moreover, in DR the reduction of RNFL thickness due to a loss of RGC [98] is more prominent in the superior quadrant, which worsens with the severity of disease and with progressing age [99,100]. Since this loss of RGC is painless, it is likely due to an apoptotic pathway as evidenced by increased expression and activation of apoptosis-related proteins [101,102].

Central to the pathology of DR, hyperglycaemia-induced mitochondrial ROS production activates four synergistic biochemical pathways that are likely causative for the loss of RGC in DR [103,104]. These pathways are initiated by increased mitochondrial ROS production, which inhibits glyceraldehyde 3-phoshate dehydrogenase (GAPDH). This inhibition of glycolysis results in increased accumulation of glycolytic metabolites and diverts the glycolysis pathway to activate polyol, hexokinase, PKC and advanced glycation end products (AGE) pathways (**Figure 6**). Activation of the polyol pathway causes osmotic damage of retinal cells through the accumulation of sorbitol. More importantly, it also reduces cellular NADPH levels, which in turn directly impairs the regeneration of the endogenous antioxidant GSH, a mechanism that further increases oxidative stress levels [103,104].

In addition, simultaneous activation of the hexokinase and PKC pathways activate transcription factors responsible for vascular complications including blood flow abnormalities, retinal capillary occlusion, stimulation of neovascularization, by upregulating vascular endothelial

growth factor (VEGF), a key element of retinal neovascularization. At the same time, PKC activation indirectly leads to the formation of AGEs from the non-enzymatic reaction of intracellular dicarbonyls with intra and extracellular amino groups of proteins. AGEs accumulate in the retinal microvasculature and activate the RAGE receptor, a process that further increases ROS levels and activates pro-inflammatory transcriptional factors such as NF-κB as well as apoptosis of the retinal cell.

Based on the activation of these pathways, it is not surprising that elevated levels of mitochondrial superoxide have also been detected in retinal cells of diabetic animal models [105]. Consistent with a central role of mitochondrial ROS in the activation of those pathways, inhibition of mitochondrial superoxide production prevented hyperglycaemia-induced activation of PKC, AGEs accumulation, sorbitol formation and NFkB activation in bovine aortic endothelial cells [106]. Furthermore, in support of a causative role of mitochondrial ROS in DR, overexpression of mitochondrial manganese superoxide dismutase (MnSOD) SOD2 protected murine and bovine retina against diabetes-induced oxidative stress and cell death [107,108]. These results strongly implicate mitochondrial dysfunction in the pathogenesis of DR.

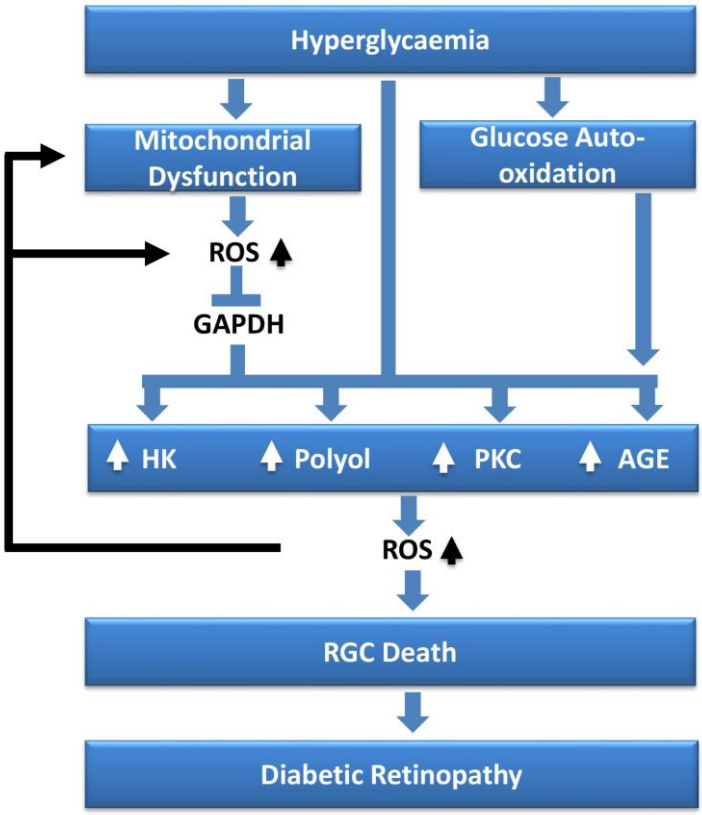

Figure 6: Mitochondrial pathology of diabetic retinopathy.
Hyperglycaemia-induced mitochondrial dysfunction and subsequent generation of excess ROS inhibits glyceraldehyde-3-phosphate dehydrogenase (GAPDH), which diverts the glycolytic pathway to the hexokinase (HK), polyol, protein kinase C (PKC), and advanced glycosylation end products (AGE) pathways. These pathways are also activated by hyperglycaemia and hyperglycaemia-induced autoxidation of glucose can activate the AGE pathway. These processes further increase ROS production, retinal ganglion cell (RGC) death and finally lead to loss of visual acuity.

1.1.3.5.2 Glaucoma

Glaucoma is a second leading cause of blindness worldwide [109]. The most common form of glaucoma is primary open-angle glaucoma (POAG), which affects nearly 70 million people worldwide [110]. POAG comprises normal tension glaucoma (NTG), in which intra-ocular pressure (IOP) is normal and high-tension glaucoma (HTG), in which increased IOP is a main

pathological feature [111]. Similar to LHON, glaucoma is associated with central but also peripheral vision loss, decreased contrast sensitivity and colour vision, which eventually progresses to blindness [112]. The major known risk factors for glaucoma include elevated intraocular pressure (IOP), age, and family history [113]. Elevated IOP is caused by reduced outflow of aqueous humor through the trabecular meshwork (TM), a connective tissue lining the iridocorneal angle of the anterior chamber of the eye [114]. The histological hallmarks of glaucoma include progressive loss of RGC and RNFL thinning [115]. Similar to LHON and ADOA the defect of RNFL thinning in glaucoma is more pronounced in the inferior and infero-temporal quadrants and is followed by the superior quadrants [115]. Moreover, decreased expression of OPA1 in patients with POAG indicates that the molecular pathology of these diseases could be very similar to LHON and ADOA [116,117]. Indeed, there is evidence that mitochondrial dysfunction-mediated oxidative stress may play a significant role in glaucoma by inducing trabecular meshwork (TM) damage and RGC loss by direct or indirect mechanisms (**Figure 7**) [118]. The damage to TM cells prevents the regulated drainage of aqueous humor from the eye, which results in elevated IOP and obstructed blood flow to the optic nerve head (ONH) resulting in ischaemic conditions. This ischemia further compromises mitochondrial energy production in the RGC [118,119]. This combined pathology renders RGC more vulnerable to light and certain astrocyte- and microglia-derived chemicals such as glutamate, prostaglandins and nitric oxide [119]. Moreover, in a mouse model of glaucoma oxidative stress was directly correlated to the development of elevated IOP [120]. It can be hypothesized that the origin of mitochondrial oxidative stress in TM cells in POAG patients is likely associated with a defect in mitochondrial oxidative phosphorylation [121]. This idea is supported by the higher than expected frequency of *OPA1* polymorphisms in POAG and especially in NTG patients [116,122]. Given the consequences of OPA1 deficiency on mitochondrial function in ADOA, it can be hypothesized that in POAG patients a defect in

mitochondrial respiration might also be present. Intriguingly, the presence of complex I dysfunction was recently described in lymphocytes obtained from POAG patients that resulted in decreased rates of complex I-driven ATP synthesis, decreased respiration and reduced cell growth, which suggest a mitochondrial defect in all cells of POAG patients [123]. The close similarities of POAG with hereditary mitochondrial diseases in terms of molecular pathology, visual defects, optic disc pallor, peripapillary atrophy and elevated IOP provide an explanation why POAG, LHON and ADOA can be easily misdiagnosed [51,124].

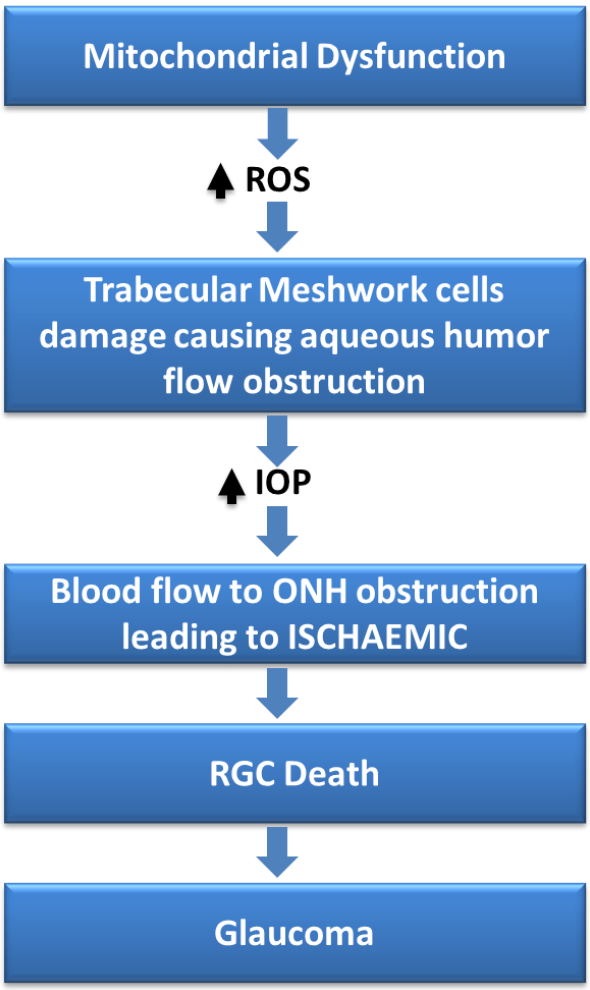

Figure 7: Mitochondrial pathology of glaucoma.

Mitochondrial dysfunction-mediated excess production of reactive oxygen species (ROS) damages trabecular meshwork cells causing aqueous humor flow obstruction as a consequence increases intraocular pressure (IOP). Subsequently, elevated IOP obstructs blood flow to optic nerve head (ONH) leading to ischaemic condition and ultimately to RGC death and development of glaucoma.

1.1.3.5.3 Age Related Macular Degeneration (AMD)

AMD is a neurodegenerative disease that affects individuals over 65 years of age and is also among the leading causes of blindness worldwide [125]. AMD is characterized by a loss of central vision as a consequence of retinal pigment epithelium (RPE) atrophy/hypertrophy and choroidal neovascularization. These predisposing factors become more pronounced as the

disease progresses and ultimately lead to complete loss of visual acuity. The underlying biochemical pathways leading to AMD are still not clear. However, like in DR, many experimental studies have pointed towards oxidative stress as a key factor (**Figure 8**) [126].

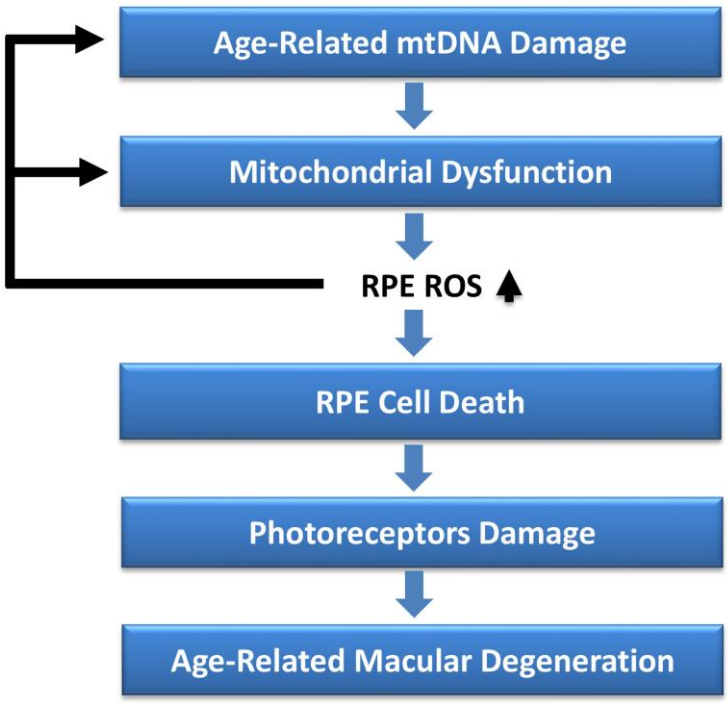

Figure 8: Mitochondrial pathology of age-related macular degeneration.
Mitochondrial DNA damage, accumulated as a result of normal aging, leads to mitochondrial dysfunction, which in turn generates excess ROS. Elevated levels of ROS impair retinal pigment epithelium (RPE) function, a process that indirectly damages photoreceptors and that leads to the development of age-related macular degeneration.

RPE cells continuously engulf, recycle and nourish the photoreceptor outer layer in order to maintain healthy photoreceptors. Therefore, the RPE has a high metabolic rate and as a result mitochondrial density in this region is particularly high [125]. Although a significant decrease in mitochondrial density in the RPE with increasing age was documented in the elderly, in AMD patients these age-related changes are even more pronounced [127]. Furthermore, with increasing age, decreased mitochondrial respiration, increased oxidative damage of mtDNA

and a decreased capacity to repair oxidative damage in the RPE is linked to AMD [128]. In support of a central role of mitochondrial ROS in AMD, knockdown of mitochondrial superoxide dismutase (MnSOD) in the murine RPE recapitulates the AMD phenotype such as RPE dysfunction, damage to photoreceptors and choroidal damage [129]. Comparable to the situation in LHON and ADOA, spectral-domain optical coherence tomography (SD-OCT) examination of AMD patients showed a decrease in RGC numbers despite no significant difference in RNFL thickness compared to healthy individuals [130]. RPE atrophy and pigmentary retinopathy, hallmarks of AMD, are reported for the majority cases of mitochondrial encephalopathies such as MELAS and MERRF that have mutations in mtDNA (3243A>G and 8344T>C) suggesting that mtDNA defect could also be associated with RPE abnormalities in AMD [63]. Supporting evidence that mtDNA mutations could be the underlying cause of AMD comes from a recent study that compared the localization of mtDNA damage in the diseased retina among human retinal samples obtained from different stages of AMD [131]. This study showed that mtDNA damage was specific to the RPE region in the retina. MtDNA of both the macular and peripheral RPE were equally damaged and the mutations localized to regions of the mtDNA that influence overall mitochondrial function. These observations led the authors to speculate that mitochondria of the RPE could be a therapeutic target to treat AMD.

Given that the major ocular diseases not only share very similar visual phenotypes with hereditary mitochondrial diseases and the growing evidence that mitochondrial dysfunction predisposes to ocular disease, most ocular diseases could, in fact, be regarded as mitochondrial diseases.

1.1.4 Drug-induced Mitochondrial Optic Neuropathy

The tight connection between vision and mitochondrial function is also illustrated at the pharmacological level. A number of widely used drugs are reported to induce mitochondrial dysfunction (**Table 1**). As a consequence, many drugs have been withdrawn from the market and in fact, about 80 % of drugs that received black box warnings by the FDA are known to cause mitochondrial toxicity [132]. These drugs cause mitochondrial defects through different mechanisms including impairing the function of ETC enzymes, generating ROS (particularly from complexes I and III) and depleting levels of the endogenous anti-oxidant, glutathione. These drugs represent a large range of drug classes that include antibiotics, anti-arrhythmics, anti-tuberculosis, anti-depressants, analgesics and anti-inflammatory drugs [133]. Drug-induced mitochondrial toxicity has been implicated in organ toxicity such as hepatotoxicity, cardiotoxicity and toxic optic neuropathy (TON) [134]. The clinical features of TON include insidious onset, slow progressive and painless bilateral central vision loss, normal, oedematous or hyperaemic optic disc at an early stage, which may progress to temporal optic disc pallor at the later stages [134]. Patients may also present with colour vision loss [134]. OCT examinations in patients with TON show a marked reduction in RNFL, predominantly due to loss of small-caliber axons within the papillomacular bundle [135-137], consistent with the mitochondrial optic neuropathy seen in LHON and ADOA. Thus, mitochondrial impairment is central to the pathology of drug-induced optic neuropathy and RGCs are the main target in toxic optic neuropathy cases.

At the same time, there is evidence that drug-induced mitochondrial optic neuropathies could also be the consequence of a pre-existing genetic mitochondrial dysfunction such as LHON and ADOA that are activated by drug use. Severe vision loss, defects in colour vision and

bilateral optic nerve pallor have been observed in a LHON patient after initiation of antiretroviral drugs belonging to the class of nucleoside reverse transcriptase inhibitors that have a clear mitochondrial liability [138,139]. Antituberculosis drugs, such as ethambutol and antibiotics, such as erythromycin have also been reported to activate LHON and induce vision loss in individuals with asymptomatic LHON or ADOA [140-143].

Table 1: Drugs associated with mitochondrial dysfunction and optic neuropathy

Drugs	**Effect on Mitochondria**									
	CI	**CII**	**CIII**	**CIV**	**CV**	**β- OX**	**mtDNA replication**	**ANT**	**Monograph Listed**	**Ref**
Amiodarone	X	X	X	X	X	X			X	[144-146]
Amitriptyline	X	X		X					--	[147,148]
Aspirin	X				X	X			--	[148,149]
Chloramphenicol							X		X	[150]
Chlorpromazine	X								--	[144,148,151]
Cocaine	X								--	[152]
Desipramine	X			X					--	[147,148]
Dexamethasone				X					--	[148,153]
Didanosine							X	X	X	[148,154]
Ethambutol	X			X					X	[145,150]
Fluphenazine	X								--	[148,151]
Gentamycin							X		--	[148,155]
Hexachlorophene					X				--	[148,156]
Hydrocortisone				X					--	[148,153]
Imipramine	X	X		X					--	[147,148]
Indomethacin	X				X	X			--	[148,149]
Isoniazid		X							X	[148,157]
Linezolid	X			X					X	[158]
Naproxen	X				X	X			X	[148,149]
Piroxicam	X				X	X			--	[148,149]
Prednisolone					X				--	[148,153]
Streptomycin							X		--	[148,150,155]
Sulindac	X				X	X			--	[149]
Tamoxifen	X		X						X	[144,159]
Thioridazine	X								X	[148,160]
Tobramycin							X		--	[148,155]
Triamcilone					X				--	[148,153]
*Clioquinol									X	[161]

*CQ-Zn chelate has shown to cause mitochondrial dysfunction by decreasing mitochondrial membrane potential.

1.2 Clioquinol and Vision

1.2.1 Clioquinol in Neurotoxicity

Clioquinol (CQ), a quinoline derivative, has been widely used (1950 to 1969) as a topical disinfectant and anti-microbial agent that was mainly used against diarrhoea. However, in 1970 its oral form was withdrawn from the market after it was linked to about 10,000 Japanese cases of subacute myelo-optic neuropathy (SMON), a neurodegenerative disease characterised by sensory and motor disturbances in the lower limbs and visual impairment [162]. The autopsy of SMON patients revealed symmetrical and continuous degeneration of nerve fibres of a distal dominant portion of the long tracts in the spinal cord and demyelination of the retrobulbular optic nerves [162]. Severe lesions were detected in the distal end of the optic tract around the lateral geniculate body. The proximal optic nerve was less severely affected and the inner ganglion cells of the retina were the least severely affected [162] (**Figure 9**). Other associated clinical symptoms observed in SMON patients include abdominal pain, diarrhoea usually occurring before the onset of neurological symptoms, [162]. The majority of symptoms were reversible but permanent disability was reported in approximately 10 % of the SMON patients [163]. Intriguingly, there were only a few cases (220) of SMON outside Japan although this drug was used in different parts of the world at the same time and this geographical restriction has never been explained [164,165]. Soon after its ban, health records of SMON patients were examined. The health records survey conducted between 1964 and 1969 showed that of 47 SMON cases, 81 % of the patients were receiving CQ at a dose of 300 mg to 3.5 g/day before the onset of symptoms [166]. Similarly, in a review of health records of 263 patients that used CQ for their digestive ailments compared to 706 patients that did not use CQ, neurological complaints were exclusively recorded in patients taking CQ [167]. A subsequent investigation revealed that among patients on CQ treatment neurological symptoms were more prevalent if

CQ treatment persisted for more than 14 days (35 % of 110 patients), while in 153 patients receiving CQ for less than 13 days neurological symptoms were recorded in only 2.6 % [167].

To confirm the association of CQ in SMON, toxicological studies were carried out in humans. In 1973, healthy volunteers were administered oral CQ at doses of up to 1.5 g for 7 days followed by 750 mg for an additional 7 days [168], but no adverse effects were reported. Likewise, no neurological adverse effects were reported when up to 1.5 g CQ was given to prevent diarrhoea or cholera [169,170]. At present, this suggests that CQ-neurotoxicity requires continuous exposure for more than 14 days. Due to the overlapping phenotype (lesion in the posterior and lateral columns of the spinal cord) of early SMON and vitamin B12 deficiency CQ associated neurotoxicity has also been linked to vitamin B12 deficiency, [171]. Moreover, reduction in serum and cerebrospinal fluid levels of vitamin B12 has been demonstrated in mice injected with CQ for 20 days [172]. However, in SMON patients normal vitamin B12 levels in serum or CSF were observed [173]. In fact, SMON patients were largely unresponsive to vitamin B12 supplementation and neurological symptoms continue to exist in these patients through 32 years of follow-up [163,174]. The connection between CQ and SMON was confirmed after 20 months of intensive investigations that were conducted by the Japanese SMON research group. This was largely based on the evidence that the majority of SMON patients had been taking CQ before the onset of the symptoms and that after the drug was withdrawn from the market the incidence of SMON reduced [175]. Furthermore, the common pathological features of SMON, including abdominal symptoms preceding to neurotoxicity have been successfully recapitulated in animals (dogs, cats and monkeys) after CQ administration [175-177].

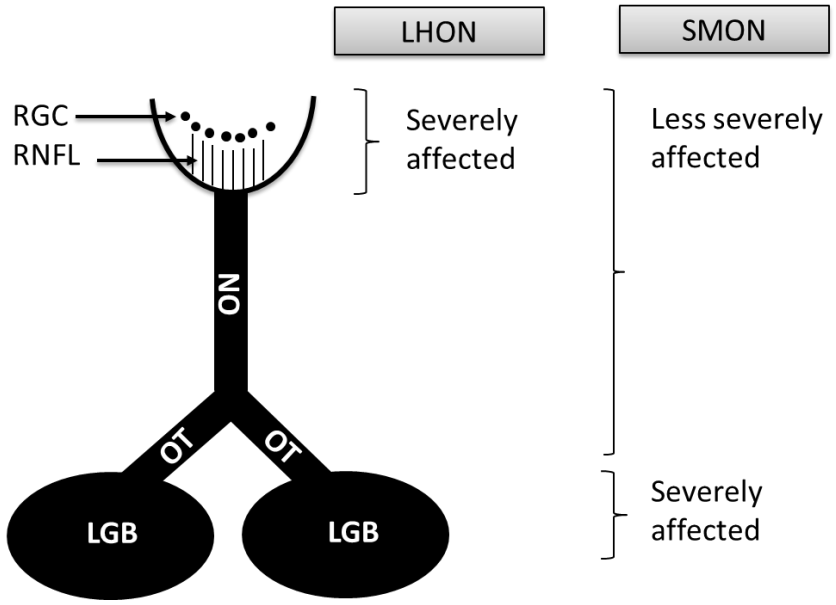

Figure 9: Comparison on severity of different damage sites between SMON and LHON.
RGC and RNFL are mainly affected in LHON whereas they are the least affected in SMON. Severe lesions were detected in the distal end of the optic tract around the lateral geniculate body in SMON. RGC: Retinal Ganglion Cells; RNFL: Retinal Nerve Fibre Layer; ON: Optic Nerve; OT: Optic Tract; LGB: Lateral Geniculate Body.

CQ is a lipophilic metal chelator of zinc (Zn), copper (Cu) and iron (Fe) and exerts its anti-parasitic effect by acting as an ionophore [178]. It has been suggested that the chelating and ionophore activities of CQ contribute to its neurotoxicity *in-vitro* [161]. This is supported by green hairy tongue and green urine, markers of iron chelates of CQ, that have been observed in SMON patients [177]. In cultured neural cells from chicken embryos, CQ-ferric chelate increased iron uptake into cells leading to increased lipid peroxidation and subsequent neuronal cell degeneration [179]. Similarly, CQ-zinc chelate (25:50 µM) has been shown to reduce mitochondrial membrane potential in human melanoma cells, which subsequently led to cellular toxicity [161]. This pro-oxidant effect of CQ was also observed in murine cortical cultures where exposure to CQ (1-3 µM) for 24 h caused 40 % neuronal death and enhanced lipid peroxidation [180]. Co-administration of metal ions such as Fe and Cu with CQ further

enhanced its neurotoxicity and caused 100 % neuronal death [180]. Consistent with these findings, a reduction in cellular viability was observed in human prostate cancer cells only when CQ was combined with zinc [181]. CQ (at and above 10 µM) induced neurotoxicity through an inhibition of superoxide dismutase 1 (SOD1) in human neuroblastoma cells [182]. CQ is believed to inhibit SOD1 by chelating Cu and Zn ions, which are essential for the activity of SOD1. CQ is also reported to inhibit the 20S proteasome by Cu-dependent and independent mechanisms and as a consequence leads to increased intracellular levels of misfolded proteins, which subsequently result in cell death [183]. A metal-independent mechanism of CQ neurotoxicity directly at the level of DNA was also suggested. CQ decreased cellular proliferation of neuroblastoma cells at concentrations of 10 µM or more [184]. Furthermore, CQ (50 µM) induced neurotoxicity by the induction of DNA double-strand breaks and the subsequent activation of the ATM/p53 signalling cascade [184]. In neuronal PC12 cells, CQ dose-dependently inhibited nerve growth factor (NGF)-induced Trk autophosphorylation and neurite outgrowth, which is essential for neuronal growth and differentiation [185]. Consistent with this inhibition, CQ also inhibited NGF-induced mitogen-activated protein kinase (MAPK) phosphorylation, which is downstream of NGF-induced signalling [185]. CQ treatment of PC12 cells also reduced histone acetylation, a process essential for transcriptional activation of genes that are responsible for cell proliferation [186]. Consistent with this activity, HDAC inhibitor treatment upregulated histone acetylation, decreased CQ-induced neurite retraction, neuronal death and finally restored Trk autophosphorylation [186].

Despite the numerous mechanisms that have been put forward to explain CQ-induced neurotoxicity, none of these have explained the restriction of CQ-induced neurotoxicity to the Japanese population. Surprisingly, despite its reported neurotoxicity, CQ is currently investigated as a disease modifying treatment for some neurodegenerative diseases such as

Alzheimer's disease (AD) and Huntington's disease (HD) with some promising preclinical and clinical outcomes.[187-189].

1.2.2 Clioquinol in Neuroprotection

1.2.2.1 Clioquinol in Alzheimer's disease (AD)

AD is a neurodegenerative disease characterised by a progressive decline in cognitive function and represents a major challenge to healthcare worldwide [190]. The major pathological hallmarks of AD include extracellular deposition of highly insoluble and proteolysis-resistant extracellular amyloid plaque also known as senile plaque, neurofibrillary tangles and cortical neuronal loss [191]. Metals such as Zn, Cu, Fe have been implicated in neocortical amyloid formation and deposition in AD's brain as a result of metal-Aβ interactions [192]. A number of pre-clinical and clinical studies have proposed possible mechanisms where the interaction of metal ions with Aβ contributes to the neurotoxicity in AD. In the presence of Cu, Aβ is shown to inhibit mitochondrial complex IV in cultured human cells [193]. These metal ions are also responsible for generating reactive oxygen species that contribute to the oxidative stress observed in AD brains [192,194]. When Cu^{2+} or Fe^{3+} binds to Aβ, metal ions are reduced by Aβ to form H_2O_2 via a two-electron transfer to oxygen [195]. In primary cortical neurons, the presence of Cu^{2+} contributes to the formation of toxic Aβ aggregates [196]. Likewise, the formation of synaptotoxic Aβ oligomers in the presence of Zn^{2+} has been observed both *in-vitro* and *in-vivo* [197,198]. It has to be pointed out that in the absence of metal ions, Aβ are degraded by matrix metalloprotease enzymes (MMP-2) [199] However, the presence of metal ions render Aβ highly protease-resistant due to metal ions-induced conformational changes in Aβ-amyloid [199]. Therefore, the therapeutic strategies to control Aβ accumulation in AD are either to promote degradation of the soluble form of Aβ by proteases or to promote the

clearance of its insoluble form through metal chelation. It was proposed that CQ as a lipophilic metal chelator and an ionophore can support both of these strategies to reduce Aβ toxicity in AD brains [200,201]. As a lipophilic molecule, CQ and its structural analogue PBT2 (Prana Biotechnology) can cross the blood-brain barrier and has a high affinity for metal ions such as copper and zinc. CQ and its derivatives are believed to function via two mechanisms. First, they out-compete Aβ-amyloid for metal ions and eventually lead to the disaggregation of Aβ-amyloid. As a second mechanism, they prevent the formation of toxic metal ions, which subsequently prevents the generation of oxidative stress and the formation of toxic Aβ aggregates [191,200,202,203]. Extracellular accumulation of metal ions implies a limited availability of intracellular metal ions, which ultimately leads to a pathological metal ion homeostasis, a condition that is reported for neurodegenerative diseases such as AD [204].

In addition to metal chelation, CQ and PBT2 are believed to act as ionophores that redistribute metal ions intracellularly to promote neuroprotective cell signalling pathways [194]. It was proposed that CQ can upregulate MMPs and thus promotes Aβ degradation when used with metal ions such as Cu^{2+} and Zn^{2+} [201,205]. Based on these mechanisms CQ administration for 9 weeks in a mouse model of AD (Tg2576) reduced insoluble Aβ by 49 % [200]. It is worth noting that administration of CQ in AD animal model has also been associated with toxicity [206]. CQ treatment induced lethality in young amyloid precursor protein (APP) transgenic mice, a model that represents only mild cognitive impairment [207]. Co-administration of CQ with Cu, however, abrogated the lethality by normalising cerebral Cu levels, increasing SOD1 activity, and reducing Aβ generation {reviewed by [207]}. In a transgenic AD mice model (APP/PS1) as well as in control animals systemic administration of CQ at 6mg/kg/day for 5 months induced myelinopathies in the dorsal lateral geniculate nucleus (DLG), which was almost devoid of amyloid plaque and is the primary site of retinal efferent projection via the

optic nerve [206], suggesting chronic systemic administration of CQ even at the lowest dose could induce neurotoxicity of the optic system. CQ-induced myelinopathies recapitulate the pathology of SMON, which includes demyelination in the lateral and posterior funicular of the spinal cord and the optic nerve [208].

Following promising *in-vivo* studies, CQ and its structural analogue PBT2 were then moved to clinical trials in patients with AD. Although the drugs were shown to be safe and tolerable in patients over the treatment durations [188,202,209,210], few neurotoxicity cases have been reported (**Table 2**).

1.2.2.2 Clioquinol in Huntington's disease (HD)

HD is an inherited neurodegenerative disease characterized by progressive and selective loss of neurons in the striatum causing motor function impairment, gradual decline in intellectual ability and personality changes. The disease is caused by an abnormally expanded CAG (polyglutamine; polyQ) repeat expansion in the *huntingtin (htt) gene* [211]. The disease starts to develop when the number of polyQ repeats reaches 40 or more [211]. Several lines of evidence indicate that ROS contributes to the pathogenesis of HD [212]. Metal ions such as Cu, Fe and Zn may be involved in ROS production, which eventually leads to the accumulation of mutant huntingtin protein [212]. Moreover, levels of Cu and Fe levels are reported to elevate in the striata of the human brain in HD [213]. In line with a role of metal ions in HD pathogenesis, treatment with a metal-chelators and ionophores including CQ and PBT2 is thought to reduce the accumulation of huntingtin protein aggregates and to restore metal homeostasis. CQ and PBT2 have shown beneficial effects in pre-clinical models of HD as well as in clinical trial [211,214]. CQ treatment of PC12 cells that overexpress polyglutamine-

expanded huntingtin exon 1, down-regulated mutant huntingtin expression and inhibited cell death in *in-vitro* [214]. In transgenic Huntington's mice and in a nematode model of HD, CQ and PBT2 treatment improved coordination (rotarod), decreased mutant huntingtin aggregates, decreased striatal atrophy and increased overall health measures such as reduced weight loss and extension of lifespan [211,214]. Based on these encouraging pre-clinical results, PBT2 (100 mg, 250 mg and placebo) was evaluated in a randomised double-blind placebo–controlled trial in 109 early to mid-stage HD patients (USA/AUS). The study was conducted in USA and Australia over a period of 26 weeks and the primary endpoint measurement was safety, tolerability. The secondary end point was cognition, measured by the change from baseline after 26 weeks in the main composite Z score of 5 cognitive tests (Category Fluency Test, Trail Making Test Part B, Map Search, Symbol Digit Modalities Test, and Stroop Word Reading Test) and scores on eight individual cognitive tests (the five aforementioned plus the Trail Making Test Part A, Montreal Cognitive Assessment, and the Speeded Tapping Test) [215]. Compared to placebo, patients receiving either PBT2 100 mg or 250 mg/day did not significantly improve the main composite cognition Z-score while those receiving PBT2 250 mg/day showed improvement only in one of the cognitive tests (trail making test part B) [215]. The European Medicines Agency (EMA) and US Food and Drug Administration (FDA) granted PBT2 orphan drug status. However, the FDA placed a partial clinical hold on PBT2 after its use in dogs induced neurotoxicity [216].

Collectively these data suggest that CQ and its structural analogue are still controversial drugs and the exact mechanism of CQ toxicity has to be understood thoroughly before CQ or its analogues can be used for the treatment of neurodegenerative diseases.

Table 2: CQ and PBT2 in clinical trial for neurodegenerative diseases

Drug	Study design/patient type/country	Dose-patient number receiving that dose	Duration (wks)	End-point measurement	Clinical findings	Ref
CQ	Open label-AD Swedish	20 mg/day-10 80 mg/ day-10	3	CSF-tau protein, growth associated protein, GAP43 measured in 1/3 weeks	Biomarkers increased in 1 week and decreased in 3 weeks, Slight improvement after 3 weeks	[202]
CQ	Pilot Phase II, double blind placebo-controlled, parallel-group/ Moderately-severe AD/ AUS	125 mg BD 250 mg BD- 18 375 mg BD Placebo-18	0-12 13-24 25-36	ADAS-cog at 4, 12, 24, 36 wks, Plasma Aβ, Zn, Cu levels	Drug well tolerated, Clinical benefit only seen in severely affected subject at 4 weeks, Plasma Aβ decreased at 20 weeks, plasma Zn increased in treated group. 3/16 receiving CQ+Vit B12 developed impaired nerve induction. Two patients receiving CQ complaint about leg numbness and one had impairment in visual acuity, colour vision	[188]
PBT2 (EURO)	Phase II a double blind randomised, placebo-controlled/ early AD in spinal fluid Sweden/AUS	50 mg-20 250 mg-29 Placebo-29	12	Safety, tolerability, Investigated levels of unaggregated soluble Abeta peptides in CSF, plasma, Cognition (ADAS-cog, MMSE, NTB)	Drug safe and well tolerated, Patients receiving 250 mg PBT2 showed decreased in CSF Aβ while no effect seen in plasma biomarker as well as metal ions (Cu, Zn) levels, significant improvement in only two executive function component of NTB test (category fluency test: 2.8 words, p=0.041; trail making part B: -	[209]

					48.0s, p=0.009) was reported in 250 mg patient group over placebo treatment.	
PBT2 (Imagine)	Phase Prodormal/ Mild AD	250mg: Placebo-15 PBT2-27	52 weeks	Safety, tolerability, PiB-PET standardized Uptake Value Ratio (SUVR)	No statistically reduction in beta-amyloid plaques compared to placebo as	[217]
Imagine extension	Open label study Extension of Imagine study	250 mg-33 No placebo group	52 weeks	Safe and well tolerated	No improvement in secondary endpoints of brain metabolic activity, cognition and function	[218]
PBT2	Randomised, double blind, placebo-controlled/ Early to mid stage HD/ USA/AUS	100 mg -38 250 mg -36 Placebo-35	26	Safety, tolerability, cognition (change in the baseline to 26 weeks in the main composite Z score of 5 cognitive test)	Drug well tolerated, No significant improvement in the main composite cognition z score observed, trail making test part B showed improvement only in group receiving 250 mg PBT2.	[215]

In order to fully understand the molecular mechanism underlying the above-mentioned mitochondrial optic neuropathies (MON), drug induced MON and to test new treatment modalities, prognostic and representative animal models are required. Pre-clinical models in several different animals have been described to study eye diseases including rats, mice and monkeys [219]. Recently, zebrafish have become a popular model to study vision and visual defects [220].

1.3 Zebrafish and Vision

1.3.1 Zebrafish as a Preclinical Model

Over the last 20 years, zebrafish (*Danio rerio*) have been increasingly used as a vertebrate model for developmental and genetic studies [221]. There are many reasons for their popularity. Zebrafish are easy to maintain and breed in large numbers at relatively low cost. They become sexually mature after 3-4 months and each pair can generate 200-300 offspring on a weekly basis. The eggs fertilize and develop into transparent embryos outside the mother, which allows real-time observation of organogenesis occurring inside the embryo. The embryos are small enough (< 1 mm in diameter) to be easily distributed and maintained in 96 well plates, which facilitates drug screening approaches using only small quantities of drug solution. In addition, embryos are permeable to many small molecules allowing easy administration of drugs [222]. Embryonic development in zebrafish is rapid and takes only a few days with the majority of organs such as brain, heart, liver, intestine and eye developing within 24 hours and becoming functional within a week. The free-swimming larvae hatch from around 72 hours post fertilization (hpf) and soon start foraging for food. All of these attributes explain the steady increase in the use of zebrafish in pharmaceutical research. A large number of embryos produced per clutch makes zebrafish a prominent model for higher throughput screening of small molecules [223], which is mandatory for preclinical drug development and toxicity assessment [224]. So far zebrafish have been used to model a wide variety of human diseases including hereditary muscle diseases [225], neurological disorders [226], tuberculosis [227], cancer[228], cardiovascular diseases [229], haematopoietic and infectious diseases [230]. In addition, zebrafish are a valuable vertebrate model for studying vision related disorders [231]. However, there are a few differences between the visual system of zebrafish and humans, which need to be taken into account.

1.3.2 The Visual System of Zebrafish

1.3.2.1 Eye Structure

The visual system of zebrafish is fundamentally similar to human subjects but exhibits some notable structural differences (**Figure 10, Table 3**) [231-241]. The lens in zebrafish eyes is spheroid and not ellipsoid as compared to the human eye and as a consequence, the zebrafish eye has a much lower volume of vitreous compared to the human eye (**Figure 10**).

Table 3: Comparison of human and zebrafish eye

Structure	Human	Zebrafish	Ref
Eye position	Frontal eyes with highly overlapped binocular vision	Lateral eyes with less overlapped binocular vision	[238]
Lens	Ellipsoidal	Completely spherical extending partially through iris providing wide-angle view.	
Retina (thickness)	≈289 μm	≈ 180 μm	[239]
Ganglion cells	Highly populated	Less densely populated	[234]
Presence of Fovea	Yes	No	[238]
Vision	Cone dominant and trichromatic vision (lacks UV sensitive colour vision.	Cone dominant and tetrachromatic vision (contains UV sensitive short single cones).	[237]
Retinotectal projection	Half of the optic fibres from each eye project on to the same side of the brain and other half crosses over at the optic chiasm and projects to the other side of the brain.	All of the optic fibres coming from each eye crosses over at the optic chiasm and extends on to the opposite side of the brain.	[238]
Myelination	The part of optic fibres before the lamina cribrosa are not myelinated while fibres after protruding from lamina cribrosa are all myelinated	Whole optic fibres are myelinated. Loose, single layer myelin sheath is present around the intra-retinal axon and optic nerve consists of compact myelin.	[232,240,241]

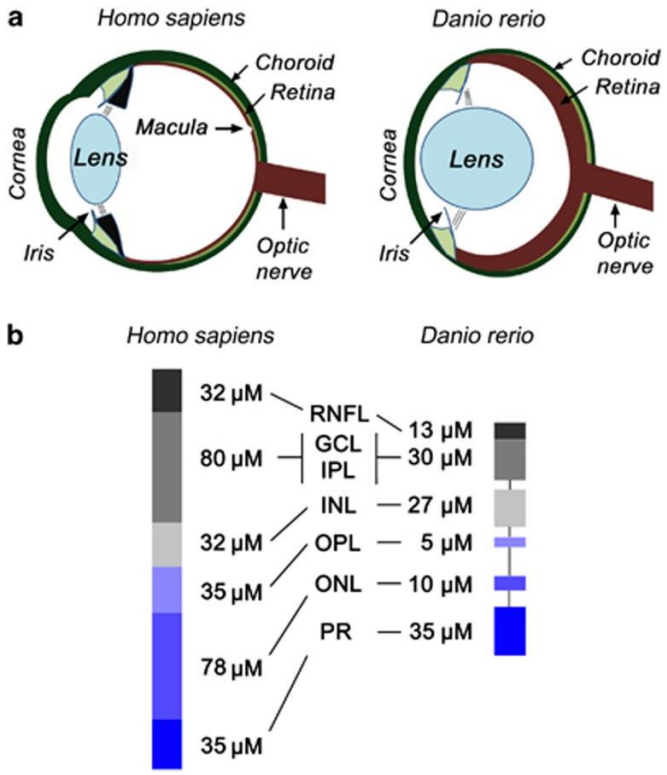

Figure 10: Comparison of the human and zebrafish eye.

(a) Comparison of the human and zebrafish eye: Human and zebrafish eyes mainly differ in lens shape and space between lens and retina. *(b)* Comparison of human and zebrafish retinal structure: Schematic representation of the differences of the retinal layers between human and zebrafish retina. Information on human retinal thickness taken from [239] and for zebrafish derived from http://zfatlas.psu.edu/view.php?atlas=18&s=207; zebrafish atlas, 12 months post fertilized male transverse section). All quantifications are approximates only and may differ between individuals and areas within the retina.

1.3.2.2 The Zebrafish Retina

Since zebrafish use vision to protect themselves against predators and depend on light to search their food, their visual system develops rapidly [237]. The retinal structure starts to develop from 32 hpf and continues to develop extraordinarily fast within 5 days post fertilization (dpf) [231]. By then the zebrafish retina becomes functional. Unlike the mammalian eye, that contains a specialized area within the retina that is responsible for high acuity vision [233], this

so called macula is notably absent in zebrafish (**Figure 10**). Comparable to the human eye, the retinal structure of zebrafish is comprised of five distinct layers (**Figure 10**); three nuclear layers - the outer nuclear layer (ONL), the inner nuclear layer (INL) and the ganglion cell layer (GCL); and two plexiform layers (PL) - the inner (IPL) and outer plexiform layers (OPL) [233]. The ONL consists of the cell bodies of photoreceptors (rods and cones) whereas the cell bodies of horizontal cells, bipolar cells and amacrine cells reside within the INL [233]. The GCL contains the cell bodies of ganglion cells while their axons are located in the retinal nerve fibre layer (RNFL) before becoming bundled into the optic nerve to carry the visual information from the eye to the brain. Synapsis between different neurons takes place at PLs [233]. The synapsis between photoreceptors and bipolar cells (and horizontal cells) occurs in the OPL and the synapsis between bipolar and ganglion cells (and amacrine cells) occurs in the IPL [233]. Horizontal and amacrine cells initiate sidewise interaction in the OPL and IPL respectively [242]. Horizontal cells are responsible for enhancing contrast while amacrine cells, in addition to detecting a change in illumination, also process movement and direction of light on the retina [242]. In contrast to human ganglion cells where part of the axon within the retina is unmyelinated while other parts of the optic nerve are myelinated, the whole axon in zebrafish is myelinated [240,241].

The photoreceptor outer segment (POS) of zebrafish consists of rods and cones, comparable to the human retina. Anatomically cones are arranged in a mosaic pattern that can be categorised into four types; short single cones (SSCs) or ultraviolet sensitive cones, long single cones (LSCs) or blue sensitive cones and double cones (DCs) consisting of short (green sensitive) and long(red sensitive) cones [235,243]. They are also classified based on the peak sensitivities of the photopigment present in each cone as follows; ultraviolet (UV, 360-361 nm), short (S, 407-417 nm), medium (M, 473-480 nm) and long (L, 556-564 nm) cones [235]. Based on the

four cone types in zebrafish, their vision is tetrachromatic. In contrast, the human eye lacks the UV-sensitive cones and therefore has the only trichromatic vision [237]. Unlike cones that have four types of opsins as their photopigment, the rods consist of only a single type and contain rhodopsin as their photopigment [237]. During the development of the zebrafish retina, the SSCs become distinct at around 5-6 dpf while LSCs appear at around 7-8 dpf and the DCs at around 10-12 dpf. However, all of the visual pigments are expressed between 50-55 hpf, so the various cone types are presumably there at 50-55 hpf, but not recognizable. The first rod cells appear at 5-6 dpf [231,244]. Although small rod responses can be detected at this stage, full rod responses are not evident until 15-21 dpf [231,245,246]. Therefore, until 15, dpf zebrafish only have functional cones that are responsible for colour vision.

1.3.2.3 Visual Processing

Light signals entering the eye are first refracted from the cornea to the lens and then projected onto the retina. The signal is then collected by the photo pigment of photoreceptor layer where the rod and cone cells convert the light signals into electrical signals [247] that are transmitted via the horizontal, amacrine and bipolar cells to the RGCs [242]. RGCs give rise to the nerve fiber layer, which is responsible for carrying the signals from the eye, via the optic nerve to the optical centers in the brain.

1.3.2.4 Eye Development

The initial development of the eye structures in zebrafish generally resembles those of other vertebrates [248,249] (**Figure 11**). Eye morphogenesis begins with the evagination of the optic vesicle from the forebrain at 11 hpf as a flat structure which then extends laterally, forming an

optic lobe [248,250]. The anterior portion of the optic lobe remains attached to the forebrain through the optic stalk [250]. The optic vesicle finally gives rise to the neural retina and pigmented epithelium at 15 hpf. By 16 to 20 hpf, the eyecups are developed through a series of different stages from the optic lobe. Surface ectoderm cells underlying the eyecups thicken and form a lens placode at around 16 hpf. Delamination of the lens placode from the surface ectoderm occurs at approximately 24 hpf and then detaches fully by 26 hpf. By 30 hpf the corneal epithelium is formed from the surface ectoderm which overlies the lens. Further morphogenesis of the eyecups forms an optic fissure by 24 hpf and closes thereafter at 48 hpf, which signals that morphogenesis of the embryonic eye is largely terminated and that only retinal neurogenesis is in progress at that time [221,248,249]. At around 32 hpf, the first ganglionic cells differentiate [251] and soon after that their axons reach the optic tectum [233]. The amacrine and horizontal cells within the INL first appear at 50 hpf and by 55 hpf, rod and cone outer segments in the ONL are developed [249]. Rods cells and Muller glial cells are the last to differentiate [252]. The presynaptic photoreceptor ribbon (**Figure 12**) develops at about 65 hpf [249]. Visual information is processed once the ribbon synapses of the bipolar cells reach maturity at 74 hpf [249], which are responsible for passing the light-induced changes in photoreceptor cell membrane potential down the retinal circuit [253]. This means that the retinal structure becomes functional at around 74 hpf [254]. At the same time, the extra-ocular muscles become fully functional, which is a prerequisite for tracking of moving objects by eye movement [255]. Consequently, visually-mediated response improves thereafter with adult-like performance after 96 hpf, where full tracking of eye movement (optokinetic response) is evident.

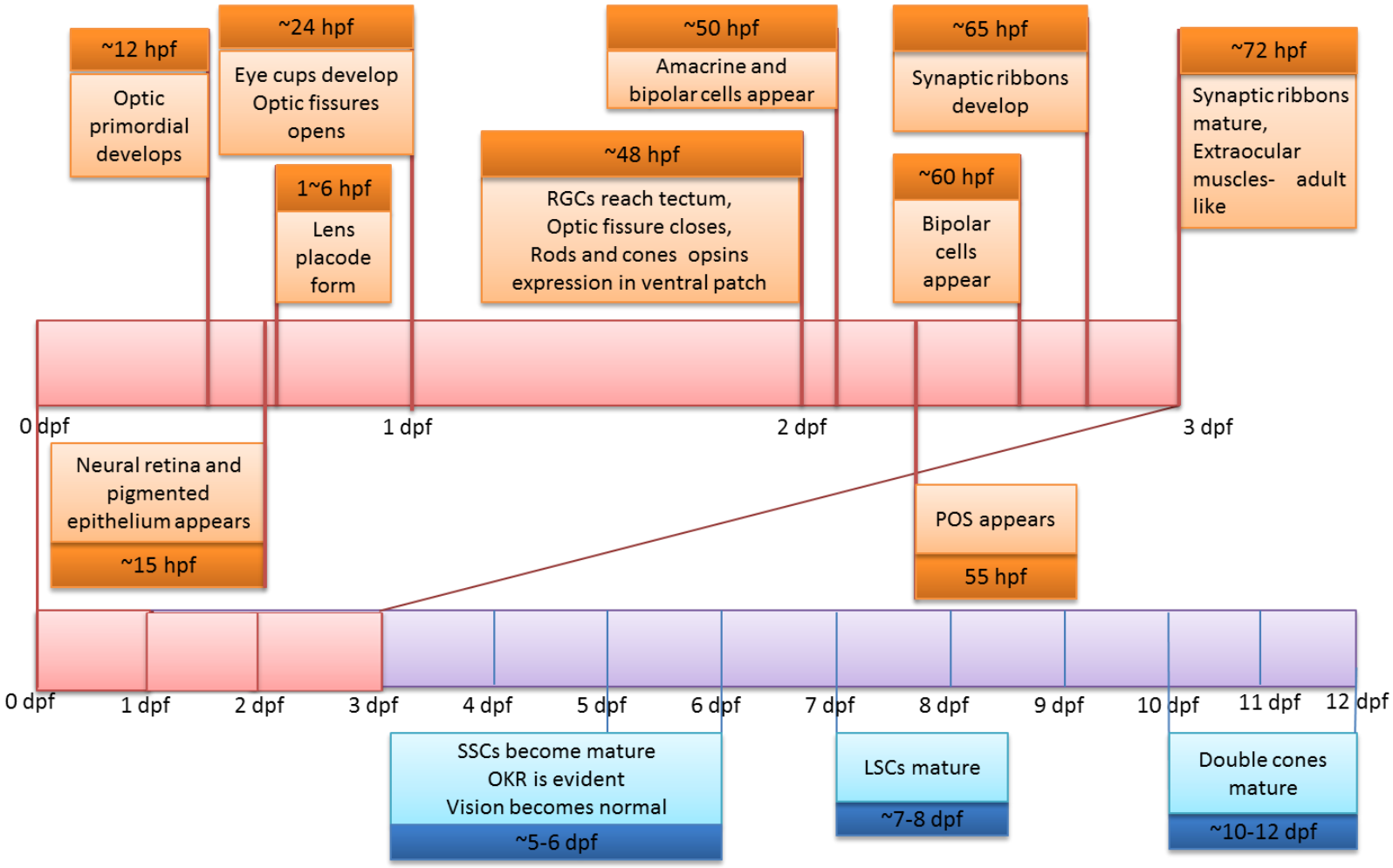

Figure 11: Sequences of eye development in zebrafish.

hpf-hours post fertilization; dpf-days post fertilization; RGCs-Retinal Ganglion cells; SSCs-short single cones; LSCs-long single cones; POS-photoreceptor outer segment; OKR-optokinetic response.

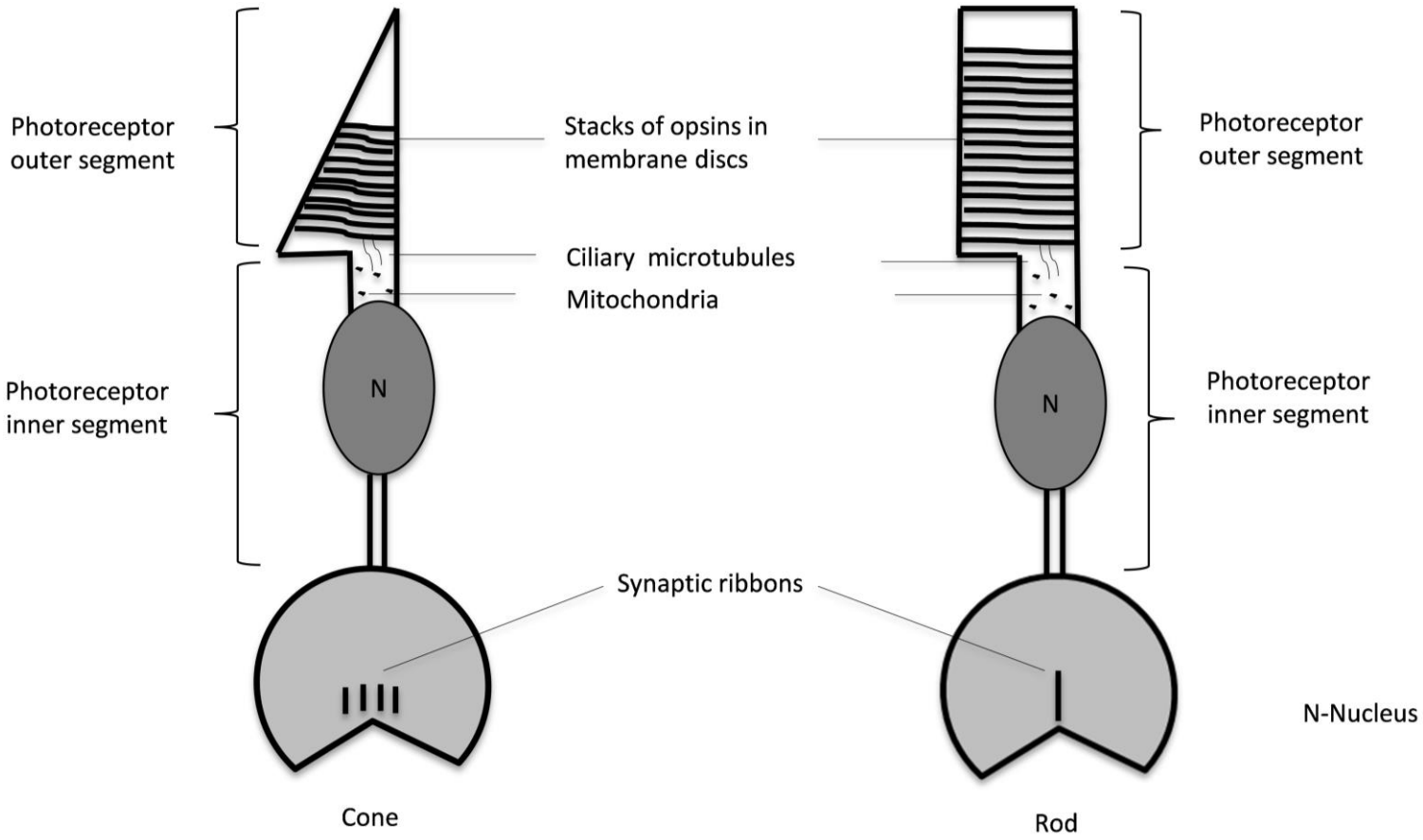

Figure 12: Synaptic ribbons.

Photoreceptors showing presynaptic ribbons, which are responsible for signal transmission from photoreceptor layer to bipolar and horizontal cells.

1.3.3 Why Zebrafish are a Good Animal Model for Ophthalmological Studies

Unlike mouse models, zebrafish are relatively easy to maintain at a fraction of the cost. Zebrafish are prolific breeders and produce as many as 100-200 eggs on every mating, while a pair of mice reliably produces a maximum 6-8 offspring. This large number of eggs per clutch in zebrafish allows higher throughput screening for the identification of mutants and potential drug candidates [231]. In many respects, the zebrafish visual system mirrors the human situation better compared to other animal models. Contrary to mice which have a rod-dominated vision, zebrafish have cone-dominant vision like humans [221], which is a prerequisite to study human disorders associated with cone degeneration such as age-related macular degeneration (AMD) [236]. In addition, the eyes of zebrafish develop fast from only 12 hpf and display a functional visual system by 5 dpf. This is significantly faster compared to mice (around 15-20 days) [256,257] and permits study visual function already in 5 day old larvae. Furthermore, the significant amount of genetic information available from zebrafish mutants associated with defective visual development and function illustrates the power of this model for understanding human ophthalmological disorders.

1.3.4 Measurement of Visual Behaviour

Behavioural responses have been utilized as an important tool for screening genetic defects of the visual system as well as to study the development of the visual system in zebrafish. Several well described behavioural responses with unique advantages and limitations have been used so far (**Table 4**).

1.3.4.1 Optokinetic Response (OKR)

The OKR is based on the eye movement reflex in response to a moving stimulus to help stabilize the image on the retina to maintain visual acuity and is evidence of a fully functional visual system in zebrafish [258,259]. The OKR is tracking eye movements which consist of smooth pursuits (slow phase) and fast resetting saccades in the opposite direction [238]. OKR begins at around 74 hpf when only 5 % of the zebrafish larvae respond to the visual stimulus which then increases steadily to 100 % by 80 hpf [248,254]. The OKR improves in terms of time spent in tracking the stimulus and velocity of tracking eye movement by 96 hpf [254,255,260]. For this method, zebrafish larvae are immobilized to restrain the body while maintaining the ability for eye movement and are then exposed to a visual stimulus that usually consists of alternate black and white stripes that move around the larvae [237,238,261,262]. The larvae respond to this stimulus by moving their eyes in the direction of the moving stripes [237]. Experimental visual stimuli, such as spatial frequency, contrast and angular velocity can be altered in this setting to gain a deeper understanding of a potential defect [262]. With some experimental adaptations, such as a constant supply of oxygen-rich water while body movement is restrained, this method can be applied to adult fish as well [263]. This assay is rapid and responses of larvae or adult fish can be processed within only a few minutes [258]. OKR was used to identify and characterize many zebrafish mutants that are associated with vision system defects (**Table 4**) such as *bumper* mutant (defect in lens development), *noir, dropje, lakritz* mutants (defect in retinal structure), *belladonna* mutant (RGCs axon misrouting) and *grumpy* and *sleepy* mutants (optic nerve disorder) [261]. Other examples of visual function defects are the *brass* mutant with a phenotype similar to glaucoma [264]. In addition, OKR was also useful in isolating a colour-blind mutant by changing the colour of visual stimulus [265]. In summary, the OKR appears to result in more robust, reliable and quantifiable behavioural

data compared to other methods described below, especially after automated commercial systems have become available [260,265].

1.3.4.2 Optomotor Response (OMR)

The OMR tests the visual behaviour of zebrafish by their tendency to swim towards moving black and white stripes [266]. Since numerous fish with possible visual function defects can be tested at once, this OMR assay enables higher throughput analysis compared to the OKR. However, it has to be noted that compared to the OKR there is a significantly higher risk to miss mutants when using OMR [266]. The set-up of OMR is similar as that of OKR except that the embryos or adult fish are not constrained and are able to swim towards the perceived black white stripes [267]. This type of behavioural response shown by zebrafish is one of the innate behaviours known as taxis where fish orient themselves in the direction of the stimulus [268]. This behaviour is important to maintain their orientation in water [268]. In the assay, the wild type fish swim towards the perceived motion and gather at one end of a chamber while zebrafish with visual defects swim in random patterns [267]. OMR is suitable to test the visual acuity of both larvae and adult zebrafish and has been used to isolate at least 17 mutants from 411 previously identified loci in zebrafish that affect visual function so far [231,254,261,267]. Furthermore, the development of visual behaviour in zebrafish under different light conditions (ON and OFF)[267] and the effects of ethanol exposure on embryonic eye development [267,269] have also been studied using OMR.

1.3.4.3 The Startle Response (SR)

The SR in zebrafish is based on a form of body movement within 2 seconds in response to a sudden exposure to a low-intensity light (~60 $\mu W/m^2$) or an acoustic signal and is also useful to determine the development and maturation of the visual system in zebrafish [254,270]. The SR is typically first seen at 68 hpf where 17 % of the fish show startle responses, which then steadily increase to 100 % at 79 hpf at a time when the POS appear abundantly together with a functional retina and fully developed synaptic ribbon [254]. This assay has been successfully used to assess visual development in zebrafish embryos as well as used to detect defects of visual development in response to exposure to toxins such as methylmercury [271]. Recently a modification of startle response has been introduced called visual motor response (VMR) which can be performed on 4 dpf zebrafish larvae to screen for visual mutants. VMR is developed to confirm the result of OKR. This assay examines whether the visual mutants that fail to detect motion under OKR can detect changes in light intensities and are not completely blind [272,273].

1.3.4.4 Phototactic Behaviour (PTB)

The PTB is based on the tendency of zebrafish with normal vision to move towards an illuminated chamber [260]. The experimental setup for this assay consists of a rectangular acrylic box with two chambers inside separated by a sliding bar. There are two methods in which PTB can be assessed [260]. The first approach is based on two chambers, which are equally illuminated. The fish are allowed to distribute between both chambers and the number of larvae in each chamber are counted after a set of the time interval. Then the same procedure is repeated with only one chamber illuminated, while the other chamber is covered. In general,

larvae between 7-14 dpf are suitable for the first method. For the second method, larvae aged between 7 to 19 days are kept in a darkened chamber for up to 2 minutes before the partition is removed and the fish are free to enter the second illuminated chamber [260]. The partition is replaced after several minutes and the numbers of fish in both chambers are quantified. Typically, fish with normal vision will move towards the illuminated chamber while fish with vision defects will not show a preference for the illuminated chamber. For this assay, it was noted that fish move towards the illuminated chamber in both methods, which is evidence of phototactic behaviour in zebrafish [260]. However, there appears to be no significant difference in the number of fish moving from one chamber to another in the light and dark condition approach, which has to be taken into account when interpreting the results. Because of this limitation, the PTB is less suitable for screening zebrafish for mutants with defective vision [260].

1.3.4.5 Escape Response (ER)

Another method to assess vision in zebrafish is the ER, which is based on the natural tendency of zebrafish to evade an approaching predator. In a typical experimental setup, zebrafish are kept inside a white circular rotating drum with a single black strip that mimics a threatening predator [274]. In this assay, zebrafish show a tendency to keep on opposite site of the black stripe. The response of zebrafish either to move towards the visual cues or to move away from it, is determined by the size of the visual cue [275]. Zebrafish orient them towards a small moving visual stimulus as in the case of OMR. As the size of the visual stimulus increases, their behavioural response change into aversive turns and they move away from it as in the case of ER. This is well explained as a transition from a prey capture related orienting response to a predator avoidance response [275]. This test is robust and has been used before in several

studies to characterize mutants that affect vision [274,276], such as *nba (night blindness a)* and *nbb (night blindness b),* which are dominant mutants with adult retinal degeneration [274]. Using ER, the role of the circadian clock in modulating visual sensitivity has also been studied in zebrafish [277,278]. When the threshold light intensity to initiate an escape response was measured over a period of 24 hours under light-dark cycle, the threshold light intensity was at its highest prior to "lights on" early in the morning and at its lowest prior to "light off" in the late afternoon. Therefore, the authors concluded that zebrafish are more sensitive towards visual stimuli at dusk than at dawn [277].

Table 4: Summary of behavioural assays used in zebrafish

Assays	Suitability	Validity	Advantages	Disadvantages	Ref
SR	≥4dpf (embryo)	Yes	Suitable for analysing simple visual function such as differentiating light from darkness. Useful to study visual function development.	Not suitable for larvae ≥ 5 dpf as spontaneous movement is often difficult to distinguish from startle response.	[254] [270]
VMR			VMR complements OKR and is useful for visual mutants screening.	Not suitable for screening visual defect mutants.	[272,273]
OKR	5-7 dpf (embryo and adult)	Yes	Suitable for complex visual function test (visual acuity, contrast sensitivity, colour blindness). Useful for mutant screens. Provides specificity in screening mutants.	Time consuming assay (test one fish at a time). Possibility of missing the strong mutants.-randomly selected	[255,261,262,266]
OMR	>6 dpf (Embryo and Adult)	Yes	Fast assay for high throughput analysis of visual mutants (large number of fish can be analysed at once). Lower risk of missing mutants while screening.	Lack of specificity in result (possibility of false result sometimes)-as it does not test each and every individual fish.	[261,267,279]
PTB	>6 dpf (embryo and adult)	No	Suitable for simple light responses.	Not suitable for mutants screening-due to unreliable result.	[260]
ER	>2 months (adult)	Yes	Simple, robust method. Provides high throughput analysis. Useful in screening visual mutants, visual sensitivities as well as for drug identification and toxicity studies.		[274] [276]

1.3.5 Limitations of Visual Behaviour-based Assays

It has to be pointed out that the assessment of visual function in zebrafish by the assays described above is entirely based on their behavioural response to the visual stimulus. As a

consequence, there is the potential that these assays could produce misleading results. In particular, it can be hypothesized that defects in tissues other than the eyes that are nevertheless crucial for behaviour, such as neuronal circuits that affect muscle function, have the potential to produce misleading results. Genetic analysis of visual behaviour in zebrafish mutants (10 loci, 12 new alleles) did reveal defective visual behaviours (OMR, OKR) with no obvious morphological defect in the retina and RGC projection [266]. This study has highlighted the potential involvement of brain functions beyond retinotectal projection, which is not unexpected given our knowledge of drugs that can alter behaviour. For example, it has been reported that acute alcohol exposure reduces the fear responses and zebrafish become unresponsive towards visual cues [280]. Nevertheless, some drugs can inhibit motility thus ending up with a false impression on visual behaviour assays that is examined by the fish movement such as OMR, therefore further assessment in such condition is necessary [281].

Finally, defects in all processes and systems that are involved, from the processing of visual information to the actual observed change of visual behaviour, such as motor function, have to be seen as possible sites that could influence results. As such, processing of the visual signal in the visual cortex (in higher vertebrates) or optic tectum (in the case of zebrafish) only serves as a prerequisite for induced behaviour, therefore dysfunction in the visual cortex but also other brain areas involved in decision-making could potentially lead to unresponsiveness to the visual stimulation. Thus, confirmation of behavioural assay results with additional methods, such as detection of pathology in the retina or optic nerve or the use of electroretinography [274,279] will significantly increase the reliability of results.

1.3.6 Drug-related Ophthalmological Toxicity Assessment in Zebrafish

More than 200 currently used drugs are associated with ophthalmic toxicity as a result of adverse drug reaction [282]. Assessment of oculotoxicity associated with drugs at the early stage of their development is crucial. However, this process is partly hindered due to a lack of predictive, convenient methods as well as the high expense associated with testing drug candidates in mammals [281,283]. For many years researchers have been using zebrafish assays for drug toxicity screening with a view to provide early drug safety assessments [284,285]. So far zebrafish have been used to predict drug-related cardiotoxicity, ototoxicity, developmental toxicity, neurotoxicity, oculotoxicity and many more [284,285]. Furthermore, zebrafish have demonstrated good prediction of toxicity associated with the effects of systemic drugs in humans [285]. More recently, a study described zebrafish as a potential animal model to predict drug related oculotoxicity at the preclinical stage [283]. In this study 3 dpf zebrafish larvae were exposed to the known oculotoxic drugs (digoxin, gentamicin, ibuprofen, minoxidil and quinine) for 48 h and toxicity was assessed using visual behaviour assay. These drugs resulted in damage to visual function in zebrafish thereby confirming the potential toxicity of these drugs to the human eye.

In addition, many studies have been carried out to validate zebrafish assays for drug toxicity assessment. In one of those, 27 drugs, 19 of which with known and 8 with no record of oculotoxicity in human were assessed in zebrafish using OMR [281]. Of the 19 compounds, 13 drug compounds including chlorpromazine, quinine, digoxin, AZ compound 1, deferoxamine, flecainide, ganciclovir, ibuprofen, minoxidil, thioridazine and vardenafil were found to be oculotoxic in zebrafish. This finding is supported by another similar study which tested 9 known drug compounds with oculotoxicity and found 7 out of 9 compounds had the

adverse effect on the visual function of zebrafish as well [286]. Furthermore, zebrafish have been used extensively as a screening tool for small molecules that modulate vertebrate development [287]. For example, small molecule screens have identified compounds that can affect vascular development in the zebrafish retina. In one study, around 2000 small molecules were tested in zebrafish embryos followed by monitoring changes in retinal vasculature and out of those, 5 compounds were identified [288], which suggests that these drugs may also contribute to the development of pathological changes in the retinal vasculature in human patients. These findings suggest that zebrafish models are successful in mirroring known oculotoxic characteristics of drugs in human and have the potential to predict oculotoxicity profiles of novel drugs.

CHAPTER 2

Chapter 2: *In-vitro Studies*

2.1 Overview and Rationale

Mitochondria generate the majority of cellular energy in the form of adenosine triphosphate (ATP) by oxidative phosphorylation and they are crucial to cellular function and survival as well as for regulating cell death. The density of mitochondria varies among different cell types such that highly metabolically active cell types such as in the visual system have higher numbers of mitochondria. Mitochondria are responsible for retinal cell function and survival as they are the major source of cellular energy supply. Therefore, defects in energy metabolism resulting from mitochondrial dysfunction often lead to visual defects. Retinal ganglion cells (RGC), one of the most metabolically active cells in the body have high numbers of mitochondria predominantly in the pre-laminar axonal region in the retina before they enter the optic nerve [15]. The reason that mitochondria are particularly abundant along the unmyelinated axons of RGCs is to sustain the energy intensive signal transduction in the absence of insulating myelin sheath. Vision impairment is a common feature of most mitochondrial disease including Leber's Hereditary Optic Neuropathy (LHON) and Autosomal Dominant Optic Atrophy (ADOA) [31]. At the same time there is evidence that ROS and mitochondrial dysfunction are at least contributing, if not causal of the pathogenesis of many ophthalmological disorders such as glaucoma, diabetic retinopathy and age related macular degeneration (AMD) [15]. Beside this, a number of widely used drugs have been reported to induce mitochondrial dysfunction and are implicated in toxic optic neuropathy [134].

Since many drugs can potentially cause mitochondrial dysfunction, this research project was designed to identity potential mitochondrial toxins by *in-vitro* screening. Around 200 selected marketed drugs (obtained from the Royal Hobart Hospital Pharmacy) and drug-like molecules

were screened using an assay to identify drug-induced mitochondrial dysfunction. Drug-induced mitochondrial dysfunction was identified by measuring cellular drug-hypersensitivity in galactose versus glucose-containing media (endpoint: drug-induced reduction in cellular ATP levels). From this screen, two compounds were identified, clioquinol (5-chloro-7-iodo-8-hydroxyquinoline) and its parent compound 8-hydroxyquinoline. Clioquinol (CQ) was widely used as a topical disinfectant for skin conditions and as an oral antibiotic to treat diarrhoea. However, after 1970, its oral form was banned in many countries after being linked to more than 10,000 cases of Subacute-Myelo-Optic Neuropathy (SMON) that were restricted mainly to Japan [167]. Despite its toxic history, there is a renewed interest to employ CQ and its derivatives as a disease modifying treatment for neurodegenerative diseases such as Alzheimer's and Huntington's diseases with some promising preclinical and clinical results [188,200,211,215]. In light of the re-emergence of CQ and its structural analogues, it is crucial to understand the underlying mechanism of CQ-induced toxicity to prevent any potential CQ-associated risks to the patients.

2.2 Aim and Objectives

The mechanism of CQ-induced neurotoxicity and the reason for restriction of this neurotoxicity to Japan are still elusive. Amidst this toxic history, CQ and its structural analogues have recently re-emerged as a neuroprotective agent. This is contradictory in itself and poses the question: how can a drug have neurotoxic as well neuroprotective effect at the same time? Therefore, the overall aim of this research project is to explore the molecular mechanism of CQ-induced neurotoxicity.

To achieve this aim, experiments were carried out to fulfil the following objectives:

- To confirm *in-vitro* screening result of CQ- and 8-HQ-induced mitochondrial dysfunction.
- To investigate if ROS is responsible for CQ-induced toxicity by measuring CQ-induced lipid peroxidation.
- To investigate if oxidative stress is the mechanism of CQ toxicity by examining if CQ-induced toxicity can be ameliorated by antioxidants.

2.3 Materials and Methods

2.3.1 Drugs and Compounds

All chemicals were obtained from Sigma-Aldrich (Castle Hill, NSW, Australia) unless otherwise specified. Clioquinol (CQ) and 8-hydroxyquinoline (8-HQ) were purchased from Ciba (Basel, Switzerland) and Ajax Chemicals Ltd (NSW, Australia) respectively. CQ and 8-HQ were dissolved in DMSO, dicoumarol (Dic) was dissolved in 0.1 % NaOH to prepare 10 mM stock solutions. The antioxidants; vitamin C, N-acetyl cysteine (NAC), trolox and vitamin E were dissolved in water or DMSO depending on their solubility in the respective vehicles to generate stock solution of 1 M Vitamin C, 0.5 M NAC, 10 mM trolox and 10 mM vitamin E. Stock solutions were stored as single-use aliquots at -20 ˚C until use. Further dilutions were made in the culture media to achieve the final concentration of drug and to keep final DMSO concentrations below 0.5 % v/v. All cell culture plastic materials were purchased from Corning-In Vitro Technologies (Victoria, Australia) unless otherwise specified.

2.3.2 Cell Culture

The human hepatocellular carcinoma cell line (HepG2) was purchased from the European Collection of Cell Culture (EACC). Rodent neuronal RGC5 cells were provided by Associate Professor Ian Trounce (Centre for Eye Research Australia, CERA, Melbourne, Australia). Human Embryonic Kidney (HEK293) cell lines stably transfected with pCI-neo expression plasmid (Promega) containing the sequence for recombinant human NQO1 were provided by Dr. Robert Dallmann (University of Warwick, UK). All cell lines were cultured under normal culture conditions (37 °C, 5 % CO_2 & 95 % RH) in Dulbecco's Modified Eagle's Medium (DMEM) containing low glucose (1 g/l) or in glucose free culture media supplemented with either 5 % or 10 % heat inactivated fetal bovine serum (FBS; Gibco, Life Technologies Victoria, Australia), 100 units/ml penicillin and 100 µg/ml streptomycin (Gibco, Life Technologies Victoria, Australia). In addition, glucose free media was supplemented with 1g/l d-(+)-galactose and 1mM sodium pyruvate for some experiments. RGC5 cells were maintained in DMEM with 5 % FBS while DMEM with 10 % FBS was used for HepG2 and HEK293 cells. Additional selection antibiotic G418 (50 mg/ml stock solution) was used for HEK293 cells at a 1:100 dilution in every fourth passage to maintain a stable transfected cell line.

All cells were routinely cultured in T25 and occasionally in T75 flask. All cells were passaged every three to four days when cell density reached around 80 % confluency. The cells were initially washed twice with phosphate-buffered saline (PBS) without Ca^{2+} or Mg^{2+} (5 ml for T25, 15 ml for T75) followed by a brief wash with 1ml of 1mg/ml EDTA solution before incubation with 1 ml of 0.05 % Trypsin solution (0.5g/l)-EDTA(0.2g/l) (Gibco-25300-054, Life Technologies, Victoria, Australia) for 3-5 min until cells were detached. Detached cells were resuspended in culture media at a 1:9 dilution (trypsin: culture media) to inactivate trypsin

and then counted manually using a Neubauer chamber. Cells were subsequently diluted in the required culture medium to the desired cell number (2.0 $*10^6$ cells for HepG2; $2.0*10^5$ cells for RGC5; $5.0*10^5$ cells for HEK293 cells) for T-25 flasks.

2.3.3 Freezing of Cells

The cells grown in T75 flasks were harvested using trypsin [**see section 2.3.2 for details**]. To harvest the cells, the cell suspension was centrifuged at 500 x g for 5 min at RT using a swinging bucket centrifuge (CM-6MT, Elmi, skyline Ltd, Riga, Latvia). The resulting pellet was resuspended in 1 ml of culture media supplemented with 20 % FBS and 10 % DMSO and then transferred to labelled cryotubes. The cells were initially cooled down at a constant rate to -80 °C over a period of 24 h in an isopropanol-containing tube box and then transferred to liquid nitrogen for long-term storage.

2.3.4 Thawing of Cells

Cryopreserved cells were thawed at 37 °C and then transferred to a T75 culture flask containing 15 ml of pre-warmed culture media. The cells were cultivated overnight and after 24 h the culture media was replaced by a fresh culture media to remove residual DMSO. Standard harvesting and subculturing was performed when the cells reached 80 % confluency.

2.3.5 Assays

2.3.5.1 Colony Formation

Colony formation is used as an *in-vitro* cell survival assay that determines the reproductive ability of the cells to grow from a single cell to a large colony that by definition should contain at least 50 cells or more [289]. The cells are generally cultivated for a period of 1-3 weeks. This is a suitable and very sensitive method to measure cellular viability and reproductive cell death in response to drug exposure. Only a fraction of cells that survive a drug treatment retain the capacity to grow into colonies [289].

Cells (RGC5, HEK293 and HepG2) were seeded at 200 cells per 100 mm cell culture petri dish and 1000 cells per well in 6 well culture plates in culture media containing low glucose. After 24 h, cells were treated as four replicates per condition with different concentrations of CQ (RGC5/HepG2: 0, 1, 2, 3, 4, 5, 10 µM; HEK293: 0, 1, 5, 6, 8, 10 µM) and 8-HQ (RGC5: 0, 1, 2, 3, 4, 5, 10 µM) and incubated 7 days for RGC5 cells, 10 days for HEK293 and 15 days for HepG2 cells due to the different growth rates of these cell lines. For comparison purposes, HepG2 cells were incubated with the drug for 7 days only, equivalent to the treatment of RGC5 cells. Culture media was not changed during the incubation period for the cell lines. For RGC5 and HepG2 cells, the colonies were washed twice with PBS, fixed with 2 % paraformaldehyde (in PBS) for 15 min and stained with 0.1 % w/v crystal violet (Oxoid, Thebarton, SA, Australia) or Coomassie blue (0.25 % Coomassie Brilliant Blue R-250, 40 % methanol, 10 % acetic acid) for 10 min before excess dye was removed with tap water and the plates were air dried. Due to the low attachment of HEK293 cells, culture plates were coated with collagen but the coating rendered cells more resistant to the effects of the drug. In addition to promoting cell adhesion, collagen is also reported to promote cell survival and proliferation [290]. Therefore, washing, fixing and staining steps were omitted and the samples were air dried instead to prevent loss of

colonies. Finally, colonies of equal to or more than 50 cells/colony were scored manually under a light microscope (Inverted Microscope, Model INV-100, Aktivlab, SA, Australia). Colony formation was expressed as the percentage of the untreated control samples. Colony formation was performed as four replicates per experiment. These four replicates provided the average for each experiment. Three independent experiments were performed and one representative experiment was shown for all cells. For HepG2 cells, however, only two independent experiments were performed.

2.3.5.2 Cellular ATP Levels

Cellular ATP levels were measured, based on an ATP-driven enzymatic reaction between the enzyme luciferase and the photon-emitting substrate luciferin, which generates a stable luminescent signal. This reaction takes place in two steps.

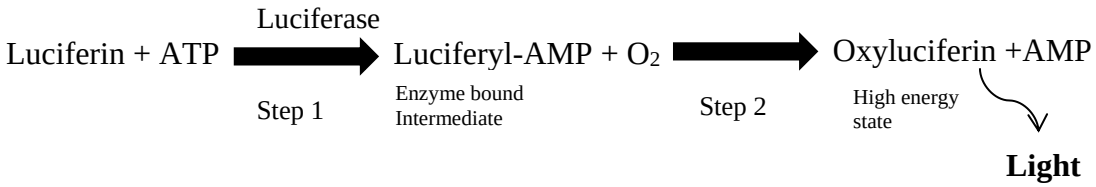

Cellular ATP levels were determined as described previously [291]. The detailed procedures for each cell type and the different conditions are discussed below.

For RGC5 and HepG2 cells ATP levels were measured after 24 h of drug treatment (chronic) and after up to 2 hours of drug treatment (acute) in culture media containing either glucose or galactose [**see section 2.3.2 for detail**]. For HEK293 cells only acute ATP measurements were performed in galactose-containing culture media. Briefly RGC5, HepG2, HEK293 cells were seeded at $1.5*10^4$ cells/well, $2.0*10^4$ cells/well and $1.5*10^4$ cells/well in 96 well culture plates

in their respective culture media. Due to low attachment of HEK293 cells, poly-l-lysine (0.01%) coated 96 well culture plates were used. After 24 h, cells were treated with CQ or 8-HQ at 0, 0.5, 1, 5, 10 µM in glucose or galactose containing culture media for either 24 h (RGC5 and HepG2) or up to 2 h (RGC5, HepG2 and HEK293). After the treatment period, cells were briefly washed twice with 100 µl PBS and lysed with 40 µl of lysis solution (4 mM EDTA, 0.2 % Triton X-100) for 5 min on a shaker at RT. 10 µl of lysate was transferred to a white 96 well culture plate and 90 µl of ATP measurement buffer containing substrate solution (25 mM HEPES pH 7.25, 600 µM D-luciferin, 75 µM DTT, 6.25 mM $MgCl_2$, 625 µM EDTA and 1 mg/ml BSA) and enzyme solution (25 mM HEPES pH 7.25, 10 µg/ml firefly luciferase, 75 µM DTT, 6.25 mM $MgCl_2$, 625 µM EDTA and 1 mg/ml BSA) at a 1:1 ratio was added to the lysate. Luminescence was quantified immediately using a multimode plate reader (Fluroskan Ascent FL Thermo Scientific, VIC, Australia). ATP levels for each individual experiment were averaged from five replicate wells/sample for both the control and each drug concentration and the data were expressed as the percentage of control values. Due to the short incubation period for acute ATP measurements, no changes in cell number were observed. Hence standardisation of ATP levels on protein contents was carried out only for long-term exposure experiments, while it was omitted for the acute experiments. ATP standard diluted in the lysis solution (concentrations: 0-10 µM) was included in each experiment for two reasons. Firstly, to generate a standard curve for the quantification of the cellular ATP concentrations and secondly as a positive control for ATP measurement. The measurement of cellular ATP levels was repeated three times for all cell types and one representative experiment was shown.

2.3.5.3 Protein Quantification

Quantification of the protein content of cell lysates was performed using the DC protein assay kit (Bio-Rad Laboratories PTY Ltd, Gladesville, NSW, Australia). This assay is based on the reaction of protein with alkaline copper tartrate (cuprous ions) yielding reactive monovalent cupric ions, which immediately reduce folin reagent thereby producing a reduced species (molybdenum/tungsten blue) that has a characteristic blue colour with a maximum absorption at 750 nm. The method was performed according to manufacturer's instruction.

Briefly, 10 µl of cell lysate or protein standards (BSA: 0 to 2 mg/ml) were added in triplicate in individual wells of a clear 96 well plate followed by the sequential addition of 25 µl of reagent A' (A' contains 20 µl of reagent S: surfactant and 1 ml of reagent A: alkaline copper tartrate) and 200 µl of reagent B (folin) into each well. After 15 min, at RT absorption at 750 nm was measured using a multimode plate reader (Thermo Scientific Multiskan GO UV/Vis microplate spectrophotometer, SkanIt Software). Protein concentrations were calculated using a standard curve derived from a BSA protein standard.

2.3.5.4 Cellular Lactate Levels

Increased lactate production is one of the hallmarks of mitochondrial dysfunction. Extracellular lactate levels after CQ treatment were determined as a supportive assay to confirm drug-induced mitochondrial dysfunction. The assay was performed according to the protocol previously described with slight modification [292]. Extracellular lactate levels were determined by measuring oxidized form of 2, 6-dichlorophenol-indophenol (ox-DCPIP; blue). Lactate is converted to pyruvate in the presence of lactate dehydrogenase enzyme (LDH) thus

generating NADH from NAD^+. Subsequently, NADH reduces phenazine methosulfate (PMS), which in turn reduces DCPIP to its reduced form (red-DCPIP; pink). In order to prevent generation of lactate from pyruvate, pyruvate is converted to glutamate by glutamate pyruvate transaminase (GPT). Briefly, HepG2 cells were seeded at a density of 60, 000 cells/ml/well in 12 well culture plates in low glucose-containing cell culture media. After 24 h the media was replaced by challenge media (DMEM-low glucose, 3.5 g/l glucose, sodium bicarbonate 3.7 g/l, penicillin and streptomycin) containing different concentrations of CQ or a known mitochondrial inhibitor, rotenone (Rot) as a positive control. After 24 h and 48 h, 10 µl of supernatant was transferred to a clear 96 well culture plate and 90 µl of lactate reaction buffer (10 mM KH_2PO_4 pH 7.8, 2 mM EDTA, 1 mg/ml BSA, 0.6 mM DCPIP, 0.5 mM PMS, 0.8 mM NAD^+, 1.5 mM glutamate, 5 U/ml glutamate-pyruvate-transaminase and 12.5 U/ml lactate dehydrogenase) was added. The oxidation of DCPIP was measured immediately spectrophotometrically at 30 ˚C at 600 nm every 2 minutes for 102 minutes. A lactate standard was run in parallel. Lactate levels were averaged from 9 replicate samples from 3 individual wells. To determine protein content, the cells were lysed in 500 µl of lysis buffer (4 mM EDTA, 0.2% NP-40, 0.2%Tween-20) for 10 minutes in a shaker and protein content was determined using Bio-rad DC method [**see section 2.3.5.3 for detail**]. Finally, lactate levels were standardised to protein content. The experiment was repeated independently three times.

2.3.5.5 Oxidative Stress

2. 3.5.5.1 Lipid Peroxidation

Lipid peroxidation is an indirect measure of oxidative stress as it measures ROS-induced membrane damage. Cellular lipid peroxidation was measured using C11-Bodipy 581/591 (D3861 Invitrogen, Eugene, Oregon, USA). It is a lipophilic dye that enters the lipid bilayer

membrane due to its C11 carbon side chain. Once inside the membrane, it can be oxidized by oxygen radicals or lipid-peroxides that result in a shift of fluorescent emission from 590 nm (red) to a shorter wavelength 510 nm (green) [293]. The green (oxidized form) and red (non-oxidized form) fluorescence of C11-Bodipy 581/591 are obtained using excitation and emission wavelength and the increase in the ratio of green to red fluorescence signifies an increase in lipid peroxidation [293]. The assay was performed using the manufacturer's instruction. Briefly RGC5, HepG2 and HEK293 cells were seeded at a density of $4*10^4$, $5*10^4$ and $5*10^4$ cells/well respectively in black 96 well culture plates. Due to low attachment rates, poly-l-lysine (0.01%) coated black 96 well culture plates were used for HEK293 cells. After 24 h the cells were washed once with 100 µl of PBS and were then incubated with 100 µM of C11-Bodipy 581/591 dye in HBSS for 30 min under normal culture conditions. The cells were once washed with 100 µl PBS before being treated with different concentrations of CQ (0, 0.5, 1, 5, 10 µM) in HBSS for different time intervals (0, 30, 60, 90 and 120 min). After the treatment period, cells were washed once with 100 µl PBS and fluorescence was quantified immediately in 40 µl PBS (Ex/Em 460/535 nm: green fluorescence and 485/600 nm: red fluorescence) using a multimode plate reader (Fluroskan Ascent FL, Thermo Scientific, VIC, Australia). The increase in the ratio of fluorescence intensity at 535 nm versus 600 nm, indicative of lipid peroxidation, was expressed as the percentage of control values. Lipid peroxidation was measured in at least three replicate wells/ sample These three replicates provided the average for each experiment. Three independent experiments were performed and one representative experiment was shown for all cells.

2. 3.5.5.2 Reactive Oxygen Species (ROS)

ROS is a direct measurement of oxidative stress. It can be measured in cells using an indicator dye such as chloromethyl derivative of 2′, 7′-dichlorodihydrofluorescein diacetate (CM-H_2DCFDA) (Molecular Probes, Life Technologies, USA). CM-H_2DCFDA passively diffuses into cells, and its acetate groups are cleaved by intracellular esterases while the chloromethyl groups react with intracellular glutathione and other thiols producing the relative water soluble, cell membrane-impermeable product H_2DCF (2′, 7′-dichlorodihydrofluorescein). This non-fluorescent compound upon oxidation by cytosolic ROS (hydrogen peroxide, peroxynitrite, hydroxy radicals) gives rise to a highly fluorescent product DCF (2′, 7′-dichlorofluorescein). Accumulation of DCF in cells is measured as an increase in fluorescence. This assay was carried out according to the manufacturer's instruction. Briefly, RGC5 cells were seeded at a density of $4*10^4$ cells per well in black 96 well culture plates. After 24 h, the wells were washed with 100 µl of PBS and incubated with 865.4 nM CM-H_2DCFDA (50 µg was dissolved in 100 µl DMSO: concentration 865.4 µM) in Hank's Buffered Saline Solution (HBSS) (865.4 µM was diluted in HBSS at a 1:1000 dilution: the final concentration of dye was 865.4 nM) for 30 min under normal culture conditions. The cells were washed with 100 µl PBS once to remove excess dye before being treated with CQ (0, 0.5, 1, 5, 10 µM) in HBSS for different time intervals (30, 60, 90 and 120 min). Finally, the cells were washed with 100 µl PBS once and fluorescence was quantified in 40 µl PBS (Ex/Em 485 nm and 535 nm) using a multimode plate reader (Fluroskan Ascent FL Thermo Scientific, VIC, Australia). The measurements were expressed as the percentage of control values. The measurement of ROS was carried out in 5 replicate wells per sample (n=1).

2. 3.5.6 Western Blot

Western blots are utilized for separation, identification and quantification of specific proteins from a protein mixture based on their molecular weight through gel electrophoresis.

2. 3.5.6.1 Protein Extraction & Protein Quantification

Cells (RGC5, HepG2 & HEK293) were cultured in T-75 flasks for 4 days. The cells were harvested by trypsinization after they reached 80 % confluency followed by pelleting them at 200 x g for 5 min at RT. The supernatant was removed and cells were resuspended in 1 ml of ice-cold PBS before again being centrifuged at 100 x g for 2 min and the supernatant discarded. Total cell lysates were obtained after extraction with lysis buffer (50 mM Tris pH 7.4, 150 mM NaCl, 2 mM EDTA, 2 mM EGTA, 0.2 % Triton X-100, 25 mM β-glycerolphosphate, 0.3 % NP-40 and freshly added 25 mM NaF, 0.1 % saturated PMSF, 1 µM DTT and 0.1 mM Na_3VO_4) for 15 min on ice with a brief mixing every 5 min. The lysates were cleared by centrifugation (14,500 x g, 20 minutes at 4 °C) to remove insoluble components and the supernatant was transferred to fresh Eppendorf tubes. Protein quantification was carried out using the Bio-rad DC method [**see section 2.3.5.3 for detail**].

2. 3.5.6.2 Protein Samples for SDS-PAGE

The protein lysates containing equal amounts of protein were used. The samples for SDS-PAGE were prepared by adding 25 % (vol/vol) of SDS-containing loading buffer (1M Tris pH 6.8, 8 % SDS, 5 % β-mercaptoethanol, 40 % glycerol, 0.01 % bromophenol blue) to each protein lysate. The samples were then stored at -20 °C until the day of analysis.

2. 3.5.6.3 Gel Electrophoresis

For western blot analysis, 12 % gels were cast (1.5 M Tris pH 8.8, 30 % acrylamide, 10 % SDS and freshly added 0.1 % APS and 1 % TEMED) in a commercial gel apparatus (Bio-Rad Laboratories PTY Ltd, Gladesville NSW, Australia). Isopropanol was layered on the top of the separating gel to smooth the border and reduce exposure of the top of the gel to oxygen. Isopropanol was removed after the polymerisation of the gel residual and isopropanol was cleaned with milliQ water before the inside of the glass plates was dried with absorbent paper. The stacking gel (1M Tris pH 6.8, 30 % acrylamide, 10 % SDS and freshly added 0.1 % APS and 1 % TEMED) was poured on the top of the separating gel and the comb was positioned. After the stacking gel was set, the comb was slowly removed and the wells were rinsed thoroughly with water. The wells were then partially filled with running buffer (25 mM Tris base, 192 mM glycine, 10 % SDS) to ease loading of samples. Protein samples were denatured for 5 min at 95 °C and loaded into each well. The gel cassette was then placed into the electrophoresis chamber, which was filled with running buffer. For two gels, electrophoresis was typically performed at a constant current of 0.06 amps for approximately one and a half hours. Protein transfer from separating gel onto a nitrocellulose membrane (GE Healthcare Life Sciences, NSW, Australia) was carried out by assembling a sandwich of gel, membrane and Whatman filter paper cut to size. The sandwich was placed inside a holder and submerged in the apparatus in the transfer buffer (25 mM Tris base, 192 mM glycine, 10 % SDS, 20 % methanol) with the gel facing the anode. The transfer was performed at constant voltage (100 V) for one hour at 4 °C. Subsequently, the membrane was briefly washed in milliQ water and subsequently non-specific binding sites were blocked using 5 % skimmed milk powder in Tris-buffered saline + 0.1 % Tween-20 (TBS-T) for 1 h. Then the membrane was incubated with the primary antibody against NQO1 (ab34173, Abcam, 1:1000) or GAPDH (ABS16, EMD

Millipore, 1:10 000) in blocking buffer overnight at 4 °C. The next day, the membrane was washed three times for 10 min with TBST and then incubated with the species-specific horseradish peroxidase-conjugated secondary antibody (ab97051, Abcam, 1:20 000) in blocking buffer for 1 hour at RT. The membrane was washed three times for 10 min with TBS-T. Antibody binding was visualized using an image analyser (Chem Smart 5000) with enhanced chemiluminescence western blotting reagent (ECL; Sigma-Aldrich, Castle Hill, NSW, Australia) according to the manufacturer's instructions. For each membrane, multiple exposures with different exposure times were routinely collected to prevent over or under exposure. Western blots were independently repeated at least three times.

2.3.5.7 NQO1-Drug Interaction and NQO1 Enzyme Activity

2.3.5.7.1 Mass Spectrometry Analysis of NQO1 and CQ Interaction

As NQO1 is known to detoxify a number of quinones, mass spectrometry analysis was performed to investigate if CQ is also converted to a potentially less toxic metabolite by NQO1. Four reactions were prepared. Reaction one contained potassium phosphate buffer pH 7.4, CQ 100 µM; the second reaction contained potassium phosphate buffer pH 7.4, CQ 100 µM, NADPH 200 µM; the third reaction contained potassium phosphate buffer pH 7.4, CQ 100 µM, NADPH 200 µM, NQO1 (10 µg/ml); and finally the fourth reaction contained potassium phosphate buffer pH 7.4, CQ 100 µM, NQO1 (10 µg/ml). The reactions were kept at 37 °C overnight for the reaction to take place before the mixtures were evaporated under vacuum using a miVac DNA centrifugal concentrator (Genevac, Suffolk, UK) at 50 °C for 2-4 h. A potential conversion of CQ in the presence of NQO1 was measured using mass spectrometry. Briefly, samples were analyzed using a Waters Acquity H-series UPLC coupled to a Waters Xevo triple quadrupole mass spectrometer. A Waters Acquity UPLC BEH C18 column (2.1 x

100mm x 1.7 micron particles) was used, with mobile phases A= 0.1 % formic acid in water and B= acetonitrile. A linear solvent gradient from 40 % A: 60 % B to 5 % A: 95 % B at 8.75 min was used followed by 3 min re-equilibration time. Flow rate was 0.4 ml/min and the column was held at 45 °C. The mass spectrometer was operated in negative ion electrospray mode and CQ was targeted by Multiple Reaction Monitoring (MRM) after the preliminary establishment of an appropriate channel. The ion source temperature was 150 °C, the desolvation gas was nitrogen at 1000 l/hr, desolvation temperature was 300 °C and the capillary voltage was 2.7 KV. The MRM channel for CQ was m/z 303.9 to 126.95. The cone voltage was 65 V and collision energy was 24 V. Dwell time was 92 ms. Simultaneous full scan data acquisition was carried out from m/z 250 to 500 over 0.3 s with a cone voltage of 60 V. 25 µl samples were injected and data were acquired and processed with Waters MassLynx software.

2.3.5.7.2 Cell-free NQO1 Enzyme Activity

The activity of human recombinant NQO1 enzyme in the presence of CQ or 8-HQ or a known-NQO1 inhibitor dicoumarol (Dic) was determined as previously described [294]. Briefly, the reaction buffer was prepared in a volume of 100 µl containing 50 mM potassium phosphate buffer (pH 7.4), 0.1 % Tween-20, 80 µM DCPIP, 1.25 µg/ml human recombinant NQO1, 200 µM NADPH. The initial reaction mixture was prepared without NADPH, which was added to the reaction buffer to initiate the reaction. Reactions were performed for 1 min at 21°C in the absence or presence of CQ, 8-HQ or Dic. Enzyme activity was determined by measuring the enzyme-dependent linear decrease in DCPIP absorbance at 600 nm every 1 second for 60 seconds. The experiment was performed independently three times.

2.3.5.7.3 Cellular NQO1 Enzyme Activity

Cellular quinone-mediated NQO1 activity in the presence of CQ was determined by conversion of water-soluble tetrazolium dye WST-1 (2-(4-iodophenyl)-3-(4-nitrophenyl)-5-(2,4-disulphonyl)-2H-tetrazolium) (SANTSC-213165, Santa Cruz Biotechnology, USA) to its corresponding formazan-product upon reduction by a hydroquinone. The assay was performed as described previously [295].

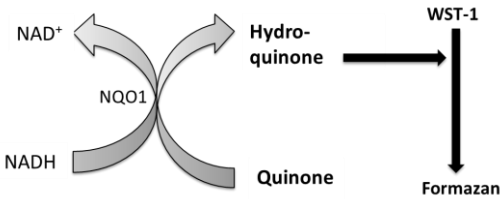

Briefly, HepG2 cells were seeded at $1.0*10^4$ cells/well in 96 well culture plates in low glucose culture media. After 6 h the culture media was replaced by challenge media containing glucose-free cell culture media, 2 % FBS, 0.3 g/l glucose for 18 h. The cells were then pre-incubated with menadione (10 µM), with or without the NQO1-inhibitor Dic (10 µM), CQ or 8HQ (10, 50, 100 µM) in challenge media for 1 hr. After the pre-incubation, the challenge media was replaced by HBSS containing 450 µM WST-1, menadione and Dic or CQ or 8HQ before WST-1 reduction was measured using a multimode plate reader (Thermo Scientific Multiskan GO UV/Vis microplate spectrophotometer, SkanIt Software, VIC, Australia) at 450 nm, 37 °C for 120 min. Cellular NQO1 enzyme activity was repeated independently three times.

2.4 Statistical Analysis

All data are expressed as mean ± standard deviation (SD) as indicated in the figure legends. Statistical significance was performed using Student t-test, one-way or two-way analysis of variance (ANOVA) where appropriate, followed by Dunnett's multiple comparison tests to

evaluate the differences between controls and treatment groups using GraphPad Prism (Version 6, GraphPad Software Inc, CA, USA). Pearson's correlation coefficient (r^2) was determined for the relationship between two variables when necessary. In all assays $p<0.05$ was considered as statistically significant.

2.5 Results

2.5.1 CQ and 8-HQ Induce Mitochondrial Dysfunction

From a previous screen of selected marketed drugs and drug-like molecules using an assay to identify drug-induced mitochondrial dysfunction; 2 strong hits were obtained: CQ and the structurally very closely related parent compound 8-HQ (data not shown) (**Figure 13**). From this point, I took over this project and started exploring the toxicity of these two compounds in more detail.

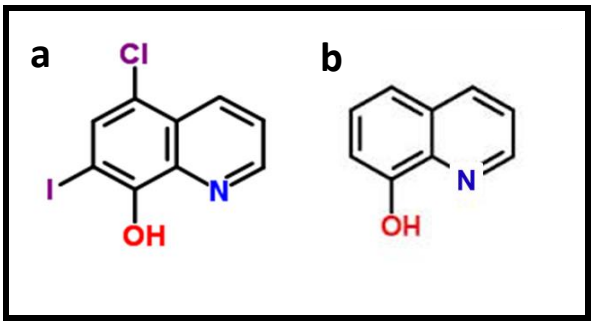

Figure 13: Structure of hits from compound screening.
Two hits, *(a)* Clioquinol (CQ) and *(b)* 8-hydroxy-quinoline (8-HQ) were identified as hits from *in-vitro* screening of compounds. These compounds are members of the hydroxy-quinoline family.

The effect of CQ and 8-HQ on cellular viability was investigated as the first experiment to determine if these compounds are cytotoxic in two different cell lines, rodent retinal (RGC5) and human hepatocarcinoma (HepG2) cells. Cellular viability was measured by incubating RGC5 and HepG2 cells with CQ (1, 2, 3, 4, 5 and 10) µM for 7 and 10 days respectively followed by counting surviving colonies against untreated control cells. In RGC5 cells CQ dose-dependently reduced viability from 3 µM ($p = 0.0033$) and at 10 µM no colonies were detected (**Figure 14a**). In contrast using the same cell line a very steep drop in viability was already observed at 2 µM ($P = 0.0001$) of 8-HQ (**Figure 14a**) and no single colony was detected from 3 µM. Compared to RGC5 cells, HepG2 cells were very sensitive to long-term exposure of CQ and a very significant drop in viability was observed from 1 µM (**Figure 14b**). Several

studies have suggested that the cytotoxicity associated with CQ can be attributed to its metal chelation property [161,182]. To test this hypothesis, different concentrations of $ZnCl_2$ alone or in combination with CQ were added to RGC5 cells and incubated for 7 days to determine if metal ion supplementation would attenuate CQ-induced cytotoxicity by replenishing the chelated metal ions. Intriguingly, $ZnCl_2$ instead of rescuing cells enhanced CQ toxicity in a dose-dependent manner (**Figure 15**). Moreover, $ZnCl_2$ *per se* was toxic to the cells reducing the cellular viability significantly to 71.85 ± 7 % ($p<0.0001$) at 50 µM and to 48.84 % ± 8.4 % at 100 µM.

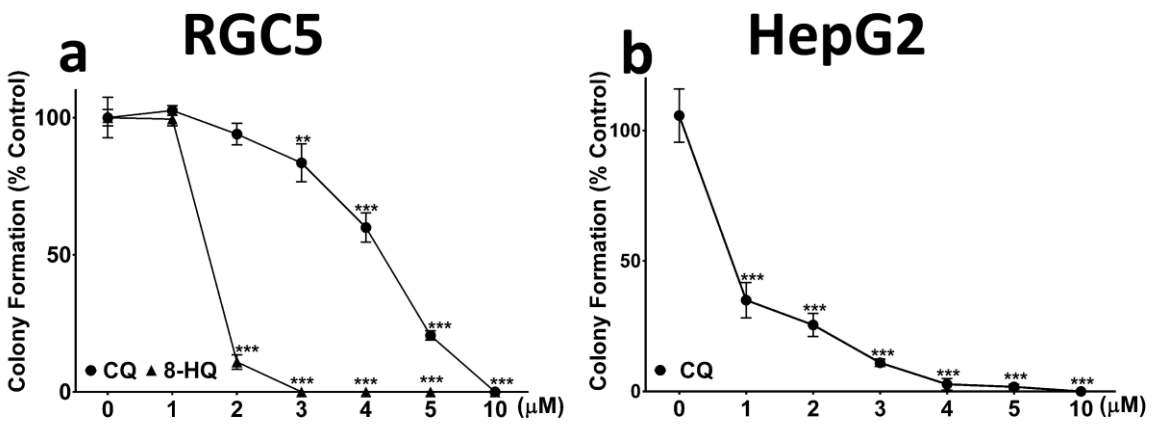

Figure 14: Clioquinol (CQ) and 8-Hydroxyquinoline (8-HQ) reduce cellular viability.

(a) RGC5 and *(b)* HepG2 cells were treated with the indicated concentrations of CQ or 8-HQ in glucose-containing culture media for *(a)* 7 days and 14 days *(b)*. The cell viability was assessed by colony formation assay. Colonies were stained and colonies ≥ 50 cells/colony were counted and presented as the percentage of control. Data represent the average of at least three individual samples per concentration of one experiment out of three independent experiments. p* <0.05, p** <0.01 and p*** <0.001 versus control using one-way analysis variance (ANOVA) followed by Dunnett's multiple comparison tests. Error bar=SD.

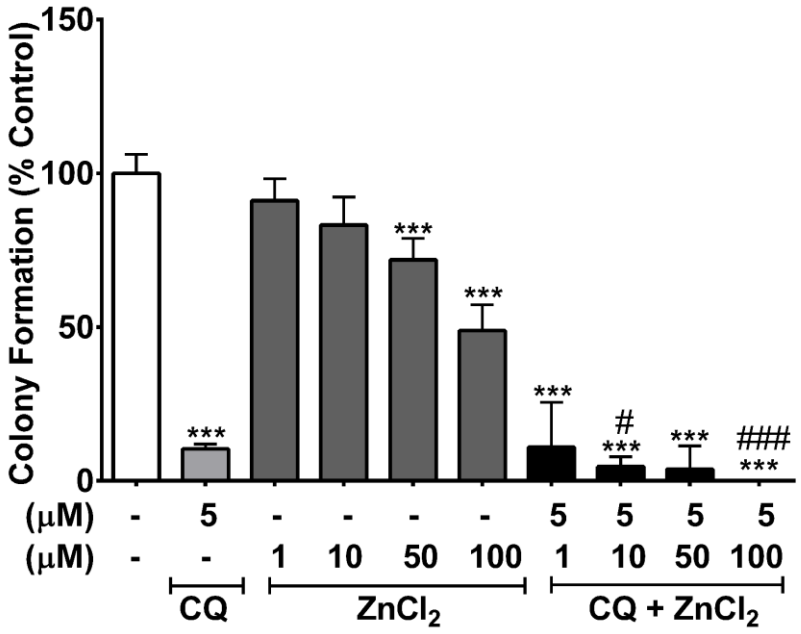

Figure 15: Effect of metal ion and clioquinol (CQ) on cellular viability.

RGC5 cells were treated with the indicated concentrations of CQ or $ZnCl_2$ or both in glucose-containing culture media for 7 days. The cell viability was assessed by colony formation assay. Colonies were stained and colonies ≥ 50 cells/colony were counted and presented as the percentage of control. Data represent the average of three individual samples per concentration of one experiment. p* <0.05, p** <0.01 and p*** <0.001 versus control using one-way analysis variance (ANOVA) followed by Dunnett's multiple comparison tests. $p^{\#}$ <0.05 and $p^{\#\#\#}$ <0.001 versus CQ using Student's t-test. Error bar=SD.

When glucose is abundant, cells *in-vitro* mainly rely on glycolysis to generate energy thus reducing the involvement of the most efficient energy source, the mitochondria [296]. However, when glucose is substituted with galactose, a net zero ATP is produced from glycolysis as a consequence this forces the cells to utilize mitochondrial-OXPHOS pathway for energy generation [296]. Under such conditions, the compounds that interfere with mitochondrial OXPHOS reduce cellular ATP levels. Therefore, to further confirm the *in-vitro* screening results, the effect of CQ and its structural related compound 8-HQ on cellular ATP levels were assessed in RGC5 cells under conditions of glucose versus galactose-containing media. Drug-induced mitochondrial dysfunction can be assessed by measuring cellular

hypersensitivity (measured as a drug-induced reduction in cellular ATP levels) in the presence of drugs in galactose- compared to glucose-containing media. RGC5 cells were hypersensitive to CQ in galactose- compared to glucose-containing media, which is a hallmark of drug-induced mitochondrial dysfunction (**Figure 16a**). In RGC5 cells, in glucose-containing culture media, a significant reduction in cellular ATP levels was observed from 5 µM of CQ and at 10 µM ATP levels were reduced to nearly 30 % of untreated cells (100 %) over 24 h (**Figure 16a**). In contrast, in galactose-containing medium, this effect was significantly more pronounced and a reduction of ATP levels by more than 90 % (0.104 ± 0.0059, $p<0.0001$) of untreated cells was detected at 10 µM of CQ. Since this response could have been due to a toxic effect on cell growth, protein content for each cell-culture condition and treatment condition was quantified. When ATP levels were standardised to protein content, no significant difference in cellular ATP levels were observed at any concentrations of CQ in glucose-containing media (**Figure 16b**). This result suggests that CQ causes toxicity and that protein degradation must have occurred simultaneously with a loss of ATP production. In galactose containing-culture media, however, the observed results resembled the data without protein standardisation (**Figure 16b**).

Similar results were also obtained for the closely related 8-HQ (**Figure 17a**). In fact, 8-HQ was more toxic than CQ in galactose-containing media where it reduced cellular ATP levels to 32 % of untreated cells (100 %) at already 0.5 µM ($P < 0.0001$) (**Figures 17a and b**). This confirmed the results derived from the initial compounds screen. This toxicity could be cell-type dependent and hence might only apply to a selective few cell lines. Therefore, mitochondrial dysfunction of CQ was attempted to confirm in a different cell line. Unlike RGC5 cells, however, HepG2 cells, showed only minor CQ toxicity at doses ≥ 5 µM ($p<0.0001$) and no major differences were observed between glucose- or galactose-containing

media after treatment with either CQ or 8-HQ (**Figures 16a and 17a**)**.** Unlike RGC5 cells, cellular ATP levels in HepG2 cells after CQ treatment also did not differ much with or without protein standardisation (**Figures 16a and b**). Consistent with the results with CQ, long-term exposure of HepG2 cells with 8-HQ in glucose-containing media was followed by higher toxicity compared to RGC5 cells (**Figures 17a and b**).

Further experiments were carried out to measure cellular ATP levels under acute exposure (up to 2h) with either CQ or 8-HQ in galactose-containing media. In RGC5 CQ or 8-HQ dose- and time-dependently reduced cellular ATP levels after short-term exposure (Figures 16c and 17c). 10 µM of CQ or 8-HQ significantly reduced cellular ATP levels to almost 45 % ($p<0.0001$) of untreated cells (100 %) at 2 h and a significant reduction was observed at 1h after CQ (10 µM) treatment (81.61 ± 2.02 %, $p<0.0001$) (**Figures 16c and 17c**). In agreement with the previous results, HepG2 cells only showed a marginal effect at the highest concentration of CQ after 2 h (**Figure 16c**), whereas significant reductions in cellular ATP levels by 8-HQ were not detected at any concentrations (**Figure 17c**). Further experiments were only performed with CQ.

CQ toxicity has been associated with elevated levels of reactive oxygen species (ROS) [182] and ROS production and ROS-mediated lipid peroxidation are the hallmarks of mitochondrial dysfunction. Therefore, CQ-mediated ROS production and lipid peroxidation were assessed in both cell lines. In RGC5 cells, treatment with CQ (up to 10 µM) for up to 2 h did not significantly increase ROS levels compared to untreated control cells (**Figure 18**). Therefore, no attempt was made to measure ROS production in HepG2 cells, which were resistant to CQ toxicity in acute ATP measurements. Consistent with CQ-induced mitochondrial dysfunction, CQ induced lipid peroxidation in RGC5 cells in a dose- and time-dependent manner, with a 50 % increase already

evident after 1h at 10 µM CQ (143.56 ± 5.77 %, $p<0.0001$) compared to untreated cells (**Figure 16d**). Consistent with the previous results, CQ failed to induce lipid peroxidation in HepG2 cells under all tested conditions (**Figure 16d**).

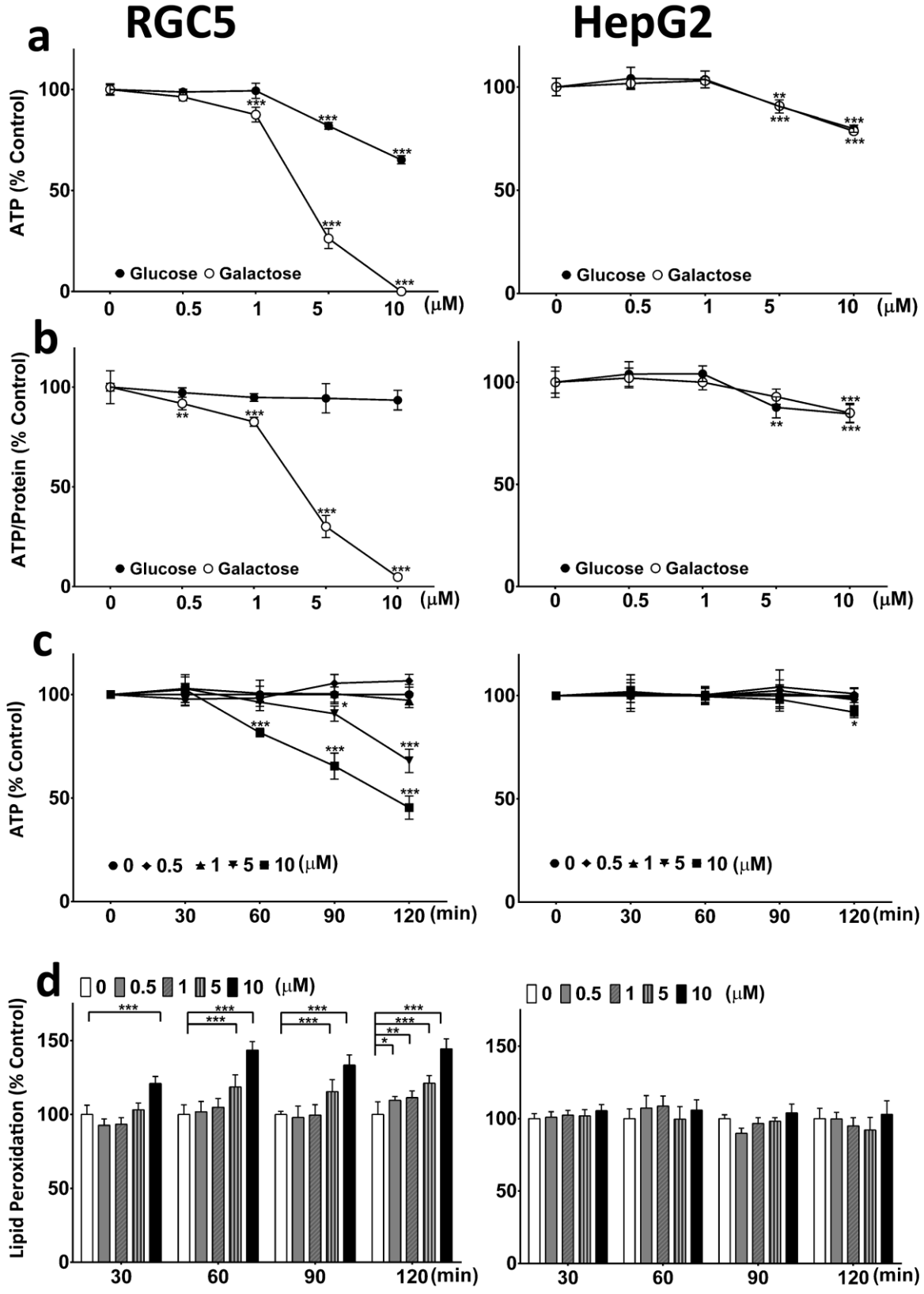
a
RGC5
HepG2
ATP (% Control)
● Glucose ○ Galactose
0 0.5 1 5 10 (μM)
b
ATP/Protein (% Control)
c
ATP (% Control)
● 0 ◆ 0.5 ▲ 1 ▼ 5 ■ 10 (μM)
0 30 60 90 120 (min)
d
0 0.5 1 5 10 (μM)
Lipid Peroxidation (% Control)
30 60 90 120 (min)

Figure 16: Clioquinol (CQ) induces mitochondrial dysfunction.

(a) Long-term effect of CQ on cellular ATP levels. ATP levels of RGC5 and HepG2 cells grown for 24 h in glucose- or galactose- containing media in the presence of CQ were measured. Data represent the average of at least four or five individual samples per concentration of one experiment out of three independent experiments. *(b) Long-term effect of CQ on cellular ATP levels/protein.* ATP levels of RGC5 and HepG2 cells grown for 24 h in glucose- or galactose-containing media in the presence of CQ were measured and standardised to protein content. Data represent the average of at least four or five individual samples per concentration of one experiment out of three independent experiments. *(c) Short-term effect of CQ on cellular ATP levels.* RGC5 and HepG2 cells were incubated in galactose-containing media in the presence of up to 10 µM CQ for 30, 60, 90 and 120 min before ATP levels were measured. Data represent the average of at least four or five individual samples per concentration of one experiment out of three independent experiments. *(d) Lipid peroxidation induced by CQ.* RGC5 cells and HepG2 cells grown in glucose-containing media were incubated with CQ up to 10 µM for up to 2 h before lipid peroxidation was measured using BODIPY-C11. Data represent the average of at least four or five individual samples per concentration of one experiment out of three independent experiments. p* <0.05, p** <0.01, p*** <0.001 versus control using one- or two-way analysis variance (ANOVA) followed by Dunnett's multiple comparison tests. Error bar=SD.

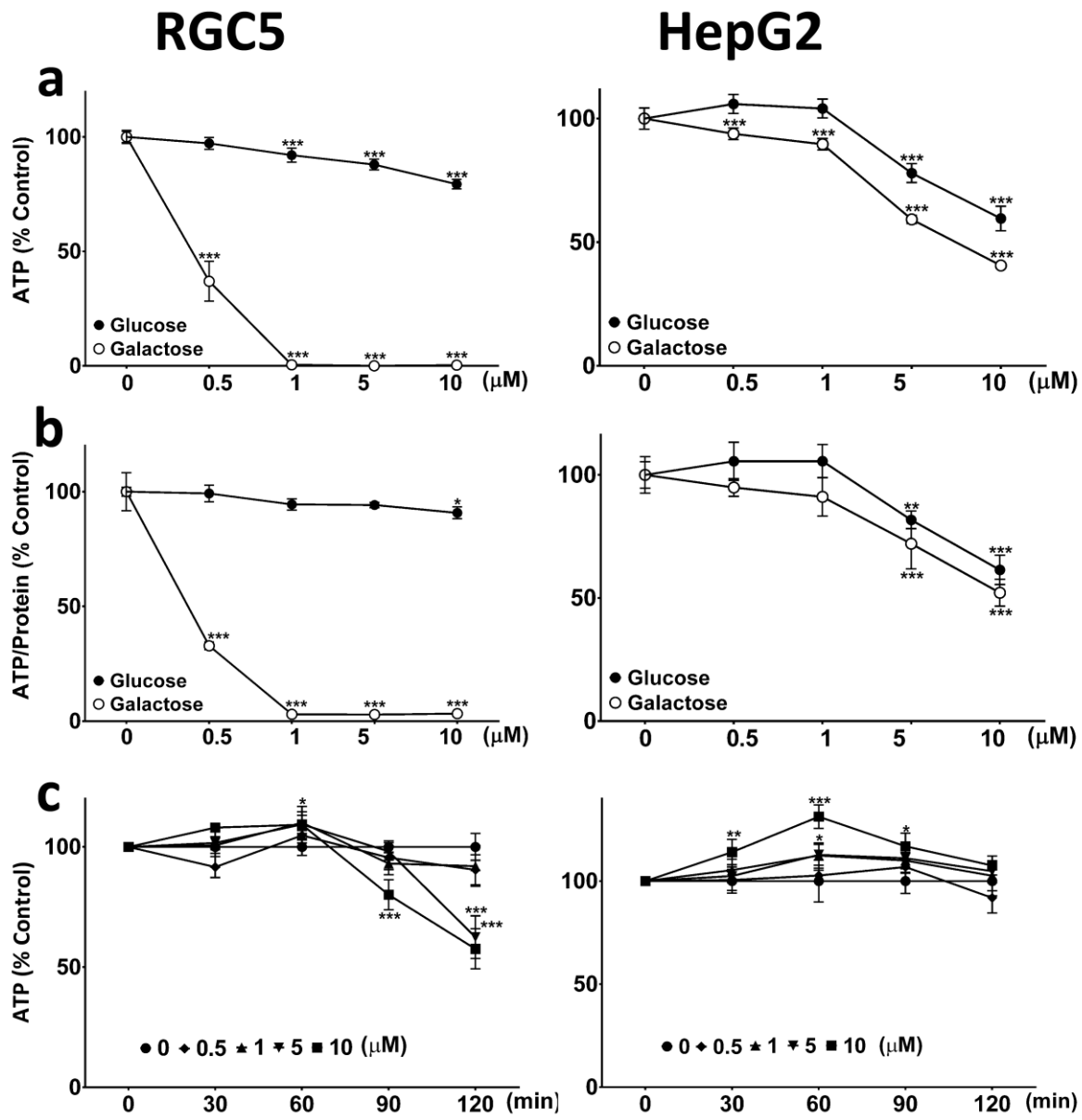

Figure 17: 8-Hydroxyquinoline (8-HQ) induces mitochondrial dysfunction.

(a) Long-term effect of 8-HQ on cellular ATP levels. ATP levels of RGC5 and HepG2 cells grown for 24 h in glucose- or galactose-containing media in the presence of 8-HQ. Data represent the average of at least four or five individual samples per concentration of one experiment out of three independent experiments. *(b) Long-term effect of 8-HQ on cellular ATP levels/protein.* ATP levels of RGC5 and HepG2 cells grown for 24 h in glucose- or galactose- containing media in the presence of 8-HQ were measured and standardised to protein content. Data represent the average of at least four or five individual samples per concentration of one experiment out of three independent experiments. *(c) Short-term effect of 8-HQ on cellular ATP levels.* RGC5 and HepG2 cells were incubated in galactose-containing media in the presence of up to 10 µM 8-HQ for 30, 60, 90 and 120 min before ATP levels were measured. Data represent the average of at least four or five individual samples per concentration

of one experiment out of three independent experiments. p* <0.05, p** <0.01 and p*** <0.001 versus control using one-way analysis variance (ANOVA) followed by Dunnett's multiple comparison tests. Error bar=SD.

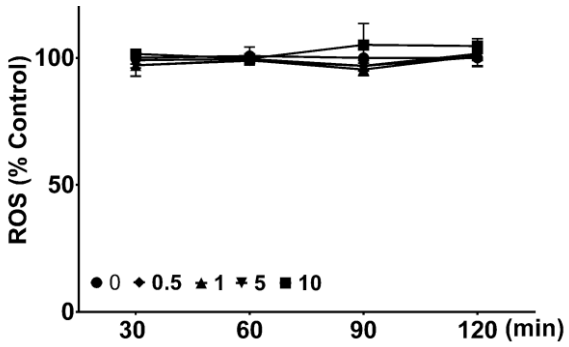

Figure 18: Clioquinol (CQ) does not contribute to cytoplasmic ROS production.
RGC5 cells grown in glucose-containing media were incubated with CQ up to 10 µM for up to 2 h before ROS was measured using CM-H_2DCFDA dye. Data represent the average of five individual samples per concentration of one experiment. p* <0.05, p** <0.01, p*** <0.001 versus control using two-way analysis variance (ANOVA) followed by Dunnett's multiple comparison tests. Error bar=SD.

Cellular toxicity was observed after long-term CQ exposure to HepG2 cells at the level of both cellular viabilities (**Figure 14b**) and ATP (**Figures 16a and b**). To further investigate the nature of this toxicity, another endpoint of mitochondrial dysfunction was measured (which is a measurement of lactate levels in HepG2 cells after CQ treatment). In a situation where mitochondrial function is impaired, cells maintain sufficient energy levels by increasing glycolysis and as a result, produce excess extracellular lactate [297]. Therefore, elevated extracellular lactate is one of the biomarkers of mitochondrial dysfunction. CQ at 10 µM only slightly increased lactate levels in HepG2 cells over 24 h (120 % ± 3.8 %) and 48 h (118.6 % ± 3.3 %) compared to untreated control cells (100 %) (**Figures 19a and b**). At the same time, treatment with the known mitochondrial inhibitor rotenone (Rot) significantly increased lactate

levels at 0.1 and 1 µM (24 h: 168.5 % ± 2.37 %, 143.36 % ± 5 %; 48 h: 174.25 ± 11.9 %) (**Figures 19a and b**). No significant increase in lactate levels was observed after 24 h treatment with Rot (10 µM). CQ even at a 100-fold higher concentration than Rot did not increase the lactate levels to the extent Rot did. Since the previous results indicated that CQ did not induce mitochondrial dysfunction in HepG2 cells, it was also expected that the lactate levels in the same cells would not change in response to CQ treatment. In contrast to our expectations, the lactate levels increased dramatically when the results were standardized on protein content. Lactate levels increased nearly 2-fold over 24 h (194.6 % ± 6 %) and 6 fold over 48 h (634.23 % ± 41.3 %) with 10 µM of CQ compared to untreated control cells (**Figures 19c and d**). In contrast, Rot at 0.1 and 1 µM only slightly increased lactate levels (24 h: 195.7 % ± 15.6 %, 223.5 % ± 18 %). Only at a higher Rot concentration (10 µM), a similar trend compared to CQ was observed, where lactate/protein increased by almost 2-fold (24 h: 199 ± 6 % 48 h: 306.4 % ± 22.3 %) compared to lactate levels that were not standardized to protein content. To understand this substantial increase, the morphology of untreated control cells, as well as CQ-treated cells, was examined. CQ-treated cells showed less number of cells compared to the untreated control cells (**Figures 19e and f**). Therefore, lower cell numbers in the CQ treated plates are responsible for the drastic increase in standardized lactate levels.

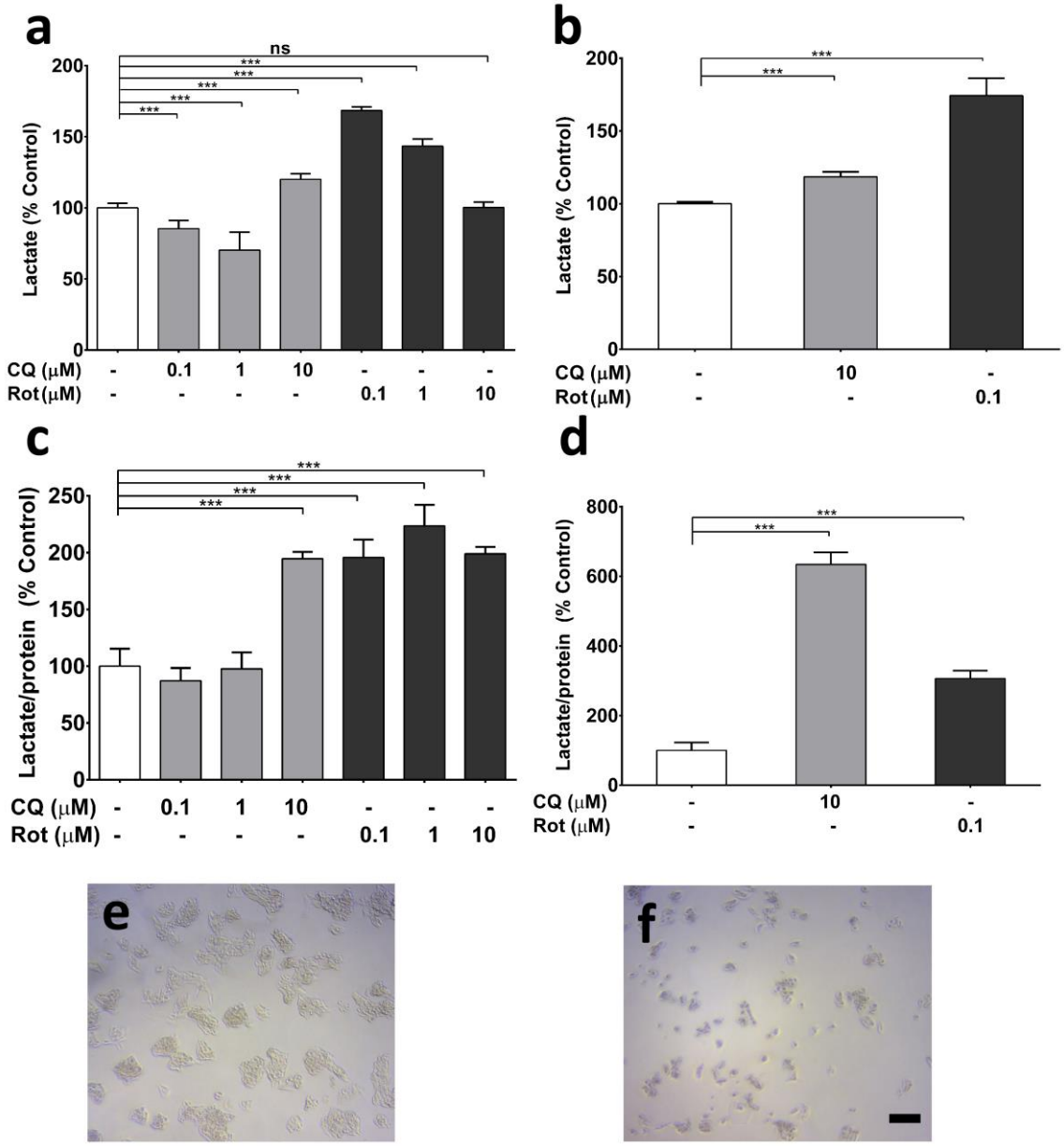

Figure 19: Lactate levels measurement in HepG2 cells.

HepG2 cells grown in glucose-containing culture media were treated with different concentrations of CQ and rotenone (Rot) in media containing high glucose for 24 h *(a, c)* and 48 h *(b, d)* before lactate levels were measured and standardised to protein content per well *(c, d). (e, f)* Representative images of HepG2 cells after 48 h of incubation with CQ (0-*e*, 10-*f*) µM. Data represent the average of at least 9 individual samples per concentration of one typical experiment from three independent experiments. p* <0.05, p** <0.01, p*** <0.001 versus control using one-way analysis variance (ANOVA) followed by Dunnett's multiple comparison tests. Error bar=SD. Scale bar=200 µm for images.

2.5.2 CQ-induced Toxicity Depends on NQO1 Levels

To understand the different response of CQ and 8-HQ in both cell types tested, differences between them were considered. Besides differing in species and tissue of origin, these two cell lines differ particularly in their ability to respond to drugs and drug-induced oxidative stress (unpublished data, N. Gueven). This ability is associated with significantly different expression levels of the antioxidant gene product NQO1 (NAD(P)H Quinone Oxidoreductase 1). NQO1 is a cytoplasmic FAD-dependent flavoprotein that catalyses the two-electron reduction of a variety of compounds [298]. In addition, NQO1 has shown to play a major role in protecting cells against oxidative stress by reducing potentially reactive compounds to their less reactive metabolites [298]. In fact, inactivation of NQO1 has been linked to many pathological conditions including cardiovascular diseases, cancer, neurodegenerative diseases and metabolic disorders [299]. Therefore, it was hypothesized that NQO1 might render cells resistant to CQ-induced toxicity. Therefore, it was tested if the NQO1 inhibitor dicoumarol (Dic) could increase the sensitivity of HepG2 cells to CQ. HepG2 cells cultured in glucose-containing media over 24 h were treated with CQ or Dic or both in galactose-containing media for 2 h. Consistent with the previous result, 10 µM CQ only mildly reduced ATP levels by less than 5 % in HepG2 cells in galactose-containing culture media (**Figure 20a**). However, the combination of CQ and Dic significantly reduced ATP levels (69 % ± 2.19, $p<0.0001$) compared to the untreated cells at 2 h. Under these conditions, Dic alone only had a marginal effect that was not statistically significant from untreated control cells ($p=0.1663$) (**Figure 20a**).

Purely based on their origin, a large number of genetic differences between the two cell lines can be postulated. Given the putative role of NQO1 to influence CQ toxicity and to rule out

cell type dependent differences, 3 isogenic cell lines based on the Human Embryonic Kidney (HEK293) cell line were used. These HEK293 cell lines have an identical background regarding their nuclear DNA and differ only in their levels of NQO1 expression that is achieved by stable transfection of a constitutively active NQO1 expression plasmid. These include, HEK293 that either overexpress human recombinant NQO1 (clones 6 and 12) or carry the empty plasmid (neo). HEK293 cells were used for this experiment as they express extremely low to undetectable levels of NQO1 and are thus well suited for this approach [291]. NQO1 expression in the three HEK293 cell lines, as well as RGC5 and HepG2 cells, was measured by western blot (**Figure 20b**). The equal loading of total cell extract (3 µg) was ensured by using glyceraldehyde-3-phosphate dehydrogenase (GAPDH) as a loading control. As previously reported [291], HepG2 cells showed very high NQO1 protein expression. In contrast, RGC5 cells showed lower NQO1 protein expression, compared to HepG2, while NQO1 levels in HEK293-neo cells were undetectable. Both NQO1 overexpressing HEK293-clones (6 and 12) showed intermediate expression levels compared to HepG2 (**Figure 20b**).

To investigate the protective role of NQO1 in ameliorating CQ-induced cellular toxicity the three previously assessed end-points were measured in these HEK293 cell lines: cellular viability, lipid peroxidation and ATP levels. The effect of NQO1 on cellular viability was examined by incubating HEK293 cells with CQ for 10 days under glucose-containing media and viability was assessed by counting number of surviving colonies compared to untreated control cultures. In cells that do not express NQO1 (HEK293-neo), CQ (8 µM) significantly reduced cellular viability to 21.85 % ± 2.85 % ($p<0.0001$) compared to untreated control cells (100 %) (**Figure 20c**). Consistent with the hypothesis that NQO1 can attenuate CQ toxicity, NQO1 expression significantly increased cellular viability in the presence of CQ by nearly 120 % in both clone 6 (47.16 ± 5.87, $p= 0.0002$) and clone 12 (47.67 ± 14.39, $p=0.0125$) compared

to CQ-treated neo cells (**Figure 20c**). Furthermore, in HEK293-neo cells, CQ significantly induced lipid peroxidation (1.5 h: 115.2 % ± 5.4 %; 2 h: 139.1 % ± 12.2 %) compared to the untreated cells (100 %). Consistent with a protective effect, expression of NQO1 significantly prevented CQ-induced lipid peroxidation in both NQO1 expressing cell lines at 1.5 h (clone 6: 98.5 % ± 10.6 %, p=0.0093; clone 12: 98.6 % ± 3.54 %, p=0.0173) and 2 h (clone 6: 117.5 % ± 8.5 %, p=0.0040; clone 12: 116.1 % ± 8.6 %, p=0.0013) compared to CQ treated neo cells (**Figure 20d**).

To investigate the mitochondrial dysfunction of CQ under a condition of undetectable NQO1, HEK293-neo cells cultured in glucose-containing media over 24 h, were treated with different concentrations of CQ (0.5, 1, 5, 10 µM) in galactose-containing media for up to 2 h followed by measurement of ATP levels. Acute incubation of HEK293-neo cells with CQ strikingly led to a pronounced reduction of ATP levels comparable to the effects seen in RGC5 cells. In a dose- and time-dependent manner, CQ reduced cellular ATP levels with a significant reduction already evident at 30 min with 10 µM CQ (80.12 ± 12.05 % P=0.0138) and at 2 h ATP levels were reduced to 36 % ± 14.3 % (P<0.0001) compared to untreated control cells (**Figure 20e**). After confirmation of CQ toxicity in HEK293-neo cells, HEK293 cells were incubated with 10 µM of CQ in galactose-containing media for 2 h and ATP levels were quantified. In HEK293-neo cells, CQ (10 µM) significantly reduced ATP levels (31.5 % ± 5.8 %, p<0.0001) compared to untreated control cells. On the other hand, under these conditions, NQO1 expression in HEK293-clone 6 and HEK293-clone 12 significantly protected against CQ-induced decrease of cellular ATP levels (clone 6: 82.8 % ± 5.87 %, p <0.0001) and (clone 12: 52.8 % ± 9.51 %, P=0.0010) (**Figure 20f**). The differences in the level of protection shown by NQO1 expressing cells led us to closely investigate this protective effect of NQO1.

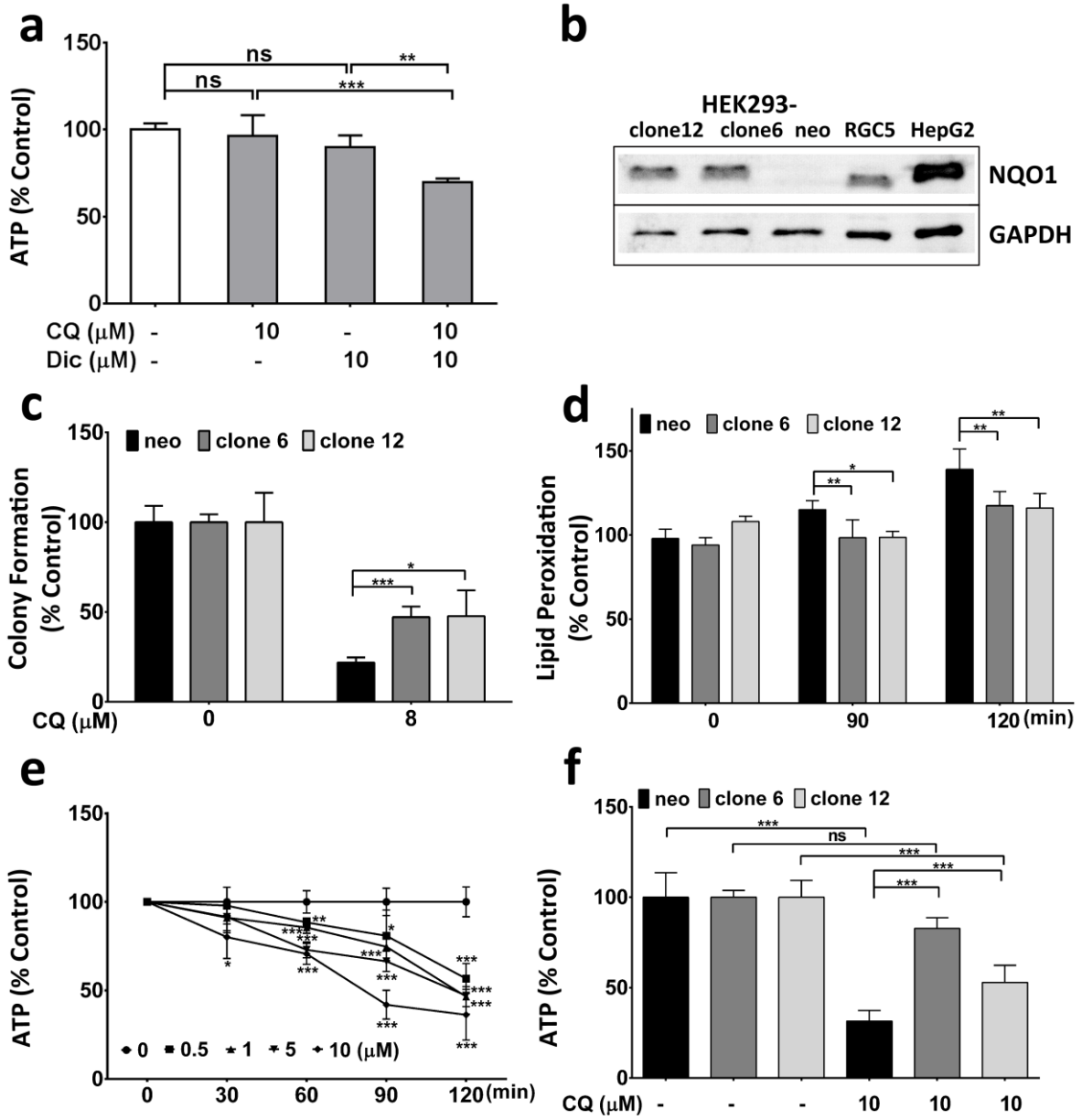

Figure 20: NQO1-dependent clioquinol (CQ) toxicity.

(a) CQ-induced reduction of cellular ATP levels in the presence of the NQO1 inhibitor dicoumarol (Dic). HepG2 cells were treated with 10 µM CQ and/or 10 µM Dic in galactose-containing media for 2 h before ATP levels were measured. Data represent the average of at least four or five individual samples per concentration of one experiment out of three independent experiments. *(b) Western blot analysis of NQO1 expression.* Representative western blot image of NQO1 and GAPDH in HepG2, RGC5, HEK293-(neo, clone 6, clone 12). Data represent one typical experiment out of 5. *(c) Cellular viability of HEK293 cells in the presence of CQ.* HEK293 cells were grown in glucose-containing media in the presence of CQ for 10 days and numbers of colonies were counted against untreated control cells. Data represent the average of four individual samples per concentration of one experiment out of three independent experiments. *(d) Effect of NQO1 on CQ-induced lipid*

peroxidation. HEK293 cells were treated with 10 µM of CQ for up to 2 h and lipid peroxidation was measured using BODIPY-C11 dye. Data represent the average of at least four or five individual samples per concentration of one experiment out of three independent experiments. *(e) Short-term effect of CQ on cellular ATP levels.* HEK29-neo cells incubated in galactose-containing media in the presence of up to 10 µM CQ for 30, 60, 90 and 120 min before ATP levels were measured. Data represent the average of at least three individual samples per concentration of one typical experiment. *(f) NQO1 dependent reduction of cellular ATP levels by CQ.* HEK293 cells were treated for 2 h with 10 µM CQ in galactose-containing media before ATP levels were measured. Data represent the average of at least four or five individual samples per concentration of one experiment out of at least three independent experiments. p* <0.05, p** <0.01 and p*** <0.001 versus control using Student's t-test or one- or two-way analysis variance (ANOVA) followed by Dunnett's multiple comparison tests where appropriate. Error bars = SD for all experiments. clone 6/clone 12 = NQO1 overexpressing cells, neo = empty vector.

Strikingly, when NQO1 expression of all cells used in this study was analysed against CQ-induced toxicity, a direct correlation was observed with cellular levels of ATP and lipid peroxidation (**Figures 21a** r^2= 0.9235 and **b** r^2= 0.8772). When NQO1 expression is very low as in HEK293-neo cells, CQ efficiently induced cellular toxicity, measured as CQ-induced reduction of cellular ATP levels and increased lipid peroxidation (**Figures 21a** and **b**). On the other hand, increased NQO1 expression showed a clear NQO1-dependent reduction in CQ-induced toxicity, which was evident by increased cellular ATP levels and decreased lipid peroxidation (**Figures 21a** and **b**).

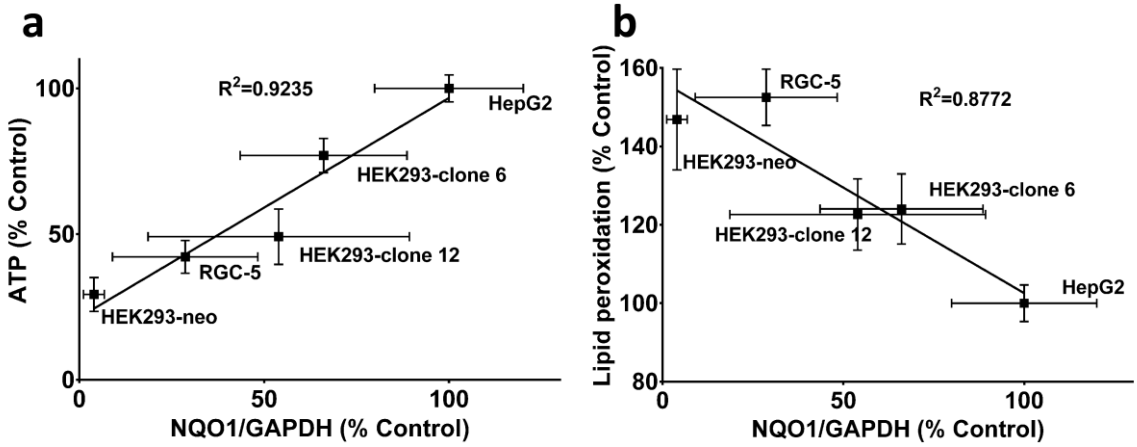

Figure 21: Correlation of clioquinol (CQ)-induced toxicity versus NQO1 expression levels. Cellular toxicity was measured as changes to *(a)* ATP (% Control) and *(b)* lipid peroxidation (% Control) after treatment with CQ (10 µM) for 2 h in galactose-containing media and HBSS respectively. ATP levels (% Control) are defined as % of CQ-induced ATP reductions in all cell lines relative to that in HepG2 cells (= 100 %). Lipid peroxidation (% Control) is defined as the % increase in lipid peroxidation by CQ in all cell lines relative to that in HepG2 cells (= 100 %). NQO1/GAPDH (% Control) is defined as % NQO1/GAPDH expression in all cell lines relative to that of HepG2 cells (= 100 %). Pearson's correlation coefficient (r2) was determined for the correlation experiment. Error bars = standard deviation (SD) for ATP, lipid peroxidation and NQO1/GAPDH.

2.5.3 CQ induces Toxicity through Generation of ROS

Since cellular protection against CQ-induced toxicity correlated with the expression of the antioxidant enzyme NQO1, oxidative stress was a possible mechanism of CQ toxicity. In order to confirm this possibility, it was tested if exogenous antioxidants could rescue CQ-induced toxicity. In order to find suitable antioxidants at their right concentrations, several different antioxidants for their ability to rescue CQ-induced lipid peroxidation were examined along with CQ in RGC5 cells. RGC5 cells, grown in glucose-containing media, were pre-treated with antioxidants; N-acetyl cysteine (NAC; 1 mM), trolox (10 µM), vitamin C (30 µM) and vitamin E (10 µM) for 30 min and co-treated with CQ (10 µM) before lipid peroxidation was measured. Consistent with the previous result, CQ treatment of RGC5 cells for 2 h significantly increased

lipid peroxidation (146.2 % ± 14.5 %, p<0.0001) compared to untreated control cells. Out of the antioxidants tested, NAC (117.7 % ± 3.5 % p=<0.0001) and trolox (126.4 % ± 5.8 %, p=0.0017) significantly reduced CQ-induced lipid peroxidation, while only a slight reduction was observed with vitamin C (131.4 % ± 2.9 %, p=0.0381) compared to untreated control cells (**Figure 22a**). Therefore, further experiments only included NAC and trolox.

The role of these antioxidants to ameliorate CQ toxicity was further explored in series of experiments where antioxidants were either used alone or in combination with CQ to determine if the CQ-mediated increase in lipid peroxidation, the decrease in cellular viability and the reduction in ATP levels could be rescued. This was tested only in HEK293-neo cells as they were highly vulnerable to CQ toxicity. Consistent with the previous lipid peroxidation results, CQ significantly increased lipid peroxidation compared to untreated control cells (126.9 % ± 1.5 %, p<0.0001). The antioxidants NAC and trolox (**Figure 22b**) showed no effect on lipid peroxidation when used alone. However, when they were used in combination with CQ (8 µM), a significant reduction in CQ-induced lipid peroxidation was observed compared to untreated control cells (NAC: 112.5 % ± 3.3 % p<0.0001; trolox: 117.3 % ± 4.3 %, p=0.0027). Similar results were obtained with regards to cellular viability measurement. Consistent with the previous result, CQ reduced cellular viability in HEK293-neo cells to 22.5 % ± 3.9 % compared to untreated control cells. NAC (1mM) and trolox (10 µM) did not affect cellular viability on their own. However, when they were combined with CQ, a significant increase in cellular viability by 200 % (NAC: 66.5 ± 7.2 %, p<0.0001) and 115 % (trolox: 70 ± 2.67 %, p<0.0001) was observed compared to CQ-treated cells (**Figures 22c** and **d**). However, the antioxidants were unable to rescue the cellular viability to the level of the untreated cells (p<0.0001). Similarly, when trolox and NAC were used at the same concentration range, CQ-

induced decreases in cellular ATP levels in HEK293-neo cells were also rescued by 112 % and 125 % respectively (p= 0.0207: trolox, p=0.0174: NAC) (**Figure 22e**).

NQO1 protein levels are generally highly inducible and NQO1 expression is modulated by a protein complex, composed of the nuclear factor erythroid 2-related factor 2 (Nrf2) and Kelch-like ECH-associated protein (keap1) [300]. NQO1 protein expression is induced as an adaptive mechanism in response to pro-oxidative conditions. Therefore, it was tested if NQO1 expression could be induced by CQ-mediated oxidative stress. This was initially examined in HepG2 cells under normal culture conditions (low glucose DMEM) using 10 µM CQ and hydrogen peroxide as a positive control (H_2O_2, 300 µM) at 24, 48 and 72 h [301]. CQ as well H_2O_2 treatment in HepG2 cells did not induce NQO1 expression at any time-points compared to untreated control cells. (**Figure 23a**). These results are in contrast to reports that pro-oxidants can induce Nrf2-regulated genes such as NQO1 in HepG2 cells [301]. However, it was shown that pro-oxidants induce NQO1 in HepG2 cells under high glucose condition [302]. Therefore, HepG2 cells were cultured in high glucose- (4.5 g/l) containing media for 6 passages before being treated with 10 µM CQ and H_2O_2 at 300 µM under high glucose conditions. Again, neither CQ nor H_2O_2 induced NQO1 expression in HepG2 cells at any time point (**Figures 23b** and **c**).

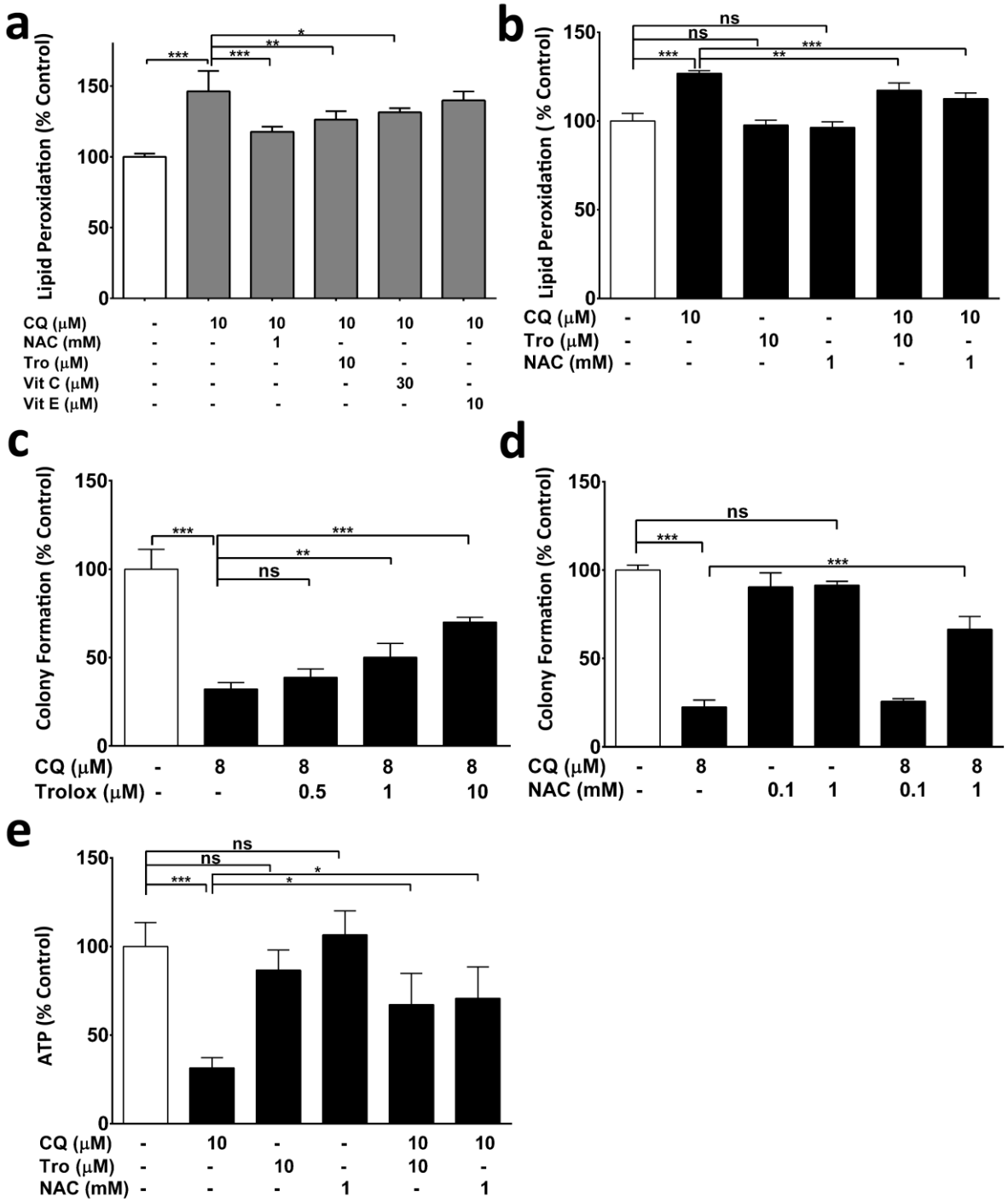

Figure 22: ROS-dependent clioquinol (CQ) toxicity.

(a, b) Antioxidants ameliorate CQ-induced increase of lipid peroxidation. (a) RGC5 cells grown in glucose-containing media were pre-treated with antioxidants N-acetyl cysteine (NAC; 1mM) and trolox (Tro; 10 µM), vitamin C (30 µM) and vitamin E (10 µM) for 30 min and co-treated with 10 µM of CQ for 2 h before lipid peroxidation was measured using Bodipy-C11 dye. Data represent the average of at least five individual samples per concentration of one typical experiment. *(b)* HEK293-neo cells grown in low glucose were co-treated with antioxidants NAC (1mM) or trolox (10 µM)

and/or 10 µM of CQ for 2 h before lipid peroxidation was measured using BODIPY-C11 dye. Data represent the average of at least four or five individual samples per concentration of one experiment out of three independent experiments. *(c, d) Antioxidants ameliorate CQ-induced reduction of cellular viability.* HEK293 cells grown in low glucose were treated with CQ and indicated concentrations of *(c)* NAC or *(d)* trolox before cellular viability was measured by colony formation. Data represent the average of at least four or five individual samples per concentration of one experiment out of three independent experiments. *(e) Antioxidants ameliorate CQ-induced reduction of cellular ATP levels.* HEK293 cells grown in glucose were co-treated with antioxidants NAC (1mM) or trolox (10 µM) and/or 10 µM of CQ for 2 h before ATP levels were measured. Data represent the average of at least four or five individual samples per concentration of one experiment out of three independent experiments. $p^* < 0.05$, $p^{**} < 0.01$ and $p^{***} < 0.001$ versus control using one-way analysis variance (ANOVA) followed by Dunnett's multiple comparison tests. Error bar=SD.

.

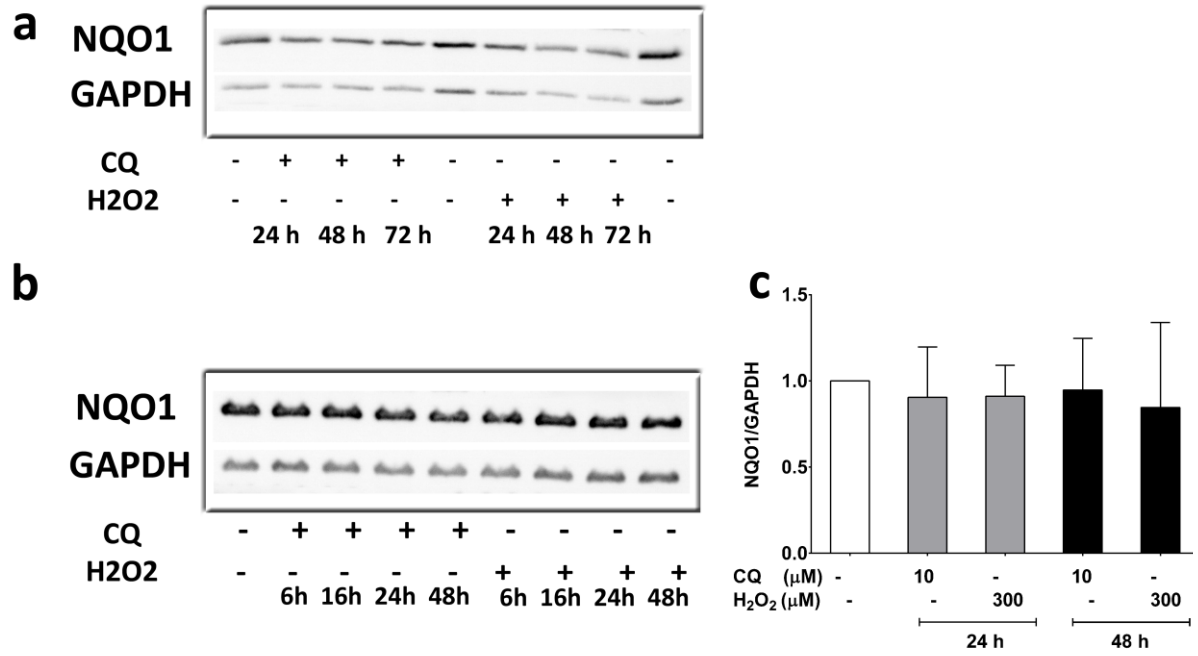

Figure 23: Effect of clioquinol (CQ) on NQO1 protein expression.

HepG2 cells were incubated with CQ (10 µM) and H_2O_2 (300 µM) for different time intervals and harvested at the same time. *(a) Western blot analysis of NQO1 expression in low glucose (1g/l).* 1 µg of cellular protein was separated on a 12 % sodium dodecyl sulfate-polyacrylamide gel. Representative western blot images of NQO1 and GAPDH are shown. Data represent one experiment. *(b) Western blot analysis of NQO1 expression in high glucose (4.5g/l).* 0.5µg of cellular protein was separated on a 12 % sodium dodecyl sulfate-polyacrylamide gel. Representative western blot images of NQO1 and GAPDH are shown. Data represent one experiment out of three independent experiments. *(c)* Densitometry of NQO1/GAPDH relative to the untreated control at 24 h and 48 h time intervals was quantified using ImageJ software. Equal loadings of western blots were ensured by GAPDH. p* <0.05 versus control using one-way analysis variance (ANOVA) followed by Dunnett's multiple comparison tests where appropriate. Error bars = SD.

2.5.4 Interaction of NQO1 with CQ and 8-HQ

The results described in the previous sections demonstrate that CQ-induced cellular toxicity is inversely correlated with NQO1 levels. NQO1 is known to be essential for cells to detoxify numerous compounds such as quinones, quinoneimines, nitroaromatic, glutathionyl-

substituted napthoquinones, dicholorophenolindophenol (DCPIP) and azo dyes into less toxic products [298]. It was therefore speculated that the cytoprotective function of NQO1 against CQ-toxicity could be based on an NQO1-dependent metabolism of CQ into a less toxic metabolite. Human recombinant NQO1 is extremely active in cell-free assays [291] and can convert its substrate compounds in a few seconds at room temperature. CQ and NQO1 were nevertheless reacted under optimal conditions of temperature and substrate availability over 24 h before a possible metabolic conversion of CQ was assessed using mass spectrometry. Under these conditions, unexpectedly no metabolic products of CQ were detected at all **(Figure 24a)**.

An inverse correlation observed between NQO1 levels and CQ toxicity supports the point that there is a possible biochemical interaction between NQO1 and CQ. In the absence of a direct conversion of CQ into a less toxic metabolite, it was therefore hypothesized that CQ might have a direct effect on NQO1 activity instead. Therefore, to explore this possibility, the activity of human recombinant NQO1 was monitored in a cell-free assay by measuring the enzyme-dependent linear decrease in DCPIP absorbance at 600 nm for 60 seconds in the absence or presence of CQ or 8-HQ or dicoumarol (Dic; NQO1 inhibitor). It became evident that both CQ and 8-HQ efficiently inhibited NQO1 activity in a dose range between 10-100 µM **(Figures 24b and c)**. The addition of 10 µM of the NQO1 inhibitor, Dic completely inhibited NQO1-induced reduction of DCPIP. Considering 100 % NQO1 inhibition by Dic, up to 70 % inhibition of NQO1activity was observed when using 100 µM of CQ or 8-HQ while 40-50 % inhibition was observed at already 10 µM of CQ and 8-HQ. This inhibitory activity was further confirmed in HepG2 cells by measuring the change in absorption of WST-1 induced by NQO1-dependent reduction of quinone (menadione). It was demonstrated that WST-1 is reduced to its formazan product only in the presence of functional NQO1, whereas NQO1 inhibitor, Dic can completely abolish the reduction of WST-1 [295]. Consistent with the results from the cell-

free assay, co-incubation of HepG2 cells with menadione as NQO1 substrate and CQ, significantly inhibited WST-1 reduction in a dose- dependent manner with a maximum inhibition at 100 µM of CQ, although a significant inhibition by CQ was already evident at 10 µM ($p=0.0005$). Interestingly, the maximum inhibition by CQ was comparable to the inhibition by the known NQO1 inhibitor Dic at 10 µM **(Figure 24d)**. The IC_{50} of CQ and 8-HQ to inhibit NQO1 activity derived from dose-response curves were 13.4 µM and 6µM respectively **(Figures 25a** and **b)**.

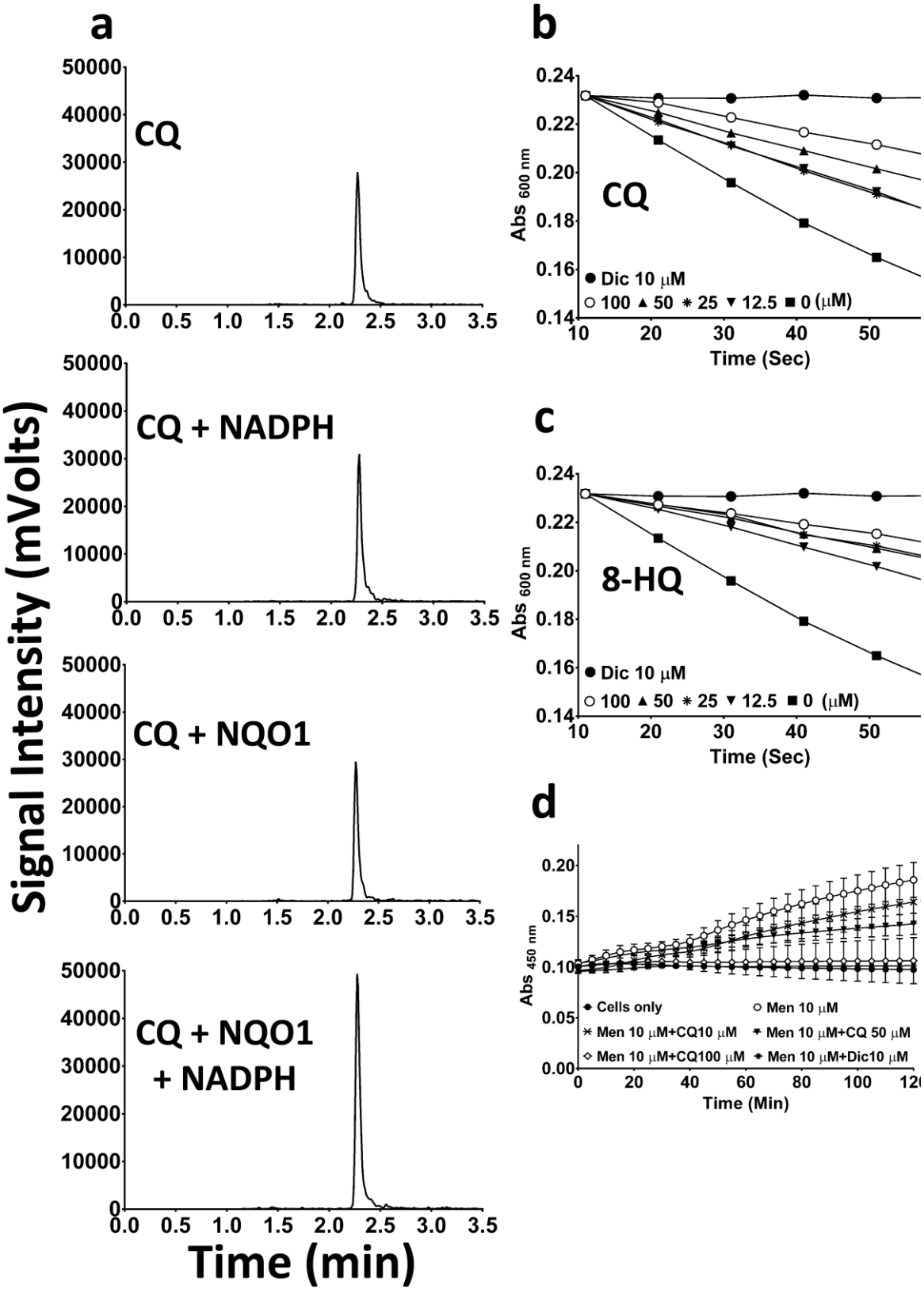

Figure 24: Interaction of CQ and 8-HQ with NQO1.

(a) Mass spectrometric analysis of CQ. Potential metabolic conversion of CQ in the presence of NQO1 and NADPH was analysed by mass spectrometry. *(b, c) Cell-free NQO1 activity*

measurement using recombinant human NQO1. NQO1 enzyme activity in the presence of 12.5-100 µM CQ *(b)* or *(c)* HQ was determined by measuring the NQO1-dependent linear decrease in DCPIP absorbance at 600 nm. *(d) Cellular measurement of CQ-mediated NQO1 inhibition.* Cellular NQO1 enzyme activity in the presence of CQ (10-100 µM) was measured using NQO1 mediated WST-1 dye reduction in HepG2 cells. p* <0.05, p** <0.01 and p*** <0.001 versus control using two-way analysis variance (ANOVA) followed by Dunnett multiple comparison tests. Error bar=SD. Men: Menadione, CQ: Clioquinol, 8-HQ: 8-Hydroxyquinoline, Dic: Dicoumarol.

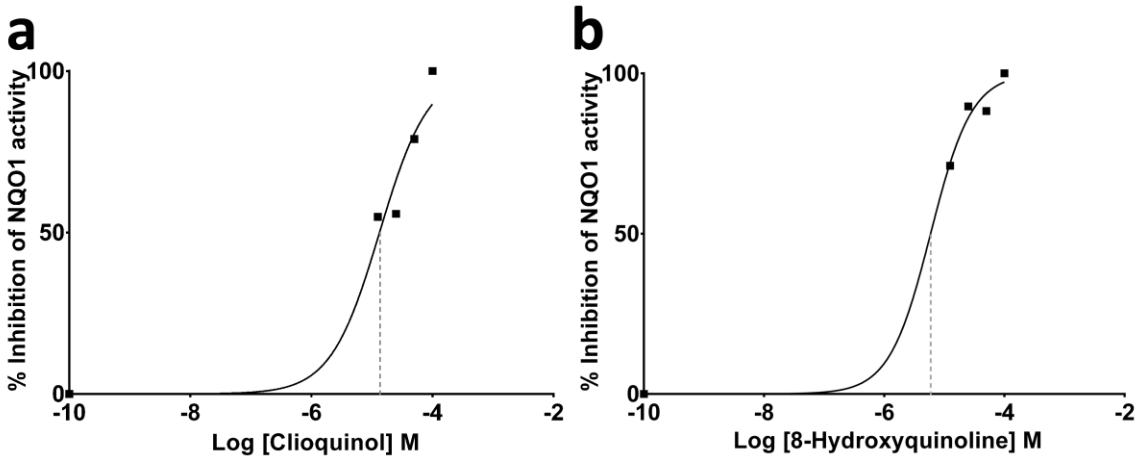

Figure 25: IC_{50} of Clioquinol (CQ) and 8-Hydroxyquinoline (8-HQ) against recombinant human NQO1 activity.

Inhibition of recombinant human NQO1 activity by CQ and 8-HQ was determined by measuring the enzyme-dependent linear decrease in DCPIP absorbance at 600 nm at 60 seconds in a cell-free assay system. IC_{50} of CQ *(a)* = 13.36 µM; IC_{50} of HQ *(b)* =5.97 µM. Data represent values from a typical experiment.

2.6 Discussion

2.6.1 General CQ Toxicity

Many drugs are converted into different metabolites in the body to elicit drug effects. In most cases, drugs are converted to chemically inactive metabolites that react with the respective receptors to evoke therapeutic effects while in some cases, they may be converted to reactive metabolites that produce a toxic response. These drugs may induce toxicity by drug overdose, drug-drug interactions, rare idiosyncratic reactions or adverse effects at therapeutic doses [303]. Some of the examples of drugs being withdrawn from the market due to adverse effects at therapeutic doses include troglitazone, rofecoxib and CQ [208,303].

The mechanism of toxicity associated with CQ has been extensively studied in *in-vitro*. CQ is a lipophilic metal-chelator of iron (Fe), zinc (Zn) and copper (Cu) and is increasingly believed to cause cytotoxicity due to its metal chelation and ionophoric activities [161,176,304]. The ionophoric property of CQ effectively transports chelated metal ions into the cells. Although CQ toxicity has also been observed to be independent of metal ions, many studies have indicated metal-dependent CQ toxicity that is aggravated by the presence of enhanced cation levels [161,176,304,305]. In this context, malignant cells that are characterised by elevated levels of metal ions (Cu, Zn and Fe) are reported to be more sensitive to CQ treatment, hence CQ has been proposed as an effective anticancer agent [176,304].

Treatment of human cancer cell lines with CQ inhibited cell growth and survival in a Zn-dependent manner [304]. Furthermore, CQ-induced cell death was more pronounced in the presence of Zn and Cu [304]. CQ-Zn chelate acted as a mitochondrial toxin in human melanoma cells that altered mitochondrial membrane potential and ultimately caused cellular

toxicity [161]. Similarly, in rat liver mitochondria, CQ uncoupled oxidative phosphorylation thus impairing energy metabolism in the presence of magnesium [306]. The mitochondrial dysfunction due to elevated levels of intracellular metal ions has also been demonstrated in malignant cells [307]. Exposure of prostate cancer cell lines to physiological levels of Zn directly affect mitochondrial function leading to a reduction in mitochondrial transmembrane potential, cytochrome c release and degradation of the anti-apoptotic Bcl-2 protein. This process subsequently triggered caspase activation followed by apoptotic cell death [307,308]. The metal–dependent cytotoxicity of CQ is displayed in malignant cells by its effect on metalloprotein (XIAPs) X-linked inhibitor of apoptosis whose primary function is to inhibit caspase activity and prevent apoptotic cell death [309,310]. CQ was reported to translocate cytoplasmic XIAPs to the nucleus and at the same time caused cytoplasmic clearance of other IAP proteins, thus promoting apoptotic cell death [309]. In addition, it is thought that CQ induces apoptosis in malignant cells by two additional mechanisms, both of which were described to be potentiated by addition of Cu or Zn ions [181,311-313]. It was recently demonstrated that CQ targets Zn to the lysosomes in human malignant cells [181]. The examination of intracellular Zn distribution after CQ treatment in human prostate cancer cells using florescence-labelled probes revealed the co-localization of Zn with lysosomes. Elevated Zn levels in lysosomes are described to disrupt the lysosomal membrane, release proteases known as cathepsins and induce apoptosis in cancer cells [181,313]. The proteasome is responsible for enzymatic degradation of misfolded proteins. Consequently, proteasome inhibition leads to accumulation of excess and misfolded proteins thus impairing regulation of proteins responsible for cell-cycle progression, DNA repair and transcriptions [176]. In malignant cells, CQ inhibits the proteasome through a copper-dependent and independent mechanism. CQ-Cu chelates in human prostate cancer cells or CQ in Cu-enriched malignant cells inhibited proteasome activity, inhibited NFkB, and subsequently induced apoptosis

[312,314]. This is further supported by a significant reduction of NFκB target genes, such as cyclin D1, which is responsible for CQ-induced cell cycle arrest, in a CQ-concentration-dependent manner [315]. In this context, it has to be noted that NFκB activity reduces ROS levels through increased expression of antioxidant proteins including MnSOD, NQO1, HO-1, GPx1 and thioredoxins [316]. Therefore, not surprising inhibition of NFκB activity may lead to excess ROS production and eventually oxidative stress.

The mechanism of CQ-induced cell death has been suggested to be mediated by oxidative stress [179,317]. Exposure of cultured human lung carcinoma cells (A549) to Fe (III) citrate chelate of CQ reportedly induced cell death through increased intracellular levels of Fe. This, in turn, increased cellular lipid peroxidation and DNA strands break, most likely as a consequence of Fenton-reaction derived ROS [317]. However, cytotoxicity of CQ was also reproduced in non-malignant cells although at twice the concentration necessary to induce toxicity in tumor cells [318]. Similar results were observed in the current study, where during long-term treatment, human hepatocarcinoma (HepG2) cells were more sensitive to low dose CQ (up to 5 µM) compared to rodent retinal ganglion cells (RGC5). Nevertheless, both cell lines were equally hypersensitive to high doses of CQ (10 µM), indicating that CQ-induced toxicity at higher concentrations can be cell type-independent. It is worth mentioning that this study addresses two different possible modes of CQ toxicity; one that is NQO1-dependent and the other that is NQO1-independent. The observed cell type-independent CQ toxicity is NQO1-independent toxicity.

It is interesting to note that the concentrations of CQ (≤ 10 µM) used in this study are clinically relevant based on pharmacokinetic studies in animals and humans. In animal models of SMON, peak serum levels of CQ that produced neurotoxicity were approximately 17 µM in monkeys

and 46 µM in dogs [177,319]. In comparison, CQ was administered orally to SMON patients typically around 1.5g/day [175]. In healthy human volunteers that received 3 x 0.5 g CQ /day p.o. over three days, peak plasma concentrations of CQ reached 30 µg/ml (98 µM) [168,177]. This concentration range of CQ is further supported by a phase II clinical trial in Alzheimer's disease (AD) patients. The steady state concentrations after oral administration of 250 mg, 500 mg and 750 mg of CQ resulted in plasma concentrations of 13.19 ±6.87 µM, 22.06 ± 12.11 µM and 24.87 ± 7.037 µM respectively in these patients [188,320]. In the context of drug-induced toxicity, it is striking that the documented plasma concentrations even at the lowest oral CQ dose used in AD patients was higher than the concentration of CQ that completely inhibited cellular viability in RGC5 and HepG2 cells (10 µM) in the present study. It has to be noted however that *in-vitro* toxicity in immortalized cell lines does not necessarily correspond to the observed neuronal side effects of systemic CQ usage in patients.

2.6.2 Is Metal Chelation a Mechanism of CQ-induced Neurotoxicity

CQ has been used extensively for the treatment of diarrhoea and acrodermatitis enteropathica (zinc malabsorption syndrome) between 1950 and 1969. However, its oral form was banned in many countries after it was linked to an endemic outbreak of SMON (subacute mylo-optic neuropathy) that affected at least 10, 000 individuals in Japan [167]. At the time, SMON was characterised by the presence of abdominal pain, subacute ascending dysesthesia, paresthesia of lower extremities and bilateral visual impairment [162,166]. To establish a possible mechanistic connection between CQ and SMON, many toxicological studies were carried out in animals {reviewed by [165,177]}. In animal studies, neurotoxicity was the most prominent adverse effect of CQ [176]. CQ administration in animals (dogs, cats and monkeys) at doses of 200 mg/kg/day for over a month or at doses of 400 mg/kg/day within a week successfully

recapitulated the common pathological features of SMON, including abdominal symptoms preceding to neurotoxicity [175-177]. These animal studies unequivocally demonstrated that CQ is neurotoxic.

In light of recent efforts to develop disease-modifying treatment options for neurodegenerative diseases, CQ and its structural analogues have gained attention and have been re-investigated in preclinical and clinical studies. This apparent emerging neuroprotective effect of CQ and its analogues is in stark contrast to its neurotoxic history. Therefore, numerous studies have attempted to explain the mechanism of CQ-induced neurotoxicity [161,182,184]. CQ is reported to cause neurotoxicity by DNA damage or by disrupting the antioxidant defence system leading to oxidative stress [180,182,184]. In human neuroblastoma cells, CQ induced neurotoxicity at 10-20 μM through DNA double-strands break that lead to the subsequent induction of apoptosis [184]. Similarly, in PC12 cells, CQ (1μM) inhibited nerve growth factor (NGF) signalling, that is essential for neuronal survival, leading to neurite retraction and neuronal death [185]. In the same cell line, CQ treatment also reduced histone acetylation, a process essential for the transcriptional activation of genes that are responsible for cell proliferation [186]. Conversely, the use of a histone deacetylase inhibitor antagonized CQ-induced histone deacetylation restored CQ-induced NGF signalling and prevented neuronal cell death [186].

There is also good evidence that CQ induces neurotoxicity through oxidative stress [180]. CQ treatment (1-3 μM) of cortical cultures containing neurons and astrocytes obtained from B6/129 mice increased oxidative stress after 24 h [180]. As shown for other cell types, the addition of metal ions (Fe^{2+}, and Cu^{2+}) enhanced CQ toxicity and caused cell death even at a previously non-toxic concentration of CQ [180]. These results support the observation of the

present study, where an addition of $ZnCl_2$ to the cell culture medium further enhanced the cytotoxicity of CQ in RGC5 cells. This result is in opposition to the recently proposed hypothesis that metal chelation, which means the removal of metal ions from the culture media, can be regarded as the mechanism of CQ toxicity [182]. CQ is demonstrated to cause neurotoxicity through its effect on the antioxidant defence mechanism which is suggested to be a consequence of its metal-chelation activity. Superoxide dismutases (SODs) are primarily cytoplasmic and mitochondrial ROS detoxifying enzymes that convert superoxide radicals into hydrogen peroxide and molecular oxygen [321]. Most cells express three distinct SOD enzymes. SOD1 (Cu/Zn SOD) is found mainly in the cytoplasm [322], although small fraction can be found in the intermembrane space of the mitochondria [23]. SOD2 (MnSOD) is exclusively present in the mitochondrial matrix [23]. SOD3 contains Cu and Zn in its active site and is mainly extracellular [321]. CQ was reported to inhibit SOD1 at a concentration between 10-50 µM by chelating the metal ions in human-derived neuroblastoma cell lines [182]. Inhibition of SOD1 caused excessive ROS generation and subsequent neuronal cell death through apoptosis [182]. If metal chelation is responsible for CQ toxicity, CQ induced toxicity should be attenuated by supplementing chelated metal ions. When this possibility was investigated in RGC5 cells, the addition of non-toxic concentration of $ZnCl_2$ did not rescue CQ-induced cellular toxicity but rather enhanced it. This suggests that CQ induces neurotoxicity through a mechanism distinct from direct metal chelation. A second hypothesis was put forward where CQ was suggested to induce toxicity through zinc ionophore activity whereby CQ transports zinc across the plasma membrane to increase intracellular Zn levels [304,323]. It has been demonstrated that increased intracellular Zn exposure is associated with oxidative stress [324]. Therefore, the results of the current study could be explained by CQ-induced increased intracellular Zn levels leading to oxidative stress and subsequent cell death of RGC5 cells. This hypothesis is directly supported by our experimental result where an

addition of premixed CQ and Zn to the human kidney cells enhanced cellular toxicity compared to CQ and Zn alone (Farooq M, unpublished data). Previous studies have shown that CQ targets Zn to specific cellular organelles such as mitochondria and lysosomes [161,181]. In the present study, intracellular Zn ions as well their localization were not explored. Based on the previous evidence of CQ-Zn targeting to mitochondria and the *in-vitro* screening results, where CQ and 8-HQ inhibited mitochondrial function (Dilek J, unpublished data), the mitochondrial liability of these compounds were further explored in RGC5 and HepG2 cells. Although RGC5 cells were used for initial experiments to confirm mitochondrial dysfunction of CQ, these cells were not used for subsequent experiments due to the uncertainty regarding the origin of this cell line [325]. The RGC5 cell line was originally described as SV-40-immortalized retinal ganglion cells derived from rat tissue [325]. There is, however, some evidence to suggest that at least some sub-strains in some laboratories are not of RGC origin but are mislabelled 661W cells, a mouse SV-40 immortalized photoreceptor cell line that was generated in the same lab as the original RGC5 line [326,327].

2.6.3 Are CQ and 8-HQ Mitochondrial Toxins?

Under normal culture conditions, cells use glycolysis to generate almost all of the ATP for their metabolic needs and are mostly resistant to the effects of xenobiotics that impair mitochondrial function [296]. However, replacing glucose with galactose yields no net ATP via glycolysis, thus forcing cells to rely entirely on mitochondrial OXPHOS to generate sufficient ATP for survival [296]. Under such conditions, the mitochondrial toxins will show pronounced effects on cellular ATP levels. Long- and short-term treatment of RGC5 cells with CQ and 8-HQ showed that these cells were very susceptible to CQ and 8-HQ toxicity in galactose-containing media compared to glucose-containing media. This selective hypersensitivity therefore

strongly suggests that drug-induced mitochondrial dysfunction as the likely mechanism of action. Since this mitochondrial dysfunction was observed both with CQ and its parent compound 8-HQ, it is likely that the toxicity is not restricted to CQ but applies to the entire class of hydroxyquinoline-compounds.

It is important to note that besides generating ATP, mitochondria are also one of the main sources of cellular ROS (80-90 %) [15]. At the same time, the function of these organelles is highly susceptible to the detrimental effects of oxidative stress [15]. Superoxide radicals can attack iron-sulfur centers in the mitochondrial ETC enzymes, which causes the release of free ferric iron [321]. This free iron then catalyzes the generation of reactive hydroxyl radicals from H_2O_2 and superoxide radicals through the Haber-Weiss reaction [321]. Depending on their concentrations, ROS are known to transmit both beneficial as well as detrimental effects on different cellular processes [13]. At low concentration, ROS regulate cellular functions through redox-dependent signalling and redox-dependent transcription factors [13]. However, at high concentrations ROS impair vital cellular processes as a consequence of their damaging effects on cellular macromolecules such as protein, lipids and DNA [13]. In this study, this effect was examined by measuring lipid peroxidation in the presence of CQ in the hypersensitive RGC5 cells. Consistent with mitochondrial impairment, CQ significantly increased lipid peroxidation in RGC5 cells. These findings support previous studies, where CQ induced cell death in *in-vitro* through mitochondrial dysfunction and enhanced lipid peroxidation [161,179].

One of the conundrums in this context is that elevated ROS levels may be causal for mitochondrial dysfunction or on the other hand, may be the result of mitochondrial dysfunction itself. In this study, there was a realistic possibility that CQ-mediated ROS could have been upstream of mitochondrial dysfunction. However, this possibility was practically ruled out by

showing that downstream events of ROS-mediated mitochondrial dysfunction, such as reduced cellular ATP levels, increased lipid peroxidation and cell death could be attenuated by several antioxidants that presumably reduced elevated ROS levels. It was surprising to observe that ROS was mainly detected at the level of lipid peroxidation whereas use of the predominantly water soluble ROS-indicator dye CM-H_2DCFDA, did not provide any evidence of ROS. This illustrates that CQ does not lead to uniformly elevated ROS production across the cell but a rather restricted localisation to the membrane compartment. Another explanation is that the particular CQ-induced ROS-species is not detected with this particular dye since most dyes do not equally react with all ROS species. For example, CM-H_2DCFDA does not react with superoxide, singlet oxygen or hypochlorous acid to produce the fluorescent product [328-330]. Based on the data of the current study, it is possible that CQ-induced ROS generation impairs mitochondrial function, and also lead to lipid peroxidation. Although, mitochondrial ROS production, in particular was not directly confirmed in CQ-treated cells in this study, overall, the results strongly indicate that oxidative stress is at the core of CQ-induced mitochondrial dysfunction.

Although HepG2 cells showed some CQ and 8-HQ cytotoxicity in long-term treatment in glucose-containing media, all attempts to confirm mitochondrial dysfunction in the form of ATP depletion or increased lipid peroxidation failed in these cells. This was further confirmed by measuring lactate levels, another characteristic metabolic signature of mitochondrial dysfunction. Using the well-known mitochondrial toxin, rotenone, mitochondrial dysfunction significantly increased lactate levels in HepG2 cells, while surprisingly a 100-fold higher CQ concentration increased lactate levels only slightly. CQ at this higher concentration was evidently cytotoxic, limiting cell proliferation and reducing clonal cell viability. This cytotoxicity explained the low lactate levels in response to CQ. When lactate levels were

standardized on residual protein levels in each reaction, lactate levels/protein showed a dramatic increase in CQ-treated cells, which suggests that cells died in response to CQ-treatment before they were able to synthesize significant levels of lactate. These results suggest that in addition to mitochondrial dysfunction in the absence of NQO1, there is likely an additional NQO1-independent mechanism of CQ cytotoxicity in HepG2 cells. Several different additional mechanisms related to CQ-induced toxicity in cancer cell lines have been proposed, such as inhibition of the 20S proteasome, disruption of a lysosomal membrane through both metal-dependent and independent mechanisms, DNA damage [176,181,183,184,313,314].

2.6.4 Is CQ-induced Mitochondrial Dysfunction Dependent on NQO1?

A growing body of evidence suggests that NQO1 plays a crucial role in modulating mitochondrial function and cellular viability [331,332]. NQO1 is an FAD-containing cytosolic protein that catalyses the two-electron reduction of quinone compounds to prevent the formation of reactive semi-quinones, free radicals and ROS, which thus protects cells from oxidative stress [333]. In addition to the indirect prevention of superoxide formation, NQO1 can directly scavenge superoxide as well. Furthermore, due to its redox activity, NQO1 can maintain the two essential endogenous antioxidants, Vitamin E and ubiquinol, in their anti-oxidant state to regulate cellular ROS levels [333]. It has been shown that NQO1 overexpression renders cells resistant against mitochondrial toxins of the electron transport chain such as rotenone and antimycin [331,332]. In contrast, cells with low or absent levels of NQO1 are characterized by increased oxidative stress, reduced ATP production as well enhanced cellular vulnerability to mitochondrial toxins [332]. This has also been demonstrated *in-vivo* where compared to the wild-type mice, NQO1 knock-out mice showed high sensitivity to drug-induced hepatotoxicity, increased ROS levels, reduced ATP synthesis and severe

mitochondrial dysfunction [331]. These findings strongly suggest that there is an association between NQO1 and mitochondrial function and a better understanding of this link would be warranted to gain insight if this process is associated with the pathology of the mitochondrial disease.

The putative role of NQO1 as endogenous antioxidant was observed in the present study where expression of NQO1 was positively correlated with cellular protection against CQ-induced toxicity. In NQO1 deficient cells (HEK293-neo), significantly reduced ATP levels, increased lipid peroxidation and reduced cellular viability were observed in the presence of CQ. However, cells with higher NQO1 levels (HEK293-clone6/12) showed protection against CQ-induced reduction in cellular ATP levels, increased lipid peroxidation and reduction in cellular viability. These results suggest a pivotal role of NQO1 in the protection against CQ-induced cellular mitochondrial-dysfunction. This protective role of NQO1 against CQ-induced toxicity observed in the present study is in good agreement with previous studies. Neuronal cell lines used as an *in-vitro* model for the study of CQ-induced neurotoxicity include the human neuroblastoma cell lines (SH-SY5Y, IMR-32) and primary neurons. These cells are characterised by low levels of endogenous antioxidant defence systems and in particular, low NQO1 expression [180,334,335]. It is likely that this reduced NQO1 expression, predisposed these cells to CQ-induced toxicity. Interestingly the neurotoxic concentrations previously reported for these cell lines are very consistent with the results of the present study [180,334,335].

Beside its antioxidant function, NQO1 is also essential to stabilize the tumor suppressor protein p53, which regulates the expression of genes that modulate cell-cycle checkpoints, apoptosis, DNA repair and the cellular stress response [298,321]. And it is important to note that p53 is

the most commonly inactivated gene in cancer cells [321]. Under normal conditions, cellular p53 levels are maintained at low levels due to a rapid degradation by the 20S proteasome [321]. However, in response to different forms of stress, NQO1 acts as a gatekeeper of the proteasome, binds to p53 and prevents its entry into the proteasome. This process causes a rapid accumulation of p53 protein levels that are then able to perform a multitude of functions [321]. In line with the p53 stabilizing role of NQO1, NQO1 knock-out mice showed lower p53 levels and consequently decreased rates of apoptosis [336]. This tight connection between NQO1 and p53 is also illustrated by the significant susceptibility of NQO1-deficient mice towards induced malignancies, which is undistinguishable from the phenotype of p53 knock-out animals [336-338]

The present study demonstrated a clear protective effect of NQO1 against CQ-induced mitochondrial-dysfunction. However, NQO1 is mainly described to be a cytoplasmic protein and has not yet been reported to translocate to the mitochondria. Therefore, it is unlikely that NQO1 exerts its mito-protective role by a direct interaction with the mitochondria but rather via some indirect activity involving additional signalling molecules or proteins. One possibility is that the NQO1-dependent protection against CQ-induced mitochondrial-dysfunction could be transmitted through an NQO1-mediated activation of p53-target genes. In addition to its regulatory function of cell death, p53 is increasingly reported to regulate the cellular antioxidant defence system and metabolic pathways that reduce glycolysis and increase oxidative phosphorylation [339,340]. The antioxidant properties of p53 are mediated to some extent through induction of the mitochondrial antioxidants ALDH4 (aldehyde dehydrogenase 4), GLS-2 (glutaminase 2) and TIGAR (TP53-induced glycolysis and apoptosis regulator) that ultimately facilitates the production of the reduced form of glutathione and the rest through transcriptional induction of the antioxidant proteins peroxiredoxin reductase and glutathione

peroxidase 1 (GPx) [340]. It is possible that this NQO1/p53-mediated upregulation of mitochondrial antioxidants is able to rescue CQ-induced mitochondrial dysfunction seen in the present study. Although both HepG2 and HEK293 cells used in the current study express wild-type p53, they differ significantly in their expression levels [341,342]. Expression of p53 in HepG2 cells is significantly higher than in HEK293 cells which correlate well with the NQO1expression in these cells. However, this study did not explore the p53 status of the cell lines used. Moreover, the HEK293 cells used in this study were stably transfected with NQO1 expression plasmids and no attempts have been made to measure differences in NQO1-mediated p53-induced gene expression. Therefore, the above hypothesis of NQO1 dependent protection against CQ-toxicity via p53-dependent gene expression needs to be further explored. In particular, the expression of p53-dependent mitochondrial antioxidant proteins such as peroxiredoxins and GPx need to be assessed.

Another possibility for NQO1-dependent protection against CQ toxicity could be due to a direct effect of NQO1 on ROS. NQO1 is also known to directly scavenge superoxide and therefore may directly inhibit CQ-induced ROS-production as well as all subsequent events such as mitochondrial dysfunction, lipid peroxidation and cell death.

2.6.5 Is NQO1 Expression Upregulated by CQ-induced Oxidative Stress?

NQO1 is generally highly inducible and NQO1 expression is regulated by a protein complex consisting of the nuclear factor erythroid 2-related factor 2 (Nrf2) and Kelch-like ECH-associated protein 1 (Keap1) [343]. Under normal physiological conditions cytoplasmic Nrf2 binds to the ubiquitin ligase systems (Cullin 3-base-E3 ligase) via Keap1, which promotes continuous ubiquitination and proteasomal degradation of Nrf2 [343]. Under conditions of

oxidative stress, some of the highly reactive cysteine residues at positions 257, 273, 288 and 297 in Keap1 are easily attacked by radicals, which destabilizes the complex with Nrf2 [298,344,345]. As a result, Nrf2 is not ubiquitinated but rather accumulates in the nucleus, where it binds to the antioxidant-response elements (ARE) in the promoter regions of its target genes. This binding promotes increased transcription of a broad range of cytoprotective genes such as heme oxygenase (HO-1), γ-glutamyl-cysteine-ligase (GCL), glutathione S-transferase (GST), glutathione peroxidase (GPX) as well as NQO1 [344,346]. A significant part of this cellular response to pro-oxidative conditions can be attributed to NQO1 since induction or knockdown of NQO1 is directly associated with decreased or increased levels of oxidative stress [298]. Since it was observed that CQ-toxicity is mediated by oxidative stress, it was hypothesised that NQO1 protein expression might increase in response to oxidative stress. When this hypothesis was examined in HepG2 cells both under low and high glucose condition, CQ at 10 µM and even H_2O_2 (300 µM) did not increase NQO1 expression at any time point compared to untreated controls. These results, however, are in contrast to previous studies in HepG2 cells where increased NQO1 expression in response to oxidative stress was shown [301,302]. One explanation for this unexpected result in the present study could be the presence of extremely high basal NQO1 expression levels in HepG2 cells, as seen in this present study, which may not allow further increase by pro-oxidants. A second possibility could be the experimental condition including pro-oxidant concentrations and their incubation periods. It is possible that the constant exposure of the cells to high concentrations of CQ and H_2O_2 may fail to upregulate NQO1 expression. The shortest incubation period of the present study was 6 hours, which might be already too long to observe oxidative stress-mediated NQO1 induction at high CQ concentrations. Therefore, it would be interesting to explore if NQO1 could be induced in HepG2 cells or other cell lines under different conditions such as lower CQ concentrations over longer exposure times or at higher CQ doses over shorter periods of time.

Additionally, it would also be of interest if NQO1 can be induced in cell lines that are characterised by a low basal NQO1 expression, such as human neuroblastoma cell lines or even primary cultures [334,347].

2.6.6 How Does NQO1 interact with CQ/8-HQ?

Generally, NQO1 is known as a detoxifying enzyme, as it detoxifies a number of compounds, such as quinones, into less-reactive and less-toxic metabolites [333]. This suggested that the cytoprotective effect of NQO1 against CQ-induced toxicity demonstrated in this study could also be the result of a direct NQO1-mediated detoxification of CQ to less reactive metabolites. However, no evidence could be found for this. First of all, CQ is chemically unrelated to all known NQO1 substrates and secondly, mass spectrometry analysis of CQ reaction products in the presence of NQO1 under optimal conditions failed to provide any evidence of metabolic conversion.

Structural and functional studies of NQO1 have shown that NQO1 contains two active binding sites that work via a "ping-pong" mechanism {reviewed by [300]}. One site binds the electron donor NAD(P)H and another site is for substrate binding such as quinones. Once NAD(P)H binds to NQO1, it reduces the tightly bound cofactor flavin adenine dinucleotide (FAD) to $FADH_2$, while $NAD(P)^+$ is released from the active site. This allows the second substrate to bind and subsequently be reduced by $FADH_2$. One of the best-studied inhibitors of NQO1 is dicoumarol [(Dic), 3,3′-methylenebis (4-hydroxycoumarin)], which is one of the most potent known competitive inhibitors of NQO1. Dic competes with NAD(P)H for binding to NQO1 and thus prevents the reduction of FAD to $FADH_2$. In the absence of a direct metabolic conversion of CQ by NQO1, it was speculated if CQ or 8-HQ may interact with the Dic-binding

site of NQO1. To explore this possibility, NQO1 enzyme activity was examined both in cell-free and cell-based systems in the presence of CQ or 8-HQ or Dic. The extent of NQO1 inhibition by CQ in cell-free and cellular system varied. At CQ (10 μM), inhibition of NQO1 activity was around 40-50 % (when considering the Dic effect as 100 % inhibition) in the cell-free system, whereas in the cellular system it was only around 25 %. It is important to note that in cells, NQO1 inhibition was measured by NADPH-dependent NQO1-mediated quinone reduction to hydroquinone, which in turn reduces WST-1. The observed differences in inhibition could, therefore, be attributed to the additional electron transfer steps inherent to the cell-based measurement system, which is absent in the cell-free system. Another point to note is the obvious difference of CQ and quinone uptake into the cells that is required to measure NQO1 activity in cells. Furthermore, varying NADPH levels and the presence of other redundant enzymes such as VKORC1 (vitamin K oxidoreductase C1) in the cells are all parameters that can influence the final results. Irrespective of these limitations, in both systems, lower CQ concentrations (10 μM) were not as potent as Dic while higher CQ concentrations (100 μM) showed comparable inhibitory activity towards NQO1. These results suggest that NQO1 inhibition by lower concentrations of CQ and its associated mitochondrial-dysfunction can become relevant in cell lines that already have a low NQO1 expression such as HEK293 and RGC5 cells. This was not the case in high NQO1 expressing HepG2 cells where a slight inhibition of NQO1 by CQ may not be sufficient to induce mitochondrial-dysfunction. Most importantly, this NQO1 expression-dependent effect can be of great importance when looking at heterozygous carriers of the inactivating NQO1 polymorphism. These individuals should be at a relatively greater risk of losing more of their residual NQO1 activity by a direct inhibition by CQ exposure. This finding is quite relevant to the SMON cases reported in Japan where the majority of the population is carrying the inactivating NQO1 polymorphism. Hence, it is possible that due to this deficiency, CQ more severely affected this population group compared

to the rest of the world.

Overall the *in-vitro* results of the present study suggest that CQ can directly inhibit NQO1 activity, especially under conditions of low NQO1 expression, which in addition to the direct CQ effects on ROS levels described above can further exacerbate toxicity.

CHAPTER 3

Chapter 3: *In-Vivo Studies*

3.1 Overview/Rationale

The *in-vitro* results described above strongly indicate that CQ-induced toxicity is negatively correlated with NQO1 expression. In order to translate the in-*vitro* results to an *in-vivo* system, a suitable animal model was required. To confirm our findings in *in-vivo*, the essential requirement of an animal model should include conditions of both high and low NQO1 expression. Zebrafish are a suitable candidate for this purpose because only recently it was reported that they lack retinal NQO1 expression during their early larval stages (7 dpf), while subsequently NQO1 is highly expressed in the adult retina [348]. The other benefits of using zebrafish lie in the possibility to perform higher-throughput drug toxicity screening, a rapid eye development that allows to test visual function already at 5 dpf, a visual system that reflects the human situation in many respects including cone-dominant vision and finally a plethora of genetic information that is available from zebrafish mutants associated with defective visual development and function [220]. Therefore, visual function was examined in zebrafish in the presence of CQ. The visual function was measured using a visual behavioural test, known as the optokinetic response (OKR). There are other visual behavioural tests described for zebrafish such as optomotor response, startle response, phototactic behaviour and escape response [220]. However, the advantages of the OKR include the ability to use larvae from only 5 dpf, reliability and specificity (tests each and every individual animal) while these characteristics not all associated with any of the other assays. Hence, in the current study, OKR was employed to examine the visual function test in zebrafish.

3.2 Aim and Objectives

The overall aim of the *in-vivo* study is to investigate the connection between NQO1 levels and CQ-induced toxicity.

To achieve this aim, I:

- investigated the effect of NQO1 expression on visual acuity of CQ-treated zebrafish
- examined histological sections of zebrafish retina
- examined NQO1 expression and activity in the adult zebrafish retina

3.3 Materials and Methods

3.3.1 Animal Husbandry

All animal experiments were approved by the Animal Ethics Committee (AEC), University of Tasmania, Australia (Animal Ethics approval numbers: A12817 and A0015097) and were carried out according to ARRIVE guidelines ([349]. The husbandry of adult wild-type zebrafish (petstore-purchased; PET and AB strains) was carried as previously described [350]. Fish were raised under standard conditions (14:10 light: dark cycle, 26-28 ˚C) in a recirculating system (Zebtec, Techniplast, USA for PET strain and Z-hab mini system, AquatiHabitats, Pentair, US for AB) that continuously aerates and filters the water in order to maintain a healthy aquatic environment. Water parameters were monitored daily and maintained to ensure a predefined target range (pH: 6.5-7.5, conductivity 690-750 µs, bicarbonates 30-35 (mg/l), nitrite: 0 mg/l, nitrate: 0-10 mg/l). Zebrafish were fed twice per day with flake food (Nutrafinmax) in the morning and in the evening and with brine shrimp (hatched in-house from artemia cysts: Inve group) in the morning (3 drops of concentrated brine shrimp per fish from a 5 ml syringe). Breeding of zebrafish was set up fortnightly. Zebrafish were allowed to spawn

and eggs were collected 4 h after the lights turned on at 8 a.m. Fertilized eggs were cultured in embryo media 0.5 x E2 (7.5 mM NaCl; 0.25 mM KCl, 0.5 mM $MgSO_4$, 0.075 mM KH_2PO_4, 0.025 mM Na_2HPO_4, 0.5 mM $CaCl_2$, 0.35 mM NaHCO3) [351] in an incubator in the dark at 28.5 ± 0.5 ˚C.

3.3.2 Maximum Tolerated Concentration (MTC) in Zebrafish Larvae

The assessment of a maximally tolerated drug concentration (MTC) in fish was performed according to a protocol described previously [281,286]. Briefly, in a 12 well culture plate, 3 dpf PET or AB strains larvae (n=10) were placed in individual wells at 2 pm. Larvae were exposed to one compound concentration per well. Seven concentrations of the drug (CQ) ranging from 1 mM, 0.3 mM, 100 µM, 30 µM, 10 µM, 3 µM, 1 µM (PET) and four concentrations of NQO1 inhibitor, dicoumarol (Dic) ranging from 0.01, 0.1, 1, 3 µM (AB) were tested. The larvae were incubated with the compounds for 48 h at 28.5 ± 0.5 ˚C in the incubator. Toxicity was assessed after 24 h and 48 h of drug exposure based on the following criteria: absence of heart beat, loss of startle response (using dish tapping and sudden exposure to light), swim position (loss of dorsoventral balance), morphological aberration (pericardial oedema, bent body, failure to inflate swim bladder). Overall, the assays were not evaluated if more than 10 % of the untreated control larvae also showed signs of toxicity.

3.3.3 Drug Treatment in Adult Zebrafish

Unlike for larvae, MTC was not determined for the adult zebrafish. Instead PET strain adult zebrafish in the age range between 1.5-2 years were treated with the CQ concentration that produced visual toxicity in larvae. Adult zebrafish (n=4) were placed in a small tank containing

a litre of system water and were left overnight to settle. Subsequently, the fish were exposed to drugs including CQ or a known NQO1 inhibitor, Dic or a combination of CQ and Dic for 48 h under standard conditions (14:10 light: dark cycle, 26-28 ˚C). The control fish were exposed to 0.1 % DMSO (solvent control). During the treatment period, feeding was carried out according to a standard husbandry. Feeding was stopped 24 h before OKR measurement to avoid regurgitation during an anaesthetic procedure. Similar to the assessment of toxicity in larvae, the assessment of toxicity in adult fish was done after 24 h and 48 h of drug exposure and was based on the following criteria: absence of a heartbeat, eating behaviour, loss of dorsoventral balance. Overall the assays were not evaluated if the control fish also showed signs of toxicity.

3.3.4 Optokinetic Response (OKR)

3.3.4.1 OKR in Zebrafish Larvae

The OKR in zebrafish larvae was measured using a commercial system (Visio Tracker TSE systems, Germany) according to a previously described protocol [352]. OKR was measured in zebrafish by a staircase approach whereby the stimulus parameter was increased from the lowest to the highest setting followed by a stepwise decrease back to the lowest setting. Each step in this staircase approach lasts for 9 secs with sinusoidal changes of direction (3 number of cycles, i.e from right to left, left to right and again from right to left, each cycle lasting for 3 secs) [263]. At 5 dpf all larvae were transferred in fresh egg media from the treatment plate and OKR was performed from 2 pm to 5 pm. Briefly, larvae were immobilized in pre-warmed 3 % methylcellulose solution in 35 mm petri-dishes. The larvae were well mixed into the methylcellulose mixture and were positioned dorsal side up. Any air bubbles generated during this process were removed using a small needle. The fish were left in methylcellulose for 5-10

min against a white background under flickering light allowing enough time for them to embed and to avoid any spontaneous body movement that could impair the experimental data during the stimulus exposure. The petri dish containing larva was placed on the Visio Tracker instrument before the camera was focused on the eyes. The fish were exposed to a computer-generated stimulus pattern that consists of rotating black and white stripes. The stimulus was run at varying absolute velocities (5, 7, 10, 15, 20, 25, 30 deg/sec) and constant contrast (10 %) and spatial frequency (0.11 cycles/ degree) for about 2 min. Before initiation of eye velocity measurements, the fish were pre-stimulated with contrast (10 %), spatial frequency (0.11 cycle/deg) and angular velocity (7.5 deg/sec) for a total of 9 secs for experiments conducted at varying absolute velocities. The word contrast refers to the difference between black and white moving stripes, spatial frequency refers to the frequency of direction changes of stripes and angular velocity refers to the speed of rotation of stripes. The raw eye velocity measurements were filtered for saccades to extract slow-phase velocity. In order to smooth the saccade-filtered eye velocity curves, averages were calculated using a sliding window of 7 frames. The average velocities of both right and left eyes at varying stimuli (angular velocities) were calculated in real time (deg/sec) and finally compared between the DMSO- and drug-treated groups.

3.3.4.2 OKR in Adult Zebrafish

The OKR in adult zebrafish was measured according to previously described protocols [262,263] (**Figure 26**). As for larvae, the OKR in adult zebrafish was also measured by staircase approach whereby the stimulus parameter was increased and then decreased stepwise with each step lasting for 6 secs in unidirectional changing direction [263]. Before initiation of eye velocity measurements, the fish was pre-stimulated for a total 9 secs at 99 % contrast, 0.2

cycle/deg spatial frequency and 12 deg/sec angular velocity. For the adult zebrafish, both eyes were stimulated with a unidirectional motion stimulus (from right to left) but the evaluation was done only in one eye (right) as this allows more precise positioning of the eye that was being examined. After 48 h of drug exposure, the fish were transferred to a tank containing system water. The fish were briefly anesthetized with 300 mg/l MS-222 dissolved in system water and clamped between two pieces of sponge and plastic to restrain the body movement while the head and gills were left free. A single fish was placed in a flow-through chamber where the gills were supplied with a constant flow of oxygenated water, which was designed to recirculate back to the supply tank through an outlet present in the flow chamber. The water in the supply tank was maintained at 28 °C ± 0.5 °C using an aquarium heater (Eheim aquatics, Germany) and oxygenated using an air pump. The flow through chamber was kept under the visual field of the camera and the fish were exposed to a computer-generated stimulus pattern consisting of black and white stripes at constant contrast of 99 %, 0.2 cycles/ degree spatial frequency and at varying absolute velocities of 5, 10, 12, 15, 20 deg/sec for nearly 2 min. The raw eye velocity measurements were filtered for saccades to extract slow-phase velocity. In order to smooth the saccade-filtered eye velocity curves, averages were calculated using a sliding window of 3 frames. The average eye velocities of only the right eyes at varying stimuli (angular velocities) were calculated in real time (deg/sec) and finally the DMSO- and drug-treated groups were compared.

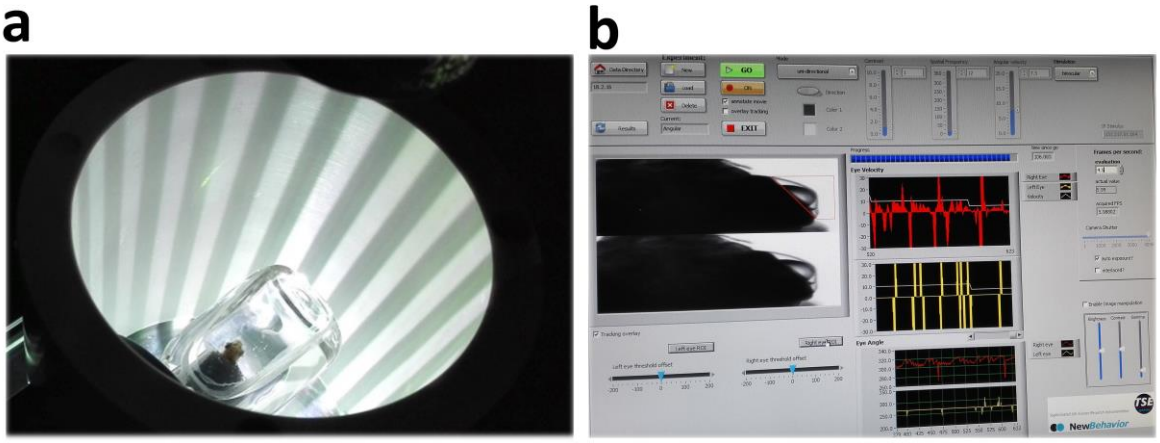

Figure 26: Experimental set-up of optokinetic response (OKR) measurement in the adult zebrafish.

(a) Adult zebrafish, immobilized in a flow-through chamber to restrain the body movement, were exposed to the visual stimulus of rotating black and white stripes. *(b)* The right eye was evaluated by precisely controlling its position.

3.3.5 Termination of Experiment and Tissue Harvesting

The larvae and adult zebrafish were euthanized using a rapid cooling technique according to the protocol in the AVMA (American Veterinary Medical Association) guidelines on euthanasia (2013), whereby the fish irrespective of age are transferred to 2-4 °C water for at least 20 minutes. In the case of adult zebrafish, the eyes were removed using a scalpel and fine forceps, whereas for the larvae the whole fish were used. The harvested tissues were either fixed in 4 % PFA (in PBS) to carry out histological analysis on paraffin sections and cryosections or snap-frozen in liquid nitrogen and stored at -80 °C for subsequent western blot analysis.

3.3.6 Histology

3.3.6.1 Mold Design

To enable higher throughput histology of zebrafish larvae an embedding mold was designed according to a previously described protocol [353] (**Figure 27a**). Briefly, the mold measures 35.5 mm by 17 mm, width 2 mm, surrounded by 4 mm walls along the length of the structure and was designed using AutoCAD 2015 Student version (**Figure 27a**). The mold consists of arrays of triangular teeth measuring 4 mm (base to apex), 0.8 mm base width and 1 mm in height (approximately equal to a dimension of 5-7 dpf larvae). Each tooth is separated by a distance of 1.2 mm. The mold-design was printed on two different 3D printers: Object Eden260VS Dental Advantage^{TM} (Stratasys) printer or Miicraft digital micromirror device (DMD)-based 3D printer (Miicraft, Hsinchu, Taiwan). The polymer called ink veroclear was used with Object Eden260VS Dental Advantage^{TM} and a colourless or blue coloured epoxy/acrylate resin was used with Miicraft. The Object Eden260VS Dental Advantage operates by spraying liquid polymer drops in tiny layers followed by a UV light curing procedure [354]. Although the proprietary clear polymer (Ink Veroclear RGD 810, Stratasys) produced a strong and durable mold, the mold lacked smooth edges, especially on the base of the triangular structures, due to insufficient resolution (**Figure 27b**). In contrast to the Dental advantage system, the Miicraft DMD printer operates by building each layer individually and adding up each successive layer on top of the previous layer and the process is repeated until the model is completed upside down, which is subsequently postcured [355]. The final products obtained from the Miicraft printer varied in resolution depending on the resin that was used. The photosensitive colourless polymer (acrylate/epoxy resins) provided strength as well as a better resolution of the finished product compared to a product obtained from Object Eden260VS Dental Advantage^{TM} printer (**Figure 27c**). However, an even higher-resolution

end product was obtained from the Miicraft printer when the proprietary blue resin was used (**Figure 27d**). The optical transparency was not critical to the function of the mold whereas the high resolution of the mold was essential to achieve the right size pockets that exactly fit the zebrafish larvae. Therefore, for experiments involving histology of zebrafish larvae, only the blue resin was used for printing the embedding mold.

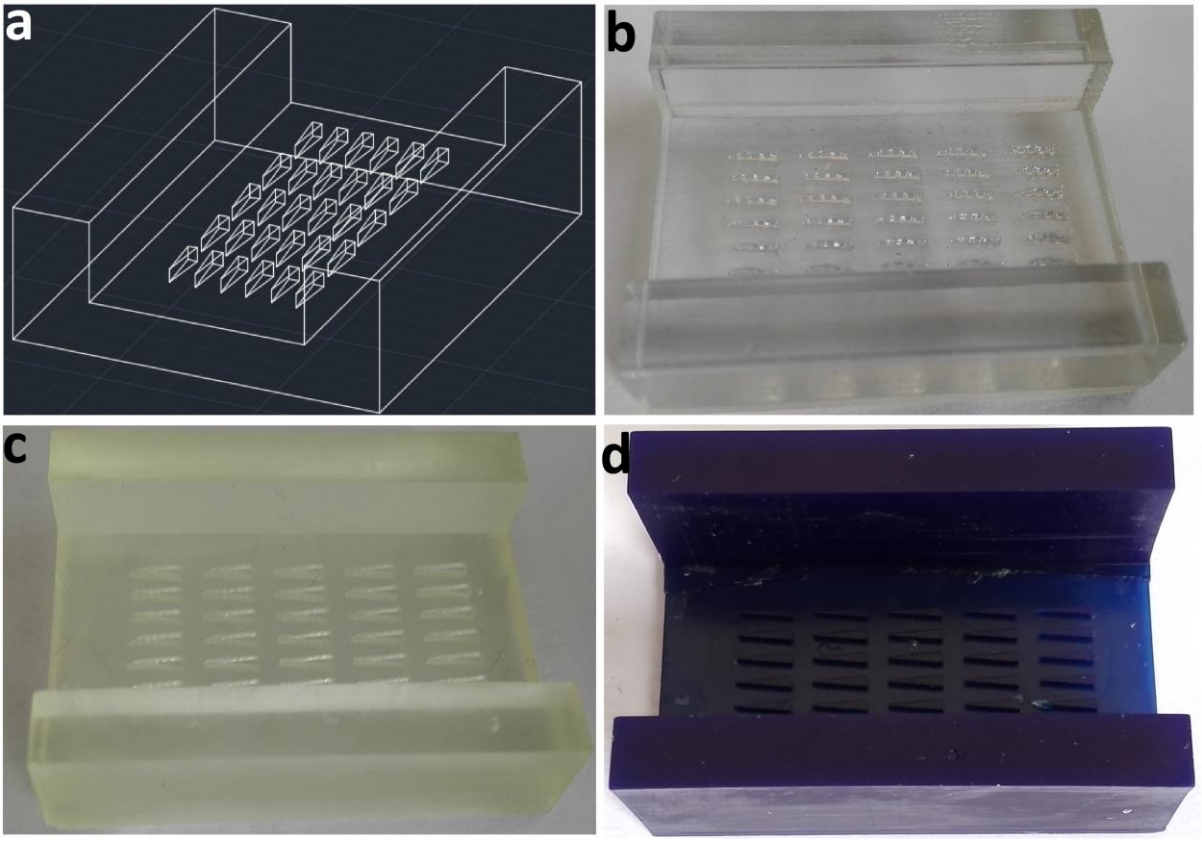

Figure 27: Mold-design for agarose embedding of zebrafish larvae.
The mold-design was printed in different materials using two different 3D printers. *(a)* AutoCAD construction image used for 3D printing, *(b)* mold printed in Object Eden260VS Dental Advantage ™ printer using Ink veroclear (polymer), *(c)* mold printed in Miicraft digital micromirror device using clear resin, *(d)* mold printed in Miicraft digital micromirror device using blue resin.

3.3.6.2 Tissue Fixation

After euthanasia in ice-cold water, 5 dpf zebrafish larvae and adult zebrafish eyes were fixed in 4 % PFA (in PBS, pH 7.4) for overnight at 4 °C.

3.3.6.3 Using the 3D-printed Embedding Mold

To fill the mold described in **3.3.6.1** with embedding agarose solution, the open slides of the mold were closed using sticky tape. 1 % agarose in distilled water was heated in a microwave for 2 min to dissolve the agarose. The solution was allowed to cool down to around 55 °C and was subsequently used to fill the mold with warm agarose solution. The volume of the solution needed to cast a mold was calculated based on the following formula:

[mold length x mold width x agarose depth (4 mm)] – [(volume of tooth) x number of teeth)]

$[35.5 \times 17 \times 4] - (0.5 \times 4 \times 1 \times 0.8) \times 30\ mm^3$

$2366\ mm^3 = 2.366\ cm^3 = 2.366\ ml$

After the agarose had solidified, the tape was removed and the agarose block peeled out of the mold. Fixed zebrafish larvae were then transferred to the wells (one in each well) using a stereomicroscope and a fine needle followed by filling the wells with 55 °C agarose solution to immobilize the embryos. The solidified agarose block was placed in a labelled cassette, immersed in 70 % ethanol and kept in the auto-processor until the tissues and agarose block were dehydrated, cleared and infiltrated.

3.3.6.4 Tissue Processing

Tissue processing was carried out using a Leica ASP 200 auto-processor (Leica Biosystems, VIC, Australia). Before the tissue was infiltrated with paraffin wax, the water in the tissue was removed completely as water and wax are immiscible. Therefore, tissue processing involved series of steps including dehydration in increasing concentrations of ethanol, clearing in xylene before finally infiltrating in paraffin wax (**Table 5**).

Table 5: Steps in zebrafish tissue processing

Solution	**Duration (Minutes)**	**Temperature (°C)**
Ethanol 70 %	15	37
Ethanol 95 %	30	37
Ethanol absolute	15	37
Ethanol absolute	15	37
Ethanol absolute	15	37
Ethanol absolute	20	37
Xylene	35	37
Xylene	35	37
Paraplast wax	60	60
Paraplast wax	60	60
Paraplast wax	60	60

3.3.6.5 Embedding and Sectioning

The agarose blocks containing larvae as well as processed adult zebrafish eyes were embedded into paraffin wax blocks using a metal mold.

A microtome (Leica 2250 microtome, Leica Biosystems, VIC, Australia) was initially adjusted to 10 µm for coarse sections followed by 4 µm sections when the area of interest was reached.

Sections were mounted on IHC microscopy slides (Dako, NSW, Australia) and dried overnight at 37 ˚C.

3.3.6.6 H & E Staining

Paraffin sections were dewaxed in fresh xylene 1 and 2 for 5 min each, 100 % ethanol, 95 % ethanol, 70 % ethanol for 2 min each. Subsequently, the sections were incubated with Mayer's haematoxylin (H) for 5 min before exposure to ammonia water for 30 sec to stain nuclei blue. The sections were counterstained with eosin (E) for 1 min and dehydrated with 95 % ethanol for 30 sec, 2 steps of 100 % ethanol for 1 min each and finally cleared in 2 steps of fresh xylene for 2 min each. Cover-slipping was done manually using a mounting agent (Dako, NSW, Australia) before the slides were dried. Finally, the mounted sections were examined using a light microscope (Leica DM 2500 microscope, Leica Biosystems, VIC, Australia). Leica Application Suite Version 3.4.1 was used to record the images. Digital images were mounted into panels and labelled using Adobe Photoshop Software (CS6). All H & E sections of larvae were evaluated for any drug-induced gross morphological changes by comparing the number of retinal ganglion cells (RGC) between DMSO-treated and drug-treated groups. The number of RGC on a 40 x image of each retina was counted and the final count was obtained by averaging n=3 retinas from each group.

3.3.6.7 Immunohistochemistry

Paraffin sections were placed in a heater maintained at 60 ˚C for 1 hour. (This step melted the paraffin and firmly attached the specimen to the slide). Dewaxing and tissue rehydration were performed as described [**see section 3.3.6.6 for detail**]. Antigen retrieval was achieved by heat

(pressure cooker method in 10 mM citrate buffer pH 6 for 10 min). The sections were washed with TBS (Tris base: 50 mM, NaCl: 150 mM pH 7.5) followed by incubation with 3 % hydrogen peroxide for 20 minutes at RT to block the activity of endogenous peroxidases. The sections were washed three times for 5 min each with TBS-T (TBS + 0.05 % Tween-20). To block non-specific background staining, the sections were incubated with 10 % goat serum, 1 % BSA, 1 % Triton X-100 in TBST 2 h at RT before incubating with primary antibodies against nitrotyrosine (AB5411-Millipore, 1:400) or NQO1 (ab34173, Abcam) in blocking buffer (1 % goat serum, 1 % BSA, 1 % Triton X-100 in TBST) overnight at 4 ˚C (nitrotyrosine) or 30 min or 2 h (NQO1). After the sections were rinsed three times with TBST for 5 min each they were allowed to react with goat anti-rabbit IgG conjugated to horseradish peroxidase (1:200, ab97051-abcam) or its isotype control antibody (rabbit immunoglobulin fraction, Dako X0903, 1:10 000) in blocking buffer (1 % goat serum, 1 % BSA, 1 % Triton X-100 in TBST) at RT for 1 h. The sections were washed three times with TBST for 5 min each. The histological signal was detected by incubating the sections in 50 µl of 3, 3'-diaminobenzidine (Abcam, England, UK) in a chromogen solution (1:50) for 5 min followed by washing with TBST once and with water before counterstaining with haematoxylin. The sections were dehydrated and mounted using mounting medium (Dako, NSW, Australia) on IHC microscopic slides. Finally, the mounted sections were examined using light microscopy (Leica DM 2500 microscope, Leica Biosystems, VIC, Australia). Leica Application Suite Version 3.4.1 was used to record the images. Digital images were mounted into panels and labelled with Adobe Photoshop Software (CS6).

3.3.7 Western Blot Analysis Using Zebrafish Tissues

3.3.7.1 Protein Lysates of Larvae

Protein lysates from zebrafish were prepared according to a protocol described previously [356]. 5 dpf euthanized zebrafish larvae (n=10) were transferred in 1 ml ice-cold PBS in Eppendorf tubes before deyolking was performed by pipetting the fish up and down 20 times using 200 µl pippette tips followed by centrifugation (Eppendorf® Micro Centrifuge, 5417R, Eppendorf, NY, USA) at 2000 rcf for 2 min. The supernatant was removed without disturbing the layer of larvae at the bottom. In order to remove remaining yolk proteins, the PBS washing and centrifugation step were repeated twice.

3.3.7.2 Protein Lysates of Adult Eyes

Adult zebrafish were euthanized in ice-cold water for 20 min and the eyes removed using forceps. The eyes were frozen down in liquid nitrogen and stored at -80 ˚C until use. On the day of protein sample preparation, the lens of the eyes was removed using sharp forceps and the humour squeezed out of the eyeball to prevent dilution of the protein extracts.

Proteins from both larvae and adult zebrafish were extracted using pre-cooled lysis buffer (50 mM Tris pH 7.4, 150 mM NaCl, 2 mM EDTA, 2 mM EGTA, 25 mM beta glycerol phosphate, 0.3 % NP-40, 0.1 % SDS, 1 % Triton X-100, 25 mM NaF, 0.1 mM Na_3VO_4, 1 mM PMSF) at 2 µl/embryo and 10 µl/adult eye followed by homogenization on ice using a Kontes Pellet Pestle (Fisher Scientific, VIC, Australia). The lysate was centrifuged (Eppendorf centrifuge, 5417R, Eppendorf, NY, USA) at 20 000 rcf at 4 ˚C for 15 min before supernatants were transferred to pre-cooled Eppendorf tubes. Determination of protein content and gel

electrophoresis was performed as previously described [**see sections 2.3.5.3** and **2.3.5.6 for detail**]. HepG2 cell extracts were used as a positive control for NQO1. NQO1 protein expression in the adult zebrafish eyes and the whole larvae was then compared.

3.3.8 Bioinformatics on Zebrafish NQO1

3.3.8.1 Subcellular Localisation of NQO1 in zebrafish

The nucleotide sequences of four different splice variants of zebrafish NQO1 were obtained from ENSEMBL (http://asia.ensembl.org/Danio_rerio/Transcript/Summary?g=ENSDARG00000010250;r=7:56401846-56420909;t=ENSDART00000004964). The nucleotide sequences of all splice variants were manually edited to remove introns and only exons were translated to protein sequences using an online nucleotide-protein translator (http://www.fr33.net/translator.php). From the different reading frames, the protein sequence from frame 1 was selected as it generated the largest open ready frame. For all the splice variants subcellular localization of NQO1 protein was predicted using online software (http://ppopen.informatik.tu-muenchen.de/).

3.3.8.2 Comparison of NQO1 Protein Sequences

Protein sequence data of NADPH dehydrogenase quinone 1 (NQO1) was obtained for zebrafish (Danio *rerio*) from NCBI (http://www.ncbi.nlm.nih.gov/protein). To compare protein homology of zebrafish NQO1 against human NQO1, protein-protein BLAST was performed between the query sequence (zebrafish NQO1) against non-redundant protein sequence of human NQO1.

(http://blast.ncbi.nlm.nih.gov/Blast.cgi?PAGE=Proteins&PROGRAM=blastp&BLAST_PROGRAMS=blastp&QUERY=AAH65622.1&LINK_LOC=protein&PAGE_TYPE=BlastSearch). The search was performed without a sequence filter. Sequences with E values of less than 1 $x10^{-4}$ can be considered as homologous.

3.3.9 NQO1 Enzyme Activity on Adult Eye Tissue

The best sectioning method for zebrafish to preserve enzyme activity is to prepare cryosections. Cryosectioning was carried out according to a protocol described previously [357,358]. Eyes from adult fish were removed immediately after the fish were euthanized and fixed in 4 % PFA (in PBS) for 2 h at 4 ˚C. PFA was replaced by 25 % sucrose (in PBS) until the eyes sank and then replaced with 35 % sucrose (in PBS) and stored overnight at 4 ˚C. Subsequently, the eyes were embedded in cryomolds (10 mm x 10 mm x 5 mm; Tissue-Tek Cryomold, Sakura, USA) containing OCT (Tissue-Tek, Sakura, USA) before freezing down in a cryostat (Leica CM 1850; Leica Biosystems, VIC, Australia) for 10 min. The frozen tissue block was sectioned into 25 µm thick sections with the cryotome maintained at -20 ˚C. Eye sections were placed on IHC microscope glass slides (Dako, NSW, Australia) and dried at RT for exactly 2 h before NQO1 enzyme activity was detected. Shorter drying periods resulted in the loss of tissue during the washing steps, while longer drying period resulted in failure to detect NQO1 enzyme activity.

NQO1 enzyme activity was detected according to a modified protocol as previously described [359]. This assay is based on the reduction of nitro-blue tetrazolium dye (NBT) into its blue formazan product in the presence of active NQO1, NAD(P)H and an NQO1 substrate. Briefly, the cryosections were washed with Tris-buffer (pH 7.4) to remove excess OCT compound and

were preincubated in preincubation solution (25 mM Tris, 0.08 % Triton-x, 2mg/ml BSA) in the presence or absence of 100 µM dicoumarol for 30 min at RT. The preincubation solution was replaced with buffer containing 100 µM NBT (ab146262, Abcam), 1 mM NADPH (final), 100 µM NQO1 substrate menadione ± 100 µM dicoumarol. The reaction was incubated at 37 ˚C for 30 min. The development of the characteristic blue stain was observed under a light microscope. Subsequently, the sections were dehydrated as described [**see section 3.3.6.6 for detail**] and finally cover-slipped using a mounting medium (Dako, NSW, Australia). Images were captured using a light microscope with a digital camera (Leica DM2500; Leica Biosystems, VIC, Australia) at a 40 x magnification. Leica Application Suite Version 3.4.1 was used to record the images. Digital images were assembled into panels and labelled using Adobe Photoshop Software (CS6).

3.4 Statistical Analysis

All data are expressed as mean ± standard error of mean (SEM) as indicated in the figure legends. Statistical significance was assessed using either Student's t-test or one-way analysis of variance (ANOVA) where appropriate, followed by Dunnett's multiple comparison tests to evaluate the differences between controls and treatment groups using GraphPad Prism (Version 6, GraphPad Software Inc, CA, USA). In all assays $p<0.05$ was considered statistically significant.

3.5 Results

3.5.1 Determination of Maximum Tolerated Concentration of CQ

In order to translate *in-vitro* findings of NQO1-dependent CQ toxicity to the *in-vivo* situation, a model system characterized by both high and low NQO1 expression was needed. Luckily, zebrafish were only recently reported to lack NQO1 expression in their retina during the early larval stages (7 dpf), while NQO1 is highly expressed in the adult retina [348]. Visual function was therefore measured in zebrafish to study CQ-induced toxicity under conditions of both high (adult) and absent retinal NQO1 (larvae). For initial dose-finding experiments the maximum tolerated concentration (MTC) was established by exposing zebrafish larvae (PET strain) at 3 days post fertilisation (dpf) to different concentrations of CQ (1 µM - 1 mM) and DMSO (0.1 %) for 48 h before startle response and morphological features were examined. No mortality was associated with the standard conditions used in this study. Larvae at 3 dpf were chosen for the experiment, as the eye development in zebrafish is very rapid [220]. By 3 dpf the retinal structure of zebrafish becomes fully functional with progressive advancement in image formation [220]. At the same time the extra-ocular muscles become functional, which is a prerequisite for the tracking of moving objects by eye movement. PET strain larvae exposed to CQ $\geq$ 30 µM showed absence of heartbeat, startle response and loss of dorso-ventral balance as well as morphological defect such as bent body (**Table 6**). For zebrafish larvae the MTC for CQ was determined to be 10 µM. Therefore, only CQ at concentrations up to 10 µM were used for visual function test, since at these concentrations the larvae were still alive, have no morphological defects and have comparable locomotory activity and dorso-ventral balance to DMSO-treated control animals. PET strain zebrafish are from an unknown source and probably have a mixed genetic background [360]. Therefore, to work with a genetically distinct laboratory strain, we also used the AB strain for the OKR experiments. When 3 dpf AB larvae

were exposed to concentrations of CQ that were tolerated in PET larvae, surprising lethality was observed at 10 µM after merely 24 h of drug exposure (**Table 6**). Due to the observed inter-strain variation in sensitivity to CQ in zebrafish larvae, the PET strain was selected over the AB strain for all further studies involving both larvae (histology) and adult zebrafish. For the adult zebrafish study, MTC was not determined, instead the concentration of CQ that severely impaired the visual function in PET strain zebrafish larvae was used (**Table 7**).

Table 6: Effect of CQ on the overall morphology and behaviour of zebrafish larvae

Strain	CQ (µM)	Heart-beat	Morphological defects*	Startle response*	Dorso-ventral balance*	MTC (µM)
PET	1	Present	No	Yes	Yes	**10**
	3	Present	No	Yes	Yes	
	10	Present	No	Yes	Yes	
	30	Absent	-	-	-	
	100	Absent	-	-	-	
	300	Absent	-	-	-	
	1000	Absent	-	-	-	
AB	1	Present	No	Yes	Yes	**3**
	3	Present	No	Yes	Yes	
	10	Absent	-	-	-	

*Due to the absence of heartbeat, morphological defects, startle response and dorso-ventral balance were not assessed at concentrations > 10 µM.

Table 7: Effect of CQ on the behaviour of PET adult zebrafish

CQ (µM)	DIC (µM)	CQ+DIC* (µM)	Swimming	Dorso-ventral balance
10			Yes	Yes
	0.5		Yes	Yes
		10 + 0.5	No	No

*Combination treatment with CQ and Dic caused death of 4 out of 4 fish within 6 h of treatment.

3.5.2 CQ Induces Visual Function Loss only in NQO1-deficient Zebrafish Larvae

OKR, a reflexive behavioural response that is elicited by a slow moving object in the visual field was employed to assess the effect of different CQ concentrations on the visual function of larvae and adult zebrafish. This response combines two eye movements: a smooth pursuit which is a slow tracking of a moving object followed by a rapid saccade which is fast resetting eye movement in the opposite direction of a moving object [279]. OKR has been extensively studied in zebrafish and is routinely used as readouts for visual performance defects in visual mutants as well as in drug-induced cases [237,281]. Drug-induced visual toxicity of the drugs has been identified by inhibition of OKR. It has to be noted that visual impairment was one of the main clinical features of CQ-linked SMON [162]. Therefore, to investigate the effect of CQ on visual function, 3 dpf zebrafish larvae were exposed to different concentrations of CQ (DMSO, 1, 3, 10 µM) for 48 h followed by measurement of OKR. It was shown that exposing larval zebrafish to unidirectional motion stimuli decreased the ratio of eye velocity to the stimulus velocity. In contrast, altering the direction of the motion of stimulus reduced saccade frequency and as a consequence increased the ratio of eye velocity to stimulus velocity [361]. Therefore, in this study, both eyes were stimulated using sinusoidal changing direction. The eye velocity was averaged over both eyes. CQ dose-dependently impaired OKR (measured in terms of average eye velocity) in the PET strain larvae (**Figures 28a** and **b**). A very significant drop in eye velocity was observed in the animals treated with ≥ 3 µM of CQ ($p=0.0236$) compared to the DMSO-treated control larvae. Animals treated with 10 µM of CQ were clearly not able to follow the visual stimuli, as a result, no eye movements were recorded ($p=0.0080$). Negative eye velocities were observed at this concentration, which could be due to the fact that zebrafish exhibited spontaneous eye movements and as a consequence, the pursuit (slow phase) movements were faster than resetting movements (**Figure 28a**). Nevertheless, this dose

response is surprisingly consistent with the results from the *in-vitro* toxicity studies (**Figure 14a**).

Using the same parameter, OKR was measured in AB strain larvae exposed to CQ (DMSO, 1, 3 μM) at 24 h and 48 h. Visual function was not altered at any concentrations of CQ at 24 h (**Figure 28c**), however at 48 h a significant reduction of visual function (**Figure 28d**) was observed compared to DMSO-treated control, which is consistent with the results from the PET larvae.

Table 8: Effect of Dic and CQ on the overall morphology and behaviour of zebrafish larvae

Strain	Dic (μM)	+CQ (μM)	Heart-beat	Morphological defects*	Startle response*	Dorso-ventral balance*
AB	0.01		Present	No	Yes	Yes
	0.1		Present	No	Yes	Yes
	1		Present	No	Yes	Yes
	3		Present	No	Yes	Yes
	0.01	1	Present	No	Yes	Yes

In order to test if CQ also induced visual impairment under conditions where NQO1 is highly expressed, OKR was measured in adult zebrafish after CQ treatment. The parameters of OKR measurement in the adult fish slightly differed from larvae in terms of stimulus direction and evaluation of eyes. A directional asymmetry has been reported supporting the movements of eyes in a temporal-nasal direction in the adult zebrafish [263]. In this study, both eyes were stimulated in one direction (from right to left and left to right) and only the right eyes were evaluated. Eye velocities in the nasal-temporal direction were found to be lower than temporal-to-nasal direction and were also less constant. Therefore, in this study, although both eyes were stimulated using a one direction motion stimulus (from right to left) only one eye (right eye) that was stimulated in temporal-nasal direction was evaluated. In contrast to the larval OKR

results, in the adult zebrafish, 10 µM CQ did not cause any significant reduction in eye velocity as compared to DMSO-treated control animals (**Figures 28e** and **f**). The obvious question was could CQ impair visual function in the adult zebrafish if NQO1 is pharmacologically inhibited? In order to address this, adult zebrafish were exposed to dicoumarol (Dic, a known NQO1 inhibitor), CQ or a combination of both followed by an examination of visual function. The concentration of Dic that was used for this experiment was 0.5 µM, which was reported to be fairly non-toxic, even to zebrafish larvae [362]. In addition, our experimental data showed that zebrafish larvae did not show any sign of toxicity when incubated with 3 µM Dic for 48 h **(Table 8)**. Treatment with Dic in the adult zebrafish also did not significantly reduce the eye velocity compared to the DMSO-treated control (**Figures 28e** and **f)**. Strikingly, when NQO1 was inhibited by Dic, 10 µM CQ was highly toxic to the fish and all fish died unexpectedly within 6 h of drugs exposure. This result drastically highlighted the significant toxicity of CQ in the absence of NQO1 activity. Due to the severe toxicity, this result was communicated to the animal ethics committee (AEC) as an unexpected adverse event. The AEC subsequently decided that it would not agree to further concentration finding experiments with the combination of Dic and CQ.

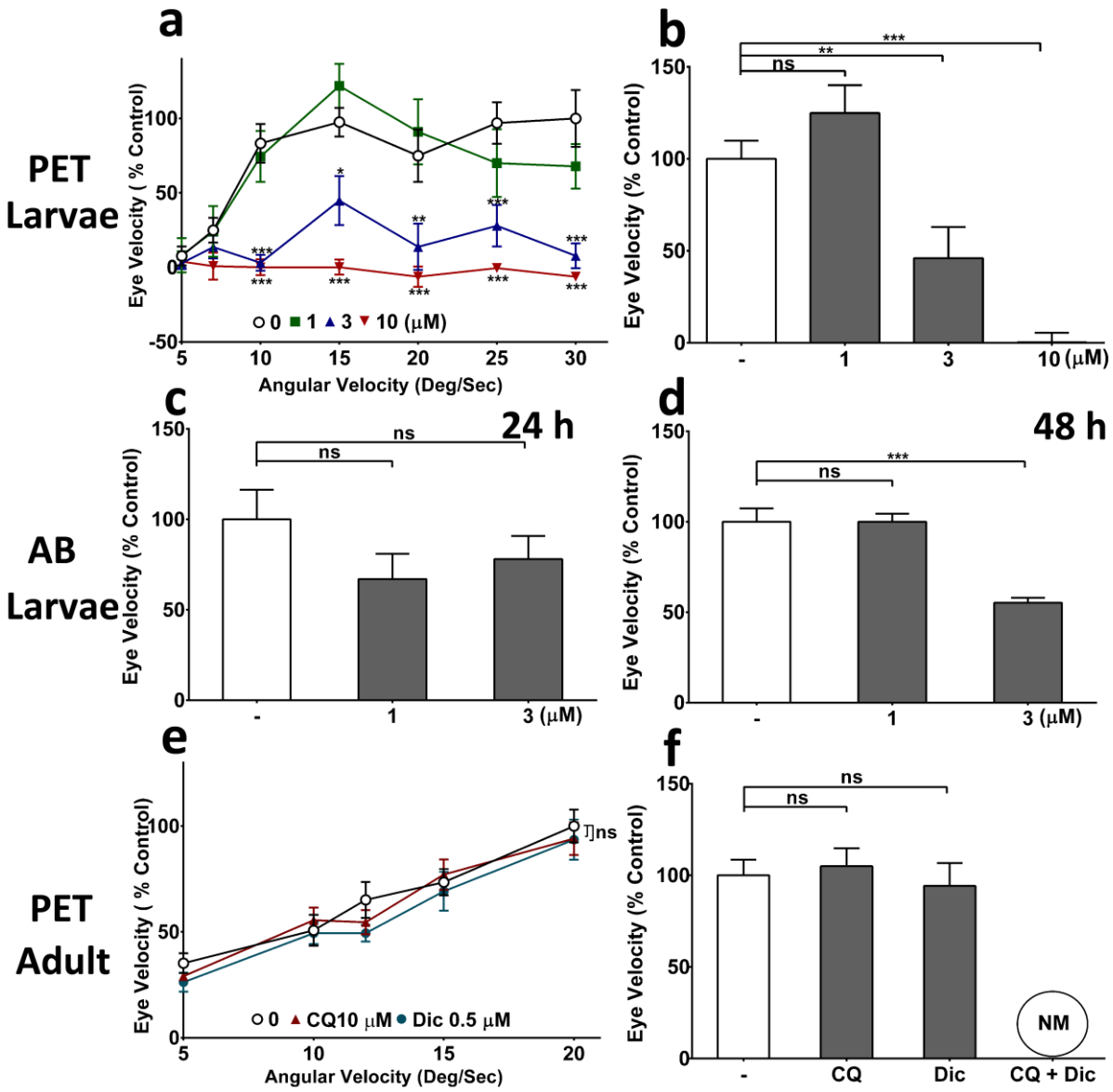

Figure 28: Effect of clioquinol (CQ) on visual function of zebrafish.

(a, b) CQ impairs visual function of petshop-purchased (PET) zebrafish larvae. 3 dpf PET strain zebrafish were exposed to up to 10 µM CQ for 48 h followed by optokinetic response (OKR) measurement at 5 dpf at *(a)* varying angular velocity of stimulus *(b)* at one angular velocity of stimulus (15 deg/sec). The visual function was measured in terms of eye velocity under bidirectional motion stimulus. The average velocity of both right and left eye was considered to compare the effect of CQ and is represented as % control. The graph shows the average eye velocity of zebrafish larvae of a typical experiment. *(c, d) CQ impairs visual function of AB strain zebrafish larvae.* 3 dpf AB strain zebrafish were exposed to CQ at concentrations up to 3 µM for 24 h *(c)* 48 h *(d)* followed by optokinetic response (OKR) measurement at days 5 dpf at one angular velocity of stimulus (15 deg/sec). The visual function was measured in terms of eye velocity under bidirectional motion stimulus. The average velocity of both right and left eye was considered to compare the effect of CQ.

The graph shows the average eye velocity of zebrafish larvae of a typical experiment. *(e, f) CQ does not impair visual function in the adult zebrafish.* Adult zebrafish were exposed to CQ 10 µM, Dic 0.5 µM and DMSO for 48 hours under 14:10 light: dark cycle before visual acuity was measured. The visual function was measured in terms of eye velocity at varying angular velocity *(e)* and at one angular velocity (15 deg/sec) *(f)* under unidirectional stimulus. Only the average velocity of right eye was considered to compare the effect of CQ. The graph shows the average eye velocity the adult zebrafish of a typical experiment. p* <0.05, ** <0.01 and p*** <0.001 versus control using one-way analysis variance (ANOVA) followed by Dunnett comparison tests. Error bar=SEM, n=10. nm: not measured.

To examine if CQ-induced loss of visual function in zebrafish larvae was the result of a CQ-mediated morphological defect in the eyes, formalin-fixed paraffin sections of the PET strain larvae were used for histopathological examination. Overall the H & E-stained eyes sections of larvae were examined for gross morphological defects and numbers of retinal ganglion cells (RGC). Although a significant visual function loss was observed in larvae treated with CQ ≥ 3 µM, no gross morphological changes were detected at any of the tested concentrations compared to the DMSO-treated control larvae (**Figures 29a-d**). However, compared to the DMSO-treated group, RGC counts were slightly but significantly (88.18 % ± 1.74 %, p=0.0095) reduced in the group treated with the highest concentration of CQ (10 µM) (**Figure 29e**).

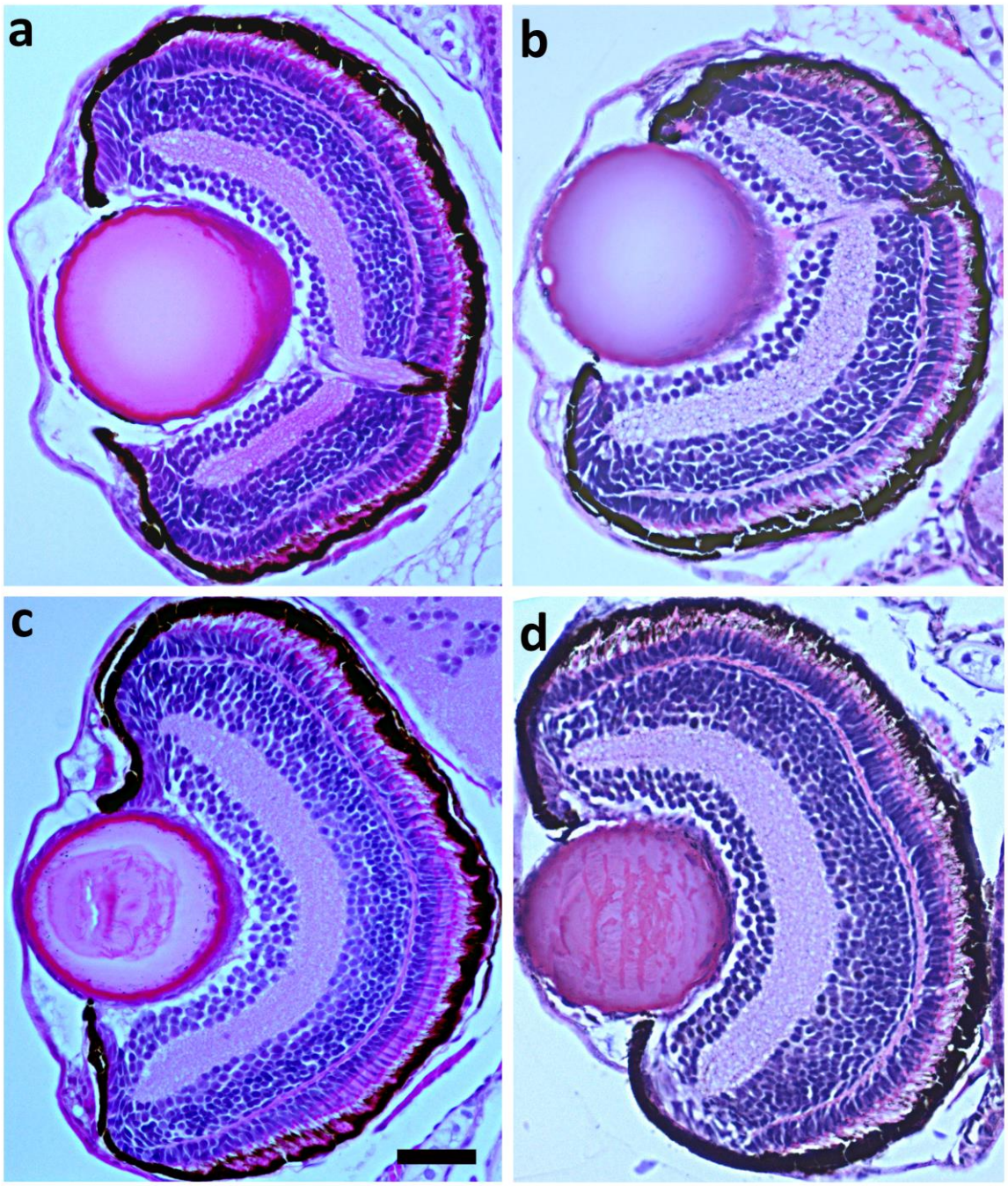
a
b
c
d

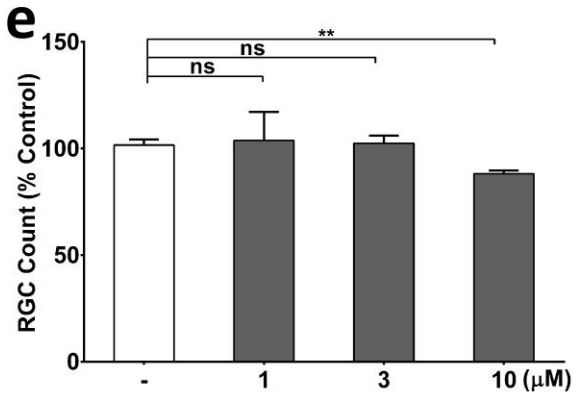
e
RGC Count (% Control)
150
100
50
0
ns
ns
**
-
1
3
10 (μM)

Figure 29: Examination of gross morphological abnormalities in the eyes of clioquinol (CQ)-treated zebrafish larvae.

(a-d) Representative images of formalin-fixed paraffin-embedded eye tissues from PET strain zebrafish larvae treated with CQ. *(a)* DMSO-treated, *(b)* (1 µM) CQ-treated, *(c)* (3 µM) CQ -treated, *(d)* (10 µM) CQ -treated. *(e)* Quantification of the retinal ganglion cells (RGC), in 40 x magnification images. Scale bar=100 µm for 40 x magnification. p* <0.05 and p** <0.01 versus control using Student's-t test. Error bar=SEM, n= at least 3.

3.5.3 Inhibiting NQO1 Does Not Contribute to CQ-mediated Visual Function Loss in Zebrafish Larvae

Although it was reported that NQO1 is not expressed in the larval retina of zebrafish, it was nevertheless of interest to confirm this by examining whether the NQO1 inhibitor, Dic could modulate CQ toxicity in larvae. Therefore, AB strain larvae were exposed to different concentrations of Dic up to 3 µM for 48 h followed by measurement of OKR to establish the concentration that does not negatively affect eye velocity. The concentration ranges of Dic used in this study were chosen based on previous studies [362,363]. In these studies, Dic was used at concentrations ranging from 50 nM – 5 µM without reported systemic toxicity in zebrafish embryos. Assuming NQO1 is present in the retina of zebrafish larvae, Dic concentrations that only inhibit NQO1 without having any effect on visual function itself were required. A non-significant trend o reduced eye velocity was nevertheless observed at all Dic concentrations between 0.1-3 µM (p=0.1049, 0.0844 and 0.1117) (**Figure 30a**). Therefore, a 10-fold lower concentration of Dic (0.01 µM) was chosen for the combination experiment with CQ to avoid direct effects of Dic on visual function. For this combination treatment 1 µM of CQ was chosen, as at this concentration a reduction in eye velocity was not observed in both strains of larvae (**Figures 28a, b** and **d**). Consistent with previous results, CQ at 1 µM had no effect on visual

function after 48 h of treatment (**Figure 30b**). Moreover, inhibition of NQO1 by Dic did not increase the toxicity of CQ in terms of both loss of visual function and lethality. In contrast, CQ appeared to counteract the negative trend induced by low-dose Dic. Overall, these results are consistent with previous reports that NQO1 is not expressed in the retina of zebrafish larvae [348].

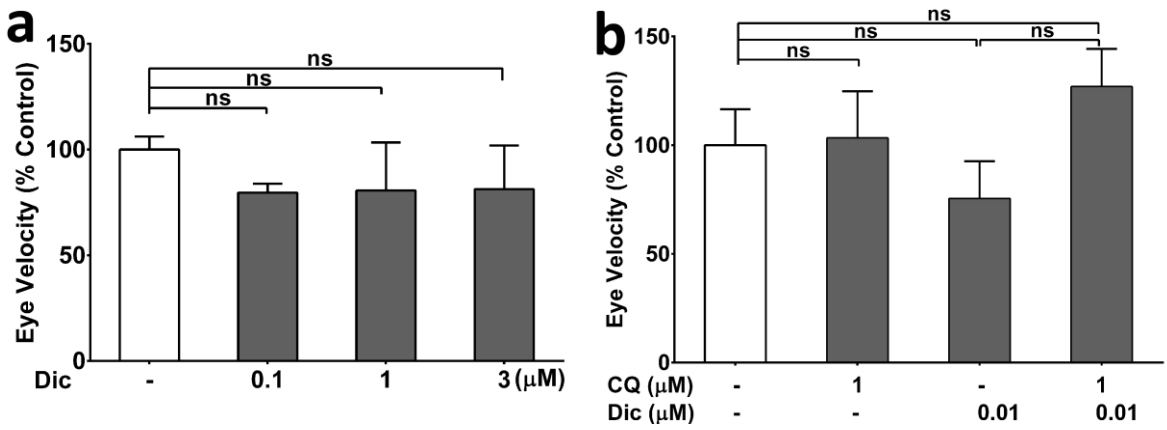

Figure 30: Inhibition of NQO1 has no effect on the visual function of zebrafish larvae.
(a) 3 dpf zebrafish (AB strain) were exposed to indicated concentrations of dicoumarol (Dic) for 48 h under dark-adapted condition before eye velocity was measured by optokinetic response (OKR) at 5 dpf under bidirectional motion stimulus at spatial frequency (0.11 cycles/deg), angular velocity (7.5 deg/sec) and contrast (7 %). *(b)* 3 dpf zebrafish (AB strain) were exposed to indicated concentrations of Dic and CQ for 48 h under dark-adapted condition before eye velocity was measured by OKR at 5 dpf under bidirectional motion stimulus at spatial frequency (0.11 cycles/deg), angular velocity (15 deg/sec) and contrast (10 %). The average eye velocity of both right and left eye was considered to compare the effect of drugs with the DMSO-treated group. The graph shows the average eye velocity of one experiment. p* <0.05, ** <0.01 and p*** <0.001 versus control using one-way analysis variance (ANOVA) followed by Dunnett comparison tests. Error bar=SEM, n=at least 5.

3.5.4 Immunohistochemical Analysis of NQO1 in Adult Zebrafish Eyes

The experiments described above showed that CQ impaired visual function in NQO1 deficient zebrafish larvae and not in the adult zebrafish that presumably express NQO1 in the retinal tissue. To confirm NQO1 expression levels in the adult zebrafish retina, formalin-fixed,

paraffin-embedded sections of zebrafish eyes were immuno-stained for NQO1. Although immunohistochemical staining for NQO1 was positive, it was only observed as nuclear staining in the inner photoreceptor layer, inner nuclear layer, outer nuclear layer and retinal ganglion cells of the retina (**Figures 31a-g**). This result was in stark contrast to previous studies that showed a primarily cytoplasmic localization of NQO1 in rat liver and pig corpus luteum [364,365]. So far, only low levels of NQO1 have been detected in the nucleus under normal conditions [366]. This nuclear immunostaining of NQO1 was observed even in sections where antibody dilutions of up to 32 times lower than the recommended dilution were used. More importantly this pattern of staining was also observed in the retina of zebrafish larvae that reportedly lack retinal NQO1 expression (**Figure 32**). Since these results would indicate non-specific staining of the primary antibody, the primary antibody was replaced with a non-specific IgG isotype (negative control). Since this control showed a complete absence of immunostaining under identical conditions, it is unclear at present with which nuclear epitope the anti-NQO1 antibody cross reacts.

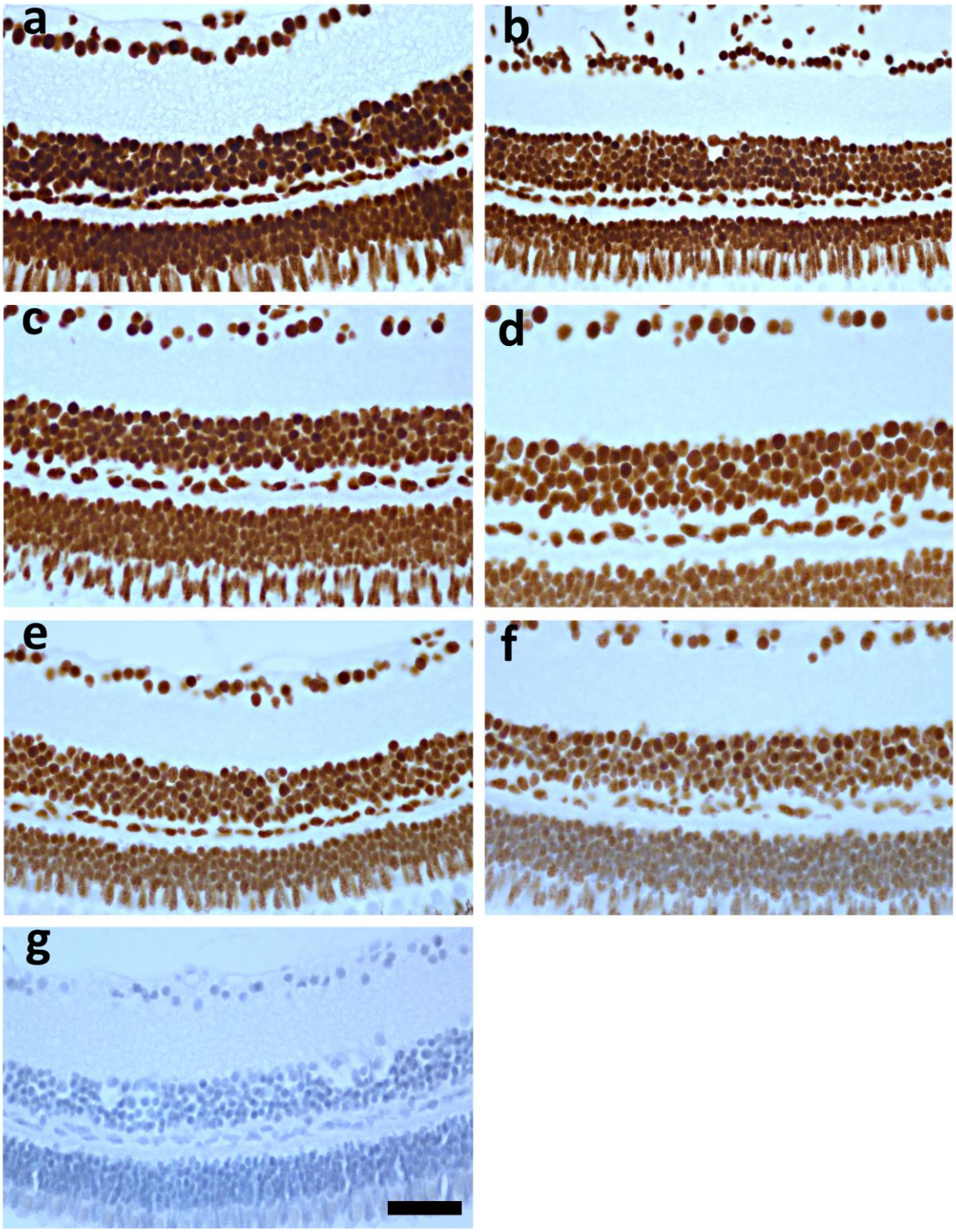

Figure 31: Anti-NQO1 antibody staining in the adult zebrafish retina.

Representative images of NQO1 staining of adult zebrafish retina. Formalin-fixed paraffin-embedded adult (PET strain) retinal-sections were incubated with anti-NQO1 antibody for 30 min at different antibody dilutions before NQO1 expression was examined. (a)1:200, (b)1:400, (c)1:800, (d)1:1600, (e)1:3200, (f)1:6400, (g) nonspecific-IgG (negative control). Scale bar indicates 100 µm for all images. Images were taken at 40 x magnification.

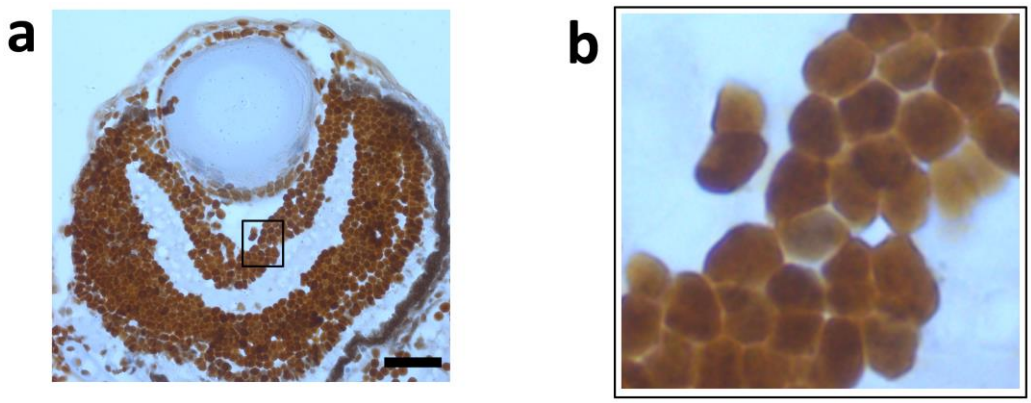

Figure 32: Anti-NQO1 antibody staining in the retina of zebrafish larvae.

a) Representative image of NQO1 staining of zebrafish larvae retina. Formalin-fixed paraffin-embedded larval (PET strain) retinal-sections were incubated with anti-NQO1 antibody for 2h at 1:200 antibody dilution before NQO1 expression was examined. *b)* Nuclear staining in RGC layer is shown at high magnification. Scale bar indicates 100 µm. Image was taken at 40 x magnification.

.

3.5.5 Western Blot Analysis of NQO1 in Adult and Larval Zebrafish

Since confirmation of NQO1expression in the retina through immunostaining provided inconclusive results, quantification of NQO1 expression was attempted by western blotting in both larvae and adult zebrafish eyes. Due to the small size of larvae (3-4mm), eyes could not be harvested and instead whole larvae were used for the analysis whereas only the eyes were harvested from the adult fish. HepG2 cells were used as a positive control. Protein bands for NQO1 in both larvae and adult eyes were detected. However, the molecular weight of the detected proteins did not correspond to the predicted size based on the protein sequences or the band detected in HepG2 cells (band size of NQO1= 31 kDa). A protein band derived from extracts from adult eyes was detected around 10 kDa whereas extracts from larvae produced a band of 45 kDa (**Figure 33**). It is worth stating that the anti-NQO1 antibody used for western blot analysis cross reacts with mouse, rat, guinea pig, human due to the significant level of NQO1 sequence homology across species but had not been evaluated for zebrafish before.

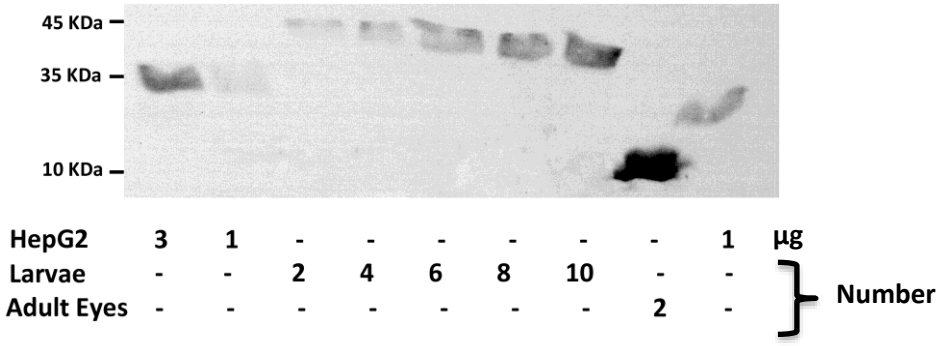

Figure 33: Western blot analysis of NQO1 in zebrafish.
Representative western blot of NQO1 in zebrafish (whole 5 dpf larvae vs. adult eyes). Protein lysate of HepG2 cells was used as a positive control.

3.5.6 Prediction of Cytoplasmic Localization of NQO1 in Zebrafish

Since the immunohistochemistry result appeared to show nuclear localization of NQO1 in zebrafish, which is contradictory to the published reports in humans and other organisms [366,367], it was of interest to explore the subcellular localisation of NQO1 in zebrafish employing bioinformatics. Five different NQO1 splice variants (one without corresponding protein) have been described in ENSEMBL. Protein sequences translated from the coding region of the reported nucleotide sequences of four NQO1 splice variants were analysed, which predicted that NQO1 in zebrafish should also be cytoplasmic as described for all other organisms (**Figures 34a-c**).

a

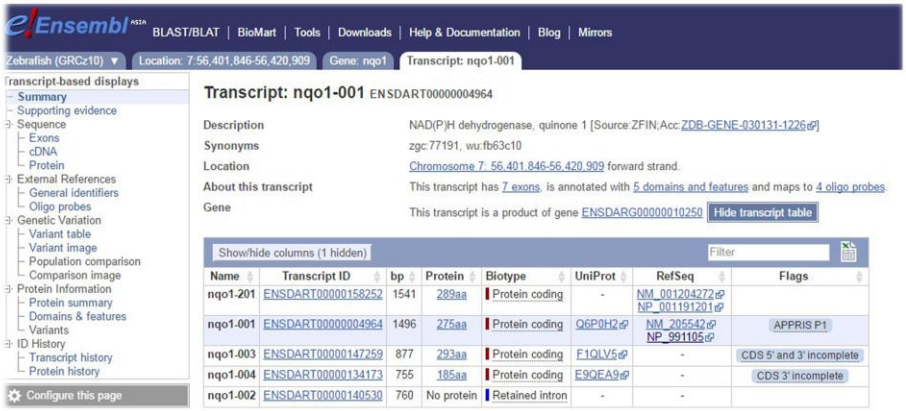

b

c

NQO1

Variants	1	2	3	4
Subcellular Localization	Cytoplasmic	Cytoplasmic	Cytoplasmic	Cytoplasmic

Figure 34: Subcellular localization of NQO1 in different splice variants of zebrafish.
(a) Five different NQO1 splice variants of zebrafish have been described in ENSEMBL [368]. *(b, c)* All four different NQO1 splice variants of zebrafish are predicted to localize exclusively to the cytoplasm with a predicted confidence of 41 %-50 %. [369].

3.5.7 Zebrafish and Human NQO1 Display Genetic Homology

After confirmation that NQO1 zebrafish should also be localised to the cytoplasm, it was suspected that NQO1 in zebrafish may not be homologous enough compared to human NQO1 for antibody detection. Consequently, it was likely that the anti-NQO1 antibody specific to human NQO1 might have resulted in false positive results. Therefore, the homology of human and zebrafish NQO1 was analysed by blasting zebrafish NQO1 protein sequence against the

non-redundant human protein sequence (**Figures 35a and b).** From the data, it was revealed that human and zebrafish NQO1 display a protein sequence homology of 47-50 % **(Figure 35c)**. To further confirm this, the manufacturer of the antibody was contacted for the exact immunogen sequence the anti-NQO1 was raised against, unfortunately, this information was not disclosed. Hence, it cannot be confirmed the NQO1 epitope the antibody was raised against is present in zebrafish NQO1 protein.

a

b

c Percentage of identity

Protein (Zebrafish)	Accession Number	Expect (E)	% Identity Human
NAD(P)H dehydrogenase [quinone] 1 isoform 1 (289 amino acid)	NP_001191201.1	2e-92	47
NAD(P)H dehydrogenase [quinone] 1 isoform 2 (275 amino acid)	NP_991105.1	3e-92	50

Figure 35: Comparison of NQO1 protein sequences.

Percentage identity of NQO1 protein between zebrafish isoform 1 *(a, c)* or isoform 2 *(b, c)* against the human NQO1 consensus sequence.

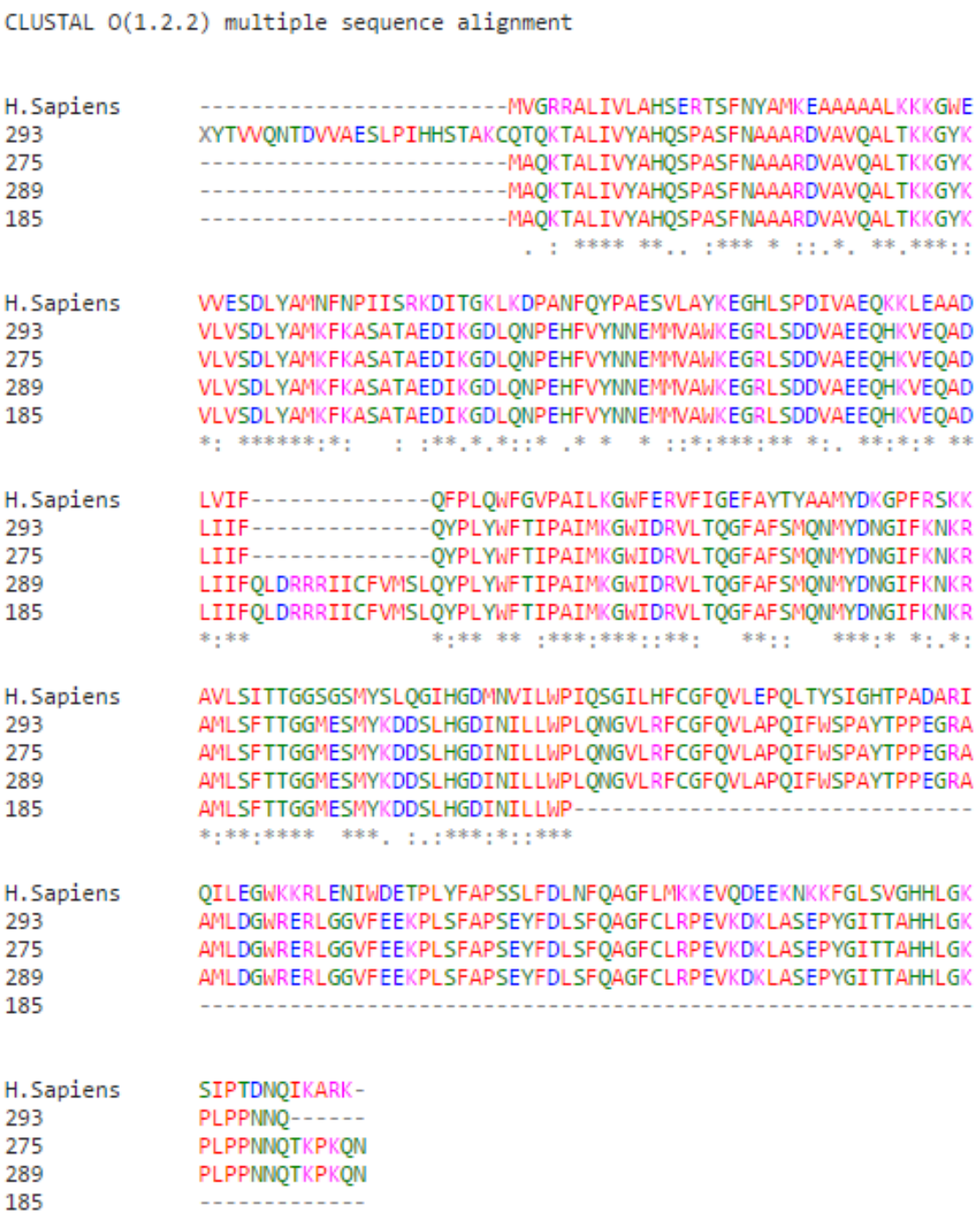

Figure 36: Multiple sequence alignments of human NQO1 and zebrafish NQO1 splice variants. Protein query sequences of all zebrafish NQO1 splice variants and human NQO1 were aligned using clustalW2 software [370].

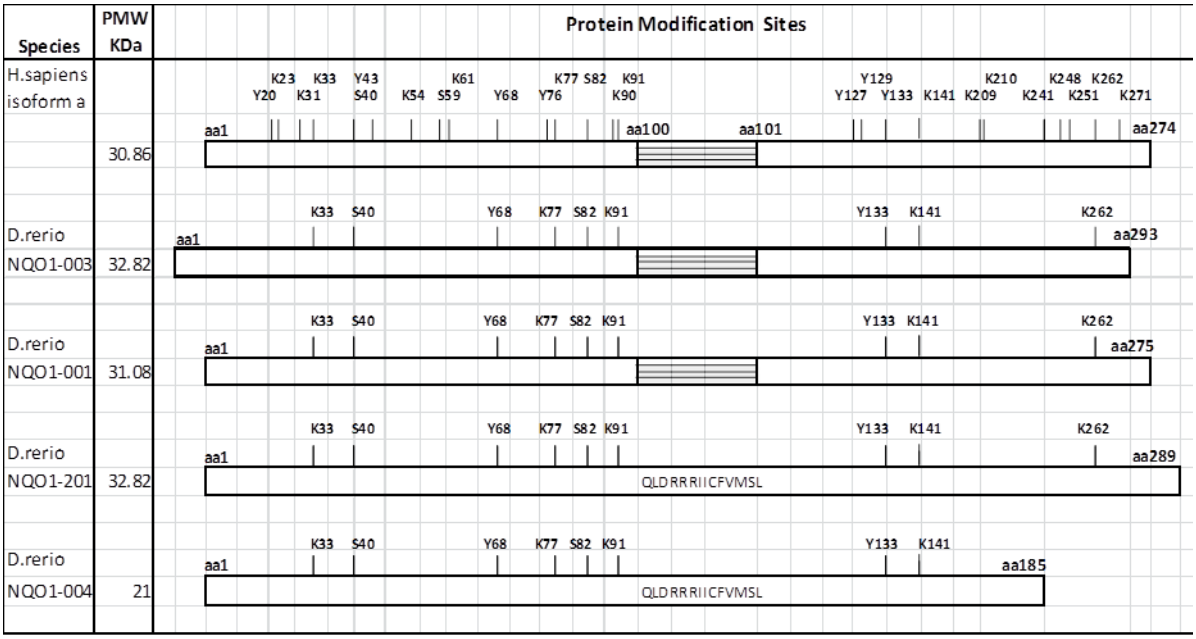

Figure 37: Post-translational modification sites in human and zebrafish NQO1 protein.
Post-translational protein modification sites of human NQO1 were obtained from PhosphoSitePlus [371]. Putative protein modification sites of zebrafish NQO1 slice variants were shown based on conserved amino acid between human and zebrafish NQO1. PMW: predicted molecular weight.

It has to be remembered that beside detecting protein bands inconsistent with the predicted size, which should be similar to human NQO1, NQO1 in larvae and adult zebrafish was detected at two different molecular weights (**Figure 33**). The detection of NQO1 protein of the same species at two different molecular weights could possibly be attributed to the existence of different NQO1 splice variants with different size. To investigate this possibility, the protein query sequences of all zebrafish splice variants were aligned using clustalW2 [370]. Alignment of multiple NQO1 sequences from all splice variants demonstrated large regions of homology to each other except for a non-coding NQO1 splice variant (**Figure 36**). Furthermore, identification of the putative post-translational protein modification sites in zebrafish NQO1 splice variants based on homologous amino acid of known protein modification sites on human NQO1, indicate that in general the NQO1 protein is very conserved between human and zebrafish (**Figure 37**).

3.5.8 NQO1 Protects Against CQ-induced Vision Loss in Adult Zebrafish

With the unsatisfactory immunohistochemistry and western blot results and more importantly due to unavailability of an anti-NQO1 antibody specific for zebrafish, NQO1 enzyme activity was detected instead, to explore the difference in NQO1 in the retinal layers of adult zebrafish **(Figure 38)**. NQO1 enzyme activity was visualized in cryosection of zebrafish retinas from DMSO- and drug-treated adult fish. A strong positive histochemical staining reaction was observed in the retina of DMSO-treated adult animals in the presence of the NQO1 substrate-menadione, NBT and NADPH. The resulting staining pattern was more diffuse as previously reported for the rat brain [359,367]. Overall, the staining extended throughout the different retinal layers, particularly in the photoreceptor layer (PR-outer segment), inner nuclear layer and retinal ganglion layer **(Figure 39a)**. Since DMSO has been reported to induce oxidative stress in yeast[372], it was of interest to confirm whether DMSO contributed to the observed NQO1 staining. However, NQO1 enzyme activity in the DMSO-treated animals did not differ from the untreated animals (data not shown), indicative of a lack of interference by DMSO. In CQ-treated fish, however, the staining intensity was reduced **(Figure 39b)** and was mainly restricted to the PR-outer segment and the inner nuclear layer. In Dic-treated animals **(Figure 39c)** the staining was only observed in the photoreceptor layer, while it could hardly be detected in CQ- and Dic-treated animals **(Figure 39d)**.

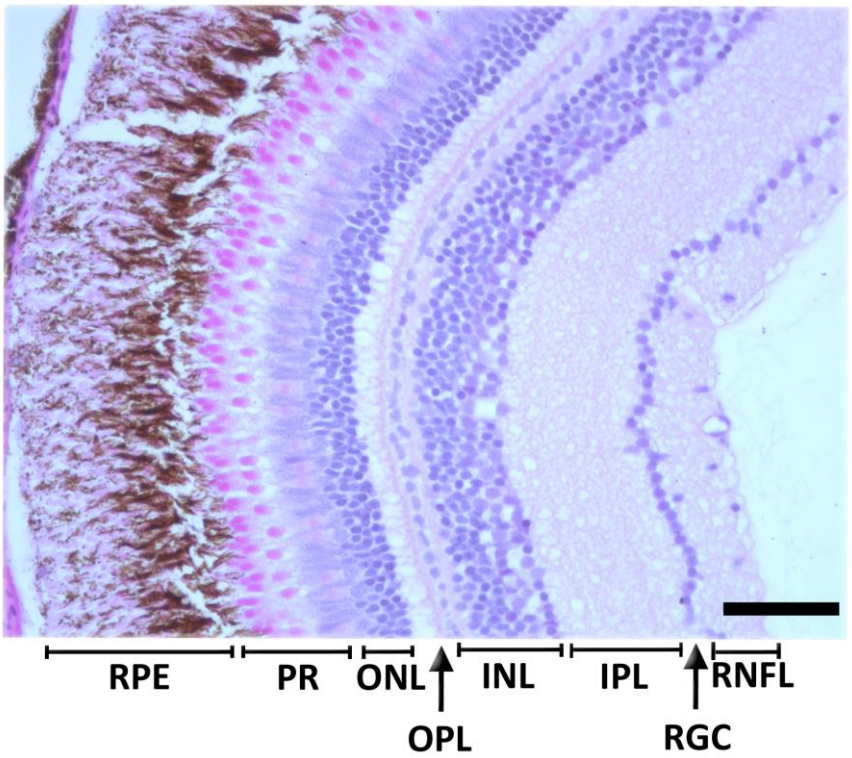

Figure 38: Retinal layer in zebrafish.

Formalin-fixed paraffin embedded H & E section of the adult zebrafish retina. The retinal layer comprises of retinal pigment epithelium layer (RPE), photoreceptor layer (PR), which consists of outer segment and inner segment, outer nuclear layer (ONL), outer plexiform layer (OPL), inner nuclear layer (ONL) and retinal ganglion cells (RGC). Scale bar indicates 100 µm. Image was taken at 40 x magnification.

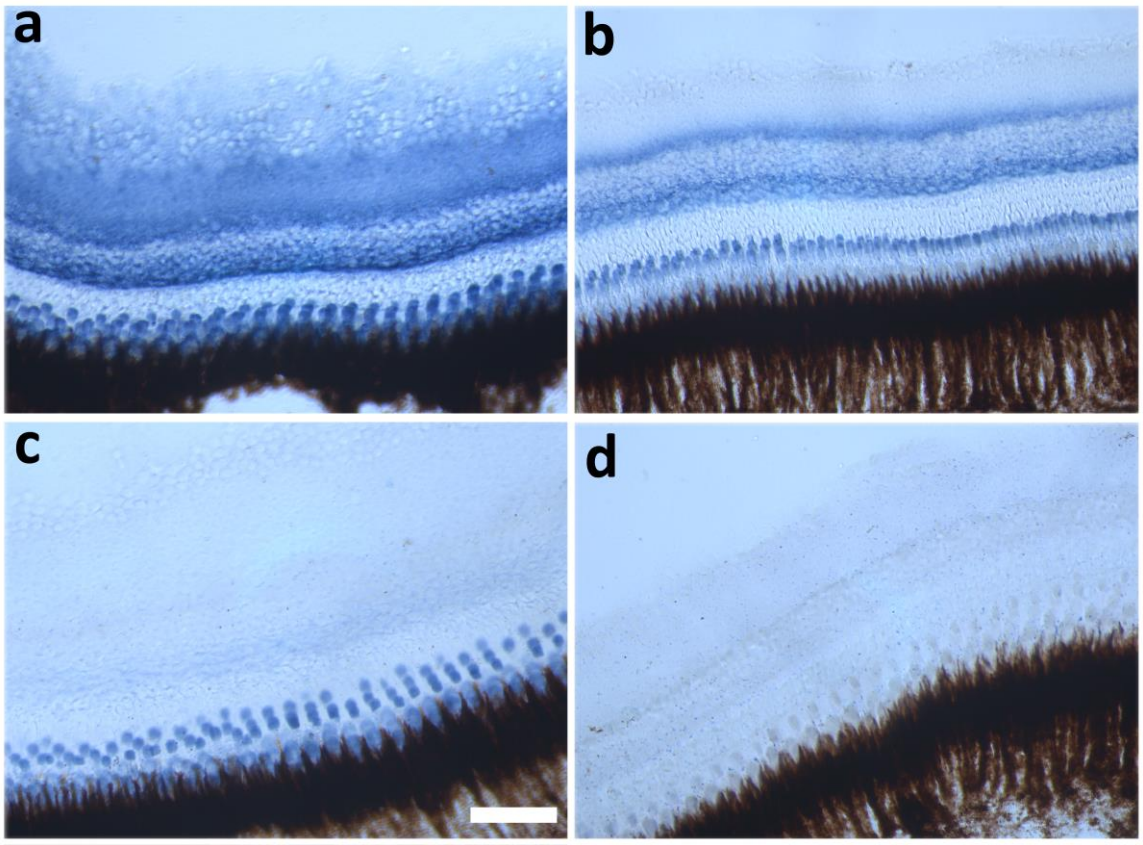

Figure 39: Histochemical detection of NQO1 enzyme activity in the adult zebrafish retina. Representative images of NQO1 enzyme activity in the adult zebrafish retina. Retinal cryosections of adult zebrafish were exposed to 100 µM menadione, 1 mM NADPH, 100 µM NBT for 30 min at 37 ˚C. A blue staining reaction was observed. *(a)* DMSO-treated *(b)* CQ- treated (10 µM), *(c)* Dic- treated (0.5 µM), *(d)* CQ and Dic- treated (10 µM and 0.5 µM). All *in-vivo* treatments were carried out for 48 hours except for the combination treatment where 4 out of 4 fish died within 6 hours of commencing the treatment. Scale bar indicates 100 µm for all images. Images were taken at 40 x magnification.

3.5.9 CQ Induces Oxidative Stress in the NQO1-Inactivated Zebrafish Retina

After observing the status of NQO1 enzyme activity in control and drug-treated animals, it was of interest to examine CQ-induced oxidative stress in the adult retina under conditions of inactivated NQO1. As a marker for oxidative stress, the presence of nitrotyrosine was detected in formalin-fixed, paraffin-embedded retinal sections of DMSO- and drug-treated adult

zebrafish. A weak immunoreactivity for nitrotyrosine was observed in Dic (0.5 µM)-treated and CQ (10 µM)-treated fish particularly around the photoreceptor and RGC layer (**Figures 40b and c)** compared to DMSO-treated fish **(Figure 40a)**. In contrast, in the CQ + Dic-treated animals, a very strong immunoreactivity for nitrotyrosine was widely detected in all retinal cell layers, indicative of significantly elevated levels of oxidative stress induced by CQ when NQO1 was inactivated **(Figure 40d)**. These results are in agreement with CQ-induced ROS production that was observed in *in-vitro*.

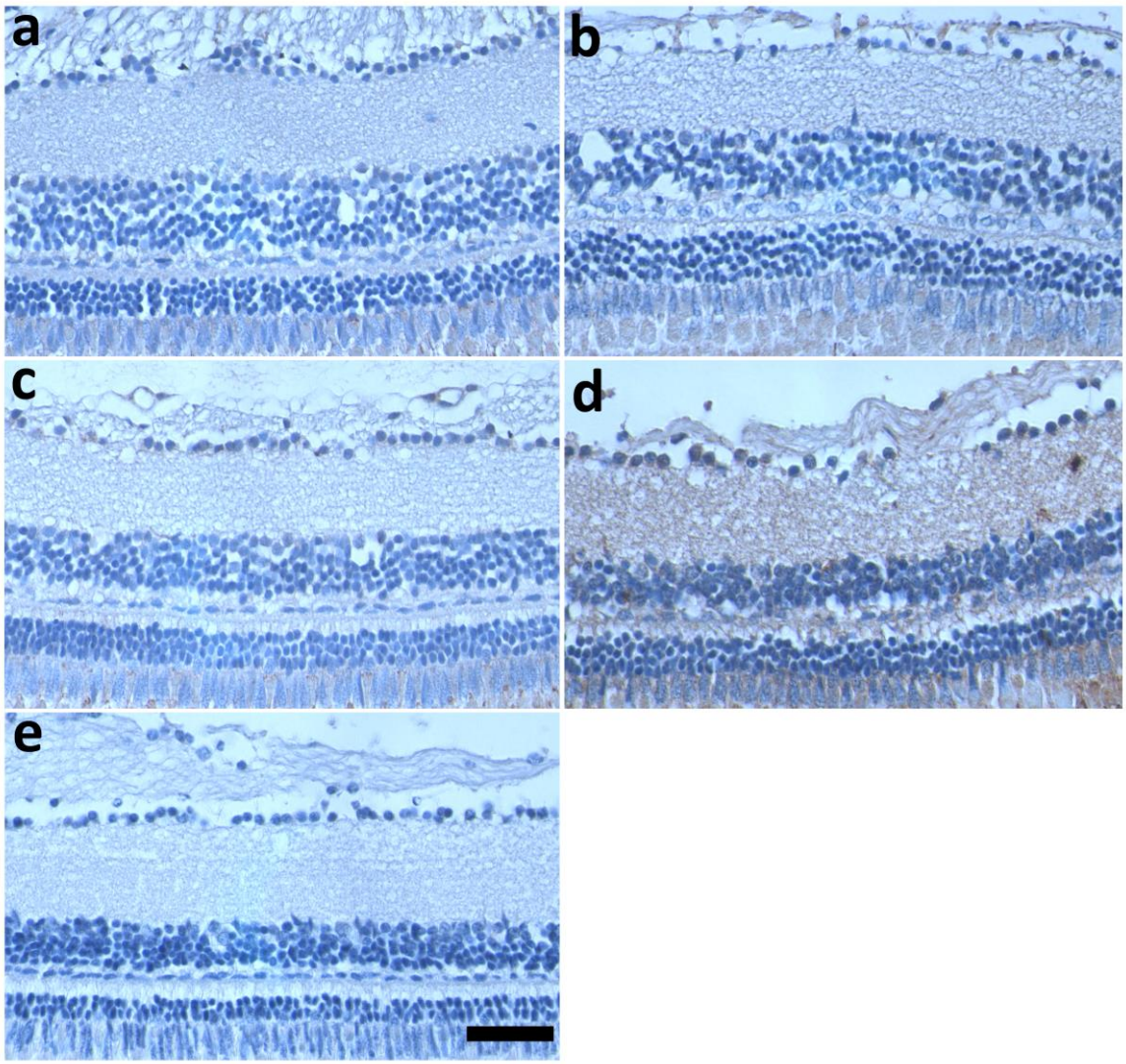

Figure 40: CQ induces oxidative stress in the NQO1 inactivated zebrafish retina.

Representative images of nitrotyrosine staining of the adult zebrafish retina. Formalin-fixed, paraffin-embedded sections of adult zebrafish retina were subjected to immunohistochemical staining for nitrotyrosine, *(a)* DMSO-treated, *(b)* CQ-treated (10 µM), *(c)* Dic-treated (0.5 µM), *(d)* CQ + Dic-treated (10 µM + 0.5 µM) *(e)* negative control (where primary antibody in *(d)* was replaced with non-specific IgG). All the treatments were carried out for 48 h except for the combination treatment (CQ + Dic; *d*) where 4 out of 4 fish died within 6 hours of treatment. Scale bar indicates 100 µm for all images. Images were taken at 40 x magnification.

3.6 Discussion

3.6.1 Suitability of an Animal Model

In order to translate the *in-vitro* results to the *in-vivo* situation, a suitable animal model was required. The described *in-vitro* results consistently indicate that CQ-induced toxicity is inversely correlated with NQO1 expression. To test this hypothesis in *in-vivo*, the essential requirement for a suitable animal model would include conditions of high and low/no NQO1 expression. Zebrafish were only recently reported to lack retinal NQO1 expression during their early larval stages (7 dpf), while NQO1 is highly expressed in the adult retina [348]. Low NQO1 activity during the early developmental stage of zebrafish is supported by a different study where the NQO1 inhibitor dicoumarol (Dic) failed to regulate the toxicity of menadione (detoxified by NQO1) and the activity of β-lapachone (bioactivated by NQO1) in zebrafish embryos [362]. This suggested that in the larvae the lack of NQO1 prevents detoxification and bioactivation of drugs [362]. This concept is further supported by the present study, where Dic failed to modulate CQ toxicity in zebrafish larvae. Incubation of zebrafish larvae with up to 3 µM Dic was non-toxic and showed no significant effect on visual performance compared to DMSO-treated controls. Furthermore, NQO1 inhibition by Dic at a non-toxic concentration of CQ (1 µM) neither affected visual function nor caused lethality in zebrafish larvae. This could be explained by the absence of retinal NQO1 but also by generally very low NQO1 enzyme activity in other tissues as previously reported (59, 60).

It has to be noted that visual impairment was one of the major adverse effects in patients that used oral CQ. Since the larvae and adult zebrafish have been reported to differ with regards to NQO1 expression in their retina, visual function was measured to study CQ-induced toxicity under conditions of both high (adult) and absent retinal NQO1 (larvae).

3.6.2 Strain-dependent Sensitivity of CQ Toxicity

In the present study CQ and Dic were added to the zebrafish media and maximum tolerated concentrations (MTC) were determined before visual acuity was assessed. Only around 3 dpf the zebrafish mouth opens, by 4-5 dpf coordinated peristalsis waves starts while the gills become functional around 14 dpf [373]. Therefore, until 3 dpf, drug absorption is only possible through the skin and until 14 dpf the drug is absorbed both through the skin and via the mouth [373]. Overall, the drug logP correlates with drug absorption in zebrafish larvae. In a study, out of 19 drugs tested with a logP >1, 18 showed pharmacological effects in zebrafish larvae, indicating that the drugs with logP >1 are successfully absorbed by zebrafish larvae [286]. In this context, CQ with log P value of 3.36 would likely be absorbed through the skin to result in significant tissue concentrations to show pharmacological effects. It can be argued that tissue drug concentrations are directly related to their pharmacological effects. Although HPLC methods have been developed to measure tissue drug exposures [374], the present study did not aim to predict drug effects quantitatively but focused instead on the qualitative examination of drug effects on visual function [286].

Although zebrafish have been increasingly used as a model organism for many years now, there is only limited information available on physiological differences underlying genetic differences among the most frequently used inbred strains of zebrafish including AB, PET, Tuebigen (TU) and Tuptel long fin (TL) [360]. Strain-dependent responses to ethanol exposure-induced disturbances in developmental processes have been reported in zebrafish [375]. With regards to embryonic lethality of ethanol exposure, zebrafish belonging to the EK (Ekkwill) strain were the most resistant strain, AB were moderately affected and TU were the most susceptible. These strain-specific differences have also been observed in the present study

with regards to CQ sensitivity of zebrafish larvae. PET strain zebrafish were more resistant to CQ-induced acute toxicity compared to the AB strain. As a consequence, the MIC for CQ in the PET strain was more than 3 times higher compared to the AB strain zebrafish larvae, which implies that genetic variation between these two strains likely contributes to the variable response to CQ exposure. Since a recent study reported a significant mtDNA diversity within different "wild-type" strains of zebrafish [376], it is likely that these differences contributed to the increased sensitivity of the AB strain to mitochondrial toxin such as CQ observed in this study.

3.6.3 Mitochondrial Function and Vision

In the present study, CQ was shown to impair mitochondrial function in *in-vitro*. There is a growing body of evidence that suggests a mitochondrial dysfunction is a primary event in many ocular diseases [31]. At the same time, typical clinical phenotypes of ocular diseases such as bilateral central vision loss, colour vision loss and loss of retinal ganglion cells are also dominant characteristics of many inherited mitochondrial diseases [31]. This connection is in agreement with the bilateral visual impairment, colour vision loss and RGC loss reported in humans after CQ administration [167]. Comparable to the responses to CQ exposure in SMON patients, CQ-treatment also significantly decreased visual function in zebrafish larvae. Intriguingly, the CQ concentration range that produced visual impairment in zebrafish larvae was surprisingly consistent with the toxic effects that were observed in this study for CQ in *in-vitro*, which further supports the hypothesis that mitochondrial dysfunction could be the key event that leads to loss of vision.

To correlate drug-induced vision loss with potential morphological defects, retinas from zebrafish larvae that were treated with CQ or DMSO were analysed histologically. Surprisingly, overall eye morphology of CQ-treated larvae was largely unaffected and therefore did not account for the observed visual defects at lower CQ concentrations up to 3 µM. Only the highest CQ concentration tested (10 µM) resulted in a small but significant decrease in RGC numbers. In addition, under these conditions, the lens appeared to be somewhat shrunk. However, since this feature was not described in SMON patients and could possibly be the result of histological artefacts, this effect was not explored any further.

It is noteworthy to mention here that autopsy of patients with SMON revealed severe lesions at the distal end of the optic tract around the lateral geniculate body. The proximal optic nerve was less severely affected and the inner ganglion cells of the retina least severely affected [162]. This specific pathology could well explain the visual defects observed in CQ-treated fish and support our finding that RGC were only slightly affected. However, CQ-induced lesions were not examined beyond the RGC layer in this study. Overall, the observed CQ-induced vision loss and RGC loss in zebrafish larvae within 48 h support the notion that low concentrations of CQ are strongly neurotoxic in *in-vivo*.

3.6.4 NQO1-dependent Protection Against CQ-induced Vision Loss

It has been suggested that NQO1 expression negatively regulates drug-induced mitochondrial dysfunction both in *in-vitro* and *in-vivo* models [377]. High NQO1 expression decreased the sensitivity of cells to mitochondrial toxin-induced oxidative stress, energy depletion and cell death [332]. Similarly, NQO1 knockout mice were highly susceptible to drug-induced hepatotoxicity resulting in elevated ROS levels, mitochondrial dysfunction-mediated energy

depletion compared to the wild-type controls [331]. Mitochondrial dysfunction has been implicated in the major ocular diseases such as age-related macular degeneration, diabetic retinopathy and glaucoma [31]. Since NQO1 is reported to be absent in zebrafish larvae, it appears not surprising that CQ induced vision loss in a dose-dependent manner in these animals. This effect is likely due to the mitochondrial-dysfunction of CQ in the absence of NQO1. The protective effect of NQO1 against CQ-induced vision loss was further examined in the adult zebrafish where NQO1 is reported to be highly expressed in the retina [348].

Consistent with the hypothesis of this study, and in contrast to the zebrafish larvae, CQ even at the highest concentration did not impair visual function compared to DMSO-treated controls in PET adult zebrafish. In an attempt to investigate the effect of CQ under conditions of inactivated NQO1, adult zebrafish were treated with CQ and/or Dic followed by assessing their visual acuity. Visual function was not impaired when NQO1 was inhibited. However, the combination of CQ and Dic led to the unexpected death of fish within only a few hours after the start of treatment. This acute toxicity can be attributed to the systemic inhibition of NQO1 in the major tissues such as heart, liver and brain. Although this study did not investigate the reason for this dramatic acute toxicity in detail due to significant concerns by the local animal ethics committee, this result strongly supports the hypothesis that CQ is very toxic under conditions where NQO1 is inactivated or absent, which is surprisingly consistent with the *in-vitro* data of this study. Overall, NQO1 expression seems to protect against CQ-induced vision loss in the adult zebrafish.

Zebrafish are reported to possess Nrf2-keap1 system [378]. In fact, Nrf2 and Nrf2-target genes such as GSTπ, NQO1 and GCSH are reasonably conserved between zebrafish and mammals [378]. Exposure of zebrafish to pro-oxidants induced Nrf2 and Nrf2-target genes such as GCLC

and NQO1 [378-381]. However, these studies only assessed mRNA expression and so far, there are no reports regarding measurement of NQO1 protein expression in zebrafish. In the current study, we were unable to confirm the presence of NQO1 protein in the retina of adult zebrafish due to the unavailability of zebrafish-specific anti-NQO1 antibodies. NQO1 is reported to localise primarily to the cytoplasm [366], which is in stark contrast to the current study where exclusively nuclear NQO1 immunostaining was observed with an anti-NQO1 antibody that was predicted to cross-react with zebrafish NQO1. Furthermore, in western blots, NQO1 protein from adult and larval zebrafish was detected at two different molecular weights and both of them did not correspond to the predicted size of human NQO1. The bioinformatics analysis predicted that all four zebrafish NQO1 splice variants to be cytoplasmic. These splice variants differ mainly in the presence or absence of a 14 amino acid region encoded by exons 4 and 5. The variants (003 and 001) lack these amino acids, which is consistent with human NQO1. In contrast, NQO1 variants (201 and 004) contain this particular amino acid sequence. There was a possibility that the detection of zebrafish NQO1 at two different molecular weights in the western blot could possibly be due to the presence of these NQO1 splice variants. However, the predicted molecular weights of these splice variants range from 21-32 kDa and are therefore unlikely to correspond to the molecular weight of about 45 and 10 kDa observed for larvae and adult fish respectively. These observations further question the specificity of the available anti-NQO1 antibody. Although this problem could have been solved by raising Zebrafish-specific NQO1 antibodies, this was clearly beyond the scope of this study but should be considered for future studies.

A linear relationship between NQO1 protein content and activity has been reported in transfected cell lines, indicating that the expressed protein is active [382]. In addition, no major posttranslational modification that would affect NQO1 activity has been described. However,

there is the possibility that despite normal NQO1 levels, the NQO1 activity can be compromised {reviewed by [300]}. Different factors are described that can affect NQO1 activity such as drugs (dicoumarol and flavonoids), advancing age, and cigarette smoke {reviewed by [300]}. Therefore, measurement of NQO1 activity can be seen as a much more relevant assessment compared to protein expression alone. Hence, NQO1 enzyme activity was measured in the retina of adult zebrafish. A strong staining reaction for NQO1 was observed in DMSO-treated adult animals, indicating high NQO1 enzyme activity. The staining was diffuse and visible in all retinal layers from the photoreceptor layer to the retinal ganglion cell (RGC) layer. This is somewhat consistent with the previous result in mice where NQO1 was reported to be expressed in the inner segment of the photoreceptor layer and RGC cells [383]. The positive staining of NQO1 activity in the photoreceptor layer in zebrafish, however, is in contrast to another study, where NQO1 mRNA expression was reported to be absent in the entire photoreceptor layer [348]. In Dic-treated fish, NQO1 staining was observed only in the photoreceptor layer. The inhibition of NQO1 activity staining in the most part of the retina of Dic-treated animals is most likely due to the inhibition of NQO1 enzyme activity, while the Dic-insensitive staining in the photoreceptor layer may be attributed to other reductase activity or different enzymes altogether [359]. It is intriguing to note that the NQO1 staining was first reduced in the RGC layer. This could indicate that RGCs have greater sensitivity to CQ treatment or could be that CQ gets access to the RGC layer first. However, these possibilities were not further explored in this study. Since the combination of CQ and Dic completely abolished the staining reaction, and the current study showed that both compounds inhibit NQO1 activity, it is likely that either NQO1 activity is measured or that CQ also inhibits the postulated unknown reductase as well. These results strongly suggest that NQO1 is present in the retina of adult zebrafish as reported and can, therefore, explain the NQO1-dependent protection against CQ-induced vision loss in adult fish versus the toxicity observed in larvae.

3.6.5 Oxidative Stress and CQ-induced Vision Loss

The retina is rich in polyunsaturated fatty acids that are highly vulnerable to ROS and thus are easily peroxidised [384]. Excess ROS are normally detoxified by antioxidants present in the retina. However, any imbalance between ROS production and detoxification, due to disturbances in the antioxidant systems or mitochondrial dysfunction-induced excessive ROS production, may result in oxidative stress in the retina [31,385]. The tight connection between excess ROS and retinal function is highlighted by several animal models of ocular diseases that are based on changing the balance between ROS production and antioxidant protection. Recently, an imbalance between pro-oxidant and Nrf2-dependent antioxidant genes (NQO1, heme oxygenase 1, glutathione S-reductase) have been shown to play an important role in the onset and progression of age-related macular degeneration [386]. Furthermore, involvement of NQO1 in retinal pathology was shown indirectly in a study where Nrf2 deficient mice developed age-related retinopathy [387]. This is in line with the result of the present study where inactivation of retinal NQO1, by itself already increased oxidative stress levels in the retina. It is likely that the level of ROS production was insufficient to alter visual function in a relatively short period of time. However, the combination of Dic and CQ in the adult zebrafish caused significant levels of oxidative damage in the retina. This result thus unequivocally supports the finding of the *in-vitro* study and suggests that oxidative stress is the mechanism of CQ–induced neurotoxicity. Therefore, our results directly support the possibility that the SMON cases in Japan could be a direct consequence of CQ exposure under conditions of absent or dysfunctional NQO1 protein.

CHAPTER 4

Chapter 4: General Conclusion

4.1 Summary

A number of widely used drugs are reported to cause mitochondrial dysfunction and many are implicated in mitochondrial dysfunction-induced optic neuropathy [31]. With the aim to identify potential mitochondrial toxins, an *in-vitro* screen of around 200 drugs and drug-like compounds was performed. Two compounds 5-chloro-7-iodo-8-hydroxyquinoline (CQ) and 8-hydroxyquinoline (8-HQ) were returned as hits. The fact that these two compounds share a common 8-hydroxyquinoline ring structure strongly supported the finding of the screen. A literature search on these two compounds revealed that CQ, a quinoline derivative, was widely used (1950 to 1969) as a topical disinfectant and as an oral anti-microbial agent to treat diarrhoea. However, its oral form was banned in many countries after being linked to endemic outbreak of SMON (subacute mylo-optic neuropathy) affecting 10, 000 people in Japan [167]. SMON was characterised by abdominal pain, subacute ascending dysesthesia, paresthesia of lower extremities and bilateral visual impairment [162,166]. Although a clear mechanistic connection remained elusive up to now, a reduction in the incidence of SMON was witnessed following the withdrawal of CQ from the market. Furthermore, the common pathological features of SMON-associated neurotoxicity have been successfully recapitulated in CQ-treated animals, which support a direct connection [176,177]. Despite ample evidence for their neurotoxicity, CQ and 8-HQ analogues have re-emerged as a potential therapeutic agent for the treatment of neurodegenerative diseases such as Alzheimer's (AD), Huntington's (HD) with some promising pre-clinical and clinical results [188,200,202,209-211,214,215]. These therapeutic outcomes are thought to be based on the metal chelating properties of CQ and its structural analogue PBT-2 [187-189,203,214,215]. Metal-induced oxidative stress by Zn, Cu, and Fe has been implicated in neocortical amyloid formation and deposition in AD brains as

well as aggregation of mutant huntingtin protein in HD [203,215]. In line with the proposed pathology of these neurodegenerative diseases, it was reported that CQ chelates and redistributes metal ions. As a consequence CQ is thought to disaggregate the existing as well as reduce de novo amyloid deposition in AD and reduce mutant huntingtin protein aggregates in HD [203,215]. In light of the obvious contradictory activities of CQ, neurotoxicity on the one hand and neuroprotection on the other, a thorough understanding of CQ-induced toxicity is warranted to prevent potential CQ-treatment associated adverse effects.

In this study, I investigated the mechanism of CQ-induced toxicity in *in-vitro* and *in-vivo*. Using a number of *in-vitro* based assays, it was observed that CQ and its parent compound 8-HQ induced mitochondrial-dysfunction in RGC5 cells both as a result of short- and long-term treatment. However, attempts to confirm this toxicity in a different cell line (HepG2) were unsuccessful. Unrelated observations from a different project suggested that one major difference between the two cell lines used (RGC5, HepG2) is their ability to respond to drugs and drug-induced oxidative stress. This ability is associated with significantly different expression levels of the antioxidant gene product NQO1. Western blot analysis revealed that RGC5 cells that were sensitive to CQ-mito toxicity have much lower NQO1 expression compared to HepG2 cells, which were CQ-resistant. NQO1 dependent CQ mitochondrial-dysfunction was then confirmed in several isogenic cell lines that differ only in their NQO1 levels. In these cells, expression of NQO1 was positively correlated with protection against CQ-induced mitochondrial-dysfunction. Furthermore, the present study clearly demonstrated that CQ-induced mitochondrial dysfunction was mediated through increased levels of oxidative stress by the observation that exogenous antioxidants were able to rescue CQ-induced mitochondrial-dysfunction. The inverse correlation between NQO1 expression and CQ toxicity observed in this study suggested a biochemical interaction between these two molecules.

Through both cell free and cell-based methods, it was revealed that CQ inhibited NQO1 enzyme activity in a dose dependent manner.

Based on the *in-vitro* results, zebrafish were chosen as a model system for many reasons. Firstly, zebrafish are reported to lack retinal NQO1 expression during their larval stage, while NQO1 is highly expressed in the adult retina. As a consequence, this model allows us to test CQ-induced toxicity in a situation of both absent and high NQO1 levels in the retina. Secondly, zebrafish are increasingly used as a model organism for toxicity screening and are a validated model for visual safety assessment of drugs [281,284]. The other reasons include a rapid eye development that allows examining visual function only 5 dpf and the high resemblance of their visual system with the human eye when compared for example to rodent models. Comparable to the human situation, CQ induced visual impairment in zebrafish larvae deficient in retinal NQO1 in a dose dependent manner. In contrast, visual function was not at all affected by CQ in the adult zebrafish that express high levels of retinal NQO1. This protective role of NQO1 against CQ-induced loss of visual function was confirmed by the presence of NQO1 enzyme activity in the retinal section of the adult zebrafish. Consistent with this activity, positive immunostaining for nitrotyrosine, a marker for oxidative damage, was observed in retinal section of CQ-treated adult zebrafish where NQO1 had been inactivated pharmacologically. Furthermore, under these conditions, CQ also caused acute systemic toxicity in the adult zebrafish. These *in-vivo* results are in line with the *in-vitro* findings suggesting CQ-induced toxicity that is mediated by increased levels of oxidative stress and is dependent on expression of functional NQO1.

Overall, the *in-vitro* and *in-vivo* results of the present investigation reinforce the concept that CQ and its parent compound 8-HQ induce mitochondrial dysfunction through oxidative stress

(Figure 41). Importantly, comparable to CQ-induced pathology in human SMON patients, the *in-vivo* data suggests that CQ treatment can lead to a clear dose-dependent loss of visual function under conditions of low or absent NQO1 expression or in the presence of an inactive NQO1 protein. Expression of NQO1 protected against CQ-induced mitochondrial-dysfunction *in-vitro* and vision loss *in-vivo*. The exact mechanism on how CQ-induced mitochondrial dysfunction and vision loss is attenuated by NQO1 still needs further investigation.

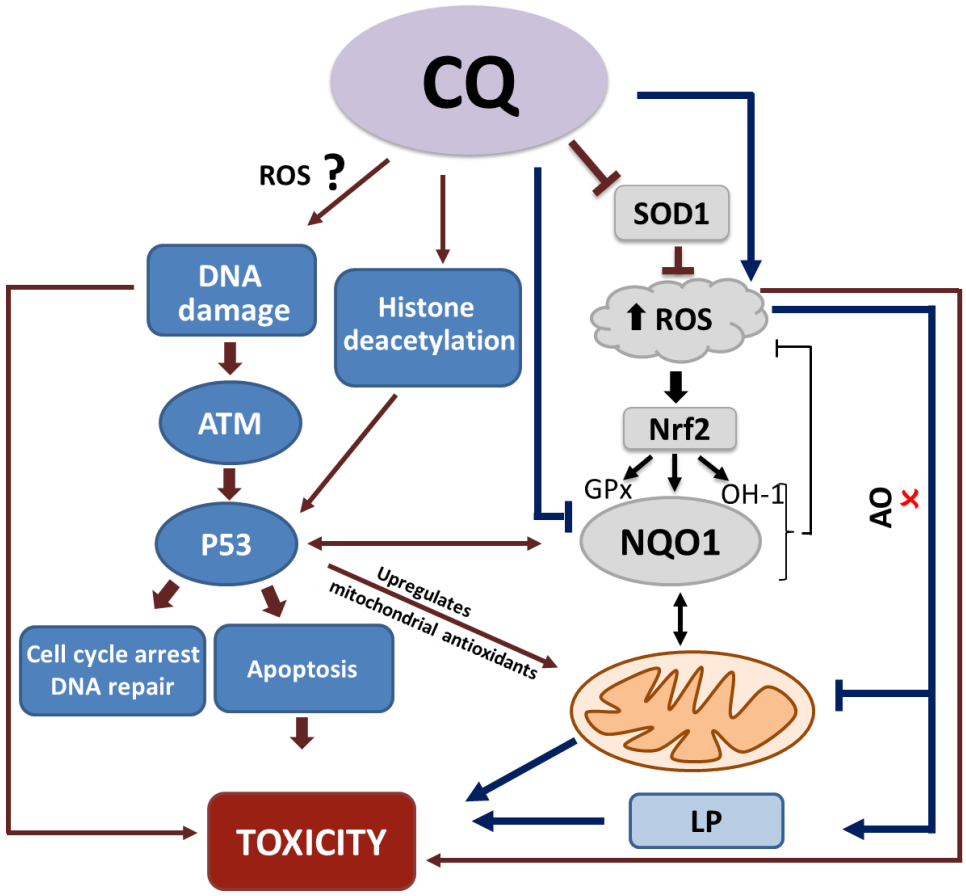

Figure 41: Possible mode of CQ-induced neurotoxicity.

CQ-induces cellular neurotoxicity through DNA breaks, activation of ATM (markers for DNA damage) and subsequent activation of p53 and its target genes that finally leads to apoptosis [184]. CQ-treatment also reduced histone acetylation, a process essential for DNA-repair and the transcriptional activation of genes that are responsible for cell proliferation [186]. CQ was also reported to produce cellular toxicity through oxidative stress by inhibition of superoxide dismutase 1 [182]. CQ induced mitochondrial dysfunction through oxidative stress which was prevented by NQO1. One possibility is that NQO1 can prevent CQ-induced mitochondrial-dysfunction through p53-dependent upregulation of

mitochondrial antioxidants genes. **Blue lines** indicate experimental results of the present study, red and black lines indicate published results from previous studies. SOD: Superoxide dismutase; ROS: Reactive oxygen species; ATM: Ataxia Telangiectasia mutated; Nrf2: Nuclear factor erythroid 2-related factor 2; GPx: Glutathione Peroxidase 1; OH-1: Heme oxygenase 1; AO: Antioxidant; LP: Lipid Peroxidation.

4.2 Implication of the Study

In this study, the mechanism of CQ-induced toxicity was investigated both in *in-vitro* and *in-vivo* and CQ-induced oxidative stress was identified as a key component of CQ toxicity. Moreover, in line with this underlying source of toxicity, a tight connection between NQO1 and CQ toxicity was identified, which for the first time could potentially explain the restriction of CQ-induced SMON to the Japanese population.

NQO1 is an FAD-containing cytosolic protein that catalyses the two-electron reduction of quinones and other compounds and prevents the production of semi-quinones, free radicals and ROS, thus protecting cells and tissues against oxidative stress. Since NQO1 expression/ activity is inversely correlated to CQ toxicity, it is essential to consider factors affecting NQO1 enzyme activity. There are several different factors that can inhibit NQO1 activity such as age, drugs (flavonoids, dicoumarol) but also a genetic predisposition. The most prominent reason for reduced NQO1 activity is NQO1 polymorphisms [300]. The most frequent and best-studied human NQO1 polymorphism is NQO1*2. NQO1*2 (C609T or Pro187Ser) is a single nucleotide polymorphism, a C to T change at position 609, which results in a proline to serine substitution at amino acid 187 of the protein. This polymorphism affects NQO1 protein stability and therefore the available NQO1 activity [388]. Heterozygote carriers (C/T) only show about 50 % NQO1 protein and activity compared to carriers of the C/C genotype. Homozygote carriers (T/T) only show very low to undetectable residual NQO1 activity

[389,390]. The striking connection of this to the Japanese SMON cases is a much higher prevalence (nearly 3-4 fold higher) of this inactivating C609T NQO1 polymorphism in Japanese and Asian populations compared to the African or European population [391,392] (**Table 9**). In the Europeans nearly 80 % of individuals harbour the normal C/C NQO1 genotype. In contrast, nearly 70 % of the Japanese population (overall Asian) carries the inactivating C/T or T/T NQO1 genotype. Given this higher prevalence of NQO1 polymorphism in Japanese patients, these individuals should be much more susceptible to the toxicity of CQ. This hypothesis exactly aligns with the *in-vitro* data of this study where CQ-induced toxicity was mainly observed in the cell lines that already have low NQO1 expression or activity. Further inhibition of NQO1 activity by CQ (10 µM), although not that strong, could further enhance CQ toxicity in those who already have 50 % or lesser NQO1 activity. In contrast, CQ-induced NQO1 inhibition might not affect those individuals with 100 % NQO1 activity. Hence the results of the present study could for the first time explain the geographic restriction of CQ-induced neurotoxicity to Japan.

Table 9: Prevalence of C609T genotypes in different ethnic groups [391,392]

Genotype			
Ethnic group	**C/C (%)**	**C/T (%)**	**T/T (%)**
Asia (overall)	31.4	48.3	20.3
Chinese	28.6	50.0	22.4
Caucasians	82	16	2
Africans	61	33.8	5.2

C/C: wild type NQO1; C/T: heterozygote NQO1; T/T: homozygote NQO1.

It is worth noting that there are clinical trials being conducted to examine the potential role of CQ and its analogues as a disease-modifying treatment in neurodegenerative diseases. In fact, these clinical trials were undertaken in Europe and Australia, where the majority of participants would be likely to harbour the active NQO1 genotype. Based on the results of this study, this population group may not show CQ toxicity. Consequently, the clinical phenotypes of CQ-induced SMON such as motor disorder and visual impairment may not have occurred in these trial participants. Nevertheless, a few cases of neurotoxicity have been reported. In a randomised placebo-controlled clinical trial in AD patients, 3 out of 16 patients that received CQ and Vitamin B 12 for 36 weeks developed impaired nerve conduction, 2 out of 16 patients complained of leg numbness and one patient developed visual impairment including loss of visual acuity and colour vision loss [188]. It is also important to note that neurotoxicity is typically a rather slow process and may take several weeks to develop, which is likely why these patients may not have developed the full neurotoxicity symptoms associated with SMON. Furthermore, due to the overlapping clinical symptoms of CQ-induced neurotoxicity and neurodegenerative diseases, drug-induced neurotoxicity (motor disorder, visual impairment) would have been difficult to distinguish from the natural progression of the disease itself.

Therefore, in light of the recent emerging interest in CQ and its analogues for the treatment of neurodegenerative disorders such as Alzheimer's and Huntington's disease the results of this study are of direct importance. This study strongly suggests that the use of CQ or its derivatives for the treatment of neurodegenerative diseases should require a prior determination of the NQO1 activity status of patients. Consequently, the results of this study represent a significant step towards personalized medicine to minimize the risks associated with CQ and its analogues.

4.3 Limitations of the Study

This study contemplated the molecular mechanism involved in CQ-induced toxicity and provides a possible explanation for the higher prevalence of this toxicity seen in the Japanese population. Although this study addresses all the aims and objectives, there were some limitations that have to be considered. The *in-vitro* results indicate that CQ is responsible for inducing ROS-mediated mitochondrial dysfunction. However, this study did not run any positive controls such as known mitochondrial inhibitors to confirm ROS production from mitochondrial dysfunction in cells. Hence, the origins of excess ROS are still unclear. Although, from the results of the study, it is possible that the ROS is generated as a consequence of the CQ-mediated increase in intracellular zinc levels or due to the inhibition of the ROS-detoxifying enzyme, NQO1, further research is warranted to confirm any of those possibilities. In addition, the *in-vitro* results also indicate that CQ can directly inhibit NQO1 activity and consequently NQO1 expression protected against CQ-induced mitochondrial dysfunction. Given the cytoplasmic localization of NQO1, it is still unclear what biochemical pathways are involved in protecting mitochondrial impairment induced by CQ. One of the possibilities would be to use dyes that can detect mitochondrial superoxide such as MitoSOX or dihydroethidium (DHE) to examine if NQO1 directly scavenges ROS and protects against CQ-toxicity.

The *in-vivo* results demonstrated that CQ-induced vision loss was negatively correlated with NQO1 expression. In this context, CQ showed a clear dose-dependent reduction of visual function in retinal-NQO1 deficient zebrafish larvae, whereas visual function was not affected in the adult zebrafish that presumably highly expressed NQO1 in the retina. However, expression of NQO1 could not be quantified due to the unavailability of antibodies that are specific to zebrafish.

The protecting role of NQO1 was confirmed in the retinal section of adult zebrafish. However, the NQO1 status in the retina of zebrafish larvae was not examined due to breeding difficulties of the PET strain in our facility. Hence, the reported absence of retinal NQO1 in zebrafish larvae was only confirmed through the indirect measurement of NQO1 activity in AB strain animals where inhibition of NQO1 failed to modulate CQ toxicity. Furthermore, CQ-induced ROS production and its effect on mitochondrial function was not explored due to a temporary unavailability of larvae for the experiments.

4.4 Future Directions

The results of this study for the first time demonstrate that oxidative stress-mediated mitochondrial dysfunction is central to CQ-induced toxicity and highlight the importance of NQO1 in determining CQ toxicity. Furthermore, previously published genomic data revealed that the known inactivating NQO1 polymorphism (C609T) is highly prevalent among the Japanese population. Based on this, the results of the present study could for the first time explain geographic restriction of SMON cases to Japan. In light of re-emergence of CQ and its structural analogues for new indications, it has become crucial to understand the mechanistic association between SMON and CQ in order to avoid any potential adverse effects of CQ administration to patients. In this context, it becomes essential to strengthen the connection of NQO1 expression and CQ toxicity by investigating this hypothesis in patients that developed SMON. Therefore, we have started the collaboration with the former Head of the Japanese Government Commission that was tasked to identify the origins of SMON. We are currently in the process of collecting DNA samples from surviving SMON patients to confirm the presence of the inactivating NQO1 polymorphism. If we can show that these patients indeed

carry the polymorphism, our research would solve the 50-year-old mystery why, despite the global use of CQ, SMON cases were largely restricted to Japan. Another possibility would be to generate immortalized cell lines from C609T carriers to directly test CQ toxicity against cell lines from non-carriers (C/C). This study could be extended to identify the drugs that have the potential to interfere with NQO1 activity. This would be beneficial in the long run to minimize the risk associated with the administration of CQ and its analogues.

References

References

1. Wong-Riley MT. Energy metabolism of the visual system. Eye Brain. 2010;2:99.
2. Yusoff AAM, Ahmad F, Idris Z, Jaafar H, Abdullah JM. Understanding Mitochondrial DNA in Brain Tumorigenesis. In: Molecular Considerations and Evolving Surgical Management Issues in the Treatment of Patients with a Brain Tumor. Terry L, editor. 2015.
3. Yu-Wai-Man P, Griffiths PG, Chinnery PF. Mitochondrial optic neuropathies - disease mechanisms and therapeutic strategies. Prog Retin Eye Res. 2011;30(2):81-114.
4. Wallace DC, Fan W, Procaccio V. Mitochondrial energetics and therapeutics. Annu Rev Pathol. 2010;5:297-348.
5. Tait SW, Green DR. Mitochondria and cell signalling. J Cell Sci. 2012;125(Pt 4):807-15.
6. Bratic I, Trifunovic A. Mitochondrial energy metabolism and ageing. Biochim Biophys Acta. 2010;1797(6-7):961-7.
7. Vander Heiden MG, Cantley LC, Thompson CB. Understanding the Warburg effect: the metabolic requirements of cell proliferation. Science. 2009;324(5930):1029-33.
8. Koopman WJ, Beyrath J, Fung CW, Koene S, Rodenburg RJ, Willems PH, et al. Mitochondrial disorders in children: toward development of small-molecule treatment strategies. EMBO Mol Med. 2016;8(4):311-27.
9. Vonck J, Schafer E. Supramolecular organization of protein complexes in the mitochondrial inner membrane. Biochim Biophys Acta. 2009;1793(1):117-24.
10. Schafer E, Seelert H, Reifschneider NH, Krause F, Dencher NA, Vonck J. Architecture of active mammalian respiratory chain supercomplexes. J Biol Chem. 2006;281(22):15370-5.

11. Floyd BJ, Wilkerson EM, Veling MT, Minogue CE, Xia C, Beebe ET, et al. Mitochondrial Protein Interaction Mapping Identifies Regulators of Respiratory Chain Function. Mol Cell 2016;63(4):621-32.
12. Zorov DB, Juhaszova M, Sollott SJ. Mitochondrial reactive oxygen species (ROS) and ROS-induced ROS release. Physiol Rev. 2014;94(3):909-50.
13. Handy DE, Loscalzo J. Redox regulation of mitochondrial function. Antioxid Redox Signal. 2012;16(11):1323-67.
14. Hancock JT, Desikan R, Neill SJ. Role of reactive oxygen species in cell signalling pathways. Biochem Soc Trans. 2001;29(Pt 2):345-50.
15. Jarrett SG, Lin H, Godley BF, Boulton ME. Mitochondrial DNA damage and its potential role in retinal degeneration. Prog Retin Eye Res. 2008;27(6):596-607.
16. Raha S, Robinson BH. Mitochondria, oxygen free radicals, and apoptosis. Am J Med Genet. 2001;106(1):62-70.
17. Quinlan CL, Orr AL, Perevoshchikova IV, Treberg JR, Ackrell BA, Brand MD. Mitochondrial complex II can generate reactive oxygen species at high rates in both the forward and reverse reactions. J Biol Chem. 2012;287(32):27255-64.
18. Desouki MM, Kulawiec M, Bansal S, Das GM, Singh KK. Cross talk between mitochondria and superoxide generating NADPH oxidase in breast and ovarian tumors. Cancer Biol Ther. 2005;4(12):1367-73.
19. Hirst J, King MS, Pryde KR. The production of reactive oxygen species by complex I. Biochem Soc Trans. 2008;36(Pt 5):976-80.
20. Balaban RS, Nemoto S, Finkel T. Mitochondria, oxidants, and aging. Cell. 2005;120(4):483-95.
21. Pereverzev MO, Vygodina TV, Konstantinov AA, Skulachev VP. Cytochrome c, an ideal antioxidant. Biochem Soc Trans. 2003;31(Pt 6):1312-5.

22. Aon MA, Stanley BA, Sivakumaran V, Kembro JM, O'Rourke B, Paolocci N, et al. Glutathione/thioredoxin systems modulate mitochondrial H2O2 emission: an experimental-computational study. J Gen Physiol. 2012;139(6):479-91.

23. Collins Y, Chouchani ET, James AM, Menger KE, Cocheme HM, Murphy MP. Mitochondrial redox signalling at a glance. J Cell Sci. 2012;125(Pt 4):801-6.

24. Lin MT, Beal MF. Mitochondrial dysfunction and oxidative stress in neurodegenerative diseases. Nature. 2006;443(7113):787-95.

25. Dai DF, Rabinovitch PS, Ungvari Z. Mitochondria and cardiovascular aging. Circ Res. 2012;110(8):1109-24.

26. Hall AM, Unwin RJ, Hanna MG, Duchen MR. Renal function and mitochondrial cytopathy (MC): more questions than answers? QJM. 2008;101(10):755-66.

27. Garcia-Ruiz C, Baulies A, Mari M, Garcia-Roves PM, Fernandez-Checa JC. Mitochondrial dysfunction in non-alcoholic fatty liver disease and insulin resistance: cause or consequence? Free Radic Res. 2013;47(11):854-68.

28. Ralph SJ, Rodriguez-Enriquez S, Neuzil J, Saavedra E, Moreno-Sanchez R. The causes of cancer revisited: "mitochondrial malignancy" and ROS-induced oncogenic transformation - why mitochondria are targets for cancer therapy. Mol Aspects Med. 2010;31(2):145-70.

29. Maechler P, Li N, Casimir M, Vetterli L, Frigerio F, Brun T. Role of mitochondria in beta-cell function and dysfunction. Adv Exp Med Biol. 2010;654:193-216.

30. Schrier SA, Falk MJ. Mitochondrial disorders and the eye. Curr Opin Ophthalmol. 2011;22(5):325-31.

31. Chhetri J, Gueven N. Targeting mitochondrial function to protect against vision loss. Expert Opin Ther Targets. 2016;20(6):721-36.

32. Smith RA, Hartley RC, Cocheme HM, Murphy MP. Mitochondrial pharmacology. Trends Pharmacol Sci. 2012;33(6):341-52.

33. Gandhi S, Abramov AY. Mechanism of oxidative stress in neurodegeneration. Oxid Med Cell Longev. 2012;2012:428010.

34. Santos JM, Tewari S, Goldberg AF, Kowluru RA. Mitochondrial biogenesis and the development of diabetic retinopathy. Free Radic Biol Med. 2011;51(10):1849-60.

35. Farrar GJ, Chadderton N, Kenna PF, Millington-Ward S. Mitochondrial disorders: aetiologies, models systems, and candidate therapies. Trends Genet. 2013;29(8):488-97.

36. Jarrett SG, Lewin AS, Boulton ME. The importance of mitochondria in age-related and inherited eye disorders. Ophthalmic Res. 2010;44(3):179-90.

37. Carelli V, Ross-Cisneros FN, Sadun AA. Mitochondrial dysfunction as a cause of optic neuropathies. Prog Retin Eye Res. 2004;23(1):53-89.

38. Wang L, Dong J, Cull G, Fortune B, Cioffi GA. Varicosities of intraretinal ganglion cell axons in human and nonhuman primates. Invest Ophthalmol Vis Sci. 2003;44(1):2-9.

39. Al-Enezi M, Al-Saleh H, Nasser M. Mitochondrial disorders with significant ophthalmic manifestations. Middle East Afr J Ophthalmol. 2008;15(2):81-6.

40. DiMauro S, Schon EA. Mitochondrial Respiratory-Chain Diseases. N Engl J Med. 2003;348(26):2656-68.

41. Fraser JA, Biousse V, Newman NJ. The neuro-ophthalmology of mitochondrial disease. Surv Ophthalmol. 2010;55(4):299-334.

42. Sadun AA, Win PH, Ross-Cisneros FN, Walker SO, Carelli V. Leber's hereditary optic neuropathy differentially affects smaller axons in the optic nerve. Trans Am Ophthalmol Soc. 2000;98:223-32; discussion 32-5.

43. Kawasaki A, Herbst K, Sander B, Milea D. Selective wavelength pupillometry in Leber hereditary optic neuropathy. Clin Experiment Ophthalmol. 2010;38(3):322-4.

44. Thouin A, Griffiths PG, Hudson G, Chinnery PF, Yu-Wai-Man P. Raised intraocular pressure as a potential risk factor for visual loss in Leber Hereditary Optic Neuropathy. PLoS One. 2013;8(5):e63446.

45. Hudson G, Carelli V, Spruijt L, Gerards M, Mowbray C, Achilli A, et al. Clinical expression of Leber hereditary optic neuropathy is affected by the mitochondrial DNA-haplogroup background. Am J Hum Genet. 2007;81(2):228-33.

46. Badura-Stronka M, Wawrocka A, Zawieja K, Silska S, Krawczynski MR. Severe manifestation of Leber's hereditary optic neuropathy due to 11778G>A mtDNA mutation in a female with hypoestrogenism due to Perrault syndrome. Mitochondrion. 2013;13(6):831-4.

47. Stone EM, Newman NJ, Miller NR, Johns DR, Lott MT, Wallace DC. Visual recovery in patients with Leber's hereditary optic neuropathy and the 11778 mutation. J Clin Neuroophthalmol. 1992;12(1):10-4.

48. Breuer M, Koopman W, Koene S, Nooteboom M, Rodenburg R, Willems P, et al. The role of mitochondrial OXPHOS dysfunction in the development of neurologic diseases. Neurobiol Dis. 2013;51:27-34.

49. Gueven N. Optic Neurodegeneration: Time to Act. Biol Med 2014;1(101):2.

50. Carelli V, Ross-Cisneros FN, Sadun AA. Optic nerve degeneration and mitochondrial dysfunction: genetic and acquired optic neuropathies. Neurochem Int. 2002;40(6):573-84.

51. Newman NJ. Hereditary optic neuropathies: from the mitochondria to the optic nerve. Am J Ophthalmol. 2005;140(3):517-23.

52. Carelli V, La Morgia C, Valentino ML, Barboni P, Ross-Cisneros FN, Sadun AA. Retinal ganglion cell neurodegeneration in mitochondrial inherited disorders. Biochim Biophys Acta. 2009;1787(5):518-28.

53. Heiduschka P, Schnichels S, Fuhrmann N, Hofmeister S, Schraermeyer U, Wissinger B, et al. Electrophysiological and Histologic Assessment of Retinal Ganglion Cell Fate in a Mouse Model for OPA1-Associated Autosomal Dominant Optic Atrophy. Invest Ophthalmol Vis Sci. 2010;51(3):1424-31.

54. Maresca A, la Morgia C, Caporali L, Valentino ML, Carelli V. The optic nerve: a "mito-window" on mitochondrial neurodegeneration. Mol Cell Neurosci. 2013;55:62-76.

55. Mayorov VI, Lowrey AJ, Biousse V, Newman NJ, Cline SD, Brown MD. Mitochondrial oxidative phosphorylation in autosomal dominant optic atrophy. BMC Biochem. 2008;9:22.

56. Ferre M, Bonneau D, Milea D, Chevrollier A, Verny C, Dollfus H, et al. Molecular screening of 980 cases of suspected hereditary optic neuropathy with a report on 77 novel OPA1 mutations. Hum Mutat. 2009;30(7):E692-705.

57. Bette S, Schlaszus H, Wissinger B, Meyermann R, Mittelbronn M. OPA1, associated with autosomal dominant optic atrophy, is widely expressed in the human brain. Acta Neuropathol. 2005;109(4):393-9.

58. Olichon A, Baricault L, Gas N, Guillou E, Valette A, Belenguer P, et al. Loss of OPA1 perturbates the mitochondrial inner membrane structure and integrity, leading to cytochrome c release and apoptosis. J Biol Chem. 2003;278(10):7743-6.

59. Van Bergen NJ, Crowston JG, Kearns LS, Staffieri SE, Hewitt AW, Cohn AC, et al. Mitochondrial oxidative phosphorylation compensation may preserve vision in patients with OPA1-linked autosomal dominant optic atrophy. PLoS One. 2011;6(6):e21347.

60. Lodi R, Tonon C, Valentino M, et al. Defective mitochondrial adenosine triphosphate production in skeletal muscle from patients with dominant optic atrophy due to opa1 mutations. Arch Neuro. 2011;68(1):67-73.

61. Abu-Amero KK, Jaber M, Hellani A, Bosley TM. Genome-wide expression profile of LHON patients with the 11778 mutation. Br J Ophthalmol. 2010;94(2):256-9.

62. Rummelt V, Folberg R, Ionasescu V, Yi H, Moore KC. Ocular pathology of MELAS syndrome with mitochondrial DNA nucleotide 3243 point mutation. Ophthalmology. 1993;100(12):1757-66.

63. Daruich A, Matet A, Borruat FX. Macular dystrophy associated with the mitochondrial DNA A3243G mutation: pericentral pigment deposits or atrophy? Report of two cases and review of the literature. BMC Ophthalmol. 2014;14:77.

64. Scaglia F, Northrop JL. The mitochondrial myopathy encephalopathy, lactic acidosis with stroke-like episodes (MELAS) syndrome: a review of treatment options. CNS Drugs. 2006;20(6):443-64.

65. Horvath R, Reilmann R, Holinski-Feder E, Ringelstein EB, Klopstock T. The role of complex I genes in MELAS: a novel heteroplasmic mutation 3380G>A in ND1 of mtDNA. Neuromuscul Disord. 2008;18(7):553-6.

66. Wang Z, Qi XK, Yao S, Chen B, Luan X, Zhang W, et al. Phenotypic patterns of MELAS/LS overlap syndrome associated with m.13513G>A mutation, and neuropathological findings in one autopsy case. Neuropathology. 2010;30(6):606-14.

67. Patsi J, Maliniemi P, Pakanen S, Hinttala R, Uusimaa J, Majamaa K, et al. LHON/MELAS overlap mutation in ND1 subunit of mitochondrial complex I affects ubiquinone binding as revealed by modeling in Escherichia coli NDH-1. Biochim Biophys Acta. 2012;1817(2):312-8.

68. Gronlund MA, Honarvar AK, Andersson S, Moslemi AR, Oldfors A, Holme E, et al. Ophthalmological findings in children and young adults with genetically verified mitochondrial disease. Br J Ophthalmol. 2010;94(1):121-7.

69. Chinnery PF, Hudson G. Mitochondrial genetics. Br Med Bull. 2013;106:135-59.

70. Nakamura M, Yabe I, Sudo A, Hosoki K, Yaguchi H, Saitoh S, et al. MERRF/MELAS overlap syndrome: a double pathogenic mutation in mitochondrial tRNA genes. J Med Genet. 2010;47(10):659-64.

71. Johri A, Beal MF. Mitochondrial dysfunction in neurodegenerative diseases. J Pharmacol Exp Ther. 2012;342(3):619-30.

72. Calabrese VP. Projected number of people with Parkinson disease in the most populous nations, 2005 through 2030. Neurology. 2007;69(2):223-4; author reply 224.

73. Cui H, Kong Y, Zhang H. Oxidative stress, mitochondrial dysfunction, and aging. J Signal Transduct 2012;2012:646354.

74. Lin TK, Cheng CH, Chen SD, Liou CW, Huang CR, Chuang YC. Mitochondrial Dysfunction and Oxidative Stress Promote Apoptotic Cell Death in the Striatum via Cytochrome c/Caspase-3 Signaling Cascade Following Chronic Rotenone Intoxication in Rats. Int J Mol Sci. 2012;13(7):8722-39.

75. Schapira AH, Cooper JM, Dexter D, Jenner P, Clark JB, Marsden CD. Mitochondrial complex I deficiency in Parkinson's disease. Lancet. 1989;1(8649):1269.

76. Ferris CF, Marella M, Smerkers B, Barchet TM, Gershman B, Matsuno-Yagi A, et al. A phenotypic model recapitulating the neuropathology of Parkinson's disease. Brain Behav. 2013;3(4):351-66.

77. Dhillon VS, Fenech M. Mutations that affect mitochondrial functions and their association with neurodegenerative diseases. Mutat Res Rev Mutat Res. 2014;759:1-13.

78. Armstrong RA. Visual symptoms in Parkinson's disease. Parkinsons Dis. 2011;2011:908306.

79. Yu JG, Feng YF, Xiang Y, Huang JH, Savini G, Parisi V, et al. Retinal nerve fiber layer thickness changes in Parkinson disease: a meta-analysis. PLoS One. 2014;9(1):e85718.

80. Brookmeyer R, Johnson E, Ziegler-Graham K, Arrighi HM. Forecasting the global burden of Alzheimer's disease. Alzheimers Dement. 2007;3(3):186-91.

81. Reddy PH. Role of mitochondria in neurodegenerative diseases: mitochondria as a therapeutic target in Alzheimer's disease. CNS Spectr. 2009;14(8 Suppl 7):8-13; discussion 6-8.

82. Hansson Petersen CA, Alikhani N, Behbahani H, Wiehager B, Pavlov PF, Alafuzoff I, et al. The amyloid beta-peptide is imported into mitochondria via the TOM import machinery and localized to mitochondrial cristae. Proc Natl Acad Sci U S A. 2008;105(35):13145-50.

83. Wang X, Su B, Siedlak SL, Moreira PI, Fujioka H, Wang Y, et al. Amyloid-beta overproduction causes abnormal mitochondrial dynamics via differential modulation of mitochondrial fission/fusion proteins. Proc Natl Acad Sci U S A. 2008;105(49):19318-23.

84. Guo L, Duggan J, Cordeiro MF. Alzheimer's disease and retinal neurodegeneration. Curr Alzheimer Res. 2010;7(1):3-14.

85. Koronyo-Hamaoui M, Koronyo Y, Ljubimov AV, Miller CA, Ko MK, Black KL, et al. Identification of amyloid plaques in retinas from Alzheimer's patients and noninvasive in vivo optical imaging of retinal plaques in a mouse model. Neuroimage. 2011;54(Suppl 1):S204-17.

86. Krantic S, Torriglia A. Retina: source of the earliest biomarkers for Alzheimer's disease? J Alzheimers Dis. 2014;40(2):237-43.

87. Nolan JM, Loskutova E, Howard AN, Moran R, Mulcahy R, Stack J, et al. Macular pigment, visual function, and macular disease among subjects with Alzheimer's disease: an exploratory study. J Alzheimers Dis. 2014;42(4):1191-202.

88. Su K, Bourdette D, Forte M. Mitochondrial dysfunction and neurodegeneration in multiple sclerosis. Front Physiol. 2013;4:169.

89. Siger M, Dziegielewski K, Jasek L, Bieniek M, Nicpan A, Nawrocki J, et al. Optical coherence tomography in multiple sclerosis: thickness of the retinal nerve fiber layer as a potential measure of axonal loss and brain atrophy. J Neurol. 2008;255(10):1555-60.

90. Palace J. Multiple sclerosis associated with Leber's Hereditary Optic Neuropathy. J Neurol Sci. 2009;286(1-2):24-7.

91. Pfeffer G, Burke A, Yu-Wai-Man P, Compston DA, Chinnery PF. Clinical features of MS associated with Leber hereditary optic neuropathy mtDNA mutations. Neurology. 2013;81(24):2073-81.

92. Su KG, Banker G, Bourdette D, Forte M. Axonal degeneration in multiple sclerosis: the mitochondrial hypothesis. Curr Neurol Neurosci Rep. 2009;9(5):411-7.

93. Stitt AW, Lois N, Medina RJ, Adamson P, Curtis TM. Advances in our understanding of diabetic retinopathy. Clin Sci (Lond). 2013;125(1):1-17.

94. Catala J, Munoz S. Proliferative diabetic retinopathy and hemovitreous: red flag for blindness. ScientificWorldJournal. 2008;8:409-10.

95. Andrade LC, Souza GS, Lacerda EM, Nazima MT, Rodrigues AR, Otero LM, et al. Influence of retinopathy on the achromatic and chromatic vision of patients with type 2 diabetes. BMC Ophthalmol. 2014;14:104.

96. Oshitari T, Roy S. Common therapeutic strategies for diabetic retinopathy and glaucoma. Curr Drug Ther. 2007;2(3):224-32.

97. Rodrigues EB, Müller Gonçalves Urias FMP, Badaró E, Novais E, Meirelles R, Farah ME. Diabetes induces changes in neuroretina before retinal vessels: a spectral-domain optical coherence tomography study. Int J Retin Vitr. 2015;1(1):4.

98. Yang Y, Mao D, Chen X, Zhao L, Tian Q, Liu C, et al. Decrease in retinal neuronal cells in streptozotocin-induced diabetic mice. Mol Vis. 2012;18:1411-20.

99. Takahashi H, Goto T, Shoji T, Tanito M, Park M, Chihara E. Diabetes-associated retinal nerve fiber damage evaluated with scanning laser polarimetry. Am J Ophthalmol. 2006;142(1):88-94.

100. Chen X, Nie C, Gong Y, Zhang Y, Jin X, Wei S, et al. Peripapillary retinal nerve fiber layer changes in preclinical diabetic retinopathy: a meta-analysis. PLoS One. 2015;10(5):e0125919.

101. Abu El-Asrar AM, Dralands L, Missotten L, Geboes K. Expression of antiapoptotic and proapoptotic molecules in diabetic retinas. Eye (Lond). 2007;21(2):238-45.

102. Oshitari T, Yamamoto S, Hata N, Roy S. Mitochondria- and caspase-dependent cell death pathway involved in neuronal degeneration in diabetic retinopathy. Br J Ophthalmol. 2008;92(4):552-6.

103. Brownlee M. Biochemistry and molecular cell biology of diabetic complications. Nature. 2001;414(6865):813-20.

104. Madsen-Bouterse SA, Kowluru RA. Oxidative stress and diabetic retinopathy: pathophysiological mechanisms and treatment perspectives. Rev Endocr Metab Disord. 2008;9(4):315-27.

105. Du Y, Miller CM, Kern TS. Hyperglycemia increases mitochondrial superoxide in retina and retinal cells. Free Radic Biol Med. 2003;35(11):1491-9.

106. Nishikawa T, Edelstein D, Du XL, Yamagishi S, Matsumura T, Kaneda Y, et al. Normalizing mitochondrial superoxide production blocks three pathways of hyperglycaemic damage. Nature. 2000;404(6779):787-90.

107. Kowluru RA, Atasi L, Ho YS. Role of mitochondrial superoxide dismutase in the development of diabetic retinopathy. Invest Ophthalmol Vis Sci. 2006;47(4):1594-9.

108. Madsen-Bouterse SA, Mohammad G, Kanwar M, Kowluru RA. Role of mitochondrial DNA damage in the development of diabetic retinopathy, and the metabolic memory phenomenon associated with its progression. Antioxid Redox Signal. 2010;13(6):797-805.

109. Pascolini D, Mariotti SP. Global estimates of visual impairment: 2010. Br J Ophthalmol. 2012; 96 (5): 614-8.

110. Cedrone C, Mancino R, Cerulli A, Cesareo M, Nucci C. Epidemiology of primary glaucoma: prevalence, incidence, and blinding effects. Prog Brain Res. 2008;173:3-14.

111. Guo Y, Chen X, Zhang H, Li N, Yang X, Cheng W, et al. Association of OPA1 polymorphisms with NTG and HTG: a meta-analysis. PLoS One. 2012;7(8):e42387.

112. Glen FC, Crabb DP, Smith ND, Burton R, Garway-Heath DF. Do patients with glaucoma have difficulty recognizing faces? Invest Ophthalmol Vis Sci. 2012;53(7):3629-37.

113. Osborne NN. Pathogenesis of ganglion "cell death" in glaucoma and neuroprotection: focus on ganglion cell axonal mitochondria. Prog Brain Res. 2008;173:339-52.

114. Zhang M, Maddala R, Rao PV. Novel molecular insights into RhoA GTPase-induced resistance to aqueous humor outflow through the trabecular meshwork. Am J Physiol Cell Physiol. 2008;295(5):C1057-70.

115. Tatham AJ, Weinreb RN, Zangwill LM, Liebmann JM, Girkin CA, Medeiros FA. Estimated retinal ganglion cell counts in glaucomatous eyes with localized retinal nerve fiber layer defects. Am J Ophthalmol. 2013;156(3):578-87.e1.

116. Buono LM, Foroozan R, Sergott RC, Savino PJ. Is normal tension glaucoma actually an unrecognized hereditary optic neuropathy? New evidence from genetic analysis. Curr Opin Ophthalmol. 2002;13(6):362-70.

117. Bosley TM, Hellani A, Spaeth GL, Myers J, Katz LJ, Moster MR, et al. Down-regulation of OPA1 in patients with primary open angle glaucoma. Mol Vis. 2011;17:1074-9.

118. Chrysostomou V, Rezania F, Trounce IA, Crowston JG. Oxidative stress and mitochondrial dysfunction in glaucoma. Curr Opin Pharmacol. 2013;13(1):12-5.

119. Osborne NN. Mitochondria: Their role in ganglion cell death and survival in primary open angle glaucoma. Exp Eye Res. 2010;90(6):750-7.

120. Liu Q, Ju WK, Crowston JG, Xie F, Perry G, Smith MA, et al. Oxidative stress is an early event in hydrostatic pressure induced retinal ganglion cell damage. Invest Ophthalmol Vis Sci. 2007;48(10):4580-9.

121. He Y, Leung KW, Zhang YH, Duan S, Zhong XF, Jiang RZ, et al. Mitochondrial complex I defect induces ROS release and degeneration in trabecular meshwork cells of POAG patients: protection by antioxidants. Invest Ophthalmol Vis Sci. 2008;49(4):1447-58.

122. Aung T, Ocaka L, Ebenezer ND, Morris AG, Brice G, Child AH, et al. Investigating the association between OPA1 polymorphisms and glaucoma: comparison between normal tension and high tension primary open angle glaucoma. Hum Genet. 2002;110(5):513-4.

123. Lee S, Sheck L, Crowston JG, Van Bergen NJ, O'Neill EC, O'Hare F, et al. Impaired complex-I-linked respiration and ATP synthesis in primary open-angle glaucoma patient lymphoblasts. Invest Ophthalmol Vis Sci. 2012;53(4):2431-7.

124. O'Neill EC, Danesh-Meyer HV, Kong GX, Hewitt AW, Coote MA, Mackey DA, et al. Optic disc evaluation in optic neuropathies: the optic disc assessment project. Ophthalmology. 2011;118(5):964-70.

125. Khandhadia S, Cherry J, Lotery AJ. Age-related macular degeneration. Adv Exp Med Biol. 2012;724:15-36.

126. Blasiak J, Petrovski G. Oxidative stress, hypoxia, and autophagy in the neovascular processes of age-related macular degeneration. Biomed Res Int. 2014;2014:768026.

127. Feher J, Kovacs I, Artico M, Cavallotti C, Papale A, Balacco Gabrieli C. Mitochondrial alterations of retinal pigment epithelium in age-related macular degeneration. Neurobiol Aging. 2006;27(7):983-93.

128. Lin H, Xu H, Liang FQ, Liang H, Gupta P, Havey AN, et al. Mitochondrial DNA damage and repair in RPE associated with aging and age-related macular degeneration. Invest Ophthalmol Vis Sci. 2011;52(6):3521-9.

129. Mao H, Seo SJ, Biswal MR, Li H, Conners M, Nandyala A, et al. Mitochondrial oxidative stress in the retinal pigment epithelium leads to localized retinal degeneration. Invest Ophthalmol Vis Sci. 2014;55(7):4613-27.

130. Savastano MC, Minnella AM, Tamburrino A, Giovinco G, Ventre S, Falsini B. Differential vulnerability of retinal layers to early age-related macular degeneration: evidence by SD-OCT segmentation analysis. Invest Ophthalmol Vis Sci. 2014;55(1):560-6.

131. Terluk MR, Kapphahn RJ, Soukup LM, Gong H, Gallardo C, Montezuma SR, et al. Investigating mitochondria as a target for treating age-related macular degeneration. J Neurosci. 2015;35(18):7304-11.

132. Dykens JA, Will Y. The significance of mitochondrial toxicity testing in drug development. Drug Discov Today. 2007;12(17-18):777-85.

133. Neustadt J, Pieczenik SR. Medication-induced mitochondrial damage and disease. Mol Nutr Food Res. 2008;52(7):780-8.

134. Kerrison JB. Optic neuropathies caused by toxins and adverse drug reactions. Ophthalmol Clin North Am. 2004;17(3):481-8; viii.

135. Zoumalan CI, Agarwal M, Sadun AA. Optical coherence tomography can measure axonal loss in patients with ethambutol-induced optic neuropathy. Graefes Arch Clin Exp Ophthalmol. 2005;243(5):410-6.

136. Kim YK, Hwang JM. Serial retinal nerve fiber layer changes in patients with toxic optic neuropathy associated with antituberculosis pharmacotherapy. J Ocul Pharmacol Ther. 2009;25(6):531-5.

137. Moura FC, Monteiro ML. Evaluation of retinal nerve fiber layer thickness measurements using optical coherence tomography in patients with tobacco-alcohol-induced toxic optic neuropathy. Indian J Ophthalmol. 2010;58(2):143-6.

138. Shaikh S, Ta C, Basham AA, Mansour S. Leber hereditary optic neuropathy associated with antiretroviral therapy for human immunodeficiency virus infection. Am J Ophthalmol. 2001;131(1):143-5.

139. Mackey DA, Fingert JH, Luzhansky JZ, McCluskey PJ, Howell N, Hall AJ, et al. Leber's hereditary optic neuropathy triggered by antiretroviral therapy for human immunodeficiency virus. Eye (Lond). 2003;17(3):312-7.

140. Ikeda A, Ikeda T, Ikeda N, Kawakami Y, Mimura O. Leber's hereditary optic neuropathy precipitated by ethambutol. Jpn J Ophthalmol. 2006;50(3):280-3.

141. Luca CC, Lam BL, Moraes CT. Erythromycin as a potential precipitating agent in the onset of Leber's hereditary optic neuropathy. Mitochondrion. 2004;4(1):31-6.

142. Seo JH, Hwang JM, Park SS. Antituberculosis medication as a possible epigenetic factor of Leber's hereditary optic neuropathy. Clin Experiment Ophthalmol. 2010;38(4):363-6.

143. Guillet V, Chevrollier A, Cassereau J, Letournel F, Gueguen N, Richard L, et al. Ethambutol-induced optic neuropathy linked to OPA1 mutation and mitochondrial toxicity. Mitochondrion. 2010;10(2):115-24.

144. Nadanaciva S, Bernal A, Aggeler R, Capaldi R, Will Y. Target identification of drug induced mitochondrial toxicity using immunocapture based OXPHOS activity assays. Toxicol In Vitro. 2007;21(5):902-11.

145. Pula JH, Kao AM, Kattah JC. Neuro-ophthalmologic side-effects of systemic medications. Curr Opin Ophthalmol. 2013;24(6):540-9.

146. Kervinen M, Falck A, Hurskainen M, Hautala N. Bilateral optic neuropathy and permanent loss of vision after treatment with amiodarone. J Cardiovasc Pharmacol. 2013;62(4):394-6.

147. Hroudova J, Fisar Z. Activities of respiratory chain complexes and citrate synthase influenced by pharmacologically different antidepressants and mood stabilizers. Neuro Endocrinol Lett. 2010;31(3):336-42.

148. Lloyd MJ, Fraunfelder FW. Drug-induced optic neuropathies. Drugs Today (Barc). 2007;43(11):827-36.

149. Sandoval-Acuna C, Lopez-Alarcon C, Aliaga ME, Speisky H. Inhibition of mitochondrial complex I by various non-steroidal anti-inflammatory drugs and its protection by quercetin via a coenzyme Q-like action. Chem Biol Interact. 2012;199(1):18-28.

150. Wang MY, Sadun AA. Drug-related mitochondrial optic neuropathies. J Neuroophthalmol. 2013;33(2):172-8.

151. Balijepalli S, Boyd MR, Ravindranath V. Inhibition of mitochondrial complex I by haloperidol: the role of thiol oxidation. Neuropharmacology. 1999;38(4):567-77.

152. Fosslien E. Mitochondrial medicine--molecular pathology of defective oxidative phosphorylation. Ann Clin Lab Sci. 2001;31(1):25-67.

153. Simon N, Jolliet P, Morin C, Zini R, Urien S, Tillement JP. Glucocorticoids decrease cytochrome c oxidase activity of isolated rat kidney mitochondria. FEBS Lett. 1998;435(1):25-8.

154. Moreno-Sanchez R, Bravo C, Vasquez C, Ayala G, Silveira LH, Martinez-Lavin M. Inhibition and uncoupling of oxidative phosphorylation by nonsteroidal anti-

inflammatory drugs: study in mitochondria, submitochondrial particles, cells, and whole heart. Biochem Pharmacol. 1999;57(7):743-52.

155. Shulman E, Belakhov V, Wei G, Kendall A, Meyron-Holtz EG, Ben-Shachar D, et al. Designer aminoglycosides that selectively inhibit cytoplasmic rather than mitochondrial ribosomes show decreased ototoxicity: a strategy for the treatment of genetic diseases. J Biol Chem. 2014;289(4):2318-30.
156. Hynes J, Nadanaciva S, Swiss R, Carey C, Kirwan S, Will Y. A high-throughput dual parameter assay for assessing drug-induced mitochondrial dysfunction provides additional predictivity over two established mitochondrial toxicity assays. Toxicol In Vitro. 2013;27(2):560-9.
157. Lee KK, Fujimoto K, Zhang C, Schwall CT, Alder NN, Pinkert CA, et al. Isoniazid-induced cell death is precipitated by underlying mitochondrial complex I dysfunction in mouse hepatocytes. Free Radic Biol Med. 2013;65:584-94.
158. Javaheri M, Khurana RN, O'Hearn T M, Lai MM, Sadun AA. Linezolid-induced optic neuropathy: a mitochondrial disorder? Br J Ophthalmol. 2007;91(1):111-5.
159. Theodossiou TA, Yannakopoulou K, Aggelidou C, Hothersall JS. Tamoxifen subcellular localization; observation of cell-specific cytotoxicity enhancement by inhibition of mitochondrial ETC complexes I and III. Photochem Photobiol. 2012;88(4):1016-22.
160. Rana P, Nadanaciva S, Will Y. Mitochondrial membrane potential measurement of H9c2 cells grown in high-glucose and galactose-containing media does not provide additional predictivity towards mitochondrial assessment. Toxicol In Vitro. 2011;25(2):580-7.
161. Arbiser JL, Kraeft SK, van Leeuwen R, Hurwitz SJ, Selig M, Dickersin GR, et al. Clioquinol-zinc chelate: a candidate causative agent of subacute myelo-optic neuropathy. Mol Med. 1998;4(10):665-70.

162. Tateishi J. Subacute myelo-optico-neuropathy: clioquinol intoxication in humans and animals. Neuropathology. 2000;20 Suppl:S20-4.

163. Konagaya M, Matsumoto A, Takase S, Mizutani T, Sobue G, Konishi T, et al. Clinical analysis of longstanding subacute myelo-optico-neuropathy: sequelae of clioquinol at 32 years after its ban. J Neurol Sci. 2004;218(1-2):85-90.

164. Gilland O. A neurological evaluation of purported cases of SMON in Sweden. Acta Neurol Scand Suppl. 1984;100:165-9.

165. Clifford Rose F, Gawel M. Clioquinol neurotoxicity: an overview. Acta Neurol Scand Suppl. 1984;100:137-45.

166. Nakae K, Yamamoto S, Shigematsu I, Kono R. Relation between subacute myelo-optic neuropathy (S.M.O.N.) and clioquinol: nationwide survey. Lancet. 1973;1(7796):171-3.

167. Tsubaki T, Honma Y, Hoshi M. Neurological syndrome associated with clioquinol. Lancet. 1971;1(7701):696-7.

168. Jack DB, Riess W. Pharmacokinetics of iodochlorhydroxyquin in man. J Pharm Sci. 1973;62(12):1929-32.

169. Richards DA. Prophylactic value of clioquinol against travellers' diarrhoea. Lancet. 1971;1(7688):44-5.

170. Woodward WE, Rahman AS. Trial of clioquinol in cholera. Lancet. 1969;2(7614):270.

171. Helmuth L. Neuroscience. An antibiotic to treat Alzheimer's? Science. 2000;290(5495):1273-4.

172. Yassin MS, Ekblom J, Xilinas M, Gottfries CG, Oreland L. Changes in uptake of vitamin B(12) and trace metals in brains of mice treated with clioquinol. J Neurol Sci. 2000;173(1):40-4.

173. Taguchi H, Sanada H, Hara K, Miyoshi I, Hiraki K. Vitamin B12 levels of cerebrospinal fluid in patients with a variety of neurological disorders. J Nutr Sci Vitaminol (Tokyo). 1977;23(4):299-304.

174. Toyokura Y, Takasu T. Clinical features of SMON. Jpn J Med Sci Biol. 1975;28 Suppl:87-99.

175. Egashira Y, Matsuyama H. Subacute myelo-optico-neuropathy (SMON) in Japan. With special reference to the autopsy cases. Acta Pathol Jpn. 1982;32 Suppl 1:101-16.

176. Mao X, Schimmer AD. The toxicology of Clioquinol. Toxicol Lett. 2008;182(1-3):1-6.

177. Bareggi SR, Cornelli U. Clioquinol: review of its mechanisms of action and clinical uses in neurodegenerative disorders. CNS Neurosci Ther. 2012;18(1):41-6.

178. Andersson DA, Gentry C, Moss S, Bevan S. Clioquinol and pyrithione activate TRPA1 by increasing intracellular Zn2+. Proc Natl Acad Sci U S A. 2009;106(20):8374-9.

179. Yagi K, Ohtsuka K, Ohishi N. Lipid peroxidation caused by chinoform-ferric chelate in cultured neural retinal cells. Experientia. 1985;41(12):1561-3.

180. Benvenisti-Zarom L, Chen J, Regan RF. The oxidative neurotoxicity of clioquinol. Neuropharmacology. 2005;49(5):687-94.

181. Yu H, Zhou Y, Lind SE, Ding WQ. Clioquinol targets zinc to lysosomes in human cancer cells. Biochem J. 2009;417(1):133-9.

182. Kawamura K, Kuroda Y, Sogo M, Fujimoto M, Inui T, Mitsui T. Superoxide dismutase as a target of clioquinol-induced neurotoxicity. Biochem Biophys Res Commun. 2014;452(1):181-5.

183. Schimmer AD. Clioquinol - a novel copper-dependent and independent proteasome inhibitor. Curr Cancer Drug Targets. 2011;11(3):325-31.

184. Katsuyama M, Iwata K, Ibi M, Matsuno K, Matsumoto M, Yabe-Nishimura C. Clioquinol induces DNA double-strand breaks, activation of ATM, and subsequent activation of p53 signaling. Toxicology. 2012;299(1):55-9.

185. Asakura K, Ueda A, Kawamura N, Ueda M, Mihara T, Mutoh T. Clioquinol inhibits NGF-induced Trk autophosphorylation and neurite outgrowth in PC12 cells. Brain Res. 2009;1301:110-5.

186. Fukui T, Asakura K, Hikichi C, Ishikawa T, Murai R, Hirota S, et al. Histone deacetylase inhibitor attenuates neurotoxicity of clioquinol in PC12 cells. Toxicology. 2015;331:112-8.

187. Cuajungco MP, Faget KY, Huang X, Tanzi RE, Bush AI. Metal chelation as a potential therapy for Alzheimer's disease. Ann N Y Acad Sci. 2000;920:292-304.

188. Ritchie CW, Bush AI, Mackinnon A, Macfarlane S, Mastwyk M, MacGregor L, et al. Metal-protein attenuation with iodochlorhydroxyquin (clioquinol) targeting Abeta amyloid deposition and toxicity in Alzheimer disease: a pilot phase 2 clinical trial. Arch Neurol. 2003;60(12):1685-91.

189. Wilkins S, Masters CL, Bush AI, Cherny RA, Finkelstein DI. Clioquinol protects against cell death in parkinson’s disease models in vivo and in vitro. In: The Basal Ganglia IX: Springer; 2009. p. 431-42.

190. Kader RA, El-Desouki M. New insights on Alzheimer's disease. J Microsc Ultrastruct. 2014;2(2):57-66.

191. Jenagaratnam L, McShane R. Clioquinol for the treatment of Alzheimer's Disease. Cochrane Database Syst Rev. 2006(1):Cd005380.

192. Bush AI. Drug development based on the metals hypothesis of Alzheimer's disease. J Alzheimers Dis. 2008;15(2):223-40.

193. Crouch PJ, Blake R, Duce JA, Ciccotosto GD, Li QX, Barnham KJ, et al. Copper-dependent inhibition of human cytochrome c oxidase by a dimeric conformer of amyloid-beta1-42. J Neurosci. 2005;25(3):672-9.

194. Crouch PJ, Barnham KJ. Therapeutic redistribution of metal ions to treat Alzheimer's disease. Acc Chem Res. 2012;45(9):1604-11.

195. Huang X, Atwood CS, Hartshorn MA, Multhaup G, Goldstein LE, Scarpa RC, et al. The A beta peptide of Alzheimer's disease directly produces hydrogen peroxide through metal ion reduction. Biochemistry. 1999;38(24):7609-16.

196. Smith DP, Smith DG, Curtain CC, Boas JF, Pilbrow JR, Ciccotosto GD, et al. Copper-mediated amyloid-beta toxicity is associated with an intermolecular histidine bridge. J Biol Chem. 2006;281(22):15145-54.

197. Deshpande A, Kawai H, Metherate R, Glabe CG, Busciglio J. A role for synaptic zinc in activity-dependent Abeta oligomer formation and accumulation at excitatory synapses. J Neurosci. 2009;29(13):4004-15.

198. Lee JY, Cole TB, Palmiter RD, Suh SW, Koh JY. Contribution by synaptic zinc to the gender-disparate plaque formation in human Swedish mutant APP transgenic mice. Proc Natl Acad Sci U S A. 2002;99(11):7705-10.

199. Crouch PJ, Tew DJ, Du T, Nguyen DN, Caragounis A, Filiz G, et al. Restored degradation of the Alzheimer's amyloid-beta peptide by targeting amyloid formation. J Neurochem. 2009;108(5):1198-207.

200. Cherny RA, Atwood CS, Xilinas ME, Gray DN, Jones WD, McLean CA, et al. Treatment with a copper-zinc chelator markedly and rapidly inhibits beta-amyloid accumulation in Alzheimer's disease transgenic mice. Neuron. 2001;30(3):665-76.

201. White AR, Du T, Laughton KM, Volitakis I, Sharples RA, Xilinas ME, et al. Degradation of the Alzheimer disease amyloid beta-peptide by metal-dependent up-regulation of metalloprotease activity. J Biol Chem. 2006;281(26):17670-80.

202. Regland B, Lehmann W, Abedini I, Blennow K, Jonsson M, Karlsson I, et al. Treatment of Alzheimer's disease with clioquinol. Dement Geriatr Cogn Disord. 2001;12(6):408-14.

203. Raman B, Ban T, Yamaguchi K, Sakai M, Kawai T, Naiki H, et al. Metal ion-dependent effects of clioquinol on the fibril growth of an amyloid {beta} peptide. J Biol Chem. 2005;280(16):16157-62.

204. Ayton S, Lei P, Bush AI. Metallostasis in Alzheimer's disease. Free Radic Biol Med. 2013;62:76-89.

205. Stix B, Kahne T, Sletten K, Raynes J, Roessner A, Rocken C. Proteolysis of AA amyloid fibril proteins by matrix metalloproteinases-1, -2, and -3. Am J Pathol. 2001;159(2):561-70.

206. Zhang YH, Raymick J, Sarkar S, Lahiri DK, Ray B, Holtzman D, et al. Efficacy and toxicity of clioquinol treatment and A-beta42 inoculation in the APP/PSI mouse model of Alzheimer's disease. Curr Alzheimer Res. 2013;10(5):494-506.

207. Schafer S, Pajonk FG, Multhaup G, Bayer TA. Copper and clioquinol treatment in young APP transgenic and wild-type mice: effects on life expectancy, body weight, and metal-ion levels. J Mol Med (Berl). 2007;85(4):405-13.

208. Konagaya M. [SMON: toxicity of clioquinol and the status quo]. Brain Nerve. 2015;67(1):49-62.

209. Lannfelt L, Blennow K, Zetterberg H, Batsman S, Ames D, Harrison J, et al. Safety, efficacy, and biomarker findings of PBT2 in targeting Abeta as a modifying therapy for

Alzheimer's disease: a phase IIa, double-blind, randomised, placebo-controlled trial. Lancet Neurol. 2008;7(9):779-86.

210. Faux NG, Ritchie CW, Gunn A, Rembach A, Tsatsanis A, Bedo J, et al. PBT2 rapidly improves cognition in Alzheimer's Disease: additional phase II analyses. J Alzheimers Dis. 2010;20(2):509-16.
211. Cherny RA, Ayton S, Finkelstein DI, Bush AI, McColl G, Massa SM. PBT2 Reduces Toxicity in a C. elegans Model of polyQ Aggregation and Extends Lifespan, Reduces Striatal Atrophy and Improves Motor Performance in the R6/2 Mouse Model of Huntington's Disease. J Huntingtons Dis. 2012;1(2):211-9.
212. Maksimovic ID, Jovanovic MD, Colic M, Mihajlovic R, Micic D, Selakovic V, et al. Oxidative damage and metabolic dysfunction in experimental Huntington's disease: selective vulnerability of the striatum and hippocampus. Vojnosanit Pregl. 2001;58(3):237-42.
213. Dexter DT, Carayon A, Javoy-Agid F, Agid Y, Wells FR, Daniel SE, et al. Alterations in the levels of iron, ferritin and other trace metals in Parkinson's disease and other neurodegenerative diseases affecting the basal ganglia. Brain. 1991;114 (Pt 4):1953-75.
214. Nguyen T, Hamby A, Massa SM. Clioquinol down-regulates mutant huntingtin expression in vitro and mitigates pathology in a Huntington's disease mouse model. Proc Natl Acad Sci U S A. 2005;102(33):11840-5.
215. Safety, tolerability, and efficacy of PBT2 in Huntington's disease: a phase 2, randomised, double-blind, placebo-controlled trial. Lancet Neurol. 2015;14(1):39-47.
216. FDA End of Phase 2 Status Update. News Room. February 13, 2015 [cited 2016 Januanry 7]; Available from: http://pranabio.com/news/fda_phase2_meeting/#.V9D-e01f06Z
217. Prana Biotechnology announces preliminary results of Phase 2 IMAGINE trial of PBT2 in Alzheimer's disease PR Newswire Press Release; March 31, 2014 [cited 2016 Januanry

8]; Available from: http://www.prnewswire.com/news-releases/prana-biotechnology-announces-preliminary-results-of-phase-2-imagine-trial-of-pbt2-in alzheimers-disease-253173581.html

218. Prana Announces Safety Outcomes of Alzheimer's IMAGINE Extension Trial; June 30, 2015 [cited 2016 May 6]; Available from: http://pranabio.com/news/prana-announces-safety-outcomes-alzheimers-imagine-extension-trial#.VywrjlVcRBc
219. Iwata T, Tomarev S. Animal Models for Eye Diseases and Therapeutics. In: Conn PM, editor. Sourcebook of Models for Biomedical Research. Totowa, NJ: Humana Press; 2008. p. 279-87.
220. Chhetri J, Jacobson G, Gueven N. Zebrafish-on the move towards ophthalmological research. Eye. 2014;7(10):19.
221. Bibliowicz J, Tittle RK, Gross JM. Toward a better understanding of human eye disease insights from the zebrafish, Danio rerio. Prog Mol Biol Transl Sci. 2011;100:287-330.
222. Mathias JR, Saxena MT, Mumm JS. Advances in zebrafish chemical screening technologies. Future Med Chem. 2012;4(14):1811-22.
223. Chakraborty C, Hsu CH, Wen ZH, Lin CS, Agoramoorthy G. Zebrafish: a complete animal model for in vivo drug discovery and development. Curr Drug Metab. 2009;10(2):116-24.
224. Kari G, Rodeck U, Dicker AP. Zebrafish: an emerging model system for human disease and drug discovery. Clin Pharmacol Ther. 2007;82(1):70-80.
225. Lin YY. Muscle diseases in the zebrafish. Neuromuscul Disord. 2012;22(8):673-84.
226. Norton WH. Toward developmental models of psychiatric disorders in zebrafish. Front Neural Circuits. 2013;7:79.
227. Ramakrishnan L. Looking within the zebrafish to understand the tuberculous granuloma. Adv Exp Med Biol. 2013;783:251-66.

228. Amatruda JF, Shepard JL, Stern HM, Zon LI. Zebrafish as a cancer model system. Cancer Cell. 2002;1(3):229-31.

229. Lien CL, Harrison MR, Tuan TL, Starnes VA. Heart repair and regeneration: recent insights from zebrafish studies. Wound Repair Regen. 2012;20(5):638-46.

230. Lohi O, Parikka M, Ramet M. The zebrafish as a model for paediatric diseases. Acta Paediatr. 2013;102(2):104-10.

231. Bilotta J, Saszik S. The zebrafish as a model visual system. Int J Dev Neurosci. 2001;19(7):621-9.

232. Villegas GM. Comparative ultrastructure of the retina in fish, monkey and man. In: Neurophysiologie und Psychophysik des Visuellen Systems/The Visual System: Neurophysiology and Psychophysics: Springer; 1961. p. 3-13.

233. Dowling J. The retina: An approachable part of the brain. 1987. Belknap Press of Harvard University Press;18:12-32.

234. Curcio CA, Allen KA. Topography of ganglion cells in human retina. J Comp Neurol. 1990;300(1):5-25.

235. Robinson J, Schmitt EA, Harosi FI, Reece RJ, Dowling JE. Zebrafish ultraviolet visual pigment: absorption spectrum, sequence, and localization. Proc Natl Acad Sci U S A. 1993;90(13):6009-12.

236. Goldsmith P, Harris WA. The zebrafish as a tool for understanding the biology of visual disorders. Semin Cell Dev Biol. 2003;14(1):11-8.

237. Fleisch VC, Neuhauss SC. Visual behavior in zebrafish. Zebrafish. 2006;3(2):191-201.

238. Maurer CM, Huang YY, Neuhauss SC. Application of zebrafish oculomotor behavior to model human disorders. Rev Neurosci. 2011;22(1):5-16.

239. Yousef YA, Finger PT. Optical coherence tomography of radiation optic neuropathy. Ophthalmic Surg Lasers Imaging. 2012;43(1):6-12.

240. Schweitzer J, Gimnopoulos D, Lieberoth BC, Pogoda HM, Feldner J, Ebert A, et al. Contactin1a expression is associated with oligodendrocyte differentiation and axonal regeneration in the central nervous system of zebrafish. Mol Cell Neurosci. 2007;35(2):194-207.

241. Zou S, Tian C, Ge S, Hu B. Neurogenesis of retinal ganglion cells is not essential to visual functional recovery after optic nerve injury in adult zebrafish. PLoS One. 2013;8(2):e57280.

242. Lagnado L. Retinal processing: amacrine cells keep it short and sweet. Curr Biol. 1998;8(17):R598-600.

243. Raymond PA, Barthel LK, Rounsifer ME, Sullivan SA, Knight JK. Expression of rod and cone visual pigments in goldfish and zebrafish: a rhodopsin-like gene is expressed in cones. Neuron. 1993;10(6):1161-74.

244. Branchek T, Bremiller R. The development of photoreceptors in the zebrafish, Brachydanio rerio. I. Structure. J Comp Neurol. 1984;224(1):107-15.

245. Saszik S, Bilotta J, Givin CM. ERG assessment of zebrafish retinal development. Vis Neurosci. 1999;16(5):881-8.

246. Moyano M, Porteros A, Dowling JE. The effects of nicotine on cone and rod b-wave responses in larval zebrafish. Vis Neurosci. 2013;30(4):141-5.

247. Baylor DA. Photoreceptor signals and vision. Proctor lecture. Invest Ophthalmol Vis Sci. 1987;28(1):34-49.

248. Schmitt EA, Dowling JE. Early eye morphogenesis in the zebrafish, Brachydanio rerio. J Comp Neurol. 1994;344(4):532-42.

249. Schmitt EA, Dowling JE. Early retinal development in the zebrafish, Danio rerio: light and electron microscopic analyses. J Comp Neurol. 1999;404(4):515-36.

250. Malicki J. Development of the retina. Methods Cell Biol. 1999;59:273-99.

251. Hu M, Easter SS. Retinal neurogenesis: the formation of the initial central patch of postmitotic cells. Dev Biol. 1999;207(2):309-21.

252. Fadool JM, Dowling JE. Zebrafish: a model system for the study of eye genetics. Prog Retin Eye Res. 2008;27(1):89-110.

253. Tsujikawa M, Malicki J. Genetics of photoreceptor development and function in zebrafish. Int J Dev Biol. 2004;48(8-9):925-34.

254. Easter SS, Jr., Nicola GN. The development of vision in the zebrafish (Danio rerio). Dev Biol. 1996;180(2):646-63.

255. Easter SS, Jr., Nicola GN. The development of eye movements in the zebrafish (Danio rerio). Dev Psychobiol. 1997;31(4):267-76.

256. Kitambi SS, Chandrasekar G, Addanki VK. Teleost fish- a powerful model for studying development, function and diseases of the human eye. Curr Sci. 2011;100(12):1815.

257. Renninger SL, Schonthaler HB, Neuhauss SC, Dahm R. Investigating the genetics of visual processing, function and behaviour in zebrafish. Neurogenetics. 2011;12(2):97-116.

258. Brockerhoff SE. Measuring the optokinetic response of zebrafish larvae. Nat Protoc. 2006;1(5):2448-51.

259. Huang YY, Neuhauss SC. The optokinetic response in zebrafish and its applications. Front Biosci. 2008;13:1899-916.

260. Brockerhoff SE, Hurley JB, Janssen-Bienhold U, Neuhauss SC, Driever W, Dowling JE. A behavioral screen for isolating zebrafish mutants with visual system defects. Proc Natl Acad Sci U S A. 1995;92(23):10545-9.

261. Neuhauss SC, Biehlmaier O, Seeliger MW, Das T, Kohler K, Harris WA, et al. Genetic disorders of vision revealed by a behavioral screen of 400 essential loci in zebrafish. J Neurosci. 1999;19(19):8603-15.

262. Huber-Reggi SP, Mueller KP, Neuhauss SC. Analysis of optokinetic response in zebrafish by computer-based eye tracking. Methods Mol Biol. 2013;935:139-60.

263. Mueller KP, Neuhauss SC. Quantitative measurements of the optokinetic response in adult fish. J Neurosci Methods. 2010;186(1):29-34.

264. Link BA, Gray MP, Smith RS, John SW. Intraocular pressure in zebrafish: comparison of inbred strains and identification of a reduced melanin mutant with raised IOP. Invest Ophthalmol Vis Sci. 2004;45(12):4415-22.

265. Brockerhoff SE, Hurley JB, Niemi GA, Dowling JE. A new form of inherited red-blindness identified in zebrafish. J Neurosci. 1997;17(11):4236-42.

266. Muto A, Orger MB, Wehman AM, Smear MC, Kay JN, Page-McCaw PS, et al. Forward genetic analysis of visual behavior in zebrafish. PLoS Genet. 2005;1(5):e66.

267. Bilotta J. Effects of abnormal lighting on the development of zebrafish visual behavior. Behav Brain Res. 2000;116(1):81-7.

268. Quentin B, Moore RH. Behavior and Cognition. In: Biology of Fishes. Third ed: Taylor & Francis Group; 2007. p. 409-33.

269. Bilotta J, Saszik S, Givin CM, Hardesty HR, Sutherland SE. Effects of embryonic exposure to ethanol on zebrafish visual function. Neurotoxicol Teratol. 2002;24(6):759-66.

270. Kimmel CB, Patterson J, Kimmel RO. The development and behavioral characteristics of the startle response in the zebra fish. Dev Psychobiol. 1974;7(1):47-60.

271. Weber DN, Connaughton VP, Dellinger JA, Klemer D, Udvadia A, Carvan MJ, 3rd. Selenomethionine reduces visual deficits due to developmental methylmercury exposures. Physiol Behav. 2008;93(1-2):250-60.

272. Emran F, Rihel J, Adolph AR, Wong KY, Kraves S, Dowling JE. OFF ganglion cells cannot drive the optokinetic reflex in zebrafish. Proc Natl Acad Sci U S A. 2007;104(48):19126-31.

273. Emran F, Rihel J, Dowling JE. A behavioral assay to measure responsiveness of zebrafish to changes in light intensities. J Vis Exp. 2008;(20).(pii):923.

274. Li L, Dowling JE. A dominant form of inherited retinal degeneration caused by a non-photoreceptor cell-specific mutation. Proc Natl Acad Sci U S A. 1997;94(21):11645-50.

275. Bianco IH, Kampff AR, Engert F. Prey capture behavior evoked by simple visual stimuli in larval zebrafish. Front Syst Neurosci. 2011;5:101.

276. Li L. Zebrafish mutants: behavioral genetic studies of visual system defects. Dev Dyn. 2001;221(4):365-72.

277. Li L, Dowling JE. Zebrafish visual sensitivity is regulated by a circadian clock. Vis Neurosci. 1998;15(5):851-7.

278. Li L, Dowling JE. Disruption of the olfactoretinal centrifugal pathway may relate to the visual system defect in night blindness b mutant zebrafish. J Neurosci. 2000;20(5):1883-92.

279. Neuhauss SC. Behavioral genetic approaches to visual system development and function in zebrafish. J Neurobiol. 2003;54(1):148-60.

280. Luca RM, Gerlai R. Animated bird silhouette above the tank: acute alcohol diminishes fear responses in zebrafish. Behav Brain Res. 2012;229(1):194-201.

281. Richards FM, Alderton WK, Kimber GM, Liu Z, Strang I, Redfern WS, et al. Validation of the use of zebrafish larvae in visual safety assessment. J Pharmacol Toxicol Methods. 2008;58(1):50-8.

282. Santaella RM, Fraunfelder FW. Ocular adverse effects associated with systemic medications : recognition and management. Drugs. 2007;67(1):75-93.

283. Deeti S, O'Farrell S, Kennedy BN. Early safety assessment of human oculotoxic drugs using the zebrafish visualmotor response. J Pharmacol Toxicol Methods. 2013;69(1):1-8.

284. Rubinstein AL. Zebrafish assays for drug toxicity screening. Expert Opin Drug Metab Toxicol. 2006;2(2):231-40.

285. Eimon PM, Rubinstein AL. The use of in vivo zebrafish assays in drug toxicity screening. Expert Opin Drug Metab Toxicol. 2009;5(4):393-401.

286. Berghmans S, Butler P, Goldsmith P, Waldron G, Gardner I, Golder Z, et al. Zebrafish based assays for the assessment of cardiac, visual and gut function--potential safety screens for early drug discovery. J Pharmacol Toxicol Methods. 2008;58(1):59-68.

287. Peterson RT, Link BA, Dowling JE, Schreiber SL. Small molecule developmental screens reveal the logic and timing of vertebrate development. Proc Natl Acad Sci U S A. 2000;97(24):12965-9.

288. Kitambi SS, McCulloch KJ, Peterson RT, Malicki JJ. Small molecule screen for compounds that affect vascular development in the zebrafish retina. Mech Dev. 2009;126(5-6):464-77.

289. Franken NA, Rodermond HM, Stap J, Haveman J, van Bree C. Clonogenic assay of cells in vitro. Nat Protoc. 2006;1(5):2315-9.

290. Somaiah C, Kumar A, Mawrie D, Sharma A, Patil SD, Bhattacharyya J, et al. Collagen Promotes Higher Adhesion, Survival and Proliferation of Mesenchymal Stem Cells. PLoS One. 2015;10(12):e0145068.

291. Haefeli RH, Erb M, Gemperli AC, Robay D, Courdier Fruh I, Anklin C, et al. NQO1-dependent redox cycling of idebenone: effects on cellular redox potential and energy levels. PLoS One. 2011;6(3):e17963.

292. Vahsen N, Cande C, Briere JJ, Benit P, Joza N, Larochette N, et al. AIF deficiency compromises oxidative phosphorylation. Embo J. 2004;23(23):4679-89.

293. Sakharov DV, Elstak EDR, Chernyak B, Wirtz KWA. Prolonged lipid oxidation after photodynamic treatment. Study with oxidation-sensitive probe C11-BODIPY581/591. FEBS Letters. 2005;579(5):1255-60.

294. Gustafson DL, Siegel D, Rastatter JC, Merz AL, Parpal JC, Kepa JK, et al. Kinetics of NAD(P)H:quinone oxidoreductase I (NQO1) inhibition by mitomycin C in vitro and in vivo. J Pharmacol Exp Ther. 2003;305(3):1079-86.

295. Tan AS, Berridge MV. Evidence for NAD(P)H:quinone oxidoreductase 1 (NQO1)-mediated quinone-dependent redox cycling via plasma membrane electron transport: A sensitive cellular assay for NQO1. Free Radic Biol Med. 2010;48(3):421-9.

296. Marroquin LD, Hynes J, Dykens JA, Jamieson JD, Will Y. Circumventing the Crabtree effect: replacing media glucose with galactose increases susceptibility of HepG2 cells to mitochondrial toxicants. Toxicol Sci. 2007;97(2):539-47.

297. Valenza F, Aletti G, Fossali T, Chevallard G, Sacconi F, Irace M, et al. Lactate as a marker of energy failure in critically ill patients: hypothesis. Crit Care. 2005;9(6):588-93.

298. Dinkova-Kostova AT, Talalay P. NAD(P)H:quinone acceptor oxidoreductase 1 (NQO1), a multifunctional antioxidant enzyme and exceptionally versatile cytoprotector. Arch Biochem Biophys. 2010;501(1):116-23.

299. Zhu H, Li Y. NAD(P)H: quinone oxidoreductase 1 and its potential protective role in cardiovascular diseases and related conditions. Cardiovasc Toxicol. 2012;12(1):39-45.

300. Chhetri J, King A, Gueven N. Alzheimer's Disease and NQO1: Is there a Link? Current Alzheimer Research 2016.(Accepted for publication)

301. Kim HJ, Zheng M, Kim SK, Cho JJ, Shin CH, Joe Y, et al. CO/HO-1 Induces NQO-1 Expression via Nrf2 Activation. Immune Netw. 2011;11(6):376-82.

302. Bak MJ, Jun M, Jeong WS. Procyanidins from wild grape (Vitis amurensis) seeds regulate ARE-mediated enzyme expression via Nrf2 coupled with p38 and PI3K/Akt pathway in HepG2 cells. Int J Mol Sci. 2012;13(1):801-18.

303. Liebler DC, Guengerich FP. Elucidating mechanisms of drug-induced toxicity. Nat Rev Drug Discov. 2005;4(5):410-20.

304. Ding WQ, Liu B, Vaught JL, Yamauchi H, Lind SE. Anticancer activity of the antibiotic clioquinol. Cancer Res. 2005;65(8):3389-95.

305. Zhai S, Yang L, Cui QC, Sun Y, Dou QP, Yan B. Tumor cellular proteasome inhibition and growth suppression by 8-hydroxyquinoline and clioquinol requires their capabilities to bind copper and transport copper into cells. J Biol Inorg Chem. 2010;15(2):259-69.

306. Yamanaka N, Imanari T, Tamura Z, Yagi K. Uncoupling of oxidative phosphorylation of rat liver mitochondria by chinoform. J Biochem. 1973;73(5):993-8.

307. Feng P, Li TL, Guan ZX, Franklin RB, Costello LC. Direct effect of zinc on mitochondrial apoptogenesis in prostate cells. Prostate. 2002;52(4):311-8.

308. Untergasser G, Rumpold H, Plas E, Witkowski M, Pfister G, Berger P. High levels of zinc ions induce loss of mitochondrial potential and degradation of antiapoptotic Bcl-2 protein in in vitro cultivated human prostate epithelial cells. Biochem Biophys Res Commun. 2000;279(2):607-14.

309. Cater MA, Haupt Y. Clioquinol induces cytoplasmic clearance of the X-linked inhibitor of apoptosis protein (XIAP): therapeutic indication for prostate cancer. Biochem J. 2011;436(2):481-91.

310. Danson S, Dean E, Dive C, Ranson M. IAPs as a target for anticancer therapy. Curr Cancer Drug Targets. 2007;7(8):785-94.

311. Daniel KG, Chen D, Orlu S, Cui QC, Miller FR, Dou QP. Clioquinol and pyrrolidine dithiocarbamate complex with copper to form proteasome inhibitors and apoptosis inducers in human breast cancer cells. Breast Cancer Res. 2005;7(6):R897-908.

312. Chen D, Cui QC, Yang H, Barrea RA, Sarkar FH, Sheng S, et al. Clioquinol, a therapeutic agent for Alzheimer's disease, has proteasome-inhibitory, androgen receptor-suppressing, apoptosis-inducing, and antitumor activities in human prostate cancer cells and xenografts. Cancer Res. 2007;67(4):1636-44.

313. Yu H, Lou JR, Ding WQ. Clioquinol independently targets NF-kappaB and lysosome pathways in human cancer cells. Anticancer Res. 2010;30(6):2087-92.

314. Mao X, Li X, Sprangers R, Wang X, Venugopal A, Wood T, et al. Clioquinol inhibits the proteasome and displays preclinical activity in leukemia and myeloma. Leukemia. 2009;23(3):585-90.

315. Zheng J, Benbrook DM, Yu H, Ding WQ. Clioquinol suppresses cyclin D1 gene expression through transcriptional and post-transcriptional mechanisms. Anticancer Res. 2011;31(9):2739-47.

316. Morgan MJ, Liu ZG. Crosstalk of reactive oxygen species and NF-kappaB signaling. Cell Res. 2011;21(1):103-15.

317. Leanderson P, Tagesson C. Iron bound to the lipophilic iron chelator, 8-hydroxyquinoline, causes DNA strand breakage in cultured lung cells. Carcinogenesis. 1996;17(3):545-50.

318. Tardito S, Barilli A, Bassanetti I, Tegoni M, Bussolati O, Franchi-Gazzola R, et al. Copper-dependent cytotoxicity of 8-hydroxyquinoline derivatives correlates with their hydrophobicity and does not require caspase activation. J Med Chem. 2012;55(23):10448-59.

319. Matsuki Y, Yoshimura S, Abe M. [SMON and pharmacokinetics of chinoform with special reference to animal species difference]. Yakugaku Zasshi. 1997;117(10-11):936-56.

320. Barnham KJ, Gautier ECL, Kok GB, Krippner G. 8-hydroxy quinoline derivatives. Google Patents; 2004.

321. Holley AK, St Clair DK. Watching the watcher: regulation of p53 by mitochondria. Future Oncol. 2009;5(1):117-30.

322. Zelko IN, Mariani TJ, Folz RJ. Superoxide dismutase multigene family: a comparison of the CuZn-SOD (SOD1), Mn-SOD (SOD2), and EC-SOD (SOD3) gene structures, evolution, and expression. Free Radic Biol Med. 2002;33(3):337-49.

323. Oyama TM, Ishida S, Okano Y, Seo H, Oyama Y. Clioquinol-induced increase and decrease in the intracellular Zn2+ level in rat thymocytes. Life Sci. 2012;91(23-24):1216-20.

324. McCord MC, Aizenman E. The role of intracellular zinc release in aging, oxidative stress, and Alzheimer's disease. Front Aging Neurosci. 2014;6:77.

325. Sippl C, Tamm ER. What is the nature of the RGC-5 cell line? Adv Exp Med Biol. 2014;801:145-54.

326. Krishnamoorthy RR, Clark AF, Daudt D, Vishwanatha JK, Yorio T. A forensic path to RGC-5 cell line identification: lessons learned. Invest Ophthalmol Vis Sci. 2013;54(8):5712-9.

327. Van Bergen NJ, Wood JP, Chidlow G, Trounce IA, Casson RJ, Ju WK, et al. Recharacterization of the RGC-5 retinal ganglion cell line. Invest Ophthalmol Vis Sci. 2009;50(9):4267-72.

328. Probes for Reactive Oxygen Species, Including Nitric Oxide. Molecular Probes™ Handbook A Guide to Fluorescent Probes and Labeling Technologies. invitrogen;

Available from: https://www.thermofisher.com/content/dam/LifeTech/global/technical-reference-library/Molecular%20Probes%20Handbook/chapter-pdfs/Ch-18-Reactive-Oxygen-Species.pdf?icid=WE216841

329. Myhre O, Andersen JM, Aarnes H, Fonnum F. Evaluation of the probes 2',7'-dichlorofluorescin diacetate, luminol, and lucigenin as indicators of reactive species formation. Biochem Pharmacol. 2003;65(10):1575-82.
330. Gomes A, Fernandes E, Lima JL. Fluorescence probes used for detection of reactive oxygen species. J Biochem Biophys Methods. 2005;65(2-3):45-80.
331. Hwang J, Kim Y-H, Noh J-R, Gang G-T, Kim K-S, Chung H, et al. The protective role of NAD(P)H:quinone oxidoreductase 1 on acetaminophen-induced liver injury is associated with prevention of adenosine triphosphate depletion and improvement of mitochondrial dysfunction. Arch Toxicol. 2014:1-8.
332. Kim J, Kim SK, Kim HK, Mattson MP, Hyun DH. Mitochondrial function in human neuroblastoma cells is up-regulated and protected by NQO1, a plasma membrane redox enzyme. PLoS One. 2013;8(7):e69030.
333. Siegel D, Gustafson DL, Dehn DL, Han JY, Boonchoong P, Berliner LJ, et al. NAD(P)H:quinone oxidoreductase 1: role as a superoxide scavenger. Mol Pharmacol. 2004;65(5):1238-47.
334. Jia Z, Zhu H, Misra HP, Li Y. Potent induction of total cellular GSH and NQO1 as well as mitochondrial GSH by 3H-1,2-dithiole-3-thione in SH-SY5Y neuroblastoma cells and primary human neurons: protection against neurocytotoxicity elicited by dopamine, 6-hydroxydopamine, 4-hydroxy-2-nonenal, or hydrogen peroxide. Brain Res. 2008;1197:159-69.

335. Li J, Lee JM, Johnson JA. Microarray analysis reveals an antioxidant responsive element-driven gene set involved in conferring protection from an oxidative stress-induced apoptosis in IMR-32 cells. J Biol Chem. 2002;277(1):388-94.

336. Iskander K, Gaikwad A, Paquet M, Long DJ, 2nd, Brayton C, Barrios R, et al. Lower induction of p53 and decreased apoptosis in NQO1-null mice lead to increased sensitivity to chemical-induced skin carcinogenesis. Cancer Res. 2005;65(6):2054-8.

337. Long DJ, 2nd, Waikel RL, Wang XJ, Perlaky L, Roop DR, Jaiswal AK. NAD(P)H:quinone oxidoreductase 1 deficiency increases susceptibility to benzo(a)pyrene-induced mouse skin carcinogenesis. Cancer Res. 2000;60(21):5913-5.

338. Yamamoto M, Tsukamoto T, Sakai H, Shirai N, Ohgaki H, Furihata C, et al. p53 knockout mice (-/-) are more susceptible than (+/-) or (+/+) mice to N-methyl-N-nitrosourea stomach carcinogenesis. Carcinogenesis. 2000;21(10):1891-7.

339. Liu B, Chen Y, St Clair DK. ROS and p53: a versatile partnership. Free Radic Biol Med. 2008;44(8):1529-35.

340. Wang DB, Kinoshita C, Kinoshita Y, Morrison RS. p53 and mitochondrial function in neurons. Biochim Biophys Acta. 2014;1842(8):1186-97.

341. Sun Y, Tao C, Huang X, He H, Shi H, Zhang Q, et al. Metformin induces apoptosis of human hepatocellular carcinoma HepG2 cells by activating an AMPK/p53/miR-23a/FOXA1 pathway. Onco Targets Ther. 2016;9:2845-53.

342. Hamid T, Kakar SS. PTTG/securin activates expression of p53 and modulates its function. Mol Cancer. 2004;3:18.

343. Dinkova-Kostova AT, Abramov AY. The emerging role of Nrf2 in mitochondrial function. Free Radic Biol Med. 2015; 88 (Pt B): 179-88.

344. Surh YJ, Kundu JK, Na HK. Nrf2 as a master redox switch in turning on the cellular signaling involved in the induction of cytoprotective genes by some chemopreventive phytochemicals. Planta Med. 2008;74(13):1526-39.

345. Nguyen T, Nioi P, Pickett CB. The Nrf2-antioxidant response element signaling pathway and its activation by oxidative stress. J Biol Chem. 2009;284(20):13291-5.

346. Marrot L, Jones C, Perez P, Meunier JR. The significance of Nrf2 pathway in (photo)-oxidative stress response in melanocytes and keratinocytes of the human epidermis. Pigment Cell Melanoma Res. 2008;21(1):79-88.

347. Warwick E, Cassidy A, Hanley B, Jouni ZE, Bao Y. Effect of phytochemicals on phase II enzyme expression in infant human primary skin fibroblast cells. Br J Nutr. 2012;108(12):2158-65.

348. Takamiya M, Weger BD, Schindler S, Beil T, Yang L, Armant O, et al. Molecular description of eye defects in the zebrafish Pax6b mutant, sunrise, reveals a Pax6b-dependent genetic network in the developing anterior chamber. PLoS One. 2015;10(2):e0117645.

349. Kilkenny C, Browne W, Cuthill IC, Emerson M, Altman DG. Animal research: reporting in vivo experiments: the ARRIVE guidelines. Br J Pharmacol 2010;160(7):1577-9.

350. Lawrence C. The husbandry of zebrafish (Danio rerio): A review. Aquaculture. 2007;269(1–4):1-20.

351. Raising Larvae in the Zebrafish International Resource Center Autonursery. ZFIN Protocol Wki; 2009.

352. Mueller KP, Schnaedelbach OD, Russig HD, Neuhauss SC. VisioTracker, an innovative automated approach to oculomotor analysis. J Vis Exp. 2011(56).

353. Sabaliauskas NA, Foutz CA, Mest JR, Budgeon LR, Sidor AT, Gershenson JA, et al. High-throughput zebrafish histology. Methods. 2006;39(3):246-54.

354. Objet Eden260VS Dental Advantage Efficiency for growing labs; [cited 2016 June 24]; Available from: http://www.stratasys.com/3d-printers/dental-series/objet-eden260vs-dental-advantage

355. Shallan AI, Smejkal P, Corban M, Guijt RM, Breadmore MC. Cost-effective three-dimensional printing of visibly transparent microchips within minutes. Anal Chem. 2014;86(6):3124-30.

356. Germana A, Sanchez-Ramos C, Guerrera MC, Calavia MG, Navarro M, Zichichi R, et al. Expression and cell localization of brain-derived neurotrophic factor and TrkB during zebrafish retinal development. J Anat. 2010;217(3):214-22.

357. Uribe RA, Gross JM. Immunohistochemistry on cryosections from embryonic and adult zebrafish eyes. CSH Protoc. 2007;2007:pdb.prot4779.

358. Macdonald R. Zebrafish immunohistochemistry. Methods Mol Biol. 1999; 127:77-88.

359. Murphy TH, So AP, Vincent SR. Histochemical detection of quinone reductase activity in situ using LY 83583 reduction and oxidation. J Neurochem. 1998;70(5):2156-64.

360. Meyer BM, Froehlich JM, Galt NJ, Biga PR. Inbred strains of zebrafish exhibit variation in growth performance and myostatin expression following fasting. Comp Biochem Physiol A Mol Integr Physiol. 2013;164(1):1-9.

361. Rinner O, Rick JM, Neuhauss SC. Contrast sensitivity, spatial and temporal tuning of the larval zebrafish optokinetic response. Invest Ophthalmol Vis Sci. 2005;46(1):137-42.

362. Pinho BR, Santos MM, Fonseca-Silva A, Valentão P, Andrade PB, Oliveira JMA. How mitochondrial dysfunction affects zebrafish development and cardiovascular function: an in vivo model for testing mitochondria-targeted drugs. Br J Pharmacol. 2013;169(5):1072-90.

363. Wu YT, Lin CY, Tsai MY, Chen YH, Lu YF, Huang CJ, et al. beta-Lapachone induces heart morphogenetic and functional defects by promoting the death of erythrocytes and the endocardium in zebrafish embryos. J Biomed Sci. 2011;18:70.

364. Edlund C, Elhammer A, Dallner G. Distribution of newly synthesized DT-diaphorase in rat liver. Biosci Rep 1982;2(11):861-5.

365. Eliasson M, Bostrom M, DePierre JW. Levels and subcellular distributions of detoxifying enzymes in the ovarian corpus luteum of the pregnant and non-pregnant pig. Biochem Pharmacol 1999;58(8):1287-92.

366. Winski SL, Koutalos Y, Bentley DL, Ross D. Subcellular localization of NAD(P)H:quinone oxidoreductase 1 in human cancer cells. Cancer Res. 2002;62(5):1420-4.

367. Ma Y, Kong J, Yan G, Ren X, Jin D, Jin T, et al. NQO1 overexpression is associated with poor prognosis in squamous cell carcinoma of the uterine cervix. BMC Cancer. 2014;14:414.

368. ENSEMBL [cited 2015 June 5]; Available from: http://asia.ensembl.org/Danio_rerio/Transcript/Summary?g=ENSDARG00000010250;r=7:56401846-56420909;t=ENSDART00000004964.

369. PredictProtein [cited 2015 June 6]; Available from: http://ppopen.informatik.tu-muenchen.de/.

370. ClustalW2 [cited 2016 July 5]; Available from: http://www.ebi.ac.uk/Tools/services/web/toolresult.ebi?jobId=clustalw2-I20150609-084749-0762-59229679-es&tool=clustalw2&showColors=true.

371. PhosphoSite Plus. Cell Signaling Technology [Cited 2016 September 17]; Available from: http://www.phosphosite.org/proteinAction?id=14721&showAllSites=true

372. Sadowska-Bartosz I, Paczka A, Molon M, Bartosz G. Dimethyl sulfoxide induces oxidative stress in the yeast Saccharomyces cerevisiae. FEMS Yeast Res. 2013;13(8):820-30.

373. Nishimura Y, Murakami S, Ashikawa Y, Sasagawa S, Umemoto N, Shimada Y, et al. Zebrafish as a systems toxicology model for developmental neurotoxicity testing. Congenit Anom (Kyoto). 2015;55(1):1-16.

374. Zhang F, Qin W, Zhang JP, Hu CQ. Antibiotic toxicity and absorption in zebrafish using liquid chromatography-tandem mass spectrometry. PLoS One. 2015;10(5):e0124805.

375. Carvan MJ, 3rd, Loucks E, Weber DN, Williams FE. Ethanol effects on the developing zebrafish: neurobehavior and skeletal morphogenesis. Neurotoxicol Teratol. 2004;26(6):757-68.

376. Flynn T, Signal B, Johnson SL, Gemmell NJ. Mitochondrial genome diversity among six laboratory zebrafish (Danio rerio) strains. Mitochondrial DNA A DNA Mapp Seq Anal 2016;27(6):4364-71.

377. Hur KY, Lee MS. New mechanisms of metformin action: Focusing on mitochondria and the gut. J Diabetes Investig. 2015;6(6):600-9.

378. Kobayashi M, Itoh K, Suzuki T, Osanai H, Nishikawa K, Katoh Y, et al. Identification of the interactive interface and phylogenic conservation of the Nrf2-Keap1 system. Genes Cells. 2002;7(8):807-20.

379. Rousseau ME, Sant KE, Borden LR, Franks DG, Hahn ME, Timme-Laragy AR. Regulation of Ahr signaling by Nrf2 during development: Effects of Nrf2a deficiency on PCB126 embryotoxicity in zebrafish (Danio rerio). Aquat Toxicol. 2015;167:157-71.

380. Liu C, Su G, Giesy JP, Letcher RJ, Li G, Agrawal I, et al. Acute Exposure to Tris(1,3-dichloro-2-propyl) Phosphate (TDCIPP) Causes Hepatic Inflammation and Leads to Hepatotoxicity in Zebrafish. Sci Rep. 2016;6:19045.

381. Hahn ME, McArthur AG, Karchner SI, Franks DG, Jenny MJ, Timme-Laragy AR, et al. The transcriptional response to oxidative stress during vertebrate development: effects of tert-butylhydroquinone and 2,3,7,8-tetrachlorodibenzo-p-dioxin. PLoS One. 2014;9(11):e113158.

382. Gustafson DL, Beall HD, Bolton EM, Ross D, Waldren CA. Expression of human NAD(P)H: quinone oxidoreductase (DT-diaphorase) in Chinese hamster ovary cells: effect on the toxicity of antitumor quinones. Mol Pharmacol. 1996;50(4):728-35.

383. Heitz FD, Erb M, Anklin C, Robay D, Pernet V, Gueven N. Idebenone protects against retinal damage and loss of vision in a mouse model of Leber's hereditary optic neuropathy. PLoS One. 2012;7(9):e45182.

384. Beatty S, Koh H, Phil M, Henson D, Boulton M. The role of oxidative stress in the pathogenesis of age-related macular degeneration. Surv Ophthalmol. 2000;45(2):115-34.

385. Jarrett SG, Boulton ME. Consequences of oxidative stress in age-related macular degeneration. Mol Aspects Med. 2012;33(4):399-417.

386. Perepechaeva ML, Kolosova NG, Stefanova NA, Fursova AZ, Grishanova AY. The influence of changes in expression of redox-sensitive genes on the development of retinopathy in rats. Exp Mol Pathol. 2016;101(1):124-32.

387. Zhao Z, Chen Y, Wang J, Sternberg P, Freeman ML, Grossniklaus HE, et al. Age-related retinopathy in NRF2-deficient mice. PLoS One. 2011;6(4):e19456.

388. Ross D, Siegel D. NAD(P)H:quinone oxidoreductase 1 (NQO1, DT-diaphorase), functions and pharmacogenetics. Methods Enzymol. 2004;382:115-44.

389. Siegel D, McGuinness SM, Winski SL, Ross D. Genotype-phenotype relationships in studies of a polymorphism in NAD(P)H:quinone oxidoreductase 1. Pharmacogenetics. 1999;9(1):113-21.

390. Hwang JH, Kim DW, Jo EJ, Kim YK, Jo YS, Park JH, et al. Pharmacological stimulation of NADH oxidation ameliorates obesity and related phenotypes in mice. Diabetes. 2009;58(4):965-74.

391. Gaedigk A, Tyndale RF, Jurima-Romet M, Sellers EM, Grant DM, Leeder JS. NAD(P)H:quinone oxidoreductase: polymorphisms and allele frequencies in Caucasian, Chinese and Canadian Native Indian and Inuit populations. Pharmacogenetics. 1998;8(4):305-13.

392. Kelsey KT, Ross D, Traver RD, Christiani DC, Zuo ZF, Spitz MR, et al. Ethnic variation in the prevalence of a common NAD(P)H quinone oxidoreductase polymorphism and its implications for anti-cancer chemotherapy. Br J Cancer. 1997;76(7):852-4.

Appendices

Appendices

Appendix 1

UTAS	University of Tasmania Animal Ethics Committee **ETHICS APPROVAL PERMIT**	University of Tasmania Research Services Ph: 03 62267283 Fax: 03 62267148 animal.ethics@utas.edu.au

To:	Dr Nuri Guven
From:	Marilyn Pugsley Ethics Officer Animal Ethics
Date:	31 October 2012
Project:	**A12817 – Role of mitochondria in the visual function of zebrafish (D.rerio)**
Approved on:	31 October 2012
Approval expires:	31 October 2015
1st Annual Report due:	31 October 2013
Number of Animals:	Adult Zebrafish – 120 for three year period Embryonic Zebrafish – 9000 for three year period

Please read this permit carefully as **approval may be withdrawn** for projects that do not comply with the conditions

The Animal Ethics Committee has approved the above project. The approval is subject to the review and approval of an annual report which is due on the approval anniversary**. Please note this date in your diary.**

If the project is to continue past the expiry date, a new initial application will need to be submitted. A project can only be approved for a maximum of 3 years.

As the Responsible Investigator, you MUST ensure that:

(a) all aspects of the work conform to the requirements of the current edition of the *Australian code of practice for the care and use of animals for scientific purposes*

(b) a full record is maintained of all animals used in this project. If at any stage you anticipate the need to use additional animals this must be communicated to the committee before use. Using additional animals without AEC approval is a breach of your ethics permit.

(c) you contact the Animal Welfare Officer (Dr Barrie Wells) to advise him when and where your experiments will be conducted. Sufficient notice needs to be given so that if the AWO wishes to make an inspection, this can be easily arranged. Dr Wells contact is 0427680782 or barrie.wells@utas.edu.au

The Animal Ethics Committee is to be promptly notified of any unexpected events which occur during the period of the approved project and impact on the welfare of the animals (2.2.28 *Australian Code of Practice*).

Autopsy should be performed by a qualified veterinarian when animals die unexpectedly. Any foreseeable departure from this requirement must have been outlined and approved in the initial application.

Detailed experimental records must be kept and must be available to the Committee on request.

Conditions (apply to some projects only):

(i) If the investigation necessitates a Parks & Wildlife permit you are required to send a copy of this permit to the AEC Secretary before commencing work.

(ii) If you intend to obtain laboratory animals directly from a source other than the University Central Animal House, the Animal Welfare Officer must be notified when the order is placed and when the animals are received.

Special Conditions of approval (if applicable):

Marilyn Pugsley
Ethics Officer Animal Ethics

University of Tasmania **Animal Ethics Committee**	
Ethics Number	A12817
Project Name	Role of mitochondria in the visual function of zebrafish (D.rerio)
Chief Investigator	Dr Nuri Guven
School	Pharmacy
Person responsible for day-to-day care	
Ethics start date	31 October 2012
Ethics approved to	31 October 2015 (with annual renewals)
No of animals approved	Adult Zebrafish – 120 for three year period Embryonic Zebrafish – 9000 for three year period
Emergency Contact	

Appendix 2

AEC Approval for Modification: A0012817

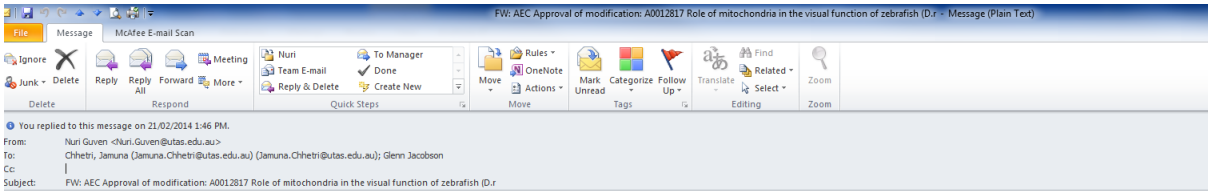

You replied to this message on 21/02/2014 1:46 PM.

From: Nuri Guven <Nuri.Guven@utas.edu.au>
To: Chhetri, Jamuna (Jamuna.Chhetri@utas.edu.au) (Jamuna.Chhetri@utas.edu.au); Glenn Jacobson
Cc:
Subject: FW: AEC Approval of modification: A0012817 Role of mitochondria in the visual function of zebrafish (D.r

FYI

-----Original Message-----
From: Marilyn.Pugsley@utas.edu.au [mailto:Marilyn.Pugsley@utas.edu.au]
Sent: Tuesday, 18 February 2014 2:01 PM
To: Nuri Guven
Subject: AEC Approval of modification: A0012817 Role of mitochondria in the visual function of zebrafish (D.r

Dear Dr Guven

RE: A0012817 Role of mitochondria in the visual function of zebrafish (D.rerio)

On behalf of the Animal Ethics Committee, I am pleased to inform you that your application to modify the above project was approved by the Animal Ethics Committee on xxxxxxxx.

To ensure currency of your ethics application, it is important that you 'accept' the tracked changes on the approved modified document. This action will update the document and allow for further modifications to be tracked if and when required.

Please file this email as evidence of your approval.

Date of modification application:10 December 2013

Description of modification: Request for utilisation of embryos generated by Dr L Foa. Request for new facility at Room 531A, Level 5, Medical Sciences Precinct.

With kind regards

Marilyn Pugsley
Executive Officer Animal Ethics Committee Office of Research Services University of Tasmania Private Bag 01 Hobart TAS 7001
Phone: (03) 6226 7283
Fax: (03) 6226 2765
Email: Marilyn.Pugsley@utas.edu.au
Web: http://www.research.utas.edu.au/

Appendix 3

UNIVERSITY of TASMANIA

Animal Ethics Committee
ETHICS APPROVAL PERMIT

Office of Research Services
Phone : 03 62267283
Fax: 03 62267148
animal.ethics@utas.edu.au

To: Dr Nuri Guven

From: Marilyn Pugsley

Date: 18 September 2015

Project: A0015097 - Role of mitochondria in the visual function of zebrafish (D.rerio)

Approved on: 11 September 2015

Approval expires: 10 September 2018

1st Annual Report due: 10 September 2016

Please read this permit carefully as **approval may be withdrawn** for non-compliance with the conditions stated below.

The Animal Ethics Committee has approved the above project and a copy of the initial application document is attached. The approval is subject to the review and AEC approval of an annual report which is due before the approval anniversary**. Please note the due date in your diary.**

As the Responsible Investigator, you MUST ensure that:

1. All aspects of the work conform to the requirements of the current edition of the *Australian code of practice for the care and use of animals for scientific purposes* 8th edition 2013

2. The project is conducted in accordance with the provisions of the Tasmanian Veterinary Surgeons Act 1987 and Veterinary Surgeons Regulations 2012. If the project involves a veterinary service or other animal service, it is **your responsibility** to contact the University Veterinarian to discuss the legal requirements of competency assessment.

3. The University Veterinarian and the Animal Ethics Committee are promptly notified of any unexpected event which was not considered in

the initial application and impacts on the welfare of any animal directly or indirectly involved in the project.

4. You contact the University Veterinarian to advise when and where your experiments will be conducted. Sufficient notice needs to be given so that an inspection can be easily arranged.

5. In the event of any unexpected death, you contact the University Veterinarian to perform an autopsy.

6. A full record is maintained of all animals used in this project. If at any stage you anticipate the need to use additional animals this must be communicated to the committee before use. Using additional animals without AEC approval is a breach of your ethics permit.

7. That all investigators attend Ethics training sessions every three years. Contact the Executive Officer Animal Ethics for the next available session.

The project is approved for a maximum of 3 years. If the project is to continue past the expiry date, a new initial application will need to be submitted.

If the investigation necessitates a Parks & Wildlife permit or other permits, you are required to send copies to animal.ethics@utas.edu.au before commencing work.

Ethics Officer
Animal Ethics Committee

University of Tasmania **Animal Ethics Committee**	
Ethics Number:	A0015097
Project Name:	Role of mitochondria in the visual function of zebrafish (D.rerio)
Chief Investigator:	Dr Nuri Guven
School:	Pharmacy
Person responsible for day-to-day care:	
Ethics start date:	11 September 2015
Ethics approved to:	10 September 2018
Emergency Contact:	

Appendix 4

Death assessment chart for zebrafish larvae

S. No	Drug Used	Absence of heart beat	Locomotory activity/startle response	Dorsoventral balance	Morphological abnormalities			% death
					Pericardial oedema	Bent body	Failure to inflate swim bladder	

Death assessment chart for adult zebrafish

Drugs	Date	S. No	Feed/temp	heart - beat	Locomotory activity	Dorso-ventral balance	% death